DEVELOPMENT OF THREE-DIMENSIONAL PATTERNING STRATEGIES FOR OSTEOCHONDRAL TISSUE ENGINEERING

Michael John Sawkins, MA

Thesis submitted to the University of Nottingham

for the degree of Doctor of Philosophy

December 2012

Abstract

Fully-realised three-dimensional patterning strategies enable the development of heterogeneous constructs which can recreate tissue architecture and cellular microenvironments over a large range of length scales. This in turn allows the development of more effective tissue models and tissue engineering therapies. The work presented in this thesis was designed to address the development of patterning methodologies and compatible biomaterial formulations.

Poly(lactic-co-glycolic acid)-based (PLGA-based) microspheres were utilised for temporally-controlled protein delivery. Robust protocols were developed for the production of microspheres with two different mean sizes to provide distinct release kinetics which could be further tailored by the addition of a PLGA-poly(ethylene glycol)-PLGA (PLGA-PEG-PLGA) triblock copolymer. A semi-automated microinjection/micromanipulation (MM) system was used to precisely position individual microspheres into cell culture substrates. This approach has the potential to replicate complex interacting signal environments as seen in developmental and repair processes.

Demineralised bovine bone, processed with or without a decellularisation step, was enzymatically digested to form solutions capable of gelation under physiological conditions. The resulting hydrogels outperformed collagen as *in vitro* culture substrates for bone-derived cells and are promising injectable scaffold materials. They were also formed into beads which could encapsulate exogenous proteins and which may be utilised in MM-based patterning strategies.

Bioplotting was used to produce alginate hydrogel constructs containing highly viable cell populations. This technique was also used to deposit a PLGA-PEG microparticulate material which could be sintered under physiological conditions to achieve bone appropriate mechanical properties. PLGA-PEG/alginate dual material

constructs could also be produced incorporating independent patterns of these two materials and of two cell populations and two protein signals. Bioplotting could therefore be used to produce sophisticated tissue engineering constructs for the repair of large, complex defects. Though this work focused on osteochondral applications much of the data is also more widely-applicable.

Publications & Presentations

The following publications and presentations have resulted from the work presented in this thesis.

Publications in Peer-Reviewed Journals

Rahman, C.V., Saeed, A., White, L.J., Gould, T.W.A., Kirby, G.T.S., Sawkins, M.J., Alexander, C., Rose, F.R.A.J. & Shakesheff, K.M. Chemistry of polymer and ceramic-based injectable scaffolds and their applications in regenerative medicine. *Chemistry of Materials* **24 (5)**, 781-795 (2012).

Published Conference Abstracts

Sawkins, M.J., Brown, B.N., Bonassar, L.J., Rose, F.R.A.J., & Shakesheff. K.M. Bioprinting as a tool for osteochondral tissue engineering. *European Cells and Materials* **22 (3)**, 51 (2011).

Sawkins, M.J., Brown, B.N., Bonassar, L.J., Cox, H., Rose, F.R.A.J., & Shakesheff. K.M. Cell, scaffold and growth factor patterning via 3D printing. *Journal of Tissue Engineering and Regenerative Medicine* **6 (Supplement 1)**, 374 (2012).

White, L.J., Sawkins, M.J., Badylak, S.F. & Shakesheff. K.M. Decellularised bone gels – novel materials for bone regeneration. *Journal of Tissue Engineering and Regenerative Medicine* **6 (Supplement 1)**, 168 (2012).

Oral Presentations

Sawkins, M.J., Brown, B.N., Bonassar, L.J., Rose, F.R.A.J., & Shakesheff. K.M. Bioprinting as a tool for osteochondral tissue engineering. Presented at the Annual Meeting of the Tissue and Cell Engineering Society 2011 (Leeds, UK).

Sawkins, M.J., Brown, B.N., Bonassar, L.J., Rose, F.R.A.J., & Shakesheff. K.M. Bioplotting of novel scaffold materials and complex constructs for osteochondral tissue engineering. Presented at the Annual Meeting of the Tissue and Cell Engineering Society 2012 (Liverpool, UK).

White, L.J., Sawkins, M.J., Badylak, S.F. & Shakesheff. K.M. Decellularised bone gels – novel materials for bone regeneration. Presented at the World Congress of the Tissue Engineering & Regenerative Medicine International Society 2012 (Vienna, Austria).

Poster Presentations

Sawkins, M.J., Brown, B.N., Bonassar, L.J., Rose, F.R.A.J., & Shakesheff. K.M. Bioprinting as a tool for osteochondral tissue engineering. Presented at UK-PharmSci 2011 (Nottingham, UK).

Sawkins, M.J., Brown, B.N., Bonassar, L.J., Rose, F.R.A.J., & Shakesheff. K.M. Bioprinting as a novel tool for osteochondral tissue engineering. Presented at the Annual Conference of TERMIS – North America 2011 (Houston, TX, USA).

Sawkins, M.J., Brown, B.N., Bonassar, L.J., Rose, F.R.A.J., & Shakesheff. K.M. Bioprinting of novel materials for bone tissue engineering. Presented at the Annual Conference of the UK Society for Biomaterials 2012 (Nottingham, UK).

White, L.J., Sawkins, M.J., Badylak, S.F. & Shakesheff. K.M. Decellularised bone gels – novel materials for bone regeneration. Presented at the Annual Conference of the UK Society for Biomaterials 2012 (Nottingham, UK).

Sawkins, M.J., Brown, B.N., Bonassar, L.J., Cox, H., Rose, F.R.A.J., & Shakesheff. K.M. Cell, scaffold and growth factor patterning via 3D printing. Presented at the World Congress of the Tissue Engineering & Regenerative Medicine International Society 2012 (Vienna, Austria).

Sawkins, M.J., Brown, B.N., Bonassar, L.J., Rose, F.R.A.J., & Shakesheff. K.M. Bioprinting as a tool for osteochondral tissue engineering. Presented at Doctoral Training Centre Joint Conference Tissue Engineering and Regenerative Medicine 2012 (Keele, UK).

Acknowledgments

First of all I must thank my supervisors Prof. Kevin Shakesheff and Dr. Felicity Rose for all their support and guidance and the opportunities that I have been afforded whilst working towards my PhD. I would also like to thank Dr. Lawrence Bonassar and Dr. Bryan Brown for supervising my work on bioplotting at Cornell University.

My thanks go to Helen Cox, Dr. Omar Qutachi, Dr. Lisa White, Giles Kirby, Dr. Glen Kirkham, Dr. Alex Huber, Dr. Stephen Badylak, Jeff Lipton, Carol Bayles, Christine Grainger-Boultby and Dr. Lloyd Hamilton for training and advice on various techniques and materials.

I am also grateful to Laura Sidney, Adam Taylor, Dr. James Dixon, Dr. Hassan Rashidi and Dr. Claudia Fischbach-Teschl for the provision of cells.

Next I must thank the staff of the histopathology department at the Queen's Medical Centre, Dr. Lisa White, Hareklea Markides, Will Bowen and Paramjeet Dhadda for providing characterisation data for extracellular matrix-derived powders.

I would like to thank everyone in the Tissue Engineering Group and in particular my fellow Doctoral Training Centre (Regenerative Medicine) students for making it such a pleasure to go to work during the past four years.

Lastly I am truly grateful to my family (Martin, Tricia & Catherine Sawkins and Matt Lee), my wife Caroline and also her family (Ian, Jo & Heather Vickers and Adrian Yemm) for their support and belief in me throughout my studies.

Table of Contents

List of Figures

List of Tables

List of Abbreviations

3DP	3D printing
αMEM	Alpha minimum essential medium
β-TCP	Beta-tricalcium phosphate
µCT	Micro-computed tomography
AB/AM	Antibiotic/antimycotic
BM	Basement membrane
BMP-2	Bone morphogenetic protein-2
CDI	1,1-Carbonyldiimidazole
CMC	Carboxymethyl cellulose
DAPI	4',6-Diamidino-2-phenylindole
DBM	Demineralised bone matrix
DCM	Dichloromethane
DECM	Decellularised extracellular matrix
dH_2O	Distilled water
DMDPP	Digital micromirror device projection photolithography
DMEM	Dulbecco's modified Eagle medium
DMSO	Dimethyl sulphoxide
(ds)DNA	(Double-stranded) deoxyribonucleic acid
ECM	Extracellular matrix

EDTA	Ethylenediaminetetraacetic acid
EMEM	Eagle's minimum essential medium
FBS	Foetal bovine serum
FFF	Fused filament fabrication
FITC	Fluorescein isothiocyanate
GAG	Glycosaminoglycan
H & E	Haemotoxylin and eosin
HA	Hydroxyapatite
hOS	Human osteosarcoma
HOT	Holographic optical tweezers
HSA	Human serum albumin
(i)hMSC	(Immortalised) human mesenchymal stem cell
MEM	Minimum essential medium
MM	Microinjection/micromanipulation
mPC	Murine primary calvarial
MPL	Multiphoton lithography
OT	Optical tweezers
PBS	Phosphate-buffered saline
PCL	Polycaprolactone
PEG	Poly(ethylene glycol)
PEGDA	Poly(ethylene glycol) diacrylate

PEGDMA	Poly(ethylene glycol) dimethacrylate
Pen/strep	Penicillin/streptomycin
PG	Proteoglycan
PLGA	Poly(lactic-co-glycolic acid)
PLLA	Poly(L-lactic acid)
PPF	Poly(propylene fumarate)
PTFE	Poly(tetrafluoroethylene)
PVA	Poly(vinyl alcohol)
RP	Rapid prototyping
$scCO_2$	Supercritical carbon dioxide
SEM	Scanning electron microscopy
SLS	Selective laser sintering
STL	Stereolithography
TCP	Tissue culture plastic
Triblock	PLGA-PEG-PLGA triblock copolymer (in-house synthesis)

1. General Introduction

Many tissue engineering strategies involve the production of biomaterial scaffolds which have largely uniform three-dimensional architectures. These scaffolds may also deliver drugs or therapeutic proteins, though usually with spatially-homogenous profiles. They can then be directly implanted *in vivo* or uniformly pre-seeded with appropriate cell types to form tissue-engineered constructs. The homogeneity of constructs produced in this way does not reflect the complexity of the tissues they are designed to emulate which may limit their ability to produce fully-functional tissue regeneration.

Heterogeneity exists *in vivo* on a wide range of length scales, arguably most obviously in the fact that a tissue may contain several cell types and a whole organ may then contain multiple tissues with distinct cell populations. Extracellular matrix (ECM) differences may also exist between different locations, in terms of mechanical properties and/or biochemical composition. Recreating these variations in tissue composition will be important to achieve truly effective, functional repair of large areas of defective or missing tissue. Another important consideration is the need for neo-tissue to become rapidly and effectively vascularised after implantation. This may necessitate the pre-vascularisation of constructs prior to delivery to the clinic. For these reasons there is a clear need for construct fabrication techniques which are capable of macro-scale ('sub-millimetre') three-dimensional patterning.

Tissues also have functional heterogeneity on a finer scale due to the arrangement and alignment of cells and ECM molecules and the presence of gradients of proteins and other signalling molecules[1-6]. These environments form the local 'niches' that play a pivotal role in the regulation of cell and tissue function. The replication of such niches *in vitro* would allow a more detailed understanding of the cell and

molecular biology of these microenvironments. Knowledge gained in this way can then support the development of more effective tissue engineering constructs.

Cell and scaffold patterning techniques can be broadly divided into three categories. Firstly there are those techniques that produce three-dimensional scaffolds but only allow the production of a restricted set of simple patterns. This category covers approaches such as electrospinning[7,8], layered moulding strategies[9] or gradient mixing[10-13]. Techniques that allow the production of complex patterns but only in two dimensions form the second category and those that facilitate the production of complex three-dimensional patterns are the third category of techniques. The complexity offered by the latter two categories is essential for the replication of tissue architectures and these techniques will be discussed further below.

For the purpose of this thesis a technique is considered to be three-dimensional if it is capable of generating macro-scale constructs suitable for tissue engineering or can exert patterning effects at any point within macro-scale constructs. In this context a macro-scale construct is taken to be a centimetre or more in size. Two-dimensional techniques such as photolithography, soft lithography, microfluidics, laser-induced forward transfer and inkjet printing have informed the development of three-dimensional techniques. However their utility is limited when it comes to the production of macro-scale tissue engineering constructs or the deduction of fundamental microenvironmental biology by dimensionality and resolution respectively. These techniques have been comprehensively reviewed elsewhere[14-23] and only three-dimensional techniques will be considered further.

1.1 Patterning of Individual Objects: Recreating Cellular Microenvironments

1.1.1 Microinjection and Micromanipulation

Microinjection involves the delivery of sub-millilitre volumes of (partially) fluid material into a substrate via the application of pressure. The pressure may be pneumatically, hydraulically or directly applied either manually or automatically. Microinjection is typically used in combination with either manual or automated micromanipulation to precisely control the site of delivery. Drugs, signalling molecules and viral vectors have been injected into both embryonic and adult tissue for the study of the mechanisms of development and disease progression[24-29].

More recently, and more relevantly for tissue engineering, microinjection/micromanipulation (MM) techniques have also been used to deliver cells[30-32] and synthetic polymer microspheres[31-34] into adult tissues. The delivery of cells and microspheres into scaffold materials could allow the creation of tissue and developmental models *in vitro*, with the microspheres responsible for controlled delivery of biological signals. These environments may permit the study of fundamental cell biology and the screening of potential tissue engineering therapies.

Automated MM platforms have recently been developed which improve the precision and repeatability of delivery[35-39]. Many of these aim to automate the manipulation of the cells, cell clusters or embryos into which the injection is to be performed. One study demonstrated a platform for automated control of injection position within a bulk collagen hydrogel[39]. Though the platform was only used to produce simple arrays of cell clusters suspended in poly(vinyl pyrollidone) the technology could allow the production of complex environments with greater speed and precision than is possible manually. Though the resolution achieved in this study compares well with many other three-dimensional patterning techniques it may not provide high enough resolution for the recreation of early developmental environments or the study of cell

biology at a single cell level. A key challenge for the future may thus be to utilise MM techniques to manipulate and deliver cells and microspheres individually.

1.1.2 (Holographic) Optical Tweezers

An optical tweezer (OT) system creates 'optical traps' by focusing a laser beam through a microscope objective with a high numerical aperture. Two distinct types of force act within the optical traps and they interact to constrain objects within the traps. The scattering force is produced by photons from the laser beam striking the object within a trap and the gradient force by a gradient in field intensity. Dielectric objects such as cells or small particles composed of silica or synthetic polymers can be optically trapped, and this enables OT systems to arrange micron-scale objects individually with high resolution (Figure 1.1)[40-43].

The science underpinning OT systems was pioneered by Arthur Ashkin and colleagues[44] and further developed in collaboration with J.M. Dziedzic[45]. The authors speculated that OT systems could be utilised in trapping and manipulating biological materials. This breakthrough was first achieved by the use of infrared lasers to effectively trap bacteria and viruses[46,47]. The low absorbance of near infrared light (wavelengths around 750 – 1500 nm) by the majority of biological materials enables their safe and effective manipulation. This development of the technique has ultimately led to the successful trapping of mammalian cells[48,49].

To allow OT systems to generate complex patterns in three dimensions they must be capable of generating multiple traps from a single laser source. Systems have now been developed which are capable of generating multiple traps in two dimensions[50-53]. Furthermore, holographic optical tweezer (HOT) systems with the ability to generate multiple traps in three dimensions have also been devised[54-61]. These systems have been used to stably trap and manipulate both eukaryotic and prokaryotic cells[62] and this has been extensively utilised in cell sorting[63-77].

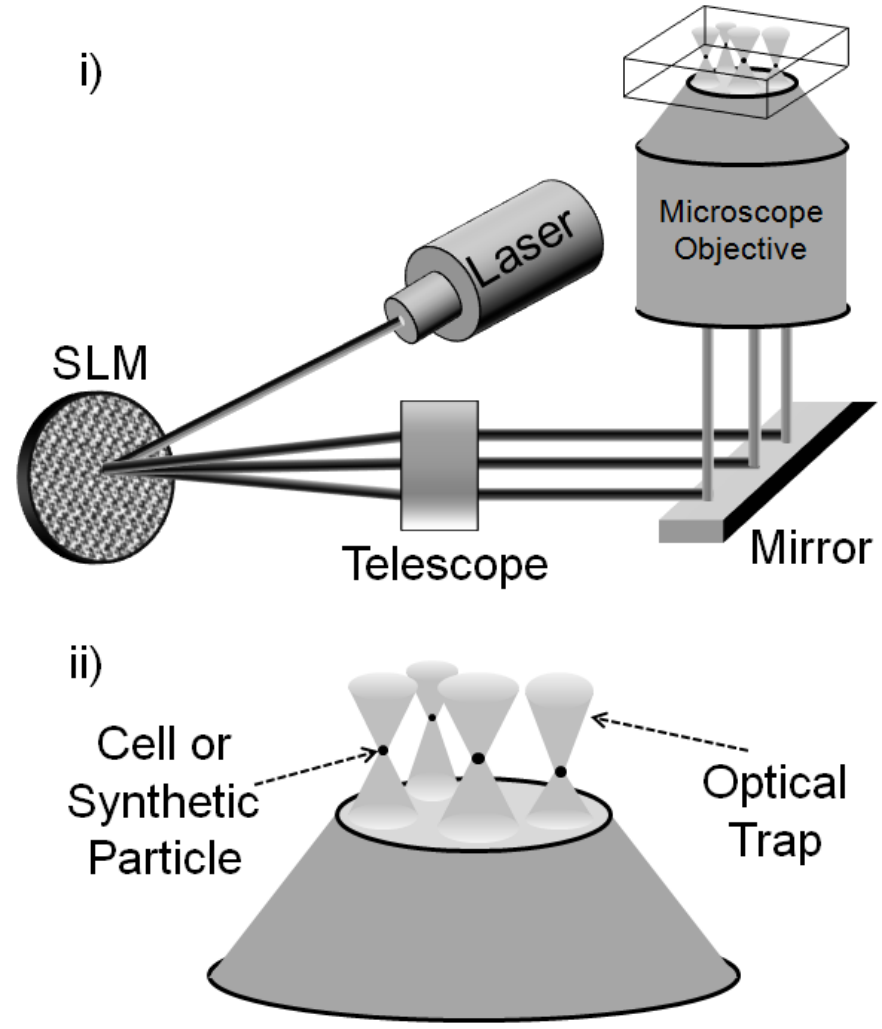

Figure 1.1 – Schematic depicting the principles of operation of a holographic optical tweezer system. i) A computer-controlled spatial light modulator (SLM) acts in combination with telescopic optics and a microscope objective to generate optical traps in 3D. ii) These traps can stably hold objects such as cells or microscopic synthetic particles in precisely defined positions.

OT systems have the ability to position trapped objects with precision on the cellular level. This high resolution manipulation has been combined with microfluidic devices to study the responses of prokaryotes to different environmental conditions[70,78]. However, effective utilisation of OT-based manipulation to perform three-dimensional patterning of mammalian cells has to date been very limited. A small number of early studies do demonstrate, at least in two dimensions, the potential of HOT systems in the study of cell-cell interactions on a single cell level[42,43,79].

In one study a single rod cell was placed next to groups of cells containing a cone cell and a multipolar neuron and it was found that prominent growth of the neuron was inhibited by the presence of the rod cell[43]. Other studies have demonstrated the 3D patterning potential of HOT systems by positioning synthetic particles into complex 3D structures with spacing of a few microns[40,68].

The practical limitations of fabrication one cell at a time may limit the use of OT systems in the production of tissue engineering constructs directly. However their high resolution offers valuable opportunities for use in *in vitro* tissue and disease modelling. OT systems could allow the study and replication of microenvironmental features at a resolution higher than that possible with any other three-dimensional patterning technique.

1.2 Production of Patterned Constructs: Recreating Macro-Scale Tissue Heterogeneity

The level of interest in the three-dimensional patterning techniques discussed below, referred to collectively as solid freeform fabrication or rapid prototyping (RP) techniques has grown rapidly in recent years. RP technologies have found significant application in tissue engineering due to their capability to produce bespoke scaffold architectures that replicate clinical defect sites. More recent research has also addressed their capacity to produce constructs which contain patterns in various

features and properties. A number of RP techniques have been utilised including stereolithography, multiphoton lithography, selective laser sintering, 3D printing, fused filament fabrication, bioplotting and bioprinting.

1.2.1 Stereolithography

Stereolithography (STL) is a maskless optical lithography technique in which a laser light is scanned across the surface of a liquid precursor bath to solidify a thin layer of the material in the desired two-dimensional pattern on a support table. Vertical motion of the table allows the generation of successive layers, each created at the liquid surface and bound to the underlying layer (Figure 1.2). STL was developed and patented by Charles Hull for high-fidelity reproduction of synthetic polymer components in industrial manufacturing[80]. Further developments of the technique have demonstrated its potential for the fabrication of biological constructs for tissue engineering and modelling[81]. STL has the potential to be used for patterning construct constituents and properties by dividing the fabrication of each layer into a series of successive steps utilising different precursor mixtures. Different mixtures may then form different final materials, encapsulate different cell types or different biological signals.

Scaffolds used in tissue engineering are typically designed to degrade or be resorbed *in vivo*, supporting and encouraging tissue repair. The compatibility of STL techniques with biodegradable/resorbable materials therefore further supports its use within the field of tissue engineering. A number of biodegradable synthetic polymers have been used successfully in STL-based scaffold fabrication, including polypropylene fumarate (PPF)[82-86], poly(D,L-lactide)[87,88] and polycaprolactone (PCL)[88,89].

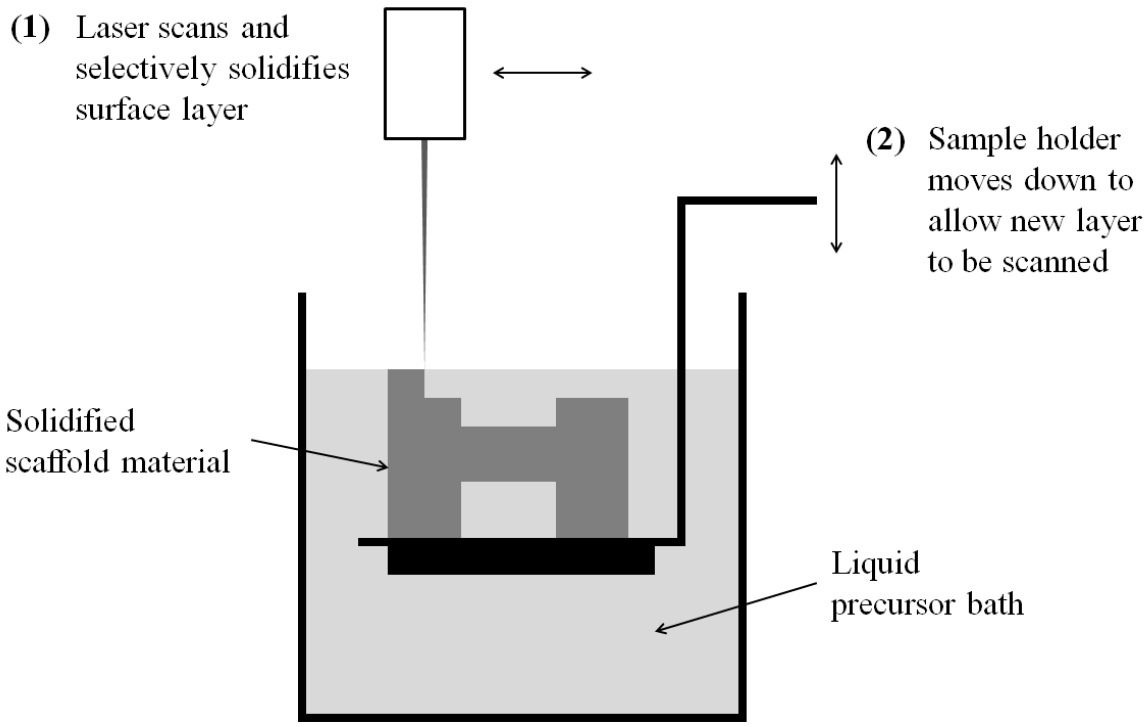

Figure 1.2 – Schematic depicting the principles of operation of a stereolithography device. A laser scans the surface of a photocurable liquid precursor to selectively solidify a thin layer close to the surface (1). The sample support table then moves down to allow a new layer to be scanned and solidified, which is bound to the first layer (2). By repetition of these steps a three-dimensional structure is built.

Photocurable forms of natural polymers including chitosan[90] have also been developed which are suitable for use in STL. Scaffolds formed from these materials have inherent bioactivity and may aid the reconstitution of natural cell-matrix interactions and the integration of the scaffold with surrounding native tissue. Wang and colleagues demonstrated that scaffolds could be produced via STL from engineered peptides containing photosensitive non-canonical amino acids[91].

STL has also been applied to a number of ceramic materials such as alumina[92-95] and β-tricalcium phosphate (β-TCP)[96]. Scaffolds are made by suspending ceramic particles in a synthetic polymer precursor to produce the initial 'green' scaffold which is then subjected to heat treatment to remove the polymer and sinter the ceramic. Scaffolds produced in this way can have compressive strengths of up to 23.54 MPa, making them suitable for the repair of load-bearing bones[96].

To increase the potential patterning complexity that can be achieved via STL, particularly for multi-tissue constructs, the incorporation of cells in the fabrication process is an important step. Whilst this is not usually possible with the materials described above, viable cells can be incorporated in scaffolds formed from hydrogels such as poly(ethylene glycol) dimethacrylate (PEGDMA)[97,98] or poly(ethylene glycol) diacrylate (PEGDA)[99]. Short-term cell survival has been demonstrated in PEGDMA, with one study showing 87% viability of human dermal fibroblasts 24 hours post-fabrication[98]. Longer term studies that demonstrate functional biological structure formation within the resulting constructs have yet to be performed. The full effectiveness of this technique for cell patterning therefore remains to be established.

Incorporation of biological proteins into the scaffold structure introduces an additional level of functionality that could further increase the efficacy of STL based construct formation[100,101]. Such incorporation has been demonstrated by a study showing the successful incorporation of the growth factor bone morphogenetic protein-2 (BMP-2). Post-fabrication bioactivity, both *in vitro* and *in vivo*, was achieved by encapsulating the protein in poly(lactic-co-glycolic acid) (PLGA) microspheres[101]. As well as

potentially protecting the protein during construct fabrication, encapsulation in polymer microspheres allowed the temporal presentation of the protein to be controlled. This is in addition to the spatial control exerted by the STL process itself.

It has been shown that STL can offer high resolution morphological control and feature sizes as small as 8.4 μm have been achieved[86]. A number of recent studies have also shown that varying simple morphological parameters such as pore size can have a significant effect on the adhesion and proliferation of cells on STL-derived scaffolds[102-104]. However these studies have largely focused on the generation of scaffolds with uniform properties.

STL can be used to pattern constructs both between and within individual layers, with the latter being more difficult to achieve but providing a greater level of functional complexity. A small number of recent studies have utilised STL to achieve both types of patterning in a variety of construct constituents[100,105-107]. Two of these have demonstrated patterning of polysaccharides and peptide-modified poly(ethylene glycol) (PEG) within hydrogel scaffolds for control of protein binding and cell adhesion respectively[100,106]. In the latter study it was qualitatively shown that human dermal fibroblasts preferentially attached to and proliferated in regions of the scaffolds which contained peptide-modified PEG[106]. Whilst these examples illustrate the potential of STL, patterns of sufficient complexity to replicate tissue macro-architectures were not generated and functionality has not been demonstrated.

Recently, a study by Chan and colleagues generated hydrogels able to support proliferation of encapsulated NIH/3T3 fibroblasts with differently-labelled cell populations able to be included in different layers of the same construct[105]. This direct approach provided constructs containing multiple cell types, which may be key to replicating tissue architecture. Similarly Zorlutuna and colleagues synthesised constructs composed of PEG and a modified photocurable alginate[107]. Some encapsulated cell types were viable and proliferative whilst others showed significant cell death, suggesting that different materials may be required to support different

cell types. The authors were subsequently able to show that cells and materials could be independently patterned and produced constructs that contained C2C12 myoblasts, hippocampal neurons and adipose-derived stem cells.

Whilst the studies discussed thus far serve to illustrate the potential of STL for the production of complex scaffold constructs, there are a number of practical limitations that must be considered for future applications of this technology. The resolution limits of STL are yet to be fully characterised. Simple applications have demonstrated the production of structures less than 10 μm in size[86] but intra-scaffold patterning has only been performed with coarser resolutions of the order of 500 μm or more[105,106]

A further limitation of STL for three-dimensional patterning is the requirement for extensive washing steps whenever the precursor materials are changed. This prevents blurring between neighbouring regions but can make the production of complex scaffolds very time-consuming. This may be particularly problematic when cells are to be incorporated since components of the photosensitive precursor mixes used for STL can be cytotoxic[97,106,107].

STL variants have been developed which utilise dynamic masking to speed up the fabrication process. Rather than a point source scanning a surface to form each two-dimensional layer, a whole layer is simultaneously illuminated as defined by a dynamic mask. The most commonly used masks are digital micromirror devices consisting of arrays of mirrors which can be switched between 'on' and 'off' states in which they do and do not reflect light[108-110].

Studies utilising digital micromirror device projection photolithography (DMDPP) in tissue engineering are far fewer in number than those using conventional STL and the development of the technique is at an earlier stage. The materials used have predominantly been synthetic polymers such as PPF[111] and a mixture of PLGA and poly(ethylene glycol) hydroxyethylmethacrylate[112]. In a small number of cases

scaffolds have also been produced from hydrogels such as PEGDA, which could be surface modified with laminin[113] or fibronectin[114] in order to promote cell attachment. Although biologically-relevant patterning has not been demonstrated with DMDPP, a study published by Choi and coworkers did show the development of a multi-material system which was utilised for patterning commercially available STL resins both within and between layers[115]. The advantages that DMDPP has over the more established STL technique make this a promising method for future biological patterning applications.

STL has been used to produce constructs for tissue engineering and *in vitro* modelling from a wide variety of materials, encapsulating a range of different cell types and biological signals. The ability of the technique to offer high-resolution morphological patterning of constructs is well-established[81] and more complex patterning of cell populations, materials and proteins has also been demonstrated[100,105-107]. The patterning resolution so far demonstrated may not be sufficient to reproduce the microenvironmental characteristics of the cell niche but significant potential still exists for the generation of macro-scale patterns.

1.2.2 Multiphoton Lithographic Techniques

Multiphoton lithography (MPL) is an adaptation of STL in which the intended effect of the illumination is produced only when two (or more) photons arrive at a point simultaneously[116-118]. This happens very precisely at the focal point of the laser optical system and it is this property that gives MPL superior spatial resolution compared to STL. The use of MPL techniques in tissue engineering and modelling is less widespread than that of conventional STL but reports published so far demonstrate the potential of the technique[119,120].

Materials utilised for freeform fabrication applications of MPL include hyaluronic acid [121], proteins such as bovine serum albumin and fibrinogen[122-125], the

organic/inorganic hybrid polymer ORMOCER® [126-128] and protein/polymer hybrids which offer the mechanical strength of polymers alongside the bioactivity of proteins[129]. As with STL, some of these techniques use digital micromirror devices to speed up construct fabrication[122,124]. The data in these publications illustrate that MPL techniques have resolutions which are at least an order of magnitude finer than those seen in conventional STL, with sub-micron features often achievable. The wide range of materials studied shows that this approach can potentially produce scaffolds suitable for application in many different tissues.

MPL techniques have also been developed to generate three-dimensional patterns within pre-existing hydrogels[130]. A series of publications by Shoichet and colleagues has focused on the development of agarose based hydrogels which can be modified by the induction of crosslinking and/or exposure of photocaged reactive moieties for protein immobilisation[131-142]. Three different routes to protein immobilisation have been demonstrated and it has been shown that all three systems are capable of producing different protein concentrations by varying the number of times an area is scanned[132-134]. The results in these studies show that the patterning resolution is 5 µm in the plane perpendicular to the incident light (40 µm in the direction parallel), that immobilised protein patterns are stable for at least 8 days and that two proteins can be patterned simultaneously.

A number of studies have demonstrated the functional effects of immobilised proteins in terms of the ability to regulate biological activities[133,136-139,141]. One study showed that murine endothelial cells would migrate significant distances into hydrogel scaffolds in response to vascular endothelial growth factor and that step gradients produced greater migration than uniform concentrations[135].

Anseth and colleagues have used a similar approach to pattern PEG-based hydrogels[143-151]. The mechanical properties of these gels can be controlled using MPL, with dynamic control possible via photocleavable crosslinks[143,145,147,150]. Modification of gel stiffness during stem cell culture has been shown to dramatically

alter the differentiation pathway of the cells[145]. Concomitant protein immobilisation via chemical conjugation can also be achieved using this method. The simultaneous photoconjugation of multiple proteins has been demonstrated with a resolution of 1 μm achieved in the plane perpendicular to incident light (~3.5 μm in the direction parallel)[143]. The ability of MPL to dynamically manipulate different gel properties simultaneously suggests that it has enhanced capability for the production of complex constructs relative to other techniques.

The MPL techniques discussed above, and others similar[152-154], can pattern protein signals and mechanical properties in cytocompatible hydrogels with resolutions which are better than most three-dimensional fabrication techniques. Coupled with hydrogel fabrication via MPL, this could potentially allow for the production of scaffolds containing an initial set of patterns which could then be dynamically altered during an *in vitro* culture period. The secondary stage of this approach does have a significant limitation in that the patterning can only extend as far into the scaffold as its optical properties will allow, which is typically no more than a few millimetres.

1.2.3 Selective Laser Sintering

In selective laser sintering (SLS) laser illumination is used to bind selected regions of sequentially deposited layers of powder in order to build three-dimensional structures in a layer-by-layer fashion (Figure 1.3). Since the technique was patented by Carl Deckard[155] a significant body of work has demonstrated that SLS can be used to produce tissue engineering scaffolds with precise control of morphology[156]. However, the range of patterning which can be performed within SLS derived constructs is inherently limited by the use of powders as starting materials into which live cells cannot be incorporated. Additionally, the difficulties that would be associated with removing unsintered powder from scaffolds during fabrication means that it is difficult to envisage individual layers containing multiple materials or biological signals.

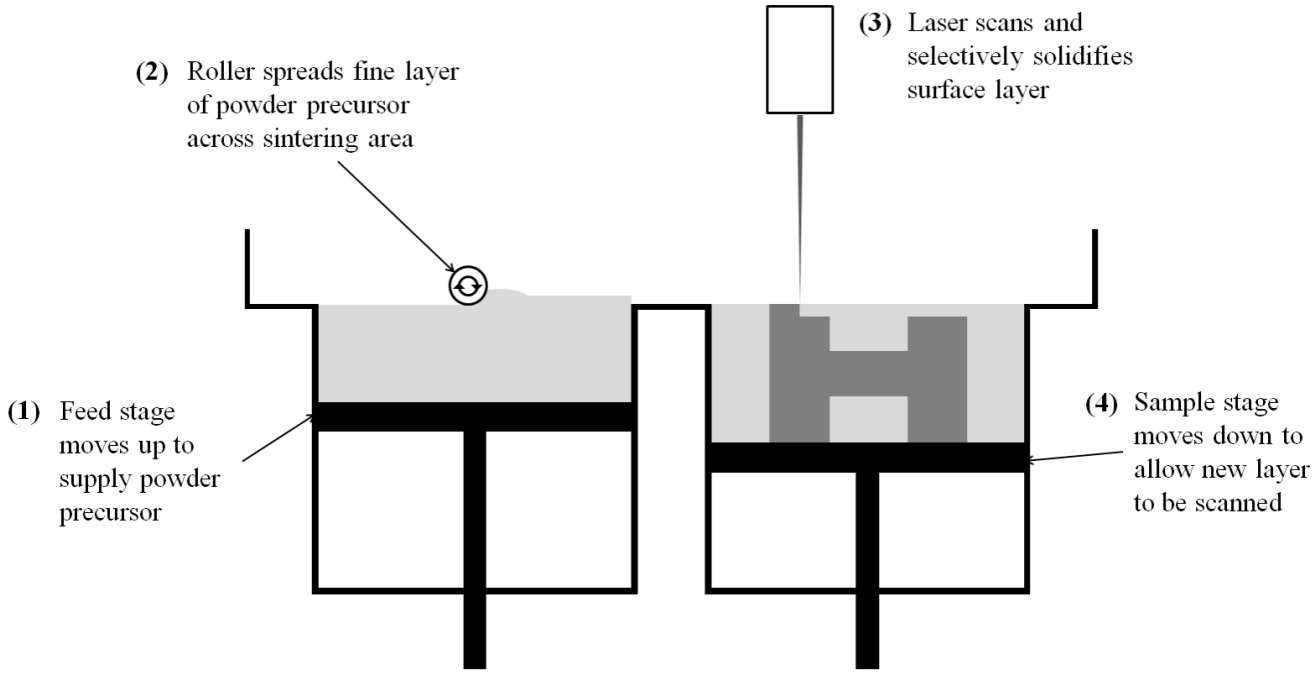

Figure 1.3 – Schematic depicting the principles of operation of a selective laser sintering device. A feed stage is raised so that a thin layer of powder precursor material stands proud (1). This layer is then spread across the sample stage by a roller (2) and the powder particles selectively bound to one another by laser irradiation-mediated melting (3). The sample stage then moves down to allow a new layer of powder to be spread across the first layer (4). By repetition of these steps, a three-dimensional structure is built.

Published work utilising SLS for tissue engineering scaffold fabrication has almost exclusively focused on synthetic polymers as scaffold materials. A wide range have been used including PCL[157-161], poly(vinyl alcohol)[162], poly(ethylene)[163], poly(L-lactic acid) (PLLA)[164], PLGA[165] and poly(hydroxybutyrate-co-hydroxyvalerate)[166,167]. To demonstrate the potential for SLS scaffold fabrication in bone applications, a number of studies have demonstrated the inclusion of ceramic micro- or nanoparticles in polymer/ceramic composite scaffolds. Ceramic materials which have been incorporated in this way include: hydroxyapatite (HA)[162-165,168,169], β-TCP[165], calcium phosphate[166,167] and apatite-wollastonite glass[170], though in the final case high temperature post-fabrication sintering was used to remove the polymer phase. Pure ceramic scaffolds have also been directly fabricated from HA[171,172]. These ceramic containing materials have been used to produce scaffolds with mechanical strengths as high as 12.06 MPa[165] which show good compatibility with bone-relevant cell types[168,170].

SLS can be used to produce scaffolds which directly incorporate biological signalling molecules[159]. A recent study demonstrated the fabrication of scaffolds from nanoparticles of (poly-3-hydroxy butyrate co-valerate) which were loaded with bovine serum albumin[167]. If the incorporation of such agents into precise positions within the bulk structure could be achieved this would enable more complex spatio-temporal patterning via SLS, but this capacity has not yet been demonstrated.

Currently there are no published reports of the use of SLS for patterning of construct constituents within the gross shape. The scaffolds that have been produced have features down to 350 μm in size within individual layers[161] but in this sense finer resolution can be achieved with other patterning techniques. The other major limiting factor to the applicability of SLS in tissue engineering and modelling is the lack of ability to incorporate cells within the bulk structure as it is formed. This would seem to be a prerequisite if effective reproduction of tissue architecture is to be achieved.

1.2.4 3D Printing

3D printing (3DP) is conceptually similar to SLS in that layers of a powdered starting material are sequentially and selectively solidified to form three-dimensional structures. The practical difference is in the use of liquid chemical binders rather than laser light to solidify the material (Figure 1.4)[173]. 3DP was originally patented by Emanuel Sachs and colleagues[174,175] but has since been applied to the production of tissue engineering scaffolds[176]. Extensive post-processing steps are required to remove unsintered powder from 3DP-produced scaffolds and consequently, as with SLS, multi-material patterning is likely to be restricted to simple layered geometries.

A small number of studies have used synthetic polymers such as PLGA[177,178] and poly(lactic acid)[177,179] in 3DP scaffolds for *in vitro* cell culture and tissue production. However the majority of publications have focused on the production of ceramic scaffolds for applications in bone tissue engineering[176,180,181]. Many of the studies published thus far have utilised some form of calcium phosphate for scaffold fabrication. The most commonly used are HA[182-190] and β-TCP[187,188,191-194], though others include tetracalcium phosphate[191], brushite[195,196] and calcium aluminate[197]. These ceramic scaffolds can contain features as small as 200 μm[197] and have compressive strengths of over 30 MPa whilst still maintaining at least 30% porosity[184,198] or at least 5 MPa where porosities of over 60% are needed[184].

Since ceramic scaffolds typically require post-fabrication sintering at very high temperatures, cells and biological signalling molecules cannot usually be incorporated in the fabrication process[185,186,188,198]. There are some studies that have attempted to solve this problem. In a 2010 study by Vorndran and co-workers BMP-2 was printed in the aqueous binder used to produce brushite ceramic scaffolds with retention of bioactivity[196]. However the post-fabrication processing steps required to fully develop the scaffolds were not applied in this case. Another publication detailed a system

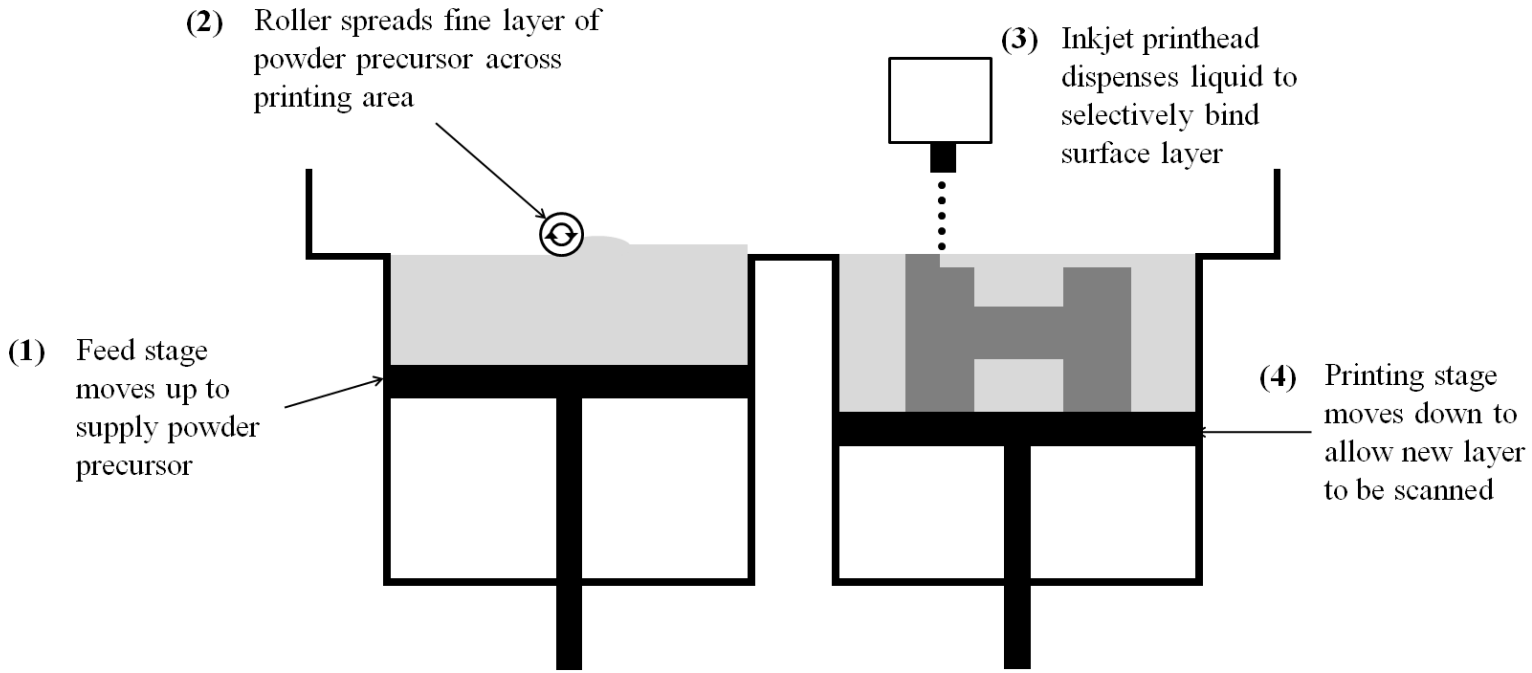

Figure 1.4 – Schematic depicting the principles of operation of a 3D printing device. A feed stage is raised so that a thin layer of powder precursor material stands proud (1). This layer is then spread across the sample stage by a roller (2) and the powder particles bound to one another by selective deposition of a liquid binder, typically by an inkjet printhead (3). The sample stage then moves down to allow a new layer of powder to be spread across the first layer (4). By repetition of these steps, a three-dimensional structure is built.

that forms patterned implants which can delay and control the presentation profile of multiple drugs[179]. Theoretically the 3DP process could be used to produce complex independent three-dimensional patterns of multiple construct constituents and properties. However for the reasons stated above and other practical limitations, the predominant use for 3DP in tissue engineering is for accurate defect shape replication and the production of defect-matched scaffolds. As with SLS, the control of macroscopic features may increase the rate of tissue in-growth *in vivo*[183,184,186,187,191,193,198] but the technique is currently unable to incorporate cells and biological signals.

1.2.5 Fused Filament Fabrication

Fused filament fabrication (FFF) (also called fused deposition modelling) involves the extrusion of synthetic polymer melts as fibres or filaments. These filaments are deposited layer-by-layer in two dimensional patterns to build three-dimensional structures (Figure 1.5). As with many other RP techniques FFF was developed as a commercial process for the fabrication of plastic parts[199]. The requirement for heating to melt the synthetic polymers renders the process incompatible with cells and in many cases biological signalling molecules. As with SLS and 3DP the technique does allow the generation of complex macro-architectural features within the bulk scaffold.

The use of FFF in tissue engineering was pioneered by Dietmar Hutmacher and colleagues[200-205], who demonstrated the potential for PCL-based scaffolds produced by FFF to be used for bone tissue engineering. The majority of scaffolds made by FFF for tissue engineering have continued to be made from PCL[206-211] with calcium phosphate incorporation in some cases to act as a cue for increased proliferation of osteogenic cells[200,206,211].

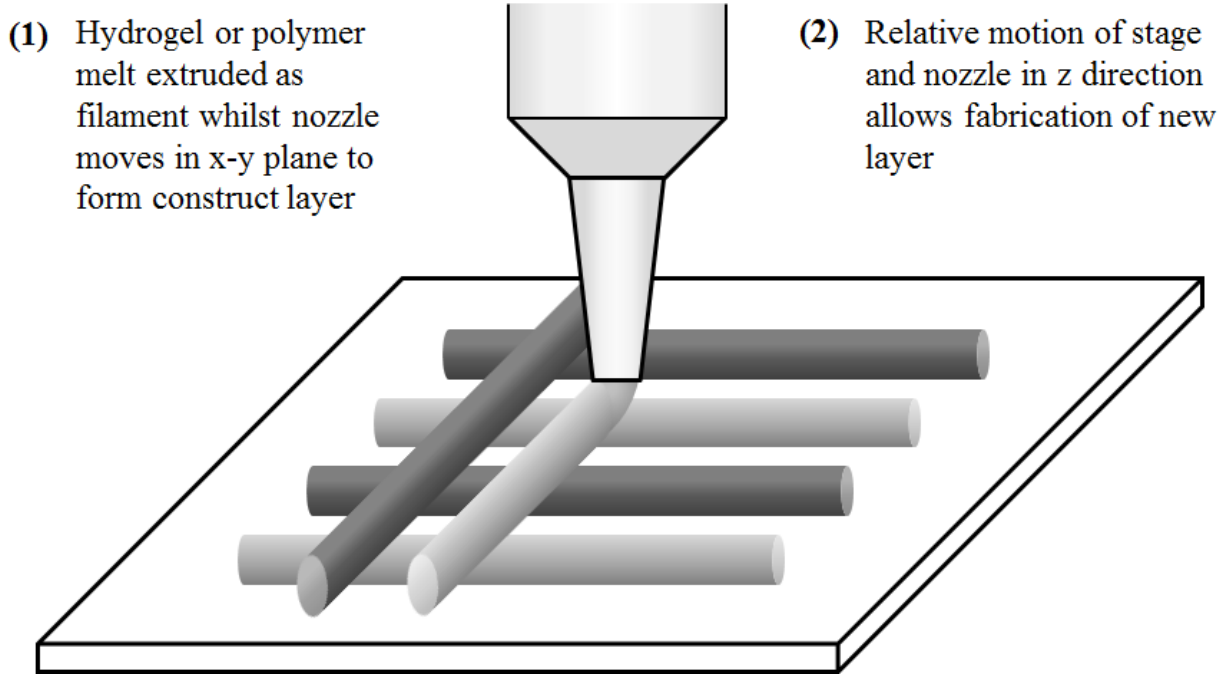

Figure 1.5 – Schematic depicting the principles of operation of a fused filament fabrication or bioplotting device. These techniques involve the extrusion of polymer melts and hydrogels respectively. In both cases, the material is extruded as a series of continuous filaments to form a single structure layer (1), and then relative motion of the deposition stage and the extrusion nozzle allows a second layer to be produced (2). By repetition of these steps, a three-dimensional structure is built.

Other synthetic polymers used include PLLA[207], PEG derivatives[212], poly(butylene tetrephthalate)[213], poly(hydroxymethylglycolide-co-ε-caprolactone)[209], polyurethane[214] and a PEG-PCL-poly(D,L-lactic acid) block copolymer[215]. Minimum scaffold feature sizes as small as 260 μm have been achieved[204], and compressive strengths as high as 3.1 MPa whilst maintaining 61% porosity[201].

FFF techniques have recently been combined with electrospinning to produce multilayer, multifunctional scaffolds[216-218]. One study aimed to produce a hybrid scaffold for osteochondral defect repair by electrospinning collagen onto an FFF scaffold which was subsequently seeded with bone marrow stromal cells[217]. While this does add a level of complexity to the bulk structure, patterning is limited to morphological features and cells cannot be placed at precise positions nor biological signalling agents incorporated.

Although FFF has the potential to produce tissue engineering scaffolds which contain complex patterns of material properties, this use of the technique has not been explored in the literature. Instead the focus has been on control of overall scaffold morphology and macropore structure to match defects and for optimisation of mechanical properties with retention of porosity respectively. Such applications have been demonstrated both *in vitro*[200,201,206,212,219] and *in vivo*[202,210,212].

1.2.6 Bioplotting

Conceptually bioplotting is similar to FFF in that it involves the extrusion of scaffold materials as fibres or filaments to build three-dimensional structures in a layer-by-layer fashion (Figure 1.5)[220,221]. In contrast to FFF bioplotting is performed at temperatures which are suitable for the incorporation of cells and biological signalling molecules. This has limited the choice of materials which have been utilised for construct fabrication to hydrogels and hydrogel precursors of both natural and synthetic origins[222-224]. Due to this restriction in choice of material, truly functional

patterning is more likely to come via the incorporation of multiple cell types or multiple signalling molecules rather than the use of different materials.

Many of the natural polymer hydrogels have the advantage of being inherently biocompatible and biofunctional. However their relatively slow gelation kinetics can be challenging to accommodate in bioplotting approaches, since the deposited material must have sufficient solidity to prevent significant flow after deposition. Nonetheless, the use of these materials in bioplotting based scaffold fabrication is widespread, with alginate being the most common[225-232]. Other materials utilised include: collagen[233-236], gelatin[237-240], fibrinogen[238], chitosan[239,240], Matrigel™ [226] and methylcellulose[226].

To overcome the problematic gelation kinetics of some of these biological hydrogels, recent studies from two groups of researchers have outlined modifications designed to induce rapid solidification after extrusion[241-243]. One approach utilised deposition at low temperatures for bioplotting chitosan[241], whilst the other sought to produce large collagen constructs by alternating deposition of a collagen solution with spray coating of nebulised sodium bicarbonate[242,243]. The minimum extruded filament diameter achieved across the studies discussed so far, which defines the potential patterning resolution, is around 100 μm[244,245]. This is broadly comparable with those achieved via other 3D fabrication techniques[244,245].

Incorporation of cells in bioplotting processes has been widely demonstrated with the majority of studies assessing cell viability *in vitro*. A wide variety of mammalian cell types have been used including liver[225,235,237-240], cartilage[230], heart[229,232], bone[235] and vascular cells[236]. Where quantitative evaluation was performed the measured viabilities immediately after production were all greater than 80%. Quantification of viability in post-fabrication culture is less commonly performed. One study did show that hepatocytes which were 98% viable immediately post-plot maintained 93% viability after one month's culture[237]. In a smaller number of cases the post-plot functionality of cells has also been demonstrated to be retained, as illustrated by

matrix synthesis[230], protein secretion[237] and expression of cell lineage markers[232]. The diversity of cell types used in these studies highlights the wide range of applications for which bioplotting may be applicable.

The use of synthetic polymers for bioplotting applications in tissue engineering and modelling is far less widespread than the use of natural polymers. A small number of recent studies have used Pluronic F-127[236], peptide-modified PEG[246], partially-polymerised acrylamide[247,248], poly(N-(2-hydroxypropyl)methacrylamide lactate-PEG-PHPMAm-lactate)[249] or methacrylated derivatives of gelatin and hyaluronic acid crosslinked with multi-arm PEG derivatives[250-252]. The majority of these studies have demonstrated the inclusion of viable cells in the fabrication process[236,246,249-251]. Qualitative assessment has shown that in some cases these cells can maintain high levels of viability for several weeks[250,251].

The major advantage of using synthetic polymers is that they can be tailored for optimal flow behaviour and gelation kinetics. They can also be rendered stimulus responsive to allow post-print induction of gelation, potentially enabling greater pattering resolution. However these filaments are often not inherently biocompatible and may require chemical modification, by peptide conjugation for instance[246]. The filament diameters achieved are broadly the same as those of natural polymers except in the case of partially polymerised acrylamide which could be deposited as a 5 μm filament[247].

In the studies discussed above the overall morphology of the scaffold could be accurately controlled, but there are only a few published studies in which bioplotted constructs have been patterned within the bulk shape. Materials[230,253], cell populations[226,242,253] and/or proteins[253] have been heterogeneously incorporated into constructs in distinct locations. However in most cases the features produced were several millimetres or more in size. One study was able to demonstrate patterning on a finer scale than this, incorporating two different fluorescent dyes into distinct regions which were around 500 μm in size[249]. This resolution is somewhat lower

than those associated with other patterning techniques such as STL. Despite this limitation, the wide variety of cell types that can be used with bioplotting gives the technique considerable advantage over many other patterning methods.

As with other patterning techniques discussed a key limitation is the current lack of assessment of pattern functionality. Two recent publications have detailed the results of the *in vivo* assessment of very simply patterned two-phase scaffolds. In the first study two-phase constructs were produced containing mesenchymal stem cells in an alginate hydrogel and endothelial progenitor cells within Matrigel™ [245]. The second study generated constructs with mesenchymal stem cells and articular chondrocytes both contained in alginate[244]. Histological staining showed distinct tissue formation and cell behaviour in the discrete phases of the scaffolds and these studies can be taken as the first successful demonstration of the capacity for functional construct patterning via bioplotting.

The inherent compatibility of the bioplotting process with the incorporation of cells and biological signalling molecules potentially allows very complex construct patterning to be performed. Cells, materials and biological signals can be independently patterned in three dimensions at the same time as controlling overall scaffold shape and morphology. However the realisation of this potential and the conversion of these patterns into heterogeneous functionality has not yet been widely demonstrated.

1.2.7 Bioprinting

Bioprinting is a fundamentally different approach to the production of tissue engineering constructs which involves three-dimensional fabrication using scaffold-free cell aggregates as a printing ink (Figure 1.6)[254,255]. Higher level aggregation and self-assembly processes then drive the conversion of bioprinted constructs into continuous tissues[254-257]. To produce uniformly sized aggregates for printing cells are

cultured in microcapillary tubes to allow them to form cell-cell junctions and deposit matrix. Once they have acquired sufficient mechanical strength they are then removed from the tubes and sub-divided[257].

In the bioprinting approach to construct production the smallest structures which can be produced consist of a single aggregate, and the patterning resolution is thus defined by the aggregate size[258]. Early studies using this technique deposited 500 μm cell aggregates into simple geometries such as rings and short tubes[259,260]. Later studies showed significantly increased pattern complexity, with scaffolds produced from multiple cell types and in more complex geometries designed, for instance, to replicate branching sections of vascular systems[261]. More recently still, published results have shown an improvement in pattern resolutions by the use of 300 μm aggregates as the printing ink[258]. Ultimately this work has culminated in the launch of the NovoGen MMX Bioprinter™ which is the first commercial rapid prototyping device to be specifically designed for biological fabrication[262-264].

In generating more complex construct morphologies, a combined bioprinting/bioplotting technique can be used to deposit both cell aggregates and size-matched hydrogels. The hydrogels used in studies referred to above act as temporary support structures during fabrication, but are designed to degrade away once aggregates are sufficiently adhered to one another[258,262,263].

Since bioprinting is an approach which does not utilise biomaterials for construct fabrication, the potential complexity of patterning which can be performed is much reduced in comparison with other technologies. However, in some respects the formation of a construct without materials simplifies its optimisation and removes some of the obstacles to its success *in vivo*. There is no need to tailor the degradation rate of the construct to maximise host tissue ingrowth, since this will be managed by the natural processes of extracellular matrix remodelling, and any potential side effects from the presence of synthetic materials are removed[254,255,261,265].

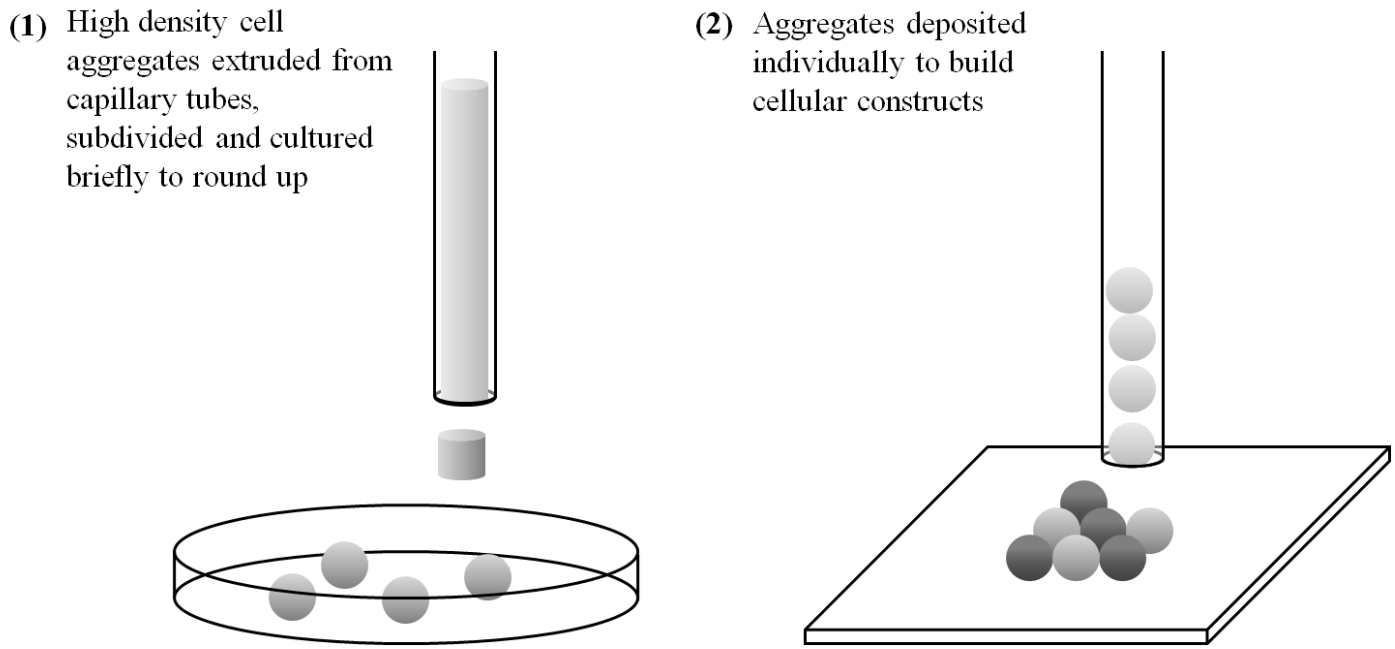

Figure 1.6 – Schematic depicting the principles of a bioprinting process. First cells are cultured at high density in capillary tubes to allow for the production of extracellular matrix and the formation of coherent structures. These cultures are then expelled, subdivided and briefly incubated to allow them to round up and form spheroid aggregates (1). These aggregates are then individually positioned layer-by-layer to form neo-tissue constructs (2).

1.3 Current and Future Directions

The more accurate replication of tissue architectures is undoubtedly an important consideration for future tissue engineering applications. MM and OT systems have great potential in the formation of *in vitro* tissue models for the reproduction and study of niche micro-architectural characteristics. Practical considerations limit their current application to macro-scale construct production but they could potentially be combined with macro-scale techniques in future applications.

The remaining patterning technologies considered have the potential to replicate macro-scale tissue features. Techniques such as STL, MPL and bioplotting are able to incorporate cellular and biological signal components to produce complex tissue engineering constructs. This gives them significant advantages over other techniques such as SLS, FFF and 3DP that are often limited to morphological patterning of scaffold materials. The maximum patterning resolution in bioplotting-based approaches is typically coarser than that achievable with STL and MPL, but the heterogeneous incorporation of cells and biological signal molecules is more easily achieved with this than with any of the other techniques discussed.

A key challenge for the field is ensuring that patterned constructs are stable in longer-term *in vitro* culture, in order that they can be used to model tissues and the progression of disease and repair. It will also become important in the future to assess pattern maintenance after *in vivo* implantation, in order that the constructs can be deemed suitable clinical therapies. Additionally more exhaustive and longer-term studies will be needed to assess post-production cell viability and demonstrate that patterns generated in tissue engineering constructs ultimately lead to the formation of heterogeneous tissues.

1.4 Thesis Aims

The overall aim of the work contained within this thesis is to explore and extend the potential of three-dimensional patterning techniques for the fabrication and modification of biological constructs for tissue engineering and modelling. More specifics aims are as follows:

- To develop synthetic polymer microsphere formulations for temporally-controlled release of growth factors.
- To produce extracellular matrix-derived biomaterials which can be used in bulk construct fabrication or as alternative microsphere formulations for controlled growth factor presentation.
- To evaluate the use of microinjection and micromanipulation techniques for the precise patterning of growth factor-releasing microspheres in *in vitro* culture environments to create functional signal gradients.
- To evaluate the use of a bioplotting platform for the production of tissue engineering constructs composed of novel scaffold materials.
- To evaluate the same platform for the production of constructs containing three-dimensional patterns of cell populations, materials and/or growth factor-releasing microspheres.

2. Materials & Methods

2.1 General Consumables & Reagents

Agar – catalogue number BP1423-500, Fisher Scientific (Loughborough, UK)

Agarose – catalogue number A2576, Sigma-Aldrich (Poole, UK)

Alginic Acid Sodium Salt (Sodium Alginate) – catalogue number 177775000, Acros Organics (Geel, Belgium) or Protanal® LF10/60, FMC BioPolymer (Philadelphia, PA, USA)

Alpha Minimum Essential Medium (αMEM) – catalogue number A10490-01, Life Technologies (Carlsbad, CA, USA)

Antibiotic/Antimycotic (AB/AM) – catalogue number 30-004-CI, Mediatech (Manassas, VA, USA)

Bone Morphogenetic Protein-2 (BMP-2) – recombinant human BMP-2 was purchased from Prof. Walter Sebald (University of Wurzburg, Germany)

Calcium Sulphate – catalogue number 237132, Sigma-Aldrich (Poole, UK) or catalogue number 40144, Alfa Aesar (Karlsruhe, Germany)

Carboxymethyl Cellulose (CMC) – catalogue number 12M8P (medium viscosity) or 12M31P (high viscosity), Ashland Speciality Ingredients (Poole, UK)

Collagen – rat tail collagen type I, catalogue number 354249, BD Biosciences (Oxford, UK)

Collagenase Type 2 – catalogue number LS004177, Worthington Biochemical Corporation (Lakewood, NJ, USA)

D,L-lactide – catalogue number L09026, Alfa Aesar (Karlsruhe, Germany)

Dulbecco's Modified Eagle Medium (DMEM) – catalogue number 10-017-CV, Mediatech (Manassas, VA, USA) or catalogue number 42430-025, Life Technologies (Paisley, UK)

Eagle's Minimum Essential Medium (EMEM) – catalogue number M2279, Sigma-Aldrich (Poole, UK)

Foetal Bovine Serum (FBS) – catalogue number 900-108, Gemini Bio-Products (West Sacramento, CA, USA) or catalogue number F9665, Sigma-Aldrich (Poole, UK)

Ethylenediaminetetraacetic acid (EDTA) – catalogue number ED2SS, Sigma-Aldrich (Poole, UK)

Gelatin – porcine type A, catalogue number G1890, Sigma-Aldrich (Poole, UK)

Glycolide – Purasorb G, Purac (Gorinchem, The Netherlands)

Human Serum Albumin (HSA) – catalogue number A9511, Sigma-Aldrich (Poole, UK)

Hydroxyproline – catalogue number H1637, Sigma-Aldrich (Poole, UK)

L-Glutamine – catalogue number G7513, Sigma-Aldrich (Poole, UK)

Live/Dead Viability/Cytotoxicity Kit – catalogue number L-3224, Life Technologies (Paisley, UK)

MEM Non-Essential Amino Acid Solution – catalogue number M7145, Sigma-Aldrich (Poole, UK)

Micro BCA Protein Assay Kit – catalogue number 23235, Fisher Scientific (Loughborough, UK)

Penicillin/Streptomycin (Pen/Strep) – catalogue number 15070-063, Life Technologies (Paisley, UK)

Pepsin – catalogue number P7012, Sigma-Aldrich (Poole, UK)

Phenol/Chloroform/Isoamyl Alcohol – catalogue number 77617, Sigma-Aldrich (Poole, UK)

Pluronic® F-127 – catalogue number P2443, Sigma-Aldrich (Poole, UK)

Poly(ethylene glycol) (PEG) – Polyglykol 400, Clariant (Leeds, UK) or catalogue number 81210, Sigma-Aldrich (Poole, UK)

Poly(lactic-co-glycolic acid) (PLGA) – various products sourced from Evonik Biomaterials (Birmingham, AL, USA)

PrestoBlue® Cell Viability Reagent – catalogue number A-13262, Life Technologies (Paisley, UK)

Quant-iT™ PicoGreen® dsDNA Assay Kit – catalogue number P11496, Life Technologies (Paisley, UK)

Trypan Blue – catalogue number SV3008401, Fisher Scientific (Loughborough, UK)

Trypsin – catalogue number T4549, Sigma-Aldrich (Poole, UK)

Trypsin/EDTA – catalogue number 25-053-CI, Mediatech (Manassas, VA, USA) or mixture of Sigma-Aldrich trypsin and EDTA products to final concentrations of 0.25% (w/v) trypsin and 0.02% (w/v) EDTA

Unless otherwise specified all other reagents are of analytical reagent grade or higher and purchased from Sigma-Aldrich (Poole, UK).

2.2 General Cell Culture

2.2.1 Murine Primary Calvarial (mPC) Cells

mPC cells were a kind gift of Laura Sidney and Adam Taylor (University of Nottingham). Cells were isolated from the calvariae of 1 to 3 day-old neonatal CD1

mice by sequential enzymatic digestion. Briefly – serial digestions were performed using collagenase type IA (1.4 mg mL^{-1}) and trypsin II S (0.5 mg mL^{-1}) and cells released during the first two digestions were discarded. Cells released during the subsequent three digestions were combined and seeded on tissue culture treated polystyrene at 6,600 cells cm^{-2}.

mPC cells were cultured in αMEM supplemented with 10% (v/v) FBS (Sigma-Aldrich), 1% (v/v) L-glutamine and 1%(v/v) pen/strep. Cultures were maintained at 37°C and 5% (v/v) CO_2 as monolayers on tissue culture treated polystyrene. At 80% confluency, cells were passaged by trypsinisation and reseeded at between 1/3rd and 1/6th of this density. Passage procedure for a T75 flask was as follows (with all volumes scaled accordingly for smaller culture vessels) – culture medium was aspirated from the flask and the cell monolayer washed with 10 mL phosphate-buffered saline (PBS). After aspiration of the PBS, 3 mL of trypsin/EDTA (Sigma-Aldrich) was added to the flask, which was incubated at 37°C until all cells had detached, resulting in a single cell suspension. The trypsin was deactivated by the addition of 7 mL of culture medium and the resulting suspension was centrifuged at 200 g for 5 minutes. The supernatant was aspirated and the cell pellet resuspended in fresh culture medium for seeding into the desired culture vessel(s).

2.2.2 Human Osteosarcoma Cell Line

HOS cells (catalogue number ATCC-CRL-1543, LGC Standards, Teddington, UK) were cultured in DMEM (Life Technologies) supplemented with 10% (v/v) FBS (Sigma-Aldrich), 1% (v/v) L-glutamine, 1%(v/v) pen/strep and 1% (v/v) non-essential amino acids. Cultures were maintained at 37°C and 5% (v/v) CO_2 as monolayers on tissue culture treated polystyrene. At 80% confluency, cells were passaged by trypsinisation and reseeded at between 1/5th and 1/8th of this density. Passage procedure for a T175 flask was as follows (with all volumes scaled accordingly for smaller culture vessels) – culture medium was aspirated from the flask and the cell

monolayer washed with 20 mL PBS. After aspiration of the PBS, 6 mL of trypsin/EDTA (Sigma-Aldrich) was added to the flask, which was incubated at 37°C until all cells had detached, resulting in a single cell suspension. The trypsin was deactivated by the addition of 9 mL of culture medium and the resulting suspension was centrifuged at 220 g for 5 minutes. The supernatant was aspirated and the cell pellet resuspended in fresh culture medium for seeding into the desired culture vessel(s).

2.2.3 Immortalised Human Mesenchymal Stem Cells

Immortalised human mesenchymal stem cells (ihMSCs) were kindly donated by Dr. Hassan Rashidi and Dr. James Dixon (University of Nottingham). Primary hMSCs (bone marrow-derived, catalogue number SC-7500, TCS Cellworks, Buckingham, UK) were immortalised using a previously published protocol[266]. This involved retrovirus-mediated transduction of the cells with human telomerase reverse transcriptase and the human papillomavirus E6 and E7 genes. The effect is to activate telomerase and inactivate the Rb/p16 pathway, circumventing the senescence normally seen in hMSCs after only a relatively short time in culture. Histological staining showed the ihMSCs had retained their ability to differentiate down the osteogenic, chondrogenic and adipogenic lineages in response to the appropriate chemical cues (data not shown).

ihMSCs were cultured in DMEM (Life Technologies) supplemented with 10% (v/v) FBS (Sigma-Aldrich), 1% (v/v) L-glutamine, 1%(v/v) pen/strep and 1% (v/v) non-essential amino acids. Cultures were maintained at 37°C and 5% (v/v) CO_2 as monolayers on tissue culture treated polystyrene. At 80% confluency, cells were passaged by trypsinisation and reseeded at between $1/5^{th}$ and $1/8^{th}$ of this density. Passage procedure for a T175 flask was as follows (with all volumes scaled accordingly for smaller culture vessels) – culture medium was aspirated from the flask and the cell monolayer washed with 20 mL PBS. After aspiration of the PBS, 6

mL of trypsin/EDTA (Sigma-Aldrich) was added to the flask, which was incubated at 37°C until all cells had detached, resulting in a single cell suspension. The trypsin was deactivated by the addition of 9 mL of culture medium and the resulting suspension was centrifuged at 220 g for 5 minutes. The supernatant was aspirated and the cell pellet resuspended in fresh culture medium for seeding into the desired culture vessel(s).

2.2.4 MC3T3-E1 Murine Pre-Osteoblast Cell Line

MC3T3-E1 cells (a kind gift from Dr. Claudia Fischbach-Teschl, Cornell University) were cultured in αMEM supplemented with 10% (v/v) FBS (Gemini Bio-Products), 1% (v/v) L-glutamine and 1%(v/v) AB/AM. Cultures were maintained at 37°C and 5% (v/v) CO_2 as monolayers on tissue culture treated polystyrene. At 80% confluency, cells were passaged by trypsinisation and reseeded at between 1/3rd and 1/6th of this density. Passage procedure for a T150 flask was as follows (with all volumes scaled accordingly for smaller culture vessels) – culture medium was aspirated from the flask and the cell monolayer washed with 20 mL PBS. After aspiration of the PBS, 5 mL of trypsin/EDTA (Mediatech) was added to the flask, which was incubated at 37°C until all cells had detached, resulting in a single cell suspension. The trypsin was deactivated by the addition of 10 mL of culture medium and the resulting suspension was centrifuged at 200 g for 5 minutes. The supernatant was aspirated and the cell pellet resuspended in fresh culture medium for seeding into the desired culture vessel(s).

2.2.5 Bovine Primary Articular Chondrocytes

The articular cartilage surfaces were removed from the femero-patellar groove of one to three day-old animals using a scalpel and placed into PBS (60 mL per joint) supplemented with 2% (v/v) AB/AM. After one hour the PBS was replaced and the

cartilage left for a further hour, after which a scalpel was used to dissect the tissue down to pieces of no more than 2 mm in any dimension. The pieces were then soaked in fresh supplemented PBS for one more hour before being transferred to DMEM (Mediatech) supplemented with 2% (v/v) AB/AM and 0.2% (v/v) collagenase type 2 (150 mL per joint). The suspension was incubated for 24 hours, stirred, at 37°C, 5% CO_2. The resulting solution was passed through a 100 µm cell strainer and centrifuged at 500 g for 3 minutes, followed by resuspension in 50 mL supplemented PBS. Centrifugation and resuspension steps were repeated twice, replacing the PBS in the second iteration with DMEM supplemented with 2% (v/v) AB/AM and 10% (v/v) FBS (Gemini Bio-Products). Cells were counted and then transferred to T150 culture flasks, at 10 million cells per flask for use within 24 – 48 hours, or as few as 1 million cells per flask for longer term culture. Medium was completely refreshed three times per week but cells were not passaged prior to use.

2.2.6 NIH 3T3 Murine Fibroblast Cell Line

3T3s (catalogue number ATCC-CRL-1658, LGC Standards, Teddington, UK) were cultured in DMEM (Life Technologies) supplemented with 10% (v/v) FBS (Sigma-Aldrich), 1% (v/v) L-glutamine and 1%(v/v) pen/strep. Cultures were maintained at 37°C and 5% (v/v) CO_2 as monolayers on tissue culture treated polystyrene. At 80 - 90% confluency, cells were passaged by trypsinisation and reseeded at between $1/8^{th}$ and $1/10^{th}$ of this density. Passage procedure for a T175 flask was as follows (with all volumes scaled accordingly for smaller culture vessels) – culture medium was aspirated from the flask and the cell monolayer washed with 20 mL PBS. After aspiration of the PBS, 6 mL of trypsin/EDTA (Sigma-Aldrich) was added to the flask, which was incubated at 37°C until all cells had detached, resulting in a single cell suspension. The trypsin was deactivated by the addition of 9 mL of culture medium and the resulting suspension was centrifuged at 200 g for 5 minutes. The

supernatant was aspirated and the cell pellet resuspended in fresh culture medium for seeding into the desired culture vessel(s).

2.2.7 C2C12 Murine Myoblast Cell Line

C2C12s (catalogue number ATCC-CRL-1772, LGC Standards, Teddington, UK) were cultured in DMEM (Life Technologies) supplemented with 10% (v/v) FBS (Sigma-Aldrich), 1% (v/v) L-glutamine and 1%(v/v) pen/strep. Cultures were maintained at 37^{o}C and 5% (v/v) CO_2 as monolayers on tissue culture treated polystyrene. At 80% confluency, cells were passaged by trypsinisation and reseeded at 1/5th of this density. Passage procedure for a T175 flask was as follows (with all volumes scaled accordingly for smaller culture vessels) – culture medium was aspirated from the flask and the cell monolayer washed with 20 mL PBS. After aspiration of the PBS, 6 mL of trypsin/EDTA (Sigma-Aldrich) was added to the flask, which was incubated at 37^{o}C until all cells had detached, resulting in a single cell suspension. The trypsin was deactivated by the addition of 9 mL of culture medium and the resulting suspension was centrifuged at 200 g for 5 minutes. The supernatant was aspirated and the cell pellet resuspended in fresh culture medium for seeding into the desired culture vessel(s).

2.2.8 Cryopreservation of Cells

In order to retain cells for later use and prevent the need for unnecessarily extended culture and the associated risk of phenotypic changes they were stored in the vapour phase of liquid nitrogen. The cryopreservation medium used for this was foetal bovine serum (as appropriate to each cell type) supplemented with 10% (v/v) dimethyl sulphoxide (DMSO) as a cryoprotectant. To prepare cells for cryopreservation they were trypsinised as for normal passage, centrifuged as appropriate to the cell type and resuspended in cryopreservation medium. A single

T75 flask was suspended in 1 to 2 mL of medium and a single T150 or T175 in 2 to 3 mL. These cell suspensions in cryopreservation medium were transferred into a Nalgene 'Mr. Frosty' (Fisher Scientific, Loughborough, UK) filled with isopropanol and placed in a -80^{o}C freezer for 48 hours. This step was designed to produce a cooling rate of approximately 1^{o}C min^{-1}. After this they were transferred to the vapour phase of liquid nitrogen for long-term storage.

To retrieve cells from liquid nitrogen for further culture cryovials containing frozen cell suspension were first thawed by placing them into a water bath set to 37^{o}C. These suspensions of cells in cryopreservation were then diluted by a factor of ten using pre-warmed complete culture medium and centrifuged as appropriate to the cell type. Finally the cell pellets were resuspended in pre-warmed complete culture medium and seeded into appropriate culture vessels.

2.2.9 Trypan Blue Counting & Viability Assessment

Trypan blue is a coloured dye which cannot cross the intact membrane of a viable cell. It can, however, cross the compromised membrane of a dead cell, and can therefore be used to quantitatively assess cell viability. For pre-bioplotting cell counting and viability assessment 100 µL of cell suspension was mixed with 100 µL of trypan blue. 10 µL of this mixture was then added to the counting chamber of an improved Neubauer haemocytometer and five cell counts performed, each covering one of the nine major square divisions of the chamber. These counts were then averaged and converted to cell numbers per mL by multiplication by a factor of 2 x 10^{4}.

2.3 PLGA-PEG-PLGA Triblock Copolymer Synthesis & Characterisation

2.3.1 Polymer Synthesis

PLGA-PEG-PLGA triblock copolymer was a kind gift of Giles Kirby (University of Nottingham)[267]. The PEG content of this copolymer means that its addition to PLGA-based microspheres increases the hydrophilicity of the microspheres. The additional water ingress into the microspheres that this encourages leads to acceleration of the release of protein encapsulated within them. This effect is both because the additional water content encourages swelling of the polymer matrix and thus greater protein diffusion through it and also because it accelerates degradation of the polymer through ester hydrolysis.

To prepare the polymer 5.5575 g PEG (Sigma-Aldrich) was heated to 120^{o}C under vacuum to achieve melting of the polymer. Under a nitrogen atmosphere the temperature was further raised to 150^{o}C and 7.5 g D,L-lactide and 2.5 g glycolide added. After 30 minutes of the reaction, 0.075 g of stannous octoate was added and the reaction maintained for a further 8 hours. After completion of the reaction and cooling of the vessel back to room temperature, the product and remaining monomers were dissolved in cold water (4^{o}C). Heating to 80^{o}C precipitated the polymer whilst leaving unreacted monomers in solution. The supernatant was decanted and the process repeated a second time. Following this the solid product was snap frozen and lyophilised for 48 hours before being stored at -20^{o}C until further use.

2.3.2 Gel Permeation Chromotography

Gel permeation chromatography measurements of the synthesised triblock copolymer using a PL-GPC 120 (Polymer Labs) indicated a molecular weight of 4590 Da and a

polydispersity index of 1.60 (analysis performed by Natasha Birkin (University of Nottingham).

2.3.3 Nuclear Magnetic Resonance

Nuclear magnetic resonance analysis of the triblock copolymer was performed by Natasha Birkin (University of Nottingham) using a DPX-300 instrument (Bruker, Coventry, UK). The solvent was deuterated chloroform and measurements at 300 MHz confirmed the purity and composition of the product.

2.4 PLGA-Based Microsphere Fabrication

For the purposes of this thesis, microparticles prepared via emulsion-based techniques will be referred to as microspheres. These techniques typically produce microparticles which are broadly spherical in nature, but it is not claimed that they are perfect spheres. To fabricate microspheres an oil phase comprising a solution of synthetic polymer in volatile organic solvent is emulsified in an aqueous phase. This aqueous phase contains an emulsifier which acts to stabilise the interfaces between the two phases and prevent oil droplets from coalescing. To minimise interfacial energy spherical oil droplets are formed, and subsequent evaporation of the organic solvent leads to the formation of solid polymer microspheres. Encapsulation of drugs and proteins into these microspheres can be by dispersion of a solid in the oil phase (solid-in-oil-in-water single emulsion), by co-dissolution in the oil phase (oil-in-water single emulsion) or by dissolution in an aqueous phase which is emulsified within the oil phase (water-in-oil-in-water double emulsion).

2.4.1 Single Emulsion Technique

PLGA (lactide-to-glycolide ratio 85:15 or 50:50, molecular weight 53 kDa or 59 kDa respectively) was dissolved in dichloromethane (DCM) (Fisher Scientific, Loughborough, UK) at 2% (w/v) with a total polymer mass of 1 g. This solution was then added to an aqueous solution of 0.3% (w/v) poly(vinyl alcohol) (PVA) (catalogue number 363170, Sigma-Aldrich, Poole, UK), with a volume of 500 mL in a 600 mL beaker. The mixture was then emulsified using a high-speed homogeniser at the desired speed (Silverson L5M, Silverson Machines Ltd., Chesham, UK at 9,000 rpm, or Ultra Turrax T25 Basic, IKA Werke GmbH, Staufen, Germany in the range 11,000 – 24,000 rpm). Homogenisation was for two minutes, and the resulting emulsion was stirred for 24 hours at 300 rpm, to allow for complete DCM evaporation and hardening of the microspheres. The resulting microsphere suspension was passed through a 0.2 µm cellulose acetate filter (Fisher Scientific, Loughborough, UK) under vacuum and washed with 1 L of deionised water (dH_2O). Small amounts of dH_2O ejected from a disposable Pasteur pipette were used to wash the microspheres off the filter and into suspension. The suspension was then transferred into a suitable container, plunge frozen in liquid nitrogen and freeze dried for at least 48 hours (Free Drier Modulyo, IMA Edwards, Alcester, UK or ModulyoD, Thermo Fisher Scientific, Waltham, MA, USA).

For the production of fluorescent microspheres via single emulsion, fluorescein (Acros Organics, Geel, Belgium) was co-dissolved with PLGA in DCM prior to homogenisation. A number of different concentrations were used, in the range 0.1 – 20% (w/w) relative to PLGA.

2.4.2 Double Emulsion Technique

PLGA was dissolved in DCM at the desired concentration. In some cases a portion of the PLGA was replaced with PLGA-PEG-PLGA triblock but the total polymer mass was

always maintained at 1 g. A small amount of water (2% (v/v) relative to the organic phase) was added to the polymer solution and this combination was homogenised for two minutes to form a primary emulsion using a Silverson L5M homogeniser (Silverson Machines Ltd., Chesham, UK, speed in the range 2,000 – 9,000 rpm). For polymer concentrations of 5% (w/v) and below the primary emulsification step was carried out in a 100 mL beaker, and for higher concentrations it was carried out in a 25 mL beaker. The primary emulsion was then added to an aqueous solution of 0.3% (w/v) PVA and this mixture homogenised to form a secondary emulsion. For polymer concentrations of 5% (w/v) and below the secondary emulsification was carried out in a 600 mL beaker using 500 mL of PVA and for higher concentrations the process utilised 200 mL of PVA and a 250 mL beaker. The secondary emulsion was stirred for 24 hours, filtered and freeze dried, as described above for microspheres produced by single emulsion.

Fluorophores and proteins could be incorporated into microspheres by dissolving them in the water which was added to the organic polymer solution to form the primary emulsion.

2.4.3 Refined Double Emulsion Technique

The refined double emulsion technique differed from the standard technique in the vessels used for the primary emulsification step. This protocol step was carried out in 30 mL poly(tetrafluoroethylene) (PTFE) beakers (catalogue number 216-0165, VWR International, Lutterworth, UK). The refined technique also utilised a shortened stirring time for microsphere hardening of only 4 hours.

2.5 Microsphere Size Distribution Analysis via Laser Diffraction

Laser diffraction-based size analysis works by laser illuminating a suspension of objects in order to generate a pattern of diffracted light which is detected under

conditions where the Fraunhofer diffraction equation applies. This allows the intensity of light at various angles from the straight-through beam to be related to the size of the objects causing the diffraction.

The size distributions of microspheres produced using the emulsion techniques described above were measured using a laser diffraction particle sizing instrument (Coulter LS230, Beckman Coulter (UK) Ltd., High Wycombe, UK). The micro volume sample module was loaded with 18 mL of dH_2O for background and calibration measurements. Following this, 1 mL was removed and a suspension of the microspheres to be sized added 100 µL at a time until the optimal obscuration for the machine's operation was reached. The module was then topped up to 18 mL once again, and readings taken over 120 s.

2.6 Scanning Electron Microscopy

In scanning electron microscopy (SEM) the sample to be imaged is bombarded by an electron beam, leading to the emission of secondary electrons by inelastic scattering from the sample surface. The relative intensity of emission of secondary electrons from different points on the sample surface then gives height information, and the topography of the surface can be deduced. In order to prevent charge build-up, which causes imaging artefacts, sample surfaces must be rendered conductive prior to imaging. This is achieved by sputter coating a very fine layer of metal (typically gold or platinum) onto samples. Furthermore, since the imaging process is conducted under vacuum, samples must be completely dry, necessitating the use of a dehydration protocol for many biological samples. Since air drying, which involves the boiling of liquids, can cause damage to samples, drying is usually achieved via gradual replacement of water with ethanol in chemically-fixed samples. To remove the ethanol, samples are subjected to critical point drying, which replaces the ethanol with supercritical carbon dioxide in which there is no distinction between gas and liquid and thus no chance of boiling.

To prepare for SEM samples were either gold coated (SC030, Balzers, Liechtenstein or EM SCD005, Leica Microsystems (UK) Ltd, Milton Keynes, UK) or platinum coated (Polaron SC7640, Quorum Technologies, East Grinford, UK). SEM was then performed using a JSM 6060LV (JEOL, Welwyn Garden City, UK) or an XL30 (Philips Research, Cambridge, UK) and the associated manufacturer's software. Images were taken at a minimum of three different magnifications and in three different quadrants of each sample where possible.

Prior to sputter coating, hydrogel samples were fixed for one hour in 3% (w/v) glutaraldehyde in PBS, washed twice in PBS and then dehydrated by soaking in increasing concentrations of ethanol. Two 15 minute soaks were performed at each of the following concentrations – 0, 30, 50, 70, 90 and 100% (v/v) and samples were then stored in 100% ethanol until they were dried in a Samdri® PVT-3 critical point dryer (tousimis, Rockville, MD, USA) and platinum coated.

2.7 Measurement of Protein Release Rate from Microspheres

In alkaline environments Cu^{2+} ions which are chelated with peptides or proteins can be reduced to Cu^{+} [268]. The subsequent chelation of these Cu^{+} ions with bicinchoninic acid (BCA) will then form a purple-coloured product which has an absorbance at 562 nm which is proportional to the protein concentration.

This reaction is utilised in the Micro BCA Protein Assay Kit, which was used to quantify the protein content of release medium in which protein-loaded microspheres had been incubated. As per manufacturer's instructions 100 µL of each sample or standard was mixed in a 96-well plate well in triplicate with 100 µL of complete working reagent. After 2 hours incubation at 37°C, the absorbance of the mixture in each well was measured at 562 nm.

2.8 Borosilicate Glass Needle Manufacture

A P-97 Flaming/Brown micropipette puller (Sutter Instrument Company, Novato, CA, USA) was used to produce closed-tip needles from borosilicate glass capillaries (1 mm outer diameter, 0.58 mm inner diameter, catalogue number 640766, Harvard Apparatus, Edenbridge, UK). The closed, drawn ends of these capillaries were then broken by hand and those with relatively smooth ends were used for semi-automated MM-based microsphere patterning.

2.9 Microinjection and Micromanipulation of PLGA Microspheres

2.9.1 Manual Microinjection/Micromanipulation System

A manual micromanipulator (catalogue number M3301R, World Precision Instruments, Hitchin, UK) was used to position the manual delivery of injection volumes of 0.1 µL or more of microsphere suspension (see Figure 2.1). These were delivered either into dH_2O for microsphere counting or into 0.75% (w/v) agar hydrogels for assessment of positional accuracy and patterning capability. Delivery was either via 701 RN syringes (catalogue number 7635-01, Hamilton Bonaduz AG, Bonaduz, Switzerland) fitted with needles of various gauges (point style 3, Hamilton Bonaduz AG, Bonaduz, Switzerland) or via plunger-in-needle syringes (catalogue numbers 00570 and 00802, SGE Europe, Milton Keynes, UK).

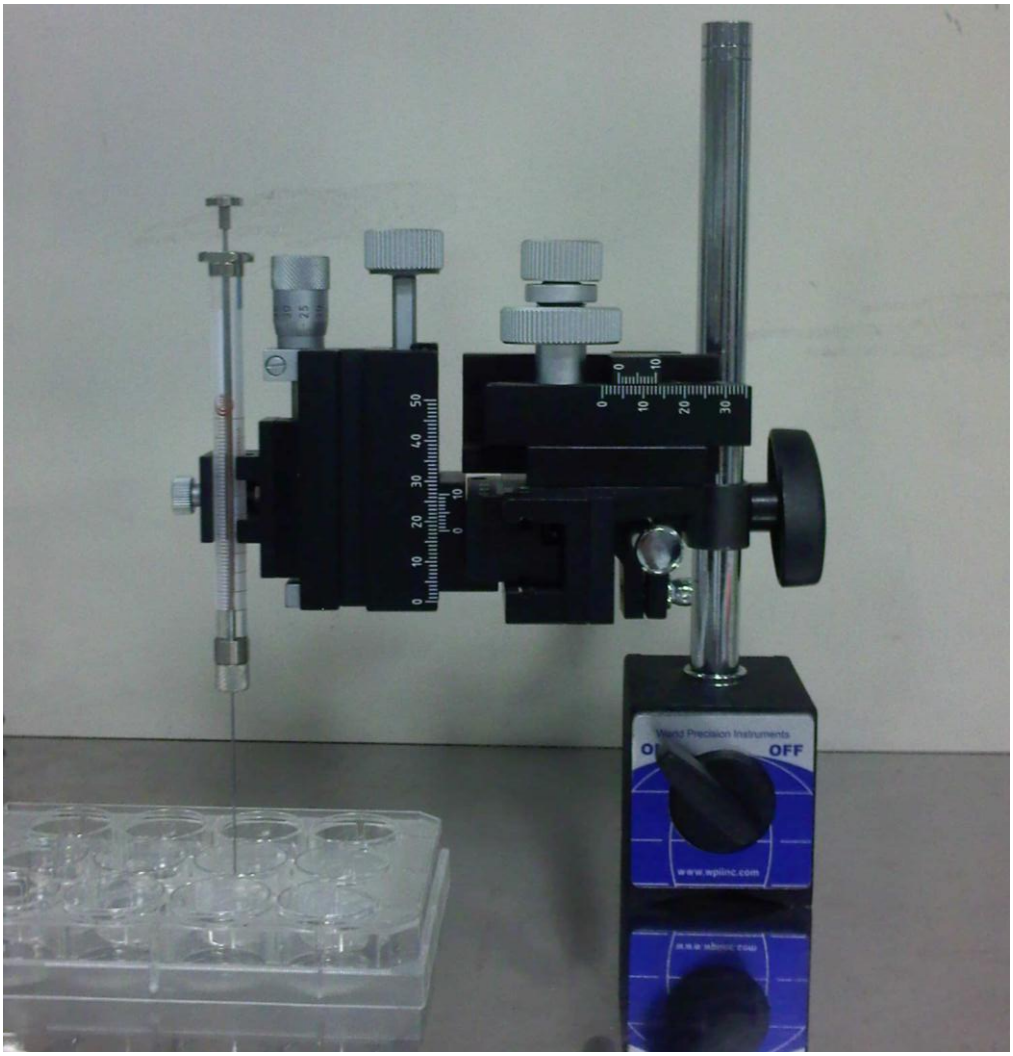

Figure 2.1 – Manual microinjection/micromanipulation system consisting of a microlitre syringe attached to a manual micromanipulator. Maximum positional accuracy of the micromanipulator is ±50 µm in the two horizontal dimensions and ±0.5 µm in the vertical direction.

2.9.2 Semi-Automated Microinjection/Micromanipulation System

A CellTram vario manual microinjector (catalogue number 5176 000.033, Eppendorf UK, Stevenage, UK) was used in conjunction with a TransferMan NK 2 semi-automated programmable micromanipulator (catalogue number 5188 000.012, Eppendorf UK, Stevenage, UK) to deliver microsphere individually or in small numbers (see Figure 2.2). Delivery was into 1% (w/v) agarose solutions as they cooled from 80^{o}C to room temperature and formed gels. A second micromanipulator was used to make small adjustments to the positions of microspheres which were disturbed by fluid movements during cooling and manipulation.

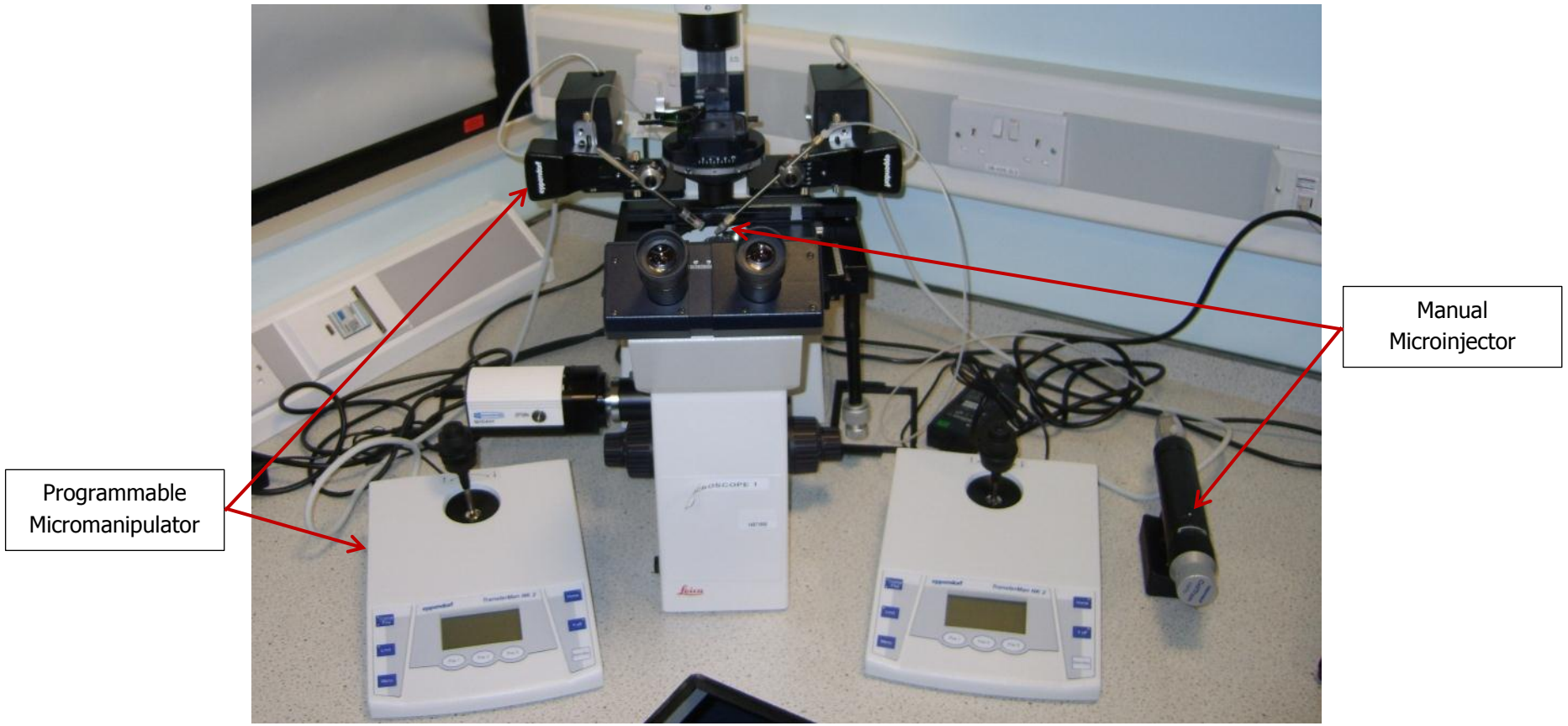

Figure 2.2 – Semi-automated microinjection/micromanipulation system comprising a pair of programmable micromanipulators and a manual microinjector. The system is mounted on an inverted microscope to allow real-time visualisation of cells and microspheres during positioning.

2.10 PLGA Microsphere Counting

2.10.1 Counting Using a Haemocytometer

Microsphere suspension ejected from Hamilton syringes was diluted with dH_2O according to the following formula:

Final Volume = 2 mL x (Ejected Volume/ 0.5 µL) x (Suspension Density/ 25% (w/v))

Each resulting, lower density suspension was loaded into both counting chambers of an improved Neubauer haemocytometer (10 µL in each chamber). Two microsphere counts were then performed on the central 5x5 square of each chamber (see Figure 2.3) in order to determine the microsphere density in the suspension, and thus the total microsphere number ejected.

2.10.2 Counting via Light Blocking

When particles are flowed in sufficiently dilute suspension that they pass individually through a region of uniform laser illumination they will block and/or scatter light depending on their size. The length of blocking and extent of scattering can be used to derive particle size distributions and the number of such events gives particle counts.

An AccuSizer 780 AD instrument (Particle Sizing Systems Europe, Dordrecht, The Netherlands) was used to count microspheres in ejected suspension volumes (see Section 2.9.1). Samples were added to the sample chamber and the chamber then drained through the detector until all liquid was gone. Microsphere counts were derived from blocking events only, to eliminate the effects of noise from very fine contaminants.

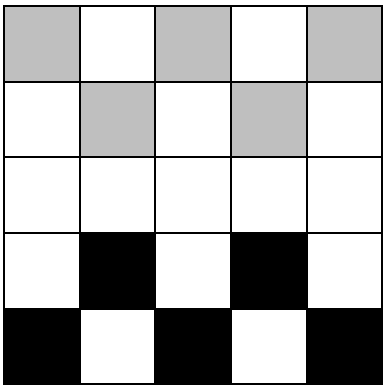

Count 1

Count 2

Counts converted to microsphere numbers per mL by multiplication by a factor of $5x10^4$

Figure 2.3 – Schematic showing counting procedure performed on microspheres using improved Neubauer haemocytometer.

2.11 Demineralisation of Bovine Bone

Fresh bovine tibias were harvested from 12 – 24 month-old animals which were slaughtered by an EU certified butcher (J Broomhall Ltd., Gloucestershire, UK). Cancellous bone segments were cleaned of residual soft tissue and washed for one hour at 37°C with PBS containing 0.1% (w/v) gentamicin (catalogue number 15750, Life Technologies, Paisley, UK). The bone fragments were then washed with dH_2O (five times the gentamicin solution volume) and finally dried under vacuum filtration (filter paper with 8 µm pores). The pieces were then briefly immersed in liquid N_2, before being wrapped in protective cotton sheet and broken up with a hammer until they were no more than 4 mm in any dimension. The resulting fragments were rinsed in a large volume of dH_2O to remove debris and dried with absorbent material. A Krups F203 mill was used to grind the pieces to a powder after they had been cooled again in liquid N_2.

The powdered bone was placed into a 0.5 M hydrochloric acid solution (25 mL per g of bone) and stirred at 300 rpm for up to 24 hours at room temperature to remove mineral from the matrix. The HCl was removed, the powder washed in dH_2O (five times the HCl volume) and then dried, all under vacuum filtration. The dried, demineralised powder was transferred into a 1:1 mix of chloroform and methanol (30 mL per g of powder, Fisher Scientific, Loughborough, UK) and incubated for 1 hour at room temperature to remove remaining lipids. Under vacuum filtration, the liquid was removed, and the powder washed in methanol (60 mL per g of demineralised bone powder) and PBS (150 mL per g of demineralised bone powder), before being dried. The resulting demineralised bone matrix (DBM) was lyophilised for 48 hours and stored at -20°C until further use.

2.12 Decellularisation of Demineralised Bone Matrix

Demineralised bone powder was stirred for 24 hours at 37°C in a 0.05% (w/v)/0.02% (w/v) trypsin/EDTA solution (Sigma-Aldrich) (enough to completely cover the powder) to cleave cell-matrix protein linkages. Under vacuum filtration, the liquid was removed, the powder washed in a volume of PBS equal to the volume of trypsin/EDTA solution and then placed in an equal volume of fresh PBS. The suspension was stirred at room temperature for 24 hours, followed by washing with a volume of dH_2O equal to the PBS volume, drying, and lyophilising for 48 hours. The resulting decellularised extracellular matrix (DECM) was stored at -20°C until further use.

2.13 Hydrogel Formation from Demineralised and Decellularised Bovine Bone

Solubilisation of extracellular matrix-derived powders (ECM powders) was achieved by pepsin digestion of the constituent proteins, producing a solution which was capable of undergoing gelation. ECM was added to a 0.01 N HCl solution at the desired digest concentration (which was higher than the final concentration of ECM in gels to be used in future experiments). Pepsin was added at 10% (w/w) relative to the ECM, and the resulting suspension was stirred at room temperature for 4 days or until all traces of solid had disappeared. Once this process was complete, ECM solution was stored at -20°C until further use.

To form a hydrogel ECM digest was mixed with sufficient 0.1 M sodium hydroxide to neutralise the solution and with 10x PBS (one ninth of the digest volume). Finally 1x PBS was used to dilute to the desired final ECM concentration. All mixing was performed at 4°C to prevent early gelation, which could be induced by raising the temperature of the pre-gel mixture to 37°C.

2.14 Haemotoxylin and Eosin Staining of Demineralised and Decellularised Bovine Bone

DBM and DECM powders were fixed overnight in 10% (v/v) neutral-buffered formalin before being embedded in 3% (w/v) agarose gel overnight. Samples were then paraffin embedded and divided into 5 – 7 μm thick sections before staining with haemotoxylin and eosin (these processing steps were performed by the Histopathology Department of the Queen's Medical Centre, Nottingham). Haemotoxylin stained cell nuclei in these sections blue-black and eosin was used as a counterstain to label ECM constituents with a pink colour.

2.15 Purification & Extraction Protocol for PicoGreen® Assay to Quantify DNA

Phenol/chloroform extraction can be used to isolate and purify nucleic acids from samples also containing large amounts of protein which may interfere with the results of quantitative DNA assays. The essence of the technique is that when a mixture of phenol and chloroform (sometimes containing isoamyl alcohol to reduce foaming) is centrifuged with an aqueous sample the proteins will partition into the organic phase and the nucleic acids into the aqueous phase. The latter can then be precipitated out by addition of alcohol and collected by centrifugation.

To quantify the double-stranded DNA (dsDNA) content of ECM-derived digests, they were first mixed 1:1 (v:v) with 25:24:1 (v:v:v) phenol/chloroform/isoamyl alcohol and centrifuged at 10000 g for 10 minutes at 4°C. The aqueous phases were carefully removed and transferred to fresh tubes. The phenol/chloroform/isoamyl alcohol addition and centrifugation steps were repeated until no white precipitate was seen at the aqueous-organic interface. At this point the aqueous phase was mixed 10:1:10 (v:v:v) with 3 M sodium acetate and ethanol and frozen on dry ice. Whilst frozen, this mixture was placed into centrifugation at 10000 g for 10 minutes at 4°C

and the supernatant carefully poured off. Four times the original digest volume of 70% (v/v) ethanol was added, centrifugation repeated and the supernatant carefully removed. Finally the samples were air dried at room temperature for 20 minutes prior to resuspension in tris-EDTA buffer as detailed below.

DNA quantification for purified samples was performed using the Quant-iT™ PicoGreen® dsDNA Assay Kit which utilises a proprietary reagent to selectively bind dsDNA and fluoresce thereafter. dsDNA standards, samples and the PicoGreen® reagent were diluted for assay in 10 mM Tris-HCl/1 mM EDTA buffer at pH 7.5. Standards and three samples of each type of digest were assayed in triplicate by mixing them with assay reagent in equal parts to a total volume of 200 µL in the wells of black 96-well plates. Fluorescence intensity was then measured at 480 nm excitation and 520 nm emission.

2.16 Micro-Computed Tomography Imaging and Three-Dimensional Analysis

In micro-computed tomography (µCT) a sample is illuminated by an x-ray source and transmission images taken at regular intervals as the sample is rotated. This produces a set of projection images which can be used to reconstruct images of the sample cross-section in a set of planes perpendicular to those of the projection images. Each cross-sectional image in fact represents the average sample density over a thin three-dimensional slice of the sample whose thickness is equal to the resolution of the instrument. These slices can then be stacked to reconstruct the three-dimensional architecture of the sample. To ensure that different materials or phases are distinguishable in the sample, they must have significantly different opacities to x-ray radiation. This typically means that they must have different physical densities.

µCT imaging of samples was undertaken using a Skyscan 1174 (Bruker microCT, Kontich, Belgium) and associated control software. Images were taken at either 6.7

or 14.5 µm resolution every 0.4° of rotation from 0 to 180° and at each rotation step a total of 6 frames were averaged to produce the final image. The NRecon software provided by the manufacturer was used to reconstruct cross-sectional slices with ring artefact reduction set to 20, beam hardening to 20% and consistent thresholding across all samples. Finally CTAn was used to produce three-dimensional models of scanned samples and to perform analyses such as measurements of total porosity and pore size distribution. As with reconstruction in NRecon, consistent thresholding was applied across all samples to be compared and despeckling was also performed to remove objects of 100 voxels or less from reconstructed images prior to analysis and modelling.

2.17 Hydroxyproline Assay for Collagen Quantification

The collagen content of both native tissues and *in vitro* engineered neo-tissues can be deduced from measurements of the hydroxyproline level, since this non-proteinogenic amino acid accounts for 14.3% by mass of naturally-occurring collagen[269]. Acid-hydrolysed samples can be oxidised by chloramine T and the hydroxyproline component subsequently reacted with p-dimethylaminobenzaldehyde (pDAB) to form a coloured product, the concentration of which is linearly related to sample absorbance at 540 nm.

First a 0.25 M sodium phosphate buffer was prepared at pH 6.5 using dibasic sodium phosphate. Next, the hydroxyproline assay stock solution was prepared, starting from a 0.24 M/2.05 M citric acid/sodium acetate solution and a 0.85 M sodium hydroxide solution. These solutions were mixed in a 13:5 ratio and glacial acetic acid was then added in a 1:75 ratio with this mixture. The solution was supplemented with the addition of dH_2O in an 11:114 ratio, and finally by the addition of toluene at a 1:2000 ratio.

The hydroxyproline assay working solution was prepared from the stock solution by mixing it with isopropanol in a 10:3 ratio, adjusting the pH to 6.0, and then supplementing with dH_2O to bring the total volume to $15/13^{th}$ of the pre-pH adjusted volume. The working solution was then used to prepare a 0.07 M solution of chloramine T, with the solvent being an 8:1 mixture of working solution and isopropanol.

The final solution to be prepared was a 1.16 M solution of p-dimethylaminobenzaldehyde (pDAB) in a 30:13 mixture of isopropanol and 60% perchloric acid.

The first step in preparing samples and standards for assay was acid hydrolysis. This was achieved through a 40 hour incubation, at 120°C, of a 1:1 mix of 10 M hydrochloric acid with either the sample to be assayed, or a blank solution of the enzyme used to digest the samples. After hydrolysis, the samples were dried by incubation at 90°C, and resuspended in 0.25 M sodium phosphate buffer (pH 6.5) at four times the volume originally hydrolysed.

Into a 96-well flat-bottomed plate was placed 50 µL of each standard and each sample in triplicate. To each well 50 µL of chloramine T solution was added and the mixture was incubated at room temperature for 20 minutes. This was followed by the addition of 50 µL of pDAB solution and incubation for 30 minutes at 60°C. The plate was cooled back to room temperature, and the absorbance of each well read at 540 nm between 10 and 30 minutes after removal from the water bath. The collagen content of each sample was then calculated as follows:

$$(\text{Collagen Content}/\ \%) = \frac{([\text{Hydroxyproline}]/\ \mu g/mL) \times (\text{Dilution Factor})}{(\text{Dry Weight of Sample}/\ g) \times 0.143 \times 10^6} \times 100$$

2.18 Spectrophotometric Analysis of Gelation Kinetics

Pre-gel mixtures (see Section 2.10) at 4°C were pipetted into 96-well plates (100 µL per well, n = 6) and loaded into a pre-warmed spectrophotometer at 37°C (Infinite 200, Tecan, Reading, UK). Sample absorbances were then measured every 3 minutes for 90 minutes at 405 nm. This wavelength falls within a band which has been used to track collagen fibril and fibre formation and thus gelation.

2.19 Rheological Analysis of Hydrogel Gelation and Mechanical Properties

Rheology is the study of the (often non-Newtonian) viscoelastic behaviour of materials such as hydrogels and amorphous polymers which neither behave completely as solids nor completely as liquids. Measurements are performed on thin samples between narrowly-separated plates in order to prevent significant edge effects or variation of mechanical properties through the sample thickness. Primarily rheological measurements involve the application of (oscillatory) strain in order to deduce the amount of energy stored by elastic behaviour and lost by viscous (flow) behaviour. Other parameters such as the strain experienced by the sample or the sample viscosity can also be measured or calculated.

ECM-derived hydrogels were subjected to rheological testing using a Physica MCR 301 rheometer (Anton Paar, Hertford, UK). Oscillatory strains were applied to deduce the rate of change of gel properties during gelation and also to assess the final mechanical properties of the fully-formed gels. Pre-gel solutions (see Section 2.10) at 4°C were loaded between 50 mm parallel plates with a 0.2 mm measuring gap which were also pre-cooled to 4°C in a humidified chamber. Samples were then subjected to a 1% oscillatory strain at 1 rad s^{-1} for 60 minutes to allow for complete gelation. During the first 75 s of measurements the plates and sample were warmed to 37°C to induce gelation.

Immediately following this, the now-gelled samples were subjected to a strain amplitude sweep from 0.1 – 200% strain at a constant strain rate of 1 rad s^{-1}. This was designed to assess whether the ECM-derived hydrogels would exhibit the strain stiffening expected of collagen hydrogels and also to define the failure strain for these gels.

2.20 Bead Formation from Alginate and ECM-Derived Hydrogels

Alginic acid is a block copolymer polysaccharide of mannuronic and guluronic acids. It is typically derived from seaweed and can be induced to form hydrogels by ion exchange. The sodium salt (sodium alginate) shows good water solubility at ambient conditions, but if the sodium ions are exchanged for divalent calcium ions they can act to crosslink the individual alginate chains and form a hydrogel. This provides a simple method for the formation of alginate hydrogel beads in which sodium alginate solutions are simply dripped into aqueous baths containing high concentrations of calcium salts, leading to almost instantaneous gelation.

This approach was used to produce beads containing or composed of ECM-derived hydrogels. 1% (w/v) sodium alginate (Acros Organics) solutions in PBS were mixed with DECM digest in varying ratios such that the DECM concentration in the final mixture was always 6 mg mL^{-1} and the total volume was always 10 mL. These mixtures were then dripped through 22G tapered dispense tips (catalogue number TTN22, Adhesive Dispensing, Milton Keynes, UK) into 100 mL baths of 5% (w/v) calcium chloride which were pre-warmed to 37^{o}C. After 1 hour's incubation to allow DECM-derived gel formation the beads could be collected and either imaged or dried at 65^{o}C for 24 hours for dry weight measurement. Alternatively the beads could be transferred to 0.25 M sodium citrate for 10 minutes to cause the alginate to revert to a liquid state and leaving the beads composed entirely of DECM-derived hydrogel.

2.21 Production and Sintering of PLGA-PEG Microparticles

Previously published work has described the production of a microparticulate synthetic polymer material which undergoes thermoresponsive liquid sintering to form a porous solid with mechanical properties suitable for bone repair[270-273]. The microparticles consist of a blend of PLGA and PEG which has a glass transition temperature higher than room temperature but lower than 37°C. This means that when the microparticles are heated to 37°C in an aqueous environment they soften and form adhesion bridges between one another. The PEG component subsequently leaches into the aqueous carrier fluid leading to an increase in the glass transition temperature and hardening of the material. As a result a solid is formed from the microparticle network which defines an interconnected pore structure.

In particular in this work, PLGA (85:15 lactide:glycolide, 53 – 56 kDa) was melt blended at 90°C with PEG in a 93.5:6.5 ratio. This melt blend was then milled in a Krups F203 mill which had been pre-cooled with liquid nitrogen. The resulting powder was manually sieved using analytical test sieves (Retsch (UK), Castleford, UK) to select the 50 – 100 μm size fraction.

To produce microparticle-based constructs these PLGA-PEG microparticles were suspended in CMC to form dense pastes which were formed into the desired construct shape via bioplotting. These constructs were incubated in a humidified environment at 37°C for two hours. Following this the constructs were submerged in 0.9% (w/v) sodium chloride in the same environment for a further 22 hours

2.22 Use of Fab@Home Bioplotting Platform

The Fab@Home solid freeform fabrication platform (Model 1)[274] was used to produce three-dimensional constructs in a layer-by-layer fashion by extrusion of scaffold materials through tapered dispense tips (catalogue number 7005006 or 7018097,

Nordson EFD, Westlake, OH, USA). Materials were loaded into 10 mL Luer lock syringes (catalogue number 26265, Exel International, Saint Petersburg, FL, USA). The pistons of these syringes were then depressed to deposit material at a computer-controlled rate utilising the FabStudio (v0.23a) software designed for the Fab@Home platform. This software also controlled the motion of the syringe tips in two dimensions and of the build stage in the third dimension in order to achieve positional control of deposition (see Figure 2.4).

In other cases the Fab@Home solid freeform fabrication platform (Model 2) was used in conjunction with alternative tapered dispense tips (catalogue number TTNx where x is the tip gauge, Adhesive Dispensing, Milton Keynes, UK). Materials were sealed into 10 mL Luer lock syringe barrels (catalogue number 7100LL1NPK, Adhesive Dispensing, Milton Keynes, UK) by the use of SmoothFlow^{TM} pistons (catalogue number 5111PE-B, Nordson EFD, Westlake, OH, USA). These pistons were then depressed to deposit material at a computer-controlled rate utilising the FabStudio (v2.0.1) and FabInterpreter software suite designed for the Fab@Home platform. This software package also controlled the motion of the syringe tips in two dimensions and of the build stage in the third dimension in order to achieve positional control of deposition (see Figure 2.5).

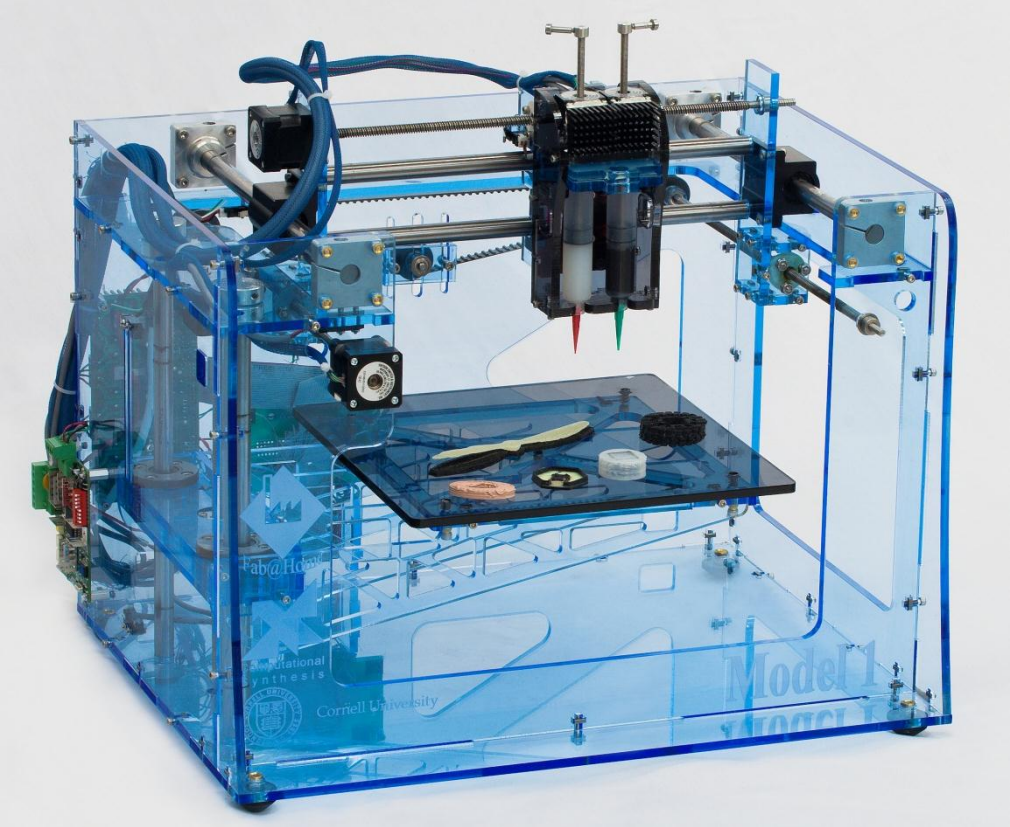

Figure 2.4 – Fab@Home Model 1 bioplotting platform. Associated software drives motion of syringe carriage in two dimensions, motion of build tray in the third dimension and rate of depression of syringe plungers to give complete control over rate and location of material deposition. Three-dimensional positioning accuracy is ±25 μm.

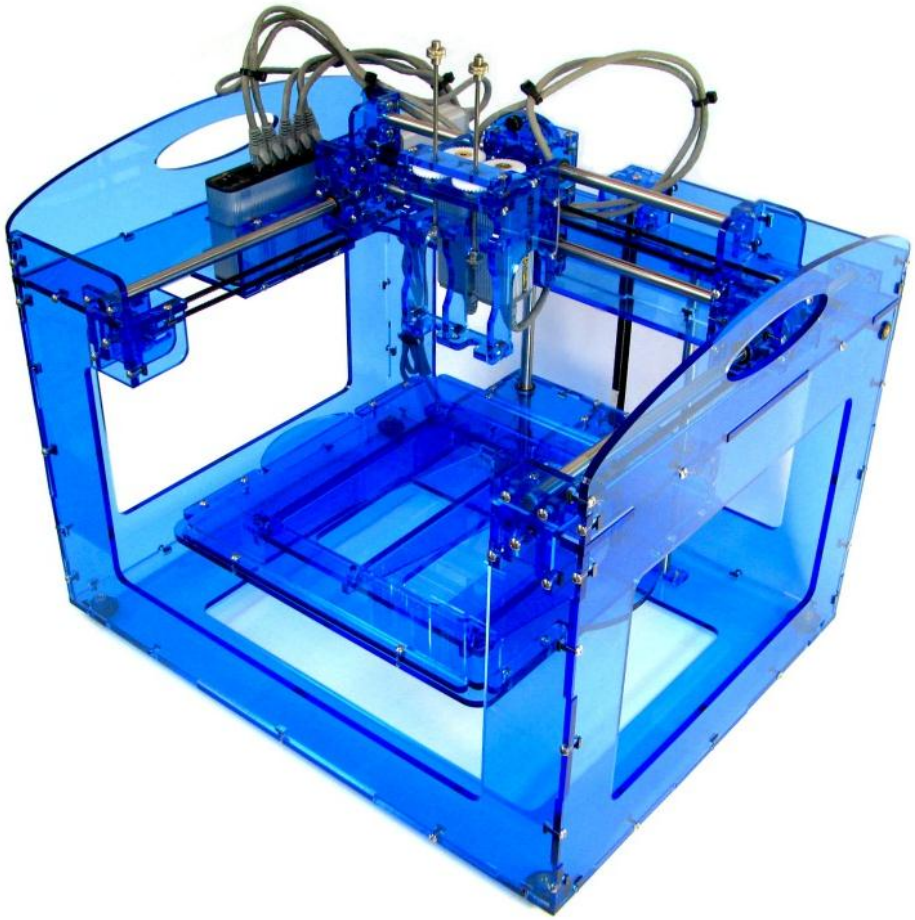

Figure 2.5 – Fab@Home Model 2 bioplotting platform. Associated software drives motion of syringe carriage in two dimensions, motion of build tray in the third dimension and rate of depression of syringe plungers to give complete control over rate and location of material deposition. Three-dimensional positioning accuracy is ±25 μm.

2.22.1 Bioplotting of Alginate Hydrogels

To achieve a consistency which was liquid enough to allow flow for deposition but solid enough to prevent significant flow after deposition sodium alginate solutions were partially calcium-crosslinked prior to bioplotting. This was achieved by mixing them with the poorly-water soluble salt calcium sulphate. In order to optimise the material for deposition a variety of alginate concentrations, calcium sulphate concentrations and ratios of the two components were tested. These were in the ranges 1 – 4% (w/v), 0.5 – 4% (w/v) and 1:1 – 3:1 (v:v, alginate:calcium sulphate) respectively.

The process of sample preparation involved drawing up the two components into separate 10 mL Luer lock syringes (catalogue number 300912, BD, Oxford, UK or catalogue number 26265, Exel International, Saint Petersburg, FL, USA) and mixing them back and forth via Luer-to-Luer connectors (catalogue number 13136, Qosina, Edgewood, NY, USA) 100 times. The post-mixing crosslinking of the alginate takes an appreciable time to reach completion, and various post-mix wait times were also assessed from 0 – 60 minutes. All deposition of alginate hydrogels was performed using 20G tapered tips and a material flow rate of 5.82 $\mu L\ s^{-1}$.

In cases where cells were to be incorporated into bioplotted alginate constructs they were either suspended directly in the uncrosslinked sodium alginate solution prior to mixing with calcium sulphate or indirectly via suspension in PBS. In this latter case the cell suspension in PBS and the uncrosslinked alginate solution were first mixed 10 times prior to the mixing of this cell-laden alginate with the calcium sulphate a further 90 times. In all cases, the pre-plotting viability of the cells to be included was assessed via trypan blue staining and the final density of cells in bioplotted constructs was always $5 \times 10^5\ mL^{-1}$.

2.22.2 Bioplotting of PLGA-PEG Microparticle Pastes

To prevent early sintering of PLGA-PEG microparticles all materials used for sample preparation were pre-cooled to 4°C and wherever possible all preparation was carried out at this temperature as well. PLGA-PEG microparticles with or without a proportion of PLGA-based microspheres were mixed with a variety of aqueous carriers (medium viscosity CMC, high viscosity CMC or Pluronic® F-127 at concentrations of 0.1 – 4% (w/v)) at the desired v:w ratio (1:1 – 1.7:1). The resulting pastes were loaded into syringe barrels for deposition which was carried out using 16G tapered tips. Material flow rates were in the range 5.82 – 38.8 μL s^{-1}.

2.23 Unconstrained Compression Testing

Compression testing involves the application of steadily increasing strain to material samples coupled with measurements of the force being exerted to achieve these strains. This allows the deduction of properties such as the yield stress (the stress at the onset of plastic deformation) and the Young's modulus (the ratio of stress to strain during elastic deformation). Constrained testing involves constriction of the samples being tested so that they cannot expand in any direction perpendicular to the axis of loading. Unconstrained testing is conducted without this restriction.

PLGA-PEG microparticulate scaffolds were subjected to unconstrained compression testing using a TA.HD*plus* texture analyser (Stable Micro Systems, Godalming, UK). Samples were tested at 37°C immediately at the end of 24 hours sintering. The probe movement rate was 0.04 mm s^{-1} (which equates to a 0.333% s^{-1} strain rate) and the test was continued to 50% strain.

2.24 Live/Dead Staining of Cells in Alginate Hydrogels

The 'live' component of the Live/Dead Viability/Cytotoxicity Kit consists of a solution of calcein AM (an acetomethoxy (AM) derivative of the fluorescent molecule calcein). The AM group which prevents fluorescence of the molecule is only cleaved by the esterases contained within living cells and the molecule is therefore only fluorescent when trapped in viable cells. The 'dead' component of the staining kit is ethidium homodimer-1 (EH-1) which can only cross cell membranes once those cells are membrane compromised (dead or dying). Upon crossing these membranes, EH-1 is then able to bind the cells' DNA at which point it becomes fluorescent.

In order to stain cells contained within bioplotted alginate hydrogels, small samples of the gels were submerged in a 2 µM/2 µM calcein AM/EH-1 solution for 30 minutes. For each bioplotted gel three samples were stained and three fields of view imaged for each sample to assess cell viability. Imaging was undertaken by removing samples from their stain solutions, pressing them between glass slides and glass coverslips and then viewing them using a Leica DM IRB inverted microscope (Leica Microsystems (UK), Milton Keynes, UK) and QCapture Pro software (QImaging, Surrey, Canada).

2.25 MTS Assay for Cell Proliferation

MTS (3-(4,5-dimethylthiazol-2-yl)-5-(3-carboxymethoxyphenyl)-2-(4-sulfophenyl)-2H-tetrazolium) and a number of closely-related tetrazolium dyes are reduced by enzymes contained within viable, metabolising cells to produce formazan products. This results in a colour change which can be measured spectrophotometrically to allow quantification of cell populations.

Here an MTS assay kit (catalogue number G3581, Promega UK, Southampton, UK) was used to assess cell proliferation in the wells of 96-well tissue culture plates. To

the 100 µL of culture medium within each well was added 20 µL of MTS reagent (n = 6, cell-free controls evaluated for each culture condition). The resulting mixture was incubated at 37^{o}C for 3 hours before the absorbance of each well was read at 490 nm using an Infinite 200 spectrophotometer (Tecan, Reading, UK).

2.26 Statistical Analysis

The homogeneity of variances across different experimental groups to be compared was determined by Levene's test. Comparisons of two experimental groups were then made using the student's t-test whilst comparisons of more than two groups were made by one way analysis of variance (ANOVA), using Welch's F statistic when group variances were found to be unequal. Appropriate *post hoc* procedures were used after ANOVA to perform pairwise comparisons between experimental groups. In cases of equal group size and equal variances Tukey's procedure was applied, whilst Gabriel's was utilised for groups of uneven size with equal variances and the Games-Howell procedure for cases of unequal variance. All statistical tests were performed at the 5% significance level.

3. Production and Patterning of PLGA-Based Microspheres

3.1 Introduction

3.1.1 Poly(lactic-co-glycolic acid)

Poly(lactic-co-glycolic acid) (PLGA) has a long and extensive history of use in biomedical science[275,276] and is approved by the Food and Drug Administration in the USA and by similar organisations around the world for a number of uses[277,278]. PLGA has excellent biocompatibility, with low-toxicity degradation products and relatively little immune response upon implantation[279-283]. PLGA is commonly-used in the fields of drug delivery and tissue engineering, where it allows the release profile of drugs or proteins encapsulated within it to be extensively tailored[276,279,284].

Well-established methodologies allow control of the morphology of PLGA scaffolds via the use of porogens[285-287] and production techniques such as supercritical fluid foaming[288]. Porous scaffolds can also be produced via microparticle sintering in which case the structural properties of the scaffolds can be controlled by varying parameters including the microparticle size and size range, sintering temperature and time and the loading regime applied during formation[289,290]. Control of scaffold structure brings the potential for control over protein release, cell growth and differentiation and also *in vivo* tissue ingrowth and architecture[291-293].

3.1.2 PLGA Microparticles

Particular attention has fallen on forming PLGA into microparticles and microparticulate scaffolds. Roughly spherical polymer microparticles can be obtained in a very broad range of sizes with well controlled protein encapsulation and release

via solvent evaporation techniques (also known as emulsion techniques)[294,295]. In single emulsion manufacture an organic polymer solution, with or without protein, is emulsified in an external aqueous phase. This external phase usually contains a surfactant or other emulsifier to stabilise the liquid organic droplets whilst the volatile solvent evaporates to leave behind solid microparticles[296-298]. The double emulsion technique is an extension of this in which an internal aqueous phase containing the protein to be encapsulated is pre-emulsified in the organic oil phase before this primary emulsion is then itself emulsified in the external aqueous phase[299-301]. A third alternative for solvent evaporation microparticle manufacture is to disperse the protein to be encapsulated in the organic polymer solution as a solid before emulsification[302-306]. The above techniques are amongst the most well-established and widely-used for microparticle manufacture but others include spray drying, electrospraying, microfluidics, ultrasonic atomisation and supercritical fluid processing[284,307-316].

3.1.3 Use of PLGA Microparticles for Controlled Delivery of Proteins

The therapeutic delivery of proteins is not a new concept, with a range of products having been in the clinic for many years[317,318]. However many potentially effective proteins are limited in their practical application by their short *in vivo* half-lives. Additionally, systemic delivery tends to lead to poor bioavailability at the desired site of action and undesirable side effects at other locations[318-320]. One solution to both of these problems is to encapsulate the protein into a synthetic polymer scaffold for controlled release over time. This methodology provides protection from degradation for the protein and significantly lengthens its half-life[317,318,321]. It also ensures that the therapeutic is available in a sustained dose form and allows the entirety of the protein load delivered to be located in or near the target organ or tissue.

Protein release from PLGA is known to follow a tri-phasic release pattern, starting with an initial burst release during the first 24 hours (quite often of a significant

proportion of the total encapsulated protein). This is followed by a lag phase during which very little protein is released and finally there is a period of sustained release of any remaining protein (Figure 3.1)[294,308].

The proportion of protein released in the initial burst is broadly dictated by the proportion that is either adsorbed to the polymer surface or encapsulated very close to it. The size of the burst can thus be altered by modification of the total scaffold surface area. This in turn can be achieved by altering the porosity and pore or structure size of the scaffold. The burst release can also be affected by modification or coating of the surface of the scaffold in a variety of ways[284,285,292,322-324].

After the release of this surface-located protein the release profile of PLGA enters a lag phase during which the polymer has yet to significantly degrade so that very little further protein is released. The final phase of release then begins at around the same time as significant polymer degradation i.e. the point at which significant mass starts to be lost from the scaffold. The degradation properties of the polymer thus define the timepoint for onset of the third phase of release. They also set the rate of release during this phase and they can be tailored by altering both the lactide-to-glycolide monomer ratio and the molecular weight of the PLGA used[276,277,325].

A significant body of work has addressed the addition of release modifiers such as poly(ethylene glycol) (PEG) and Pluronic® (a triblock copolymer of poly(ethylene oxide) and poly(propylene oxide)) to the PLGA used to make controlled-release scaffolds[277,303,305,308,326-328]. This addition may be with the aim of adjusting the rates and timescales for a typical tri-phasic release or of altering the shape of the release curve entirely. In the latter case a zero order release profile is often of particular interest since it assures a steady rate of protein delivery throughout the period of release and thus a constant level of biological activity[294]. Alternatively it is sometimes desired simply to minimise the burst release such that a steady release of active factor is achieved albeit after an initial delay[284,327,329].

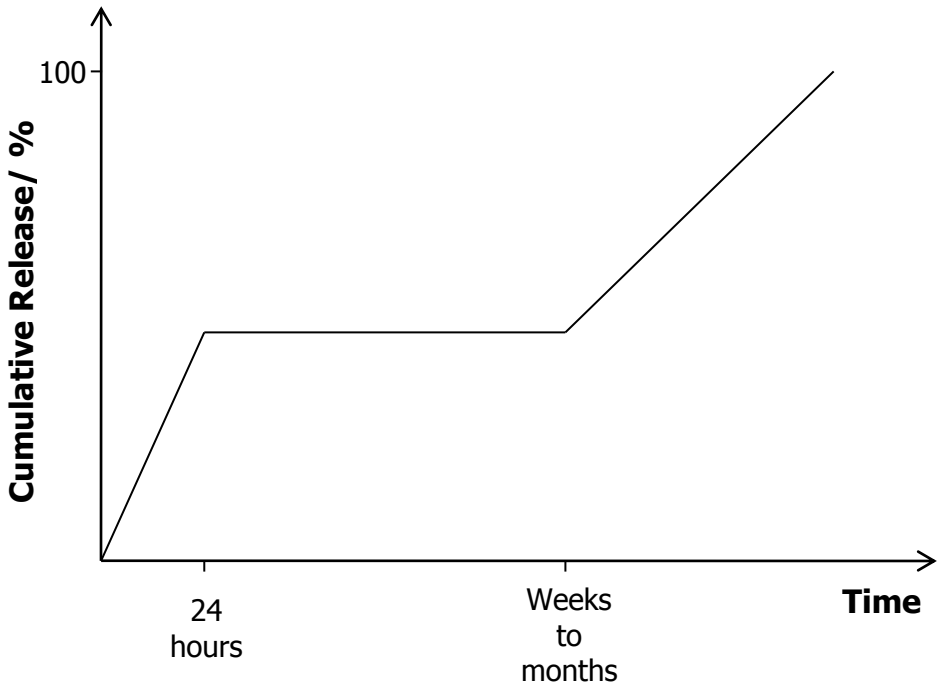

Figure 3.1 – Schematic representing typical tri-phasic protein release from PLGA scaffold.

For microparticulate scaffolds protein release can be controlled simply via size modification of microparticle size[294,298,330-333]. A number of process parameters can be altered to affect the size distribution of the resulting microparticles. The resulting change in surface area will alter both the size of the burst release and the rate of degradation of the microparticles. Coatings and material layering can easily be applied to microparticles and used to affect the release profile and/or the cellular response to PLGA-based microparticles[32,292,303,329,334-344].

Perhaps most importantly microparticles can constitute (part of) injectable scaffold formulations for tissue engineering therapies. This in turn offers the promise of minimally-invasive treatments which can be delivered into tissues or defect spaces without the need for open surgery[32]. This ultimately leads to less pain and discomfort for patients, shorter recovery times and lower infection risks.

Of particular relevance to the work presented in this thesis is the fact that the injectability of these microparticle formulations also renders them compatible with a number of patterning technologies. These include microinjection/micromanipulation and bioplotting and can be used to pattern protein-loaded microparticles within tissue engineering constructs for spatially-controlled delivery of these therapeutic agents.

3.1.4 Microinjection and Micromanipulation Techniques in Tissue Engineering

As described earlier (see Section 1.1.1) there are some examples of the use of microinjection and micromanipulation (MM) techniques in tissue engineering. These early examples have typically involved a single precisely-positioned delivery of cells and/or synthetic polymer microspheres into adult tissues[30-34]. Obstacles still remain to the application of MM techniques for three-dimensional patterning.

In order to fully utilise the positional resolution of micromanipulation systems and produce very fine scale patterns a key challenge is to achieve the delivery of very small volumes of very densely-suspended cells or microspheres. Dense suspension is

important in order to minimise the 'dead volume' of suspension fluid delivered and to prevent excessive cell or microsphere movement after delivery. The ultimate aim in this regard is to achieve precise delivery of individual objects which has been little demonstrated for rigid objects such as synthetic polymer microspheres.

3.1.5 Aims & Objectives

The first major aim of the work presented in this chapter is to generate robust protocols for the fabrication of PLGA-based microspheres demonstrating low degrees of batch-to-batch size variability. More specifically three protocols will be devised for the production of microspheres whose mean sizes vary across around two orders of magnitude. The ability to precisely define and choose the microsphere size will allow significant variation of the release profile of encapsulated proteins to tailor the presentation of each to match its native production during the biological process to be replicated. Additional modification of protein release profiles via the addition of PLGA-PEG-PLGA triblock copolymer ('Triblock') will also be evaluated.

A further task will be the production of fluorescent versions of all microsphere sizes to allow microsphere patterns in bulk scaffold materials to be imaged via fluorescence microscopy. This will be achieved via direct incorporation of fluorophores into the polymer matrix during microsphere fabrication.

The second major aim of this work is to evaluate MM techniques for their potential to pattern synthetic polymer microspheres into *in vitro* cell culture environments. Microsphere patterning would allow proteins encapsulated within them to be presented to cells in a spatially-controlled manner. This could create complex heterogeneous signal environments which would allow developmental and repair mechanisms to be modelled. The modification of these mechanisms by potential tissue engineering therapies could also be evaluated.

Initial efforts will focus on finding conditions which result in the consistent delivery of sub-microlitre volumes of microsphere suspension. Consistency will be assessed on the basis of microsphere numbers and this will involve the development of an accurate and reliable method of counting. Further to this the ability of MM techniques to precisely position these small volume deliveries within hydrogels will be evaluated. Work will progress to consider the delivery and patterning of individual microspheres and the smallest length scales on which this is possible. Finally, an important consideration will be the definition of a material environment which is suitable for both microsphere patterning and also cell adhesion and proliferation (see Appendix).

3.2 Materials and Methods

3.2.1 Microsphere Fabrication via Single Emulsion Technique

See Section 2.4.1.

3.2.2 Microsphere Fabrication via Double Emulsion Technique

See Section 2.4.2.

3.2.3 Microsphere Fabrication via Refined Double Emulsion Technique

See Section 2.4.3 for general methodology. Bone morphogenetic protein-2-loaded (BMP-2-loaded) microspheres were fabricated by utilisation of a 99:1 (w:w) mix of HSA and BMP-2 dissolved in PBS at 100 mg mL^{-1} as the aqueous phase at primary emulsification.

3.2.4 Microsphere Size Distribution Analysis via Laser Diffraction

See Section 2.5.

3.2.5 Scanning Electron Microscopy (SEM) Imaging of Microspheres

See Section 2.6.

3.2.6 PLGA-PEG-PLGA Triblock Copolymer Synthesis & Characterisation

See Section 2.3.

3.2.7 Measurement of Protein Release Rate from Microspheres

To assess the rate of release of protein from BMP-2-loaded microspheres, 100 mg samples of microspheres were incubated at 37^{o}C in 3 mL phosphate-buffered saline (PBS, pH 7.4) under gentle agitation for a total of 28 days. During this time the liquid was regularly removed to be assayed for protein content and replaced with fresh PBS. See section 2.7 for details of protein quantification assay which was run in triplicate on three separate samples from each microsphere formulation to be assessed. Blank (protein-free) microspheres were used as controls for each formulation.

3.2.8 Borosilicate Glass Needle Manufacture

See Section 2.8.

3.2.9 Microinjection and Micromanipulation of PLGA Microspheres

See Section 2.9 for general protocols for microinjection and micromanipulation utilising a fully manual system (see Section 2.9.1) and a semi-automated system (see Section 2.9.2).

3.2.10 PLGA Microsphere Counting

See Section 2.10 for general protocols for microsphere counting utilising a haemocytometer (see Section 2.10.1) or a light blocking-based particle sizing and counting system (see Section 2.10.2).

3.3 Results

Previous unpublished work on PLGA microsphere fabrication gave significant indications as to the correct choice of conditions for the production of microspheres with mean sizes of around 100 µm. This size was therefore chosen as a starting point for the work presented in this thesis and the production of smaller microspheres evaluated for the provision of the desired two order of magnitude variation (see Section 3.1.5).

3.3.1 Production of Microspheres with Size Distributions Centred on Around 100 µm ('100 µm' Microspheres)

As a result of the previous work referred to above, a 20% (w/v) PLGA (50:50, 59 kDa) concentration was chosen for fabrication targeted at this largest microsphere size. A double emulsion protocol was chosen as it had been found previously (unpublished work) to give higher encapsulation efficiency for proteins. A range of homogenisation speeds were then tested to determine that which was optimal for

production of the correct size of microspheres (1000 – 9000 rpm using Silverson L5M, identical at primary and secondary emulsification steps, Figure 3.2). Laser diffraction-based size analysis demonstrated that 2000 rpm was the correct choice of speed for future work, resulting in a mean microsphere size of 98.6 μm.

An assessment of the batch-to-batch variability of the process at this homogenisation speed was then undertaken based on size distribution consistency (n = 6, Figure 3.3). The coefficient of variance of mean microsphere size for this process was found to be 18.5% and the mean of the mean sizes to be 84.8 μm. SEM imaging (JEOL JSM 6060LV) was also undertaken (representative images shown in Figure 3.4). Microspheres were found to be predominantly spherical and smooth-surfaced with sizes that reflected the distribution seen via laser diffraction.

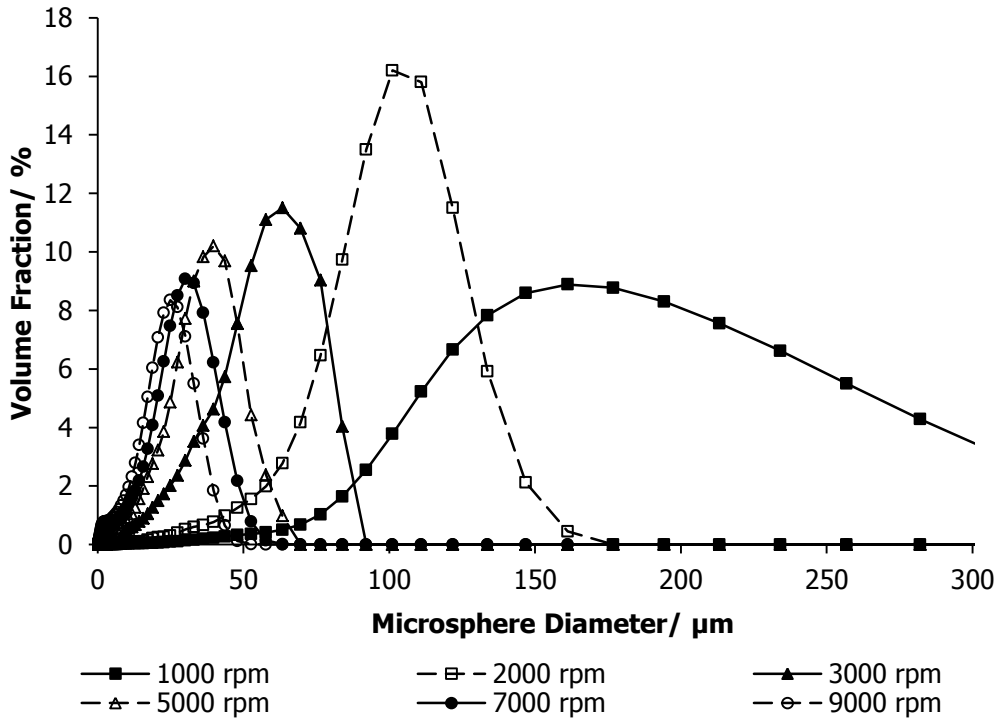

Figure 3.2 - Laser diffraction-derived size distributions demonstrating the effect on PLGA microsphere size of altering the homogenisation speeds used during double emulsion microsphere manufacture. Speeds at primary and secondary emulsification the same in all cases, polymer concentration fixed at 20% (w/v).

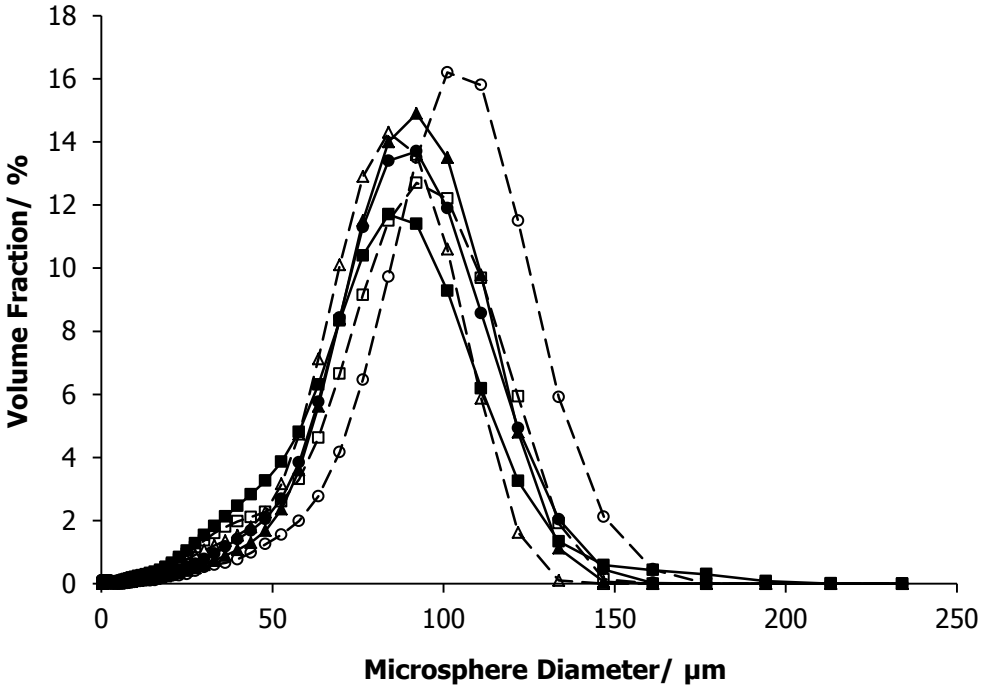

Figure 3.3 – Laser diffraction-derived size distributions showing degree of batch-to-batch variability during '100 µm' PLGA microsphere production via double emulsion using homogenisation speeds of 2000 rpm at both emulsification steps and a polymer concentration of 20% (w/v).

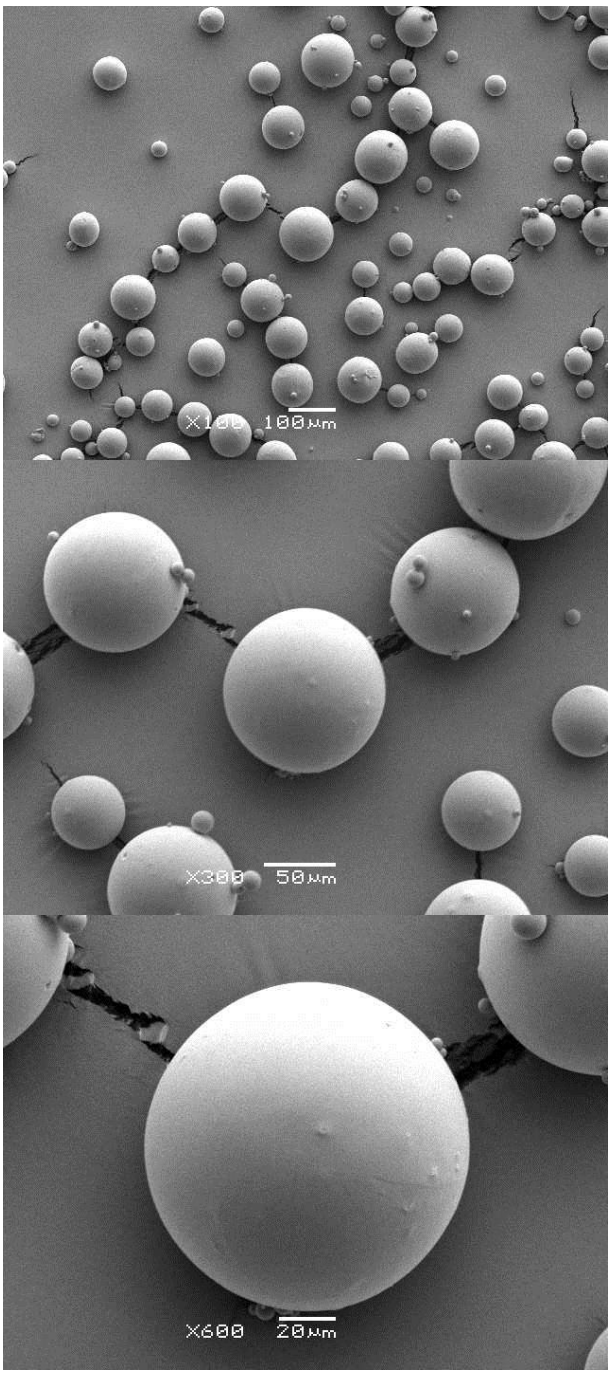

Figure 3.4 – Representative SEM images of '100 µm' PLGA microspheres produced via double emulsion with a polymer concentration of 20% (w/v) and homogenisation speeds of 2000 rpm at both emulsification steps.

Fluorescent microspheres were produced by replacing the water normally used as the inner aqueous phase with 0.1 mg mL^{-1} acridine orange. The microspheres produced were highly fluorescent and could easily be visualised via fluorescence microscopy. As with blank microspheres, an assessment of the batch-to-batch variability of the process was undertaken based on size distribution consistency (n = 6, Figure 3.5). The coefficient of variance of mean microsphere size for this process was found to be 9.1%. The mean of the mean microsphere sizes was found to be 91.0 µm indicating that the addition of fluorophore had caused a slight shift in the microsphere size distribution. SEM imaging (JEOL JSM 6060LV) was also undertaken (representative images shown in Figure 3.6). The addition of fluorophore to the microsphere formulation did not appear to have altered the predominantly spherical nature of the microspheres. However there did appear to have been an increase in the amount of surface imperfections and pores on the microspheres.

Volume-based size distributions for '100 µm' microspheres showed relatively few microspheres with sizes lower than 50 µm. However, number-based distributions highlighted the presence of a very significant number of microspheres with sizes below 10 µm (Figure 3.7(a)). To allow microspheres to flow over one another more effectively when in aqueous suspension for both microinjection (see Sections 3.3.4, 3.3.5 and 3.3.6) and bioplotting (see Chapter 5) it was necessary to remove this small size fraction. This was achieved by manual sieving using an analytical test sieve (Retsch (UK), Castleford, UK) with a 40 µm mesh. After sieving the volume-based size distribution showed little change (Figure 3.7 (b)), but the number-based distribution demonstrated the complete removal of the small microsphere fraction (Figure 3.7 (a)).

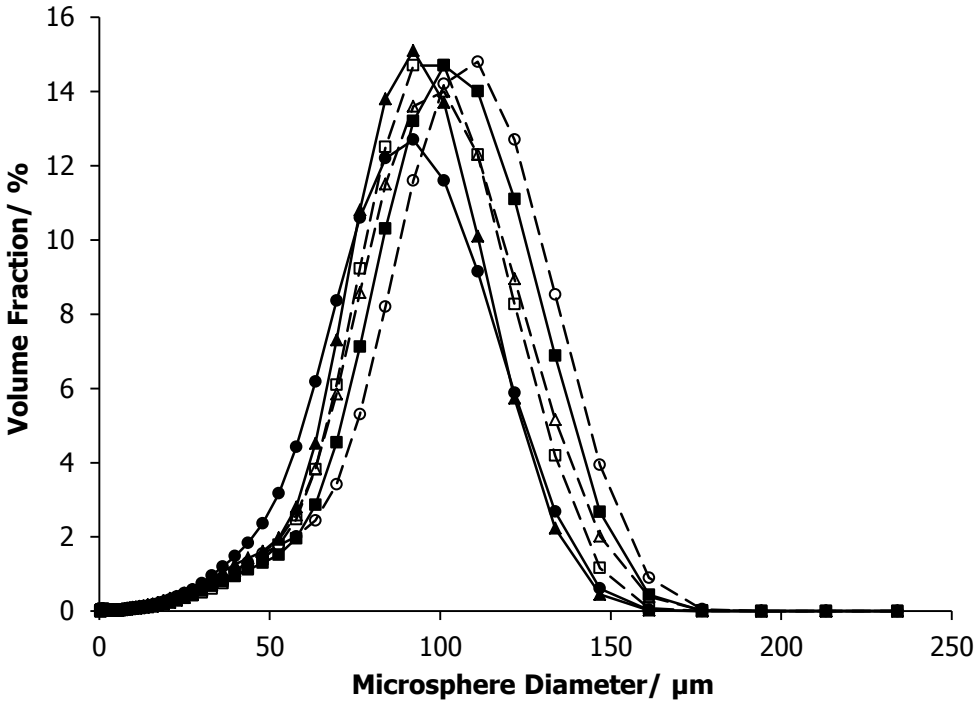

Figure 3.5 – Laser diffraction-derived size distributions showing degree of batch-to-batch variability during fluorescent '100 µm' PLGA microsphere production via double emulsion. Homogenisation speeds used were 2000 rpm at both emulsification steps, polymer concentration was 20% (w/v) and a solution of 0.1 mg mL^{-1} acridine orange was the inner aqueous phase.

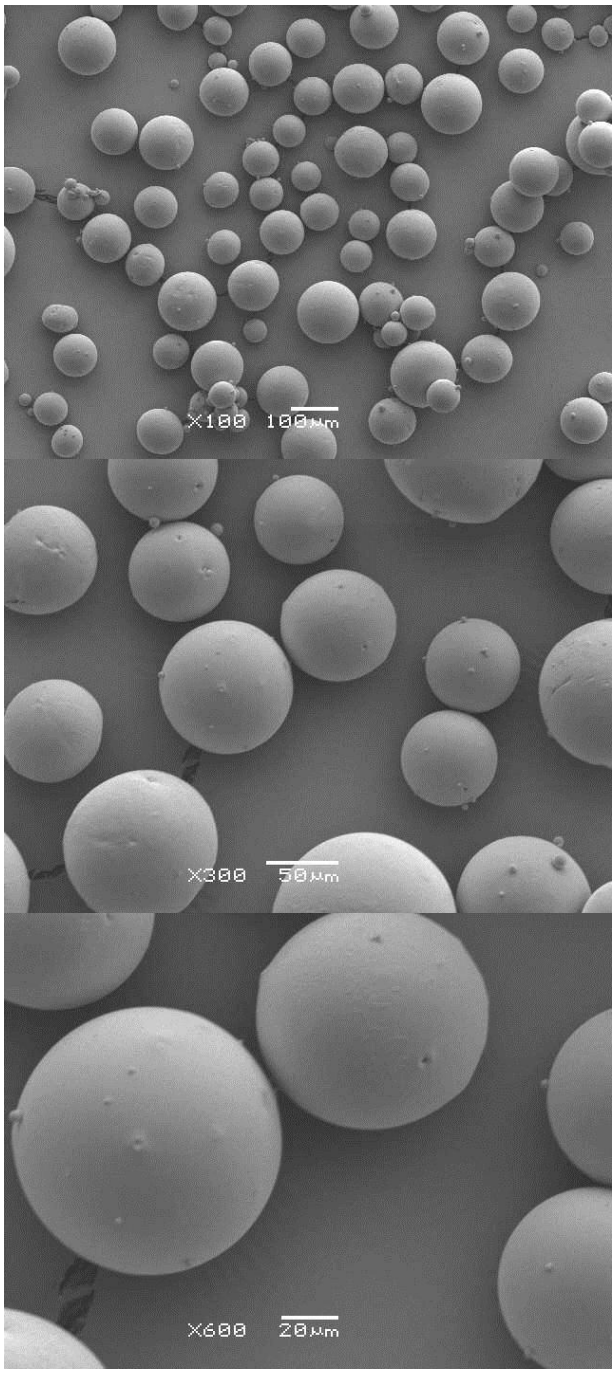

Figure 3.6 – Representative SEM images of fluorescent '100 µm' PLGA microspheres produced via double emulsion with a polymer concentration of 20% (w/v), homogenisation speeds of 2000 rpm at both emulsification steps and an inner aqueous phase consisting of 0.1 mg mL^{-1} acridine orange.

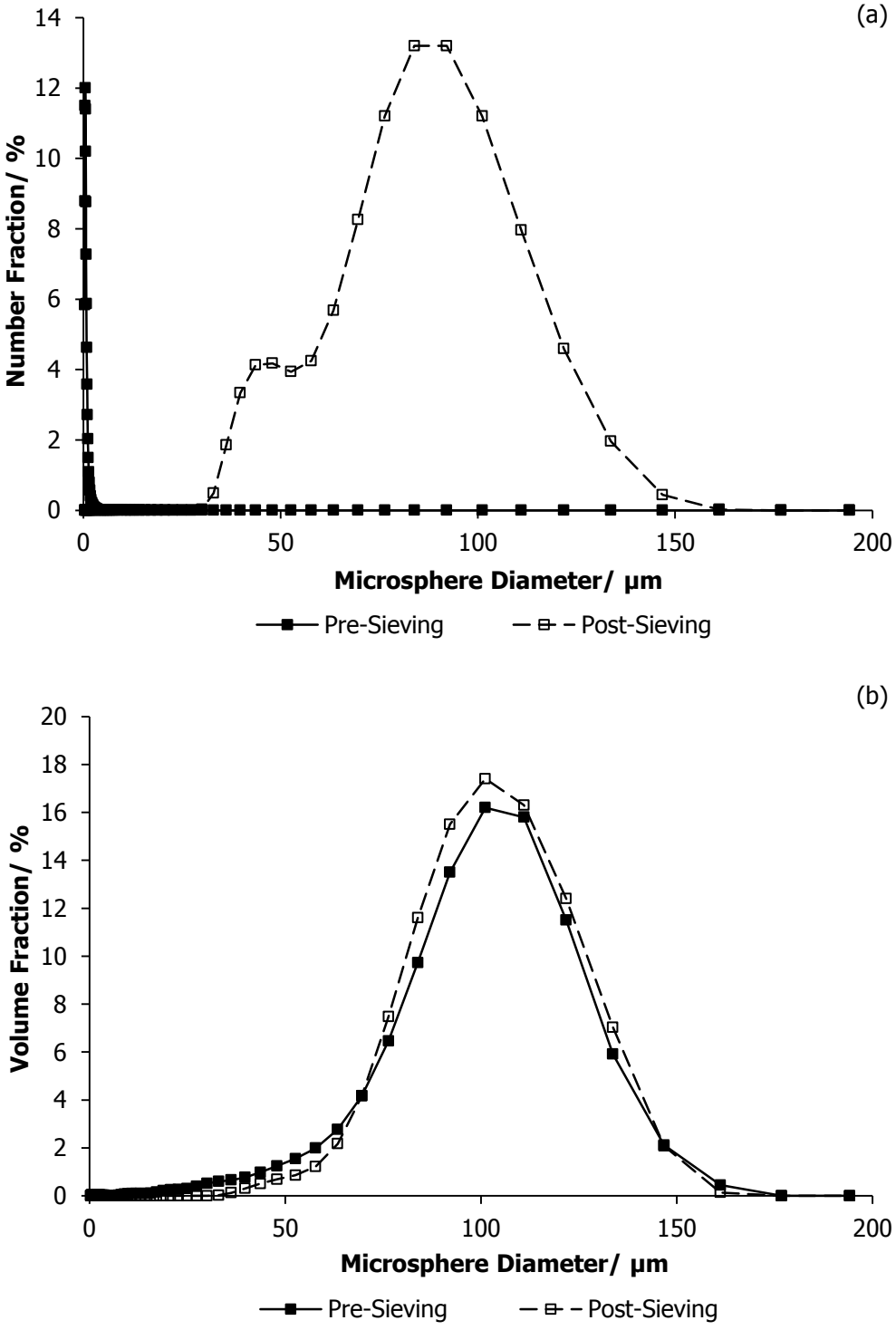

Figure 3.7 – Laser diffraction-derived size distributions, based on number fraction (a) and volume fraction (b), to show alterations achieved via sieving of '100 µm' PLGA microspheres (where the sub-40 µm fraction is discarded). Microspheres were produced via double emulsion with a polymer concentration of 20% (w/v) and homogenisation speeds of 2000 rpm at both emulsification steps.

3.3.2 Production of Microspheres with Mean Sizes Covering Two Orders of Magnitude Below 100 µm

It was clear from the work described above that mean microsphere sizes of 10 µm or less (i.e. at least one order of magnitude lower than those produced by the existing protocol) could not be produced using a polymer concentration of 20% (w/v). A range of lower PLGA (50:50, 59 kDa) concentrations (2 – 17% (w/v)) were evaluated using 9000 rpm homogenisation speeds (Silverson L5M) at both emulsification steps. The aim in this study was to produce microspheres with size distributions centred close to 1 and 10 µm without showing significant overlap with one another. Laser diffraction-based size analysis demonstrated that 2 and 17% (w/v) concentrations may be suitable for this purpose, producing size distributions centred on 1.94 and 14.4 µm respectively (Figure 3.8). To assess whether the smaller of the distributions could be shifted to further reduced size faster homogenisation speeds were tested using an alternative homogeniser (Ultra Turrax T25 Basic). No further reduction in size was observed (Figure 3.9) and the 9000 rpm homogenisation speed was carried forward for further work.

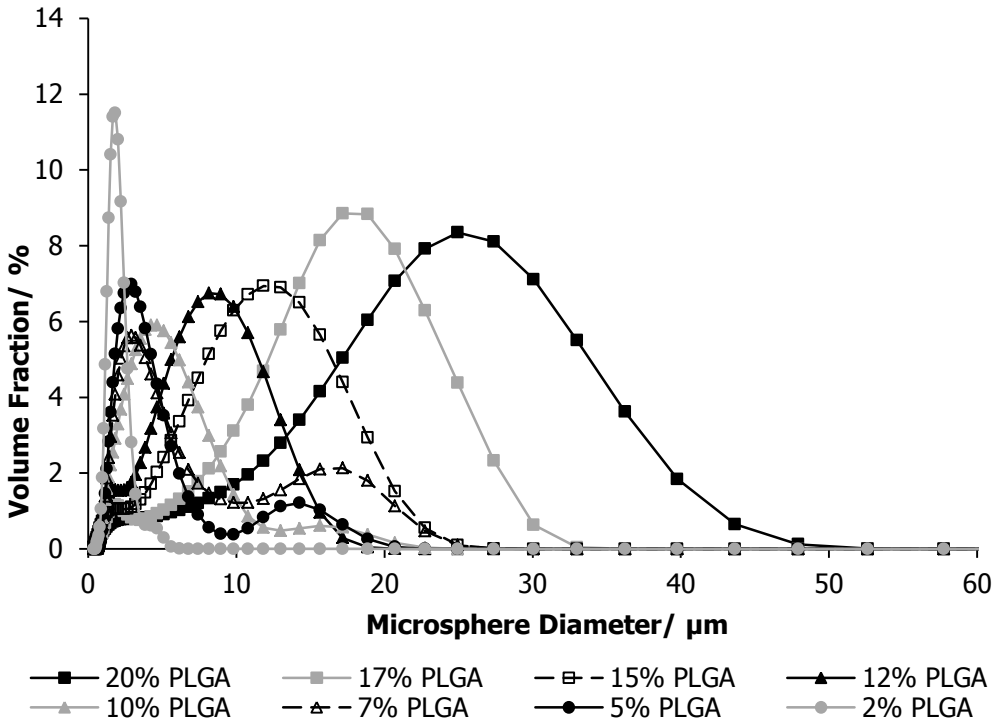

Figure 3.8 - Laser diffraction-derived size distributions demonstrating the effect on PLGA microsphere size of altering the polymer concentration used during double emulsion microsphere manufacture. Homogenisation speeds at primary and secondary emulsification are 9000 rpm in all cases.

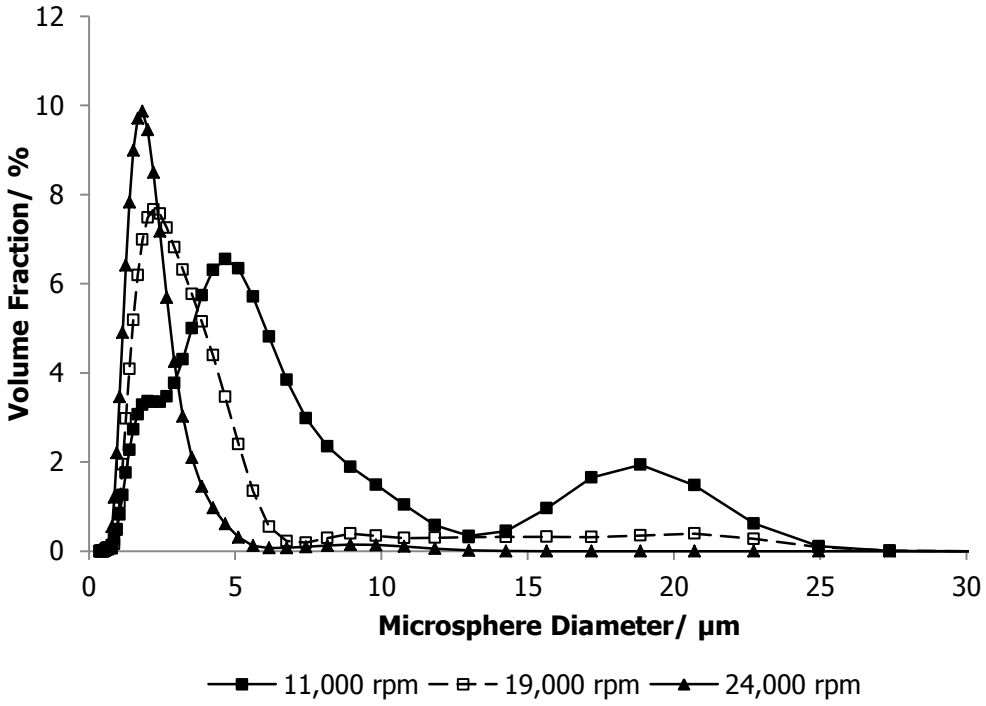

Figure 3.9 - Laser diffraction-derived size distributions demonstrating the effect on PLGA microsphere size of altering the homogenisation speeds used during double emulsion microsphere manufacture. Homogenisation speeds at primary and secondary emulsification the same in all cases, polymer concentration fixed at 2% (w/v).

The larger of these two microsphere sizes ('15 μm' microspheres) was further studied to assess batch-to-batch variability based on size distribution consistency (n = 6, Figure 3.10). The coefficient of variance of mean microsphere size for this process was found to be 9.3% and the mean of the mean sizes to be 13.6 μm. SEM imaging (JEOL JSM 6060LV) was also undertaken (representative images shown in Figure 3.11) and demonstrated that microspheres were predominantly spherical with smooth surfaces lacking pores. The microsphere sizes seen reflected the distribution seen via laser diffraction.

Similar analyses were performed for fluorescent versions of these microspheres which were produced utilising 0.1 mg mL^{-1} acridine orange as the aqueous phase at primary emulsification (Figures 3.12 & 3.13). The coefficient of variance of mean microsphere size for this process was found to be 4.9% and the mean of the mean sizes to be 14.4 μm. This indicated that as with '100 μm' microspheres (Section 3.3.1) the addition of fluorophore had slightly increased the mean microsphere size. SEM imaging (JEOL JSM 6060LV) again showed the maintenance of predominantly spherical, smooth-surfaced microsphere morphology.

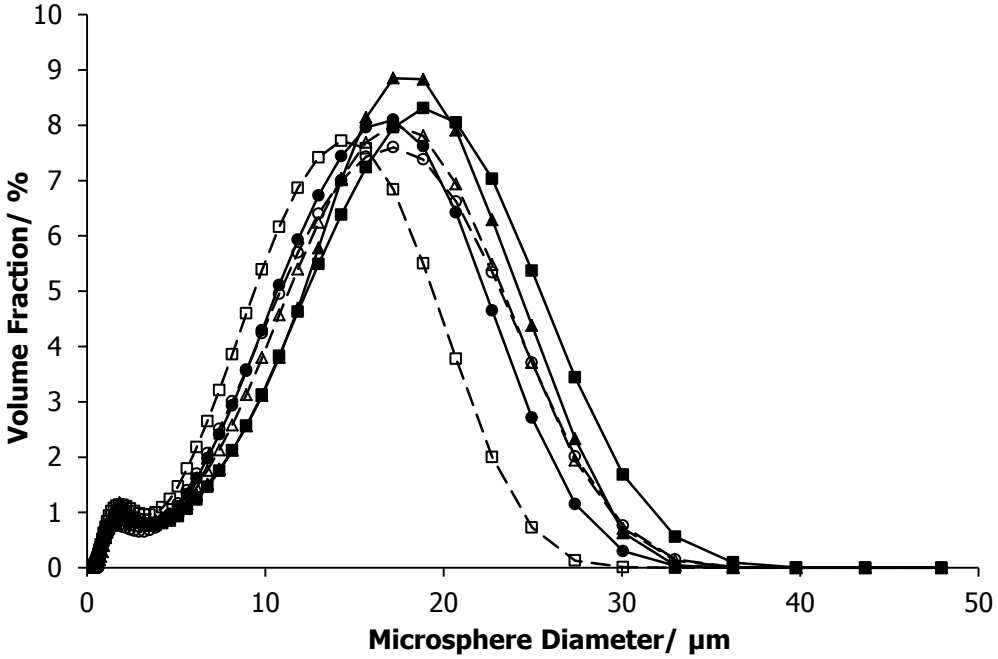

Figure 3.10 – Laser diffraction-derived size distributions showing degree of batch-to-batch variability during '15 µm' PLGA microsphere production via double emulsion. Homogenisation speeds used were 9000 rpm at both emulsification steps and polymer concentration was 17% (w/v).

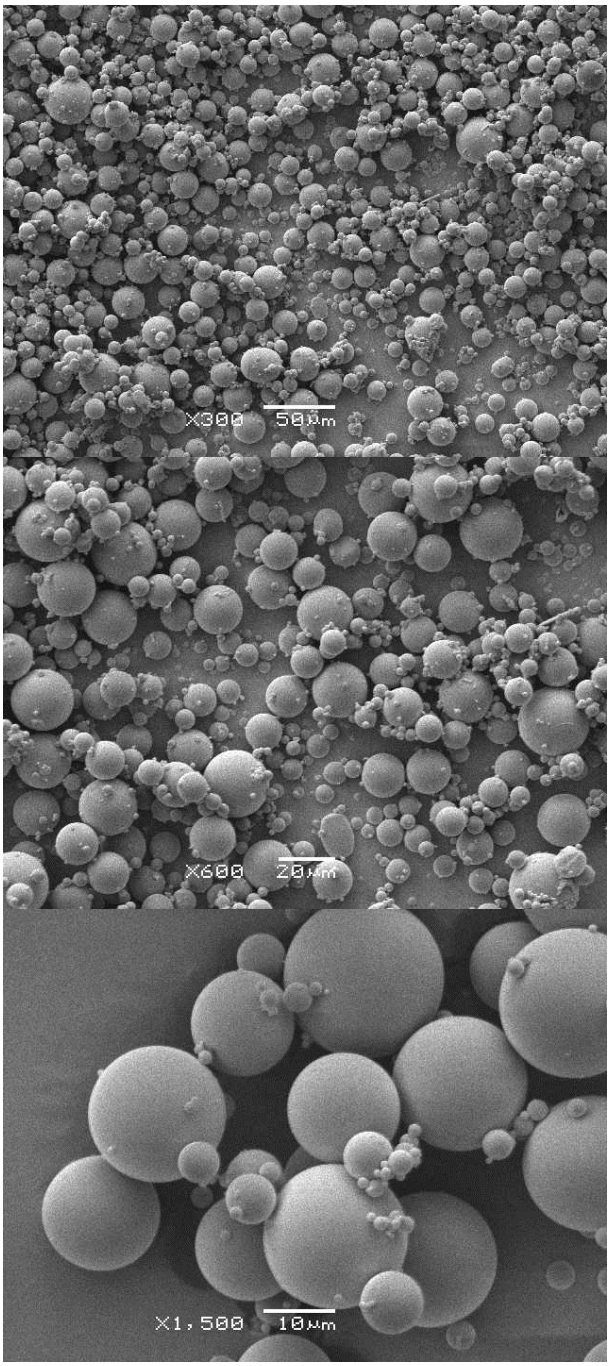

Figure 3.11 – Representative SEM images of '15 µm' PLGA microspheres produced via double emulsion with a polymer concentration of 17% (w/v) and homogenisation speeds of 9000 rpm at primary and secondary emulsifications.

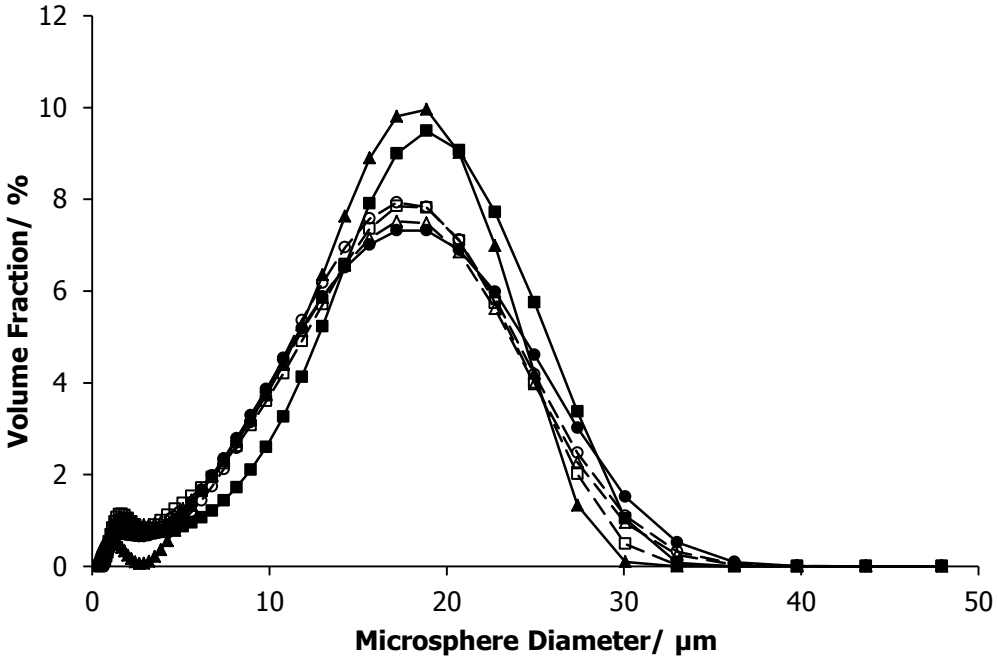

Figure 3.12 – Laser diffraction-derived size distributions showing degree of batch-to-batch variability during fluorescent '15 µm' PLGA microsphere production via double emulsion. Homogenisation speeds used were 9000 rpm at both emulsification steps, polymer concentration was 17% (w/v) and 0.1 mg mL^{-1} acridine orange was the inner aqueous phase.

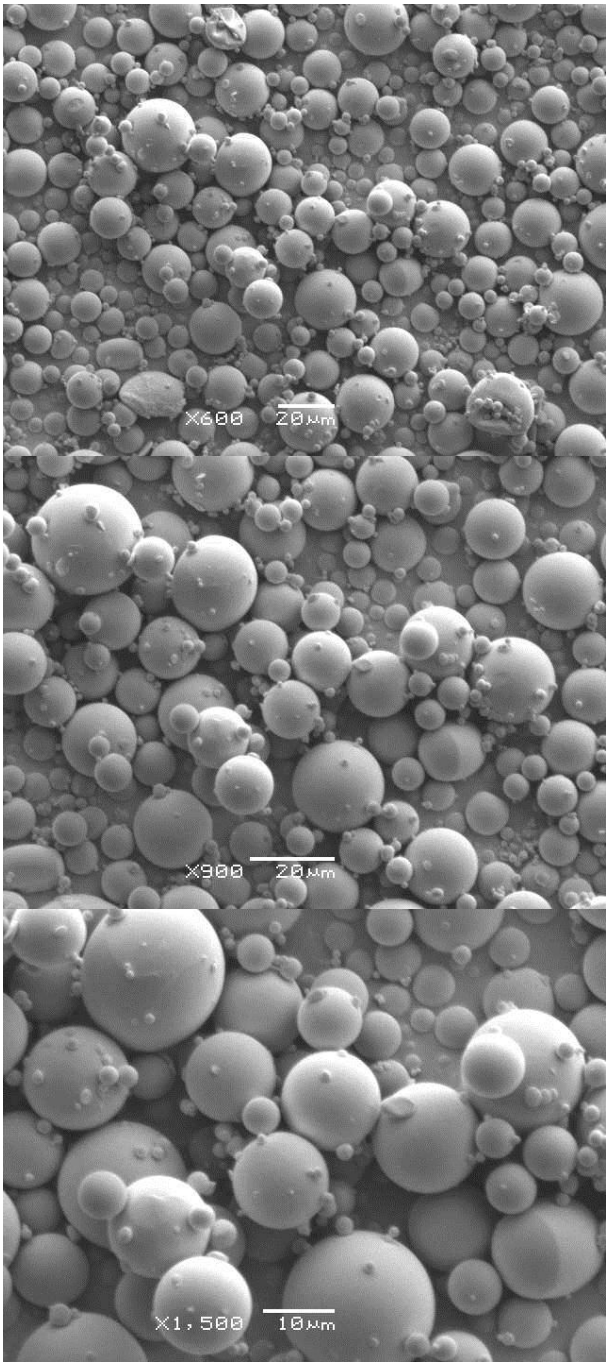

Figure 3.13 – Representative SEM images of fluorescent '15 µm' PLGA microspheres produced via double emulsion with a polymer concentration of 17% (w/v), homogenisation speeds of 9000 rpm at primary and secondary emulsifications and an inner aqueous phase of 0.1 mg mL^{-1} acridine orange.

A batch-to-batch variability study was attempted for the smallest microsphere size ('2 μm' microspheres). The first three batches produced showed a good degree of consistency (Figure 3.14 (a)) and similar predominantly spherical, smooth-surfaced morphology to that seen in other microsphere sizes (SEM imaging, Philips XL30, Figure 3.15). However subsequent batches showed very high variability and significant populations of much larger than intended microspheres (Figure 3.14 (b)).

Similar problems were seen when the production of fluorescent '2 μm' microspheres was attempted, either by co-dissolution of fluorescein with the polymer (single emulsion, see Figure 3.16) or by the use of acridine orange solutions as the aqueous phases at primary emulsification (double emulsion, see Figure 3.17).

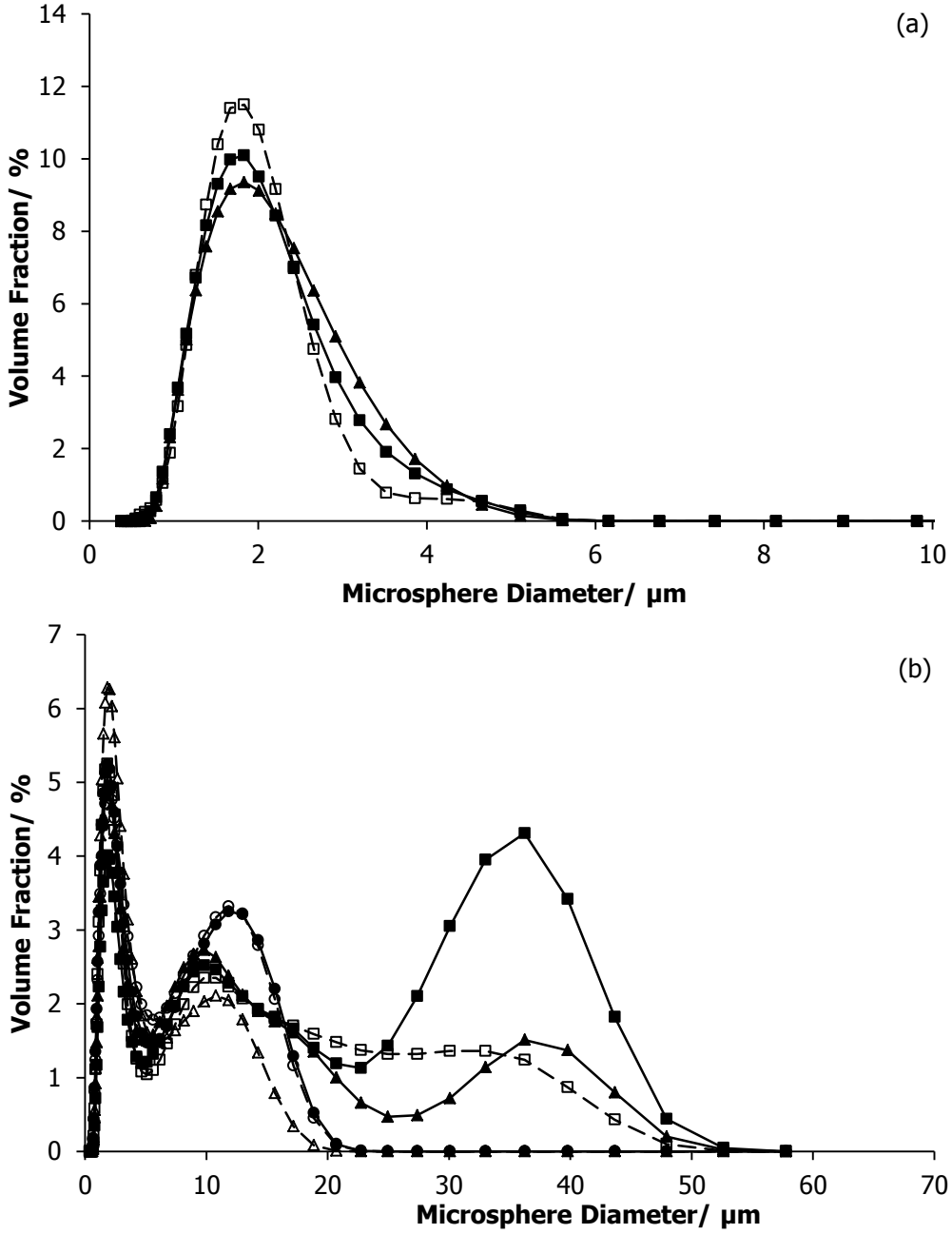

Figure 3.14 – Laser diffraction-derived size distributions for first three batches (a) and subsequent six batches (b) of '2 µm' PLGA microspheres produced via double emulsion technique using homogenisation speeds of 9000 rpm at both emulsification steps and a polymer concentration of 2% (w/v).

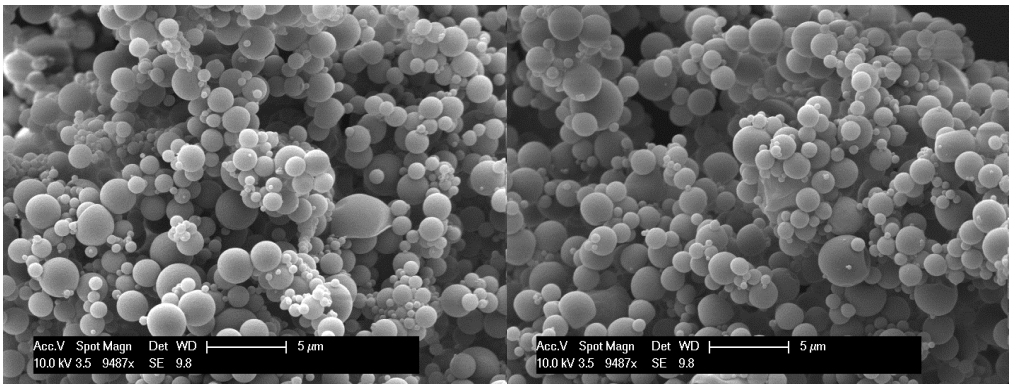

Figure 3.15 – Representative SEM images of '2 μm' PLGA microspheres (early batches, see Figure 3.14 (a)) produced via double emulsion with a polymer concentration of 2% (w/v) and homogenisation speeds of 9000 rpm at primary and secondary emulsifications.

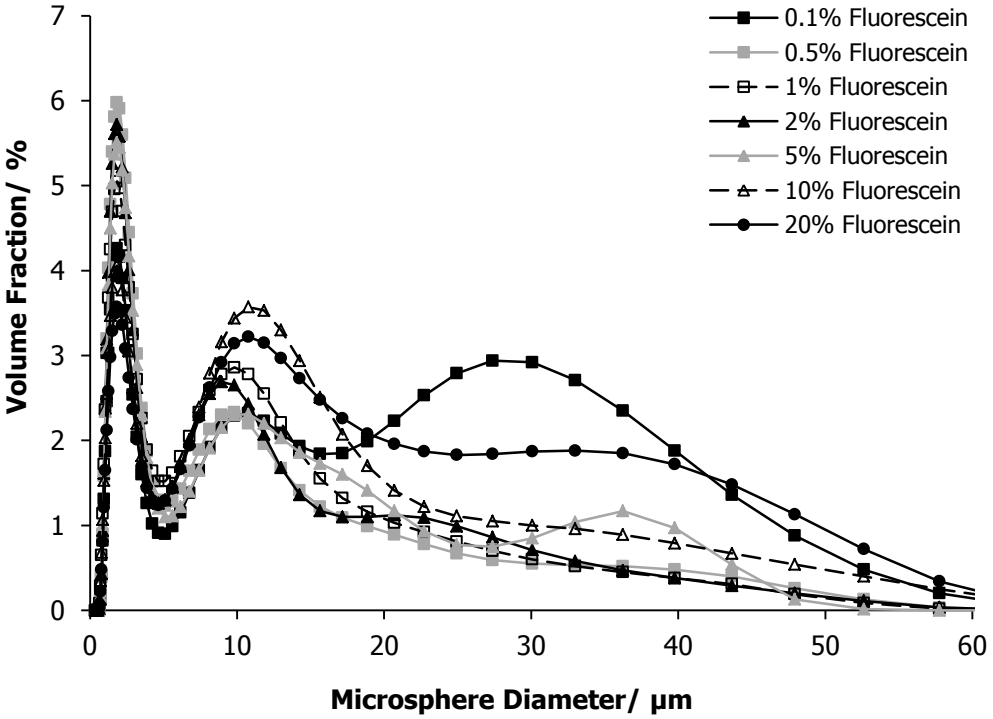

Figure 3.16 - Laser diffraction-derived size distributions demonstrating the effect on fluorescent '2 µm' PLGA microsphere size of altering the fluorescein concentration co-dissolved with the polymer during single emulsion microsphere manufacture. Speed at emulsification fixed at 24,000 rpm and polymer concentration at 2% (w/v).

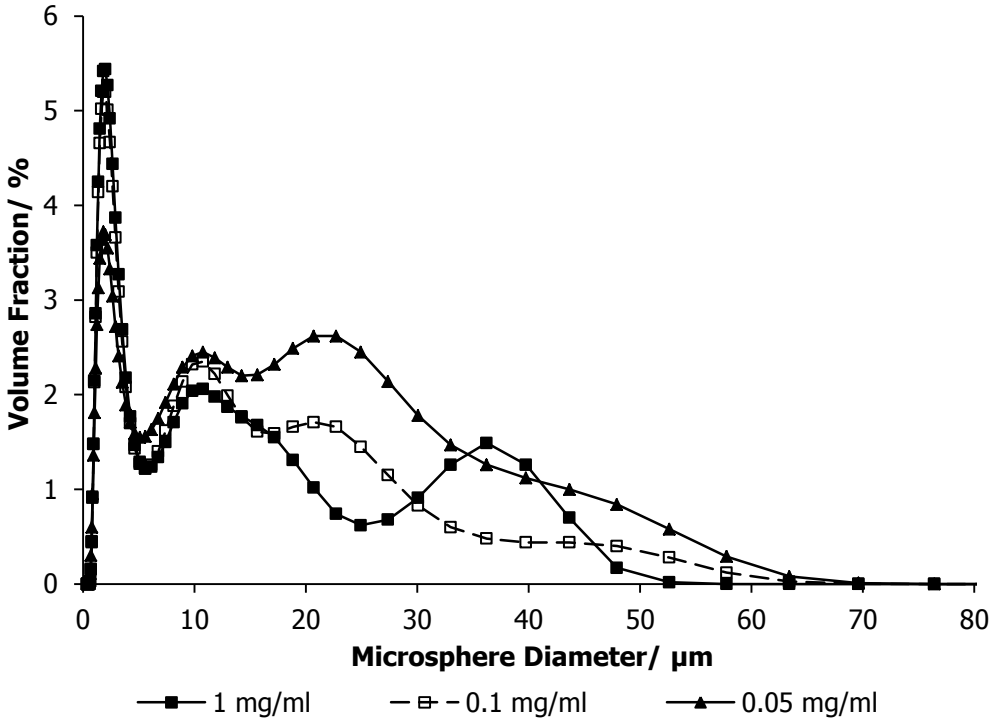

Figure 3.17 - Laser diffraction-derived size distributions demonstrating the effect on fluorescent '2 µm' PLGA microsphere size of altering the acridine orange concentration used during double emulsion microsphere manufacture. Speeds at primary and secondary emulsification steps fixed at 9000 rpm and polymer concentration at 2% (w/v).

3.3.3 The Effect of PLGA-PEG-PLGA Triblock Copolymer on Protein Release from Microspheres

The refined double emulsion technique utilised here (see Section 2.4.3) was found to produce greater yields of microspheres and to result in higher protein encapsulation efficiencies than the original double emulsion technique. The former is predominantly due to the use of PTFE containers for conducting the primary emulsification procedure and the latter due to the decreased organic solvent evaporation time. An additional result of these alterations was an improvement in the batch-to-batch consistency of the microsphere fabrication process. Figure 3.18 shows laser diffraction-derived size distributions for '100 μm' microspheres produced via the refined protocol using a PLGA (85:15, 56 kDa) concentration of 20% (w/v) and homogenisation speeds of 4000 and 2000 rpm at primary and secondary emulsifications respectively (Silverson L5M). The coefficient of variance of the mean microsphere sizes was found to be 9.1% and the mean of the mean sizes to be 74.3 μm. SEM imaging (JEOL JSM 6060LV) showed that the changes to the protocol had not changed the predominantly spherical, smooth-surfaced nature of the microspheres (representative images shown in Figure 3.19).

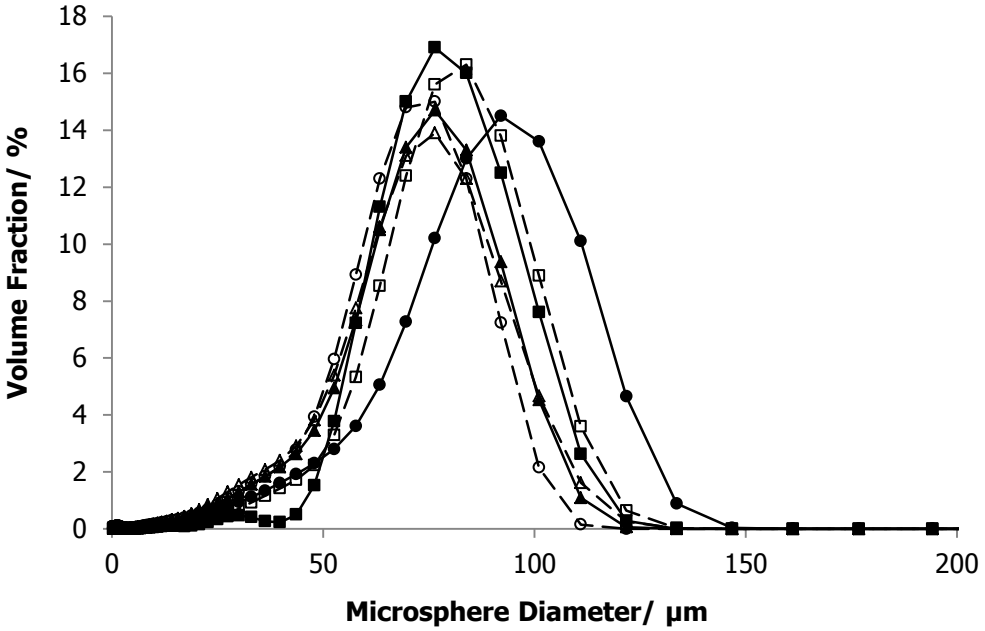

Figure 3.18 - Laser diffraction-derived size distributions showing degree of batch-to-batch variability during '100 µm' PLGA microsphere production via refined double emulsion technique. Homogenisation speeds used were 4000 and 2000 rpm at primary and secondary emulsifications respectively and polymer concentration was 20% (w/v).

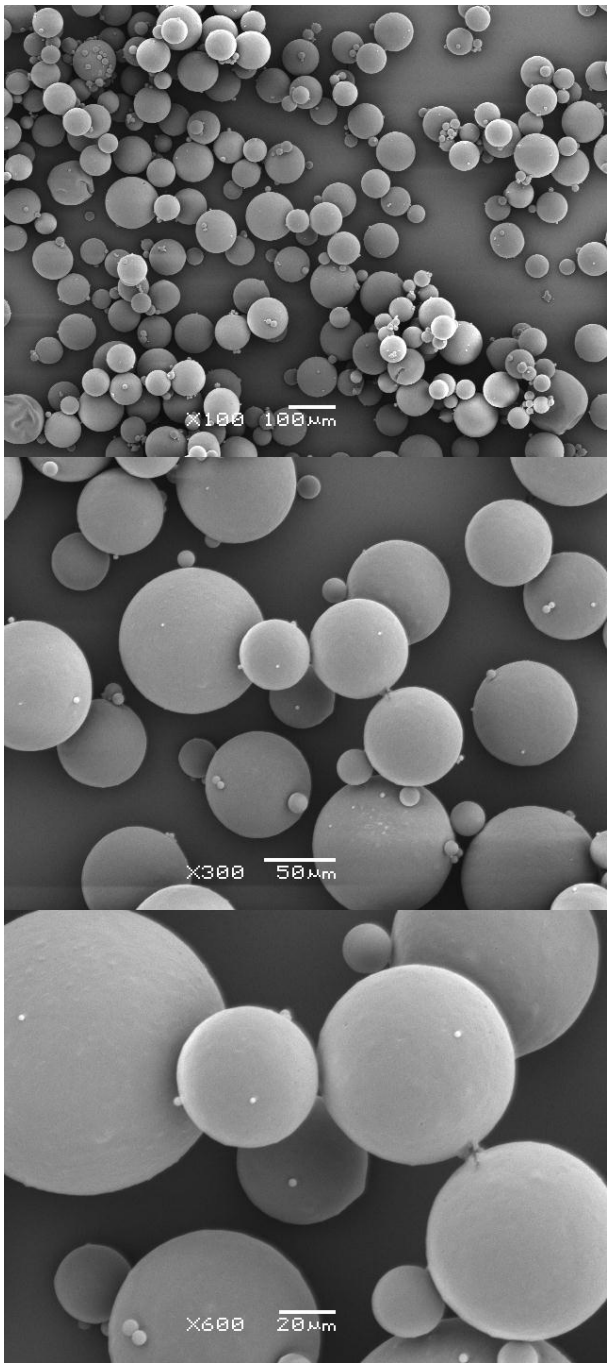

Figure 3.19 – Representative SEM images of '100 µm' PLGA microspheres produced via refined double emulsion technique with a polymer concentration of 20% (w/v) and homogenisation speeds of 4000 and 2000 rpm at primary and secondary emulsifications respectively.

As per the method detailed in Section 3.2.7 the release of protein from BMP-2-loaded PLGA-based (85:15, 56 kDa) microspheres produced using the protocol above was measured over 28 days using the MicroBCA Assay Kit. Release was assessed from microspheres containing 0, 10 and 30% (w/w) Triblock (Figure 3.20). Clear differences were seen between the release profiles produced by the different microsphere formulations.

The protein released during the first 24 hours from polymer microspheres (the 'burst release') is believed to be predominantly that which is adsorbed to the microsphere surfaces[308]. As a result the amount released in this period is typically not related to the polymer composition of the microspheres. In Figure 3.18 (b) this burst release has effectively been subtracted from the release profiles which are shown as the cumulative release of protein from 24 hours after the initiation of incubation. Once this composition-independent but variable burst is subtracted a clearer trend of more rapid release with increasing Triblock content emerges.

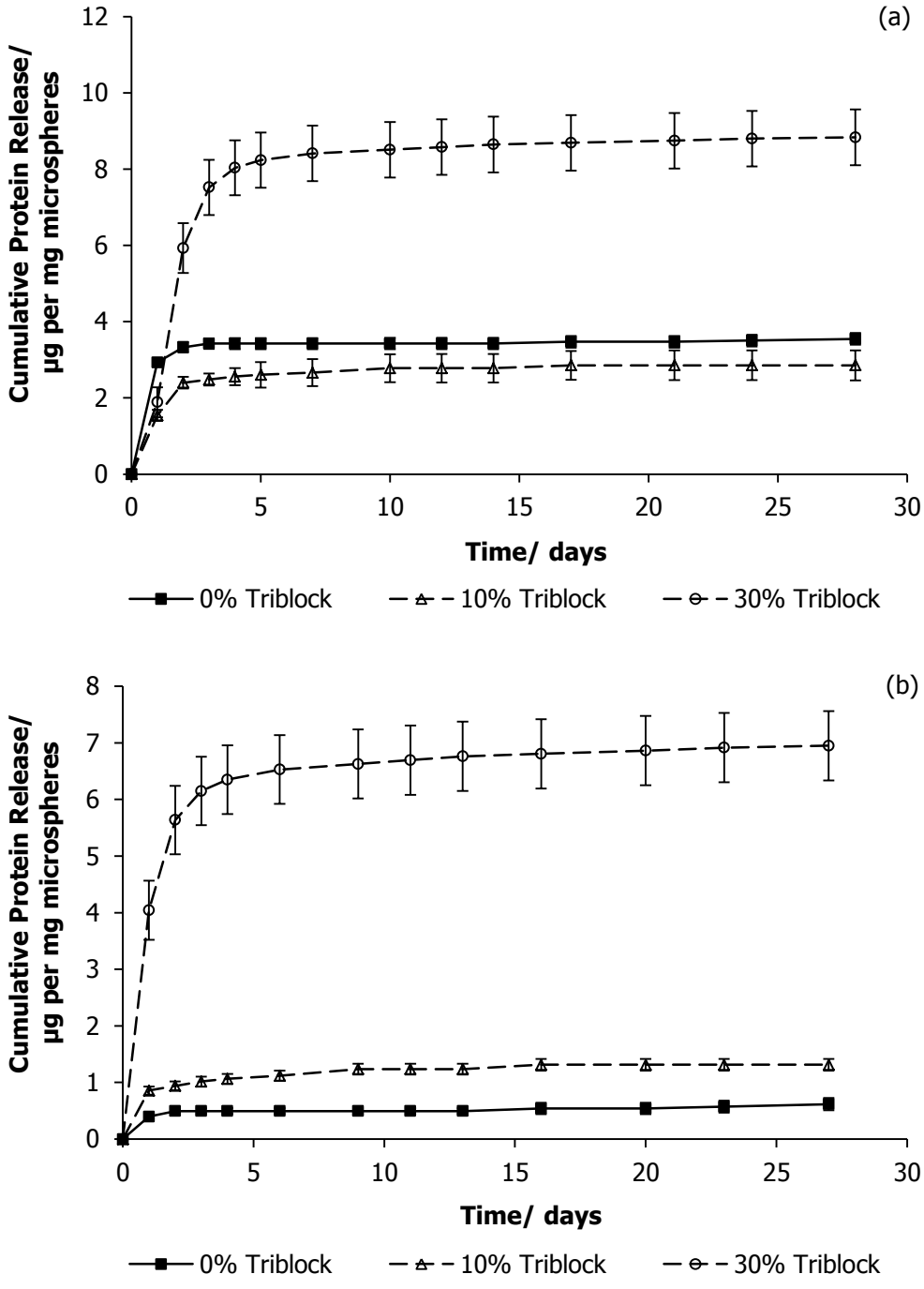

Figure 3.20 – Cumulative mass release profiles of 99:1 (w:w) HSA:BMP-2 mixture from '100 µm' PLGA-based microspheres containing varying amounts of Triblock. Profiles are shown from beginning of incubation (a) or from 24 hours after start of incubation (b) i.e. with the burst release subtracted.

3.3.4 Consistency of Delivery of Microspheres via Microlitre Syringes

Initial evaluation of the ability of microinjection to deliver PLGA microspheres was performed using microlitre Hamilton syringes and plunger-in-needle syringes. The ability to repeatedly draw up and completely eject various densities of '2 μm' microsphere suspension in water through needles of various sizes was assessed (Table 3.1).

Subsequently the ability of these syringe types to deliver microspheres consistently was assessed. The ultimate aim of the microsphere delivery and patterning work presented in this chapter was to achieve heterogeneity of protein signals. In order to produce consistent signal environments it was important that the protein load delivered under a given set of conditions was reproducible. It was on this basis that consistency was evaluated. Since the delivered protein load could not be accurately measured for small volume deliveries a surrogate measure was needed. The microsphere mass was expected to be proportional to the protein load, but this could not be accurately measured either. The number of microspheres in a delivery was considered a potential surrogate output but would only be proportional to protein load if the microsphere size distribution was found to be consistent between different deliveries.

		Suspension Density/ %(w/v)			
Needle Type	**Needle Inner Diameter/ µm**	**10**	**20**	**50**	**75**
P-i-N	340	✓	✓	✓	✓
P-i-N	260	✓	✓	✓	×
33G	110	✓	✓	✓	×

Table 3.1 - Summary of feasibility (✓) or unfeasibilty (×) of repeatedly drawing up and completely ejecting '2 µm' microsphere suspensions (early batches, see Figure 3.14 (a)) of various densities (i.e. various proportions of solid content) through various needle sizes. Note that P-i-N denotes the use of a positive displacement, plunger-in-needle syringe.

In this and subsequent work ejections were considered to be either 'repeated' or 'consecutive'. The former consisted of repeatedly drawing up and ejecting a volume in its entirety whilst the latter consisted of drawing up a volume and then ejecting it sequentially in equally-sized parts. Practical considerations dictate that the latter would be preferred for the production of microsphere patterns involving a large number of individual injections.

The similarity of size distributions resulting from different microsphere deliveries was considered to be true by definition for repeated ejections in which the complete suspension volume was delivered on each occasion. However an assessment was necessary to evaluate whether it was also true for consecutive ejections. This evaluation was performed under conditions that were considered to be the most likely to result in differences (the smallest usable needle size at the highest usable suspension density for this needle size). Three series of ejections were performed, each consisting of five consecutive 1 µL ejections of 50% (w/v) '2 µm' microsphere suspension through a 33 G needle. The mean results from these three series are shown in Figure 3.21 (with error bars omitted for clarity). The distributions were visually very similar and within experimental error of one another. The mean sizes for the five ejections were (from first to last) 1.80, 1.84, 1.79, 1.85 and 1.82 µm. Microsphere number was therefore considered an appropriate surrogate measure for protein load when delivering '2 µm' microspheres.

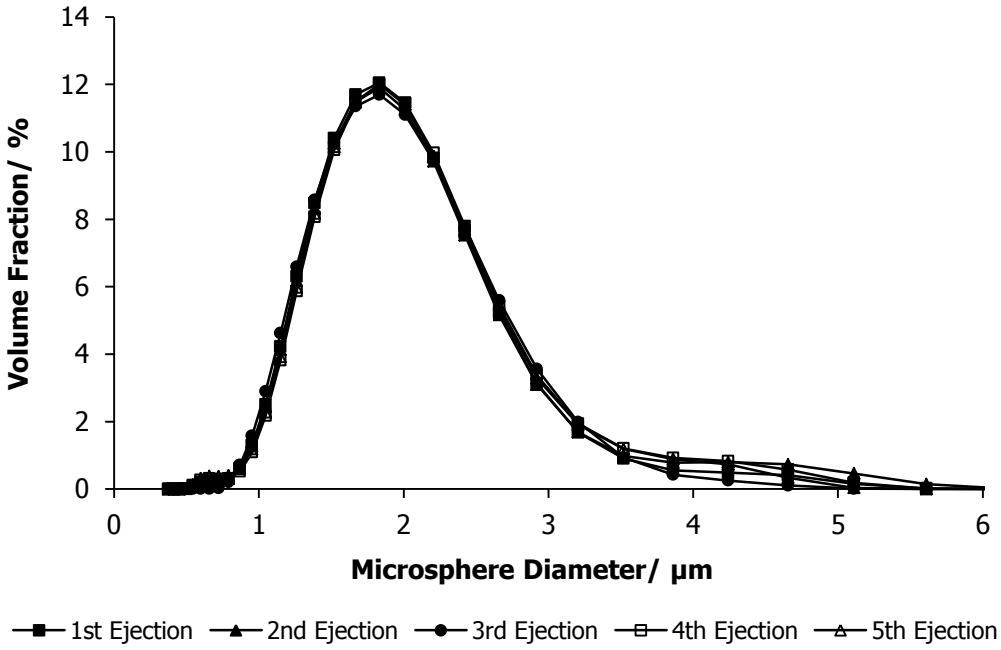

Figure 3.21 – Mean laser diffraction-derived size distributions resulting from series of five consecutive ejections of 1 µl of 50% (w/v) suspension of '2 µm' microspheres (early batches, see Figure 3.14 (a)) from a total volume of 5 µl (microlitre syringe, 33 G needle, n =3, error bars omitted for clarity).

For '2 μm' microspheres counting was performed using an improved Neubauer haemocytometer. Figure 3.22 shows exemplar microsphere counts resulting from repeated and consecutive ejections of the same volume of suspension of the same density. In this case, as was observed across many conditions, the repeated ejections contained microsphere numbers which were within experimental error of one another. On the other hand, the microsphere numbers resulting from three series of consecutive ejections showed very wide variability. This suggested that water may not be an adequate suspension fluid for achieving consistent delivery of microsphere suspensions. It was postulated that this may be due to insufficient viscosity of the fluid. This could have led both to settling of the microspheres out of suspension and also to preferential ejection of the fluid in the early ejections.

The unreliability of '2 μm' microsphere production (see Section 3.3.2 and Figure 3.14) meant that this hypothesis could not be tested on the smallest microsphere size. Instead subsequent evaluation was performed using the '15 μm' and '100 μm' microsphere sizes only. In order to try to reduce the impact of the issues discussed above carboxymethyl cellulose (CMC) was considered as a viscosity modifier for use in the delivery of microspheres.

Figures 3.23 and 3.24 show photographs of suspensions of '15 μm' and '100 μm' microspheres in various concentrations of CMC at various intervals of time after they were homogenously suspended in those fluids. CMC Concentrations higher than 1% (w/v) were not considered as they were found to be too viscous to be drawn up through the needle sizes under investigation. Microsphere batches of both sizes were found to contain subpopulations which were porous enough to float in all suspension fluids. This meant that they never reached a point at which all microspheres had settled to the bottom of the containers. The times to 'complete settling' were therefore considered to be the times beyond which no further change was observed (Table 3.2). Increasing the concentration of CMC was found to result in large increases in the times to complete settling for both microsphere sizes.

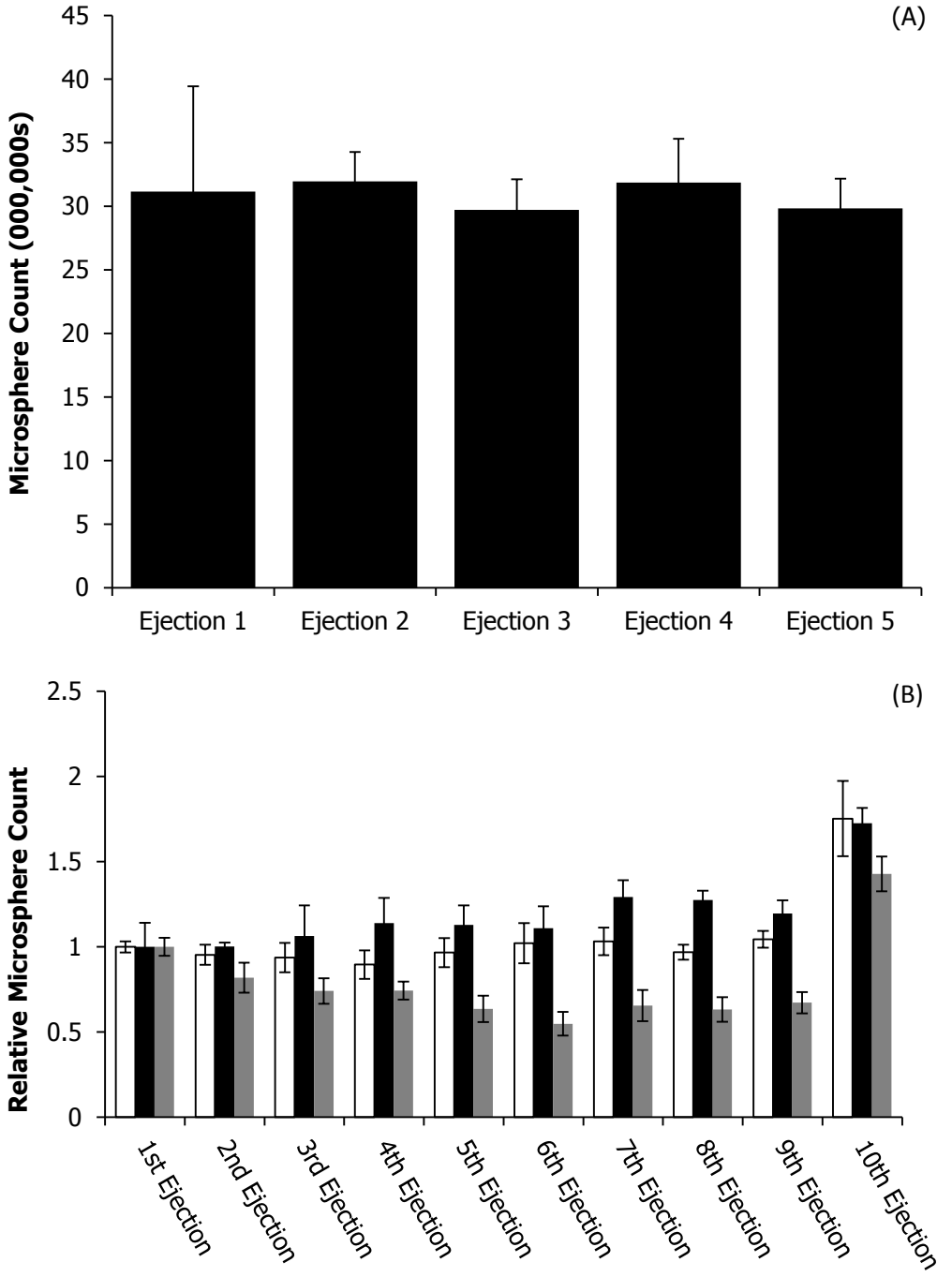

Figure 3.22 – Microsphere numbers resulting from 0.5 µL ejections of 25% (w/v) suspension of '2 µm' microspheres (early batches, see Figure 3.14 (a)) through a 33 G needle. Counting performed using an improved Neubauer haemocytometer. Error bars are one standard deviation. Shown are five repeated ejections (A) and three series of ten ejections performed consecutively from total volumes of 5 µL (B), with each series normalised to its own first ejection to allow direct comparison.

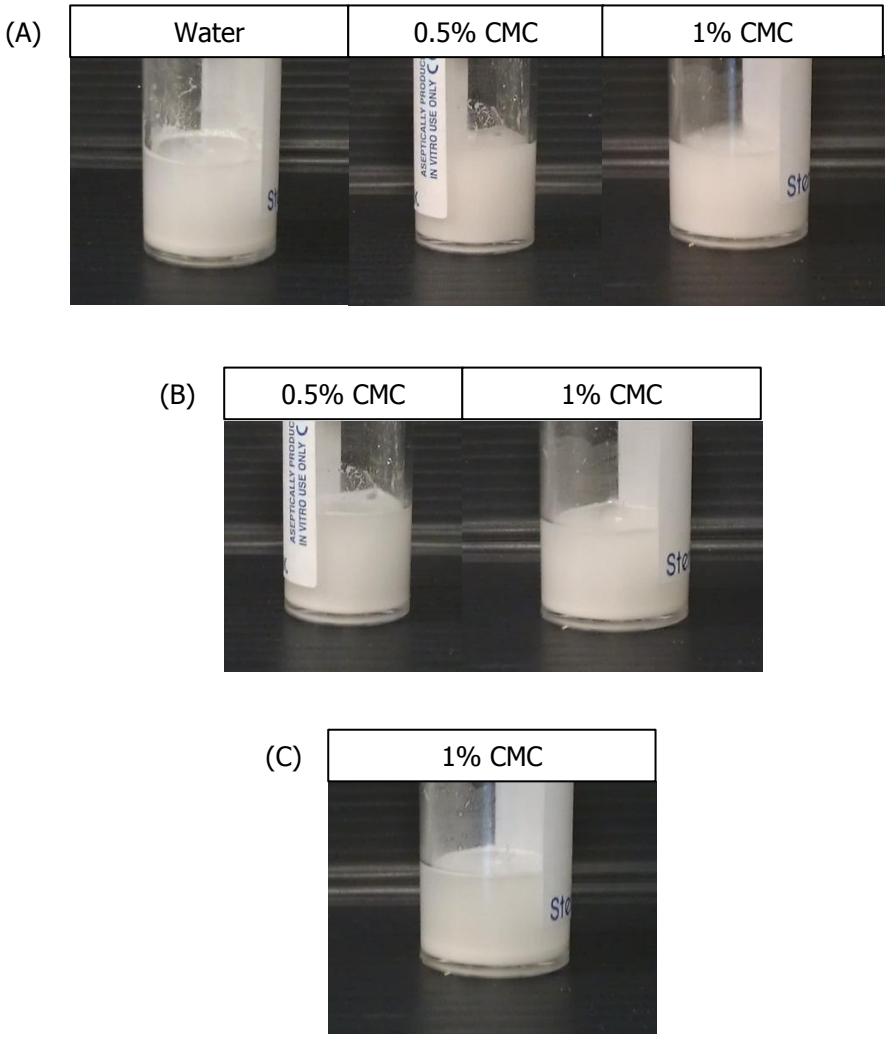

Figures 3.23 – Representative images of 10% (w/v) suspensions of '15 μm' microspheres in various concentrations of CMC and at various times after they were homogenously suspended in those fluids – 5 minutes (A), forty minutes (B) and 90 minutes (C).

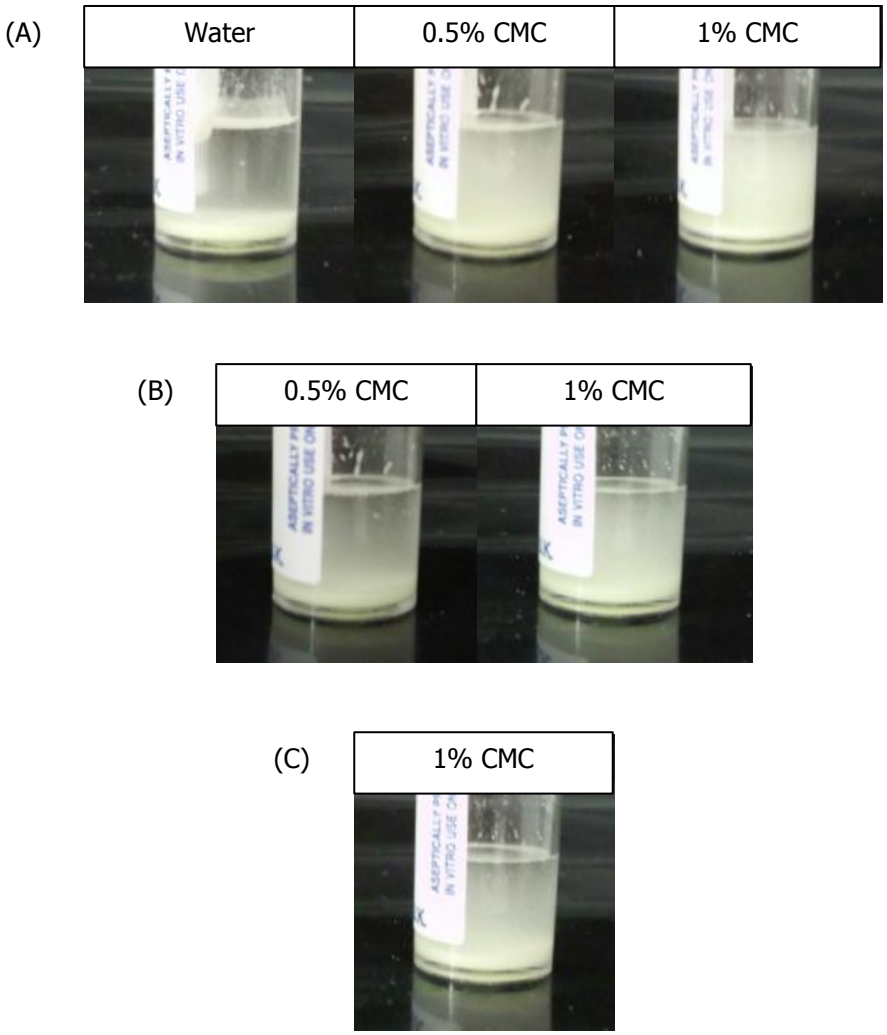

Figures 3.24 – Representative images of 10% (w/v) suspensions of '100 μm' microspheres in various concentrations of CMC and at various times after they were homogenously suspended in those fluids – 5 minutes (A), 20 minutes (B), 40 minutes (C) and 120 minutes (D).

	Time to Complete Settling/ min	
CMC Concentration/ % (w/v)	**15 µm Microspheres**	**100 µm Microspheres**
0	5	5
0.5	40	20
1.0	90	40

Table 3.2 - Times taken for PLGA microspheres to completely settle out of suspension in various concentrations of CMC as assessed visually.

Following this various combinations of CMC concentration, microsphere suspension density and needle size were assessed for their ability to allow repeated drawing up and ejection of suspension (Tables 3.3 and 3.4). For both microsphere sizes suspensions in water of up to 75% (w/v) could be drawn up and ejected with appropriate choice of needle size. It was also found in all cases that increasing the concentration of CMC used in the suspension fluid resulted in a decrease in the maximum usable suspension density for a given needle size. It also resulted in an increase in the minimum usable needle size.

			Suspension Density/ % (w/v)			
[CMC]/ % (w/v)	Needle Type	Needle Inner Diameter/ µm	10	20	50	75
0	P-i-N	340	✓	✓	✓	×
0	24G	310	✓	✓	✓	✓
0	26G	260	✓	✓	✓	✓
0	P-i-N	260	✓	✓	✓	×
0	30G	160	×	×	×	×
0.5	P-i-N	340	✓	✓	×	×
0.5	24G	310	✓	✓	✓	×
0.5	26G	260	✓	✓	×	×
0.5	P-i-N	260	✓	✓	×	×
0.5	30G	160	×	×	×	×
1.0	P-i-N	340	✓	✓	×	×
1.0	24G	310	✓	✓	×	×
1.0	26G	260	×	×	×	×
1.0	P-i-N	260	×	×	×	×
1.0	30G	160	×	×	×	×

Table 3.3 - Summary of feasibility (✓) or unfeasibility (×) of repeatedly drawing up and completely ejecting '15 µm' PLGA microsphere suspension through various needle sizes at various suspension densities (i.e. various proportions of solid content). Note that P-i-N denotes the use of a positive displacement, plunger-in-needle syringe.

			Suspension Density/ % (w/v)			
[CMC]/ % (w/v)	Needle Type	Needle Inner Diameter/ μm	10	20	50	75
0	20G	600	✓	✓	✓	✓
0	22G	410	✓	✓	×	×
0	P-i-N	340	✓	×	×	×
0	24G	310	✓	×	×	×
0	P-i-N	260	×	×	×	×
0	26G	260	×	×	×	×
0.5	20G	600	✓	✓	✓	×
0.5	22G	410	✓	✓	×	×
0.5	P-i-N	340	✓	×	×	×
0.5	24G	310	×	×	×	×
0.5	P-i-N	260	×	×	×	×
0.5	26G	260	×	×	×	×
1.0	20G	600	✓	✓	×	×
1.0	22G	410	✓	×	×	×
1.0	P-i-N	340	✓	×	×	×
1.0	24G	310	×	×	×	×
1.0	P-i-N	260	×	×	×	×
1.0	26G	260	×	×	×	×

Table 3.4 - Summary of feasibility (✓) or unfeasibility (×) of repeatedly drawing up and completely ejecting '100 μm' PLGA microsphere suspension through various needle sizes at various suspension densities (i.e. various proportions of solid content). Note that P-i-N denotes the use of a positive displacement, plunger-in-needle syringe.

Next a more comprehensive study of delivery consistency was undertaken. The first step, as for the smallest microsphere size, was to assess whether different ejections resulted in microsphere populations with the same size distributions. For both remaining microsphere sizes 5 µL volumes of suspension were ejected as series of 1 µL volumes (n = 6). In order to create sufficient obscuration to allow laser diffraction-based size analysis the ejections of the six series were combined prior to analysis. For each microsphere size the analysis was performed using the smallest needle size through which suspension could be ejected and the maximum suspension density which was usable for this needle size. Examination of the size distributions shown in Figures 3.25 and 3.26 show only very slight differences between those derived from different ejections within consecutive series. Mean sizes for the five ejections of '15 µm' microspheres were 14.5, 14.5, 15.0, 15.2 and 15.7 µm from first to last ejection. The equivalent values for '100 µm' microspheres were 78.0, 68.6, 66.6, 78.9 and 77.1 µm. As a result of these analyses, microsphere number was considered an appropriate surrogate measure for theoretical delivered protein load.

The next analysis undertaken was to determine whether light blocking-based particle counting would provide an accurate means to determine the number of microspheres contained within ejection volumes. A particle size and count standard (Count-Cal Particle Size Standard, catalogue no. CC70, Thermo Scientific, Loughborough, UK) was counted at various different nominal numbers and the coefficient of variance (the standard deviation as a proportion of the mean) derived at each point (n = 6, Figure 3.27). This coefficient provided a lower limit to the level of ejection-to-ejection variability that could reliably be measured. For measured variabilities below this level the coefficient of variance for the standard was taken as an upper limit to the true variability instead. In either case the larger of the two values was referred to as the 'process variability'.

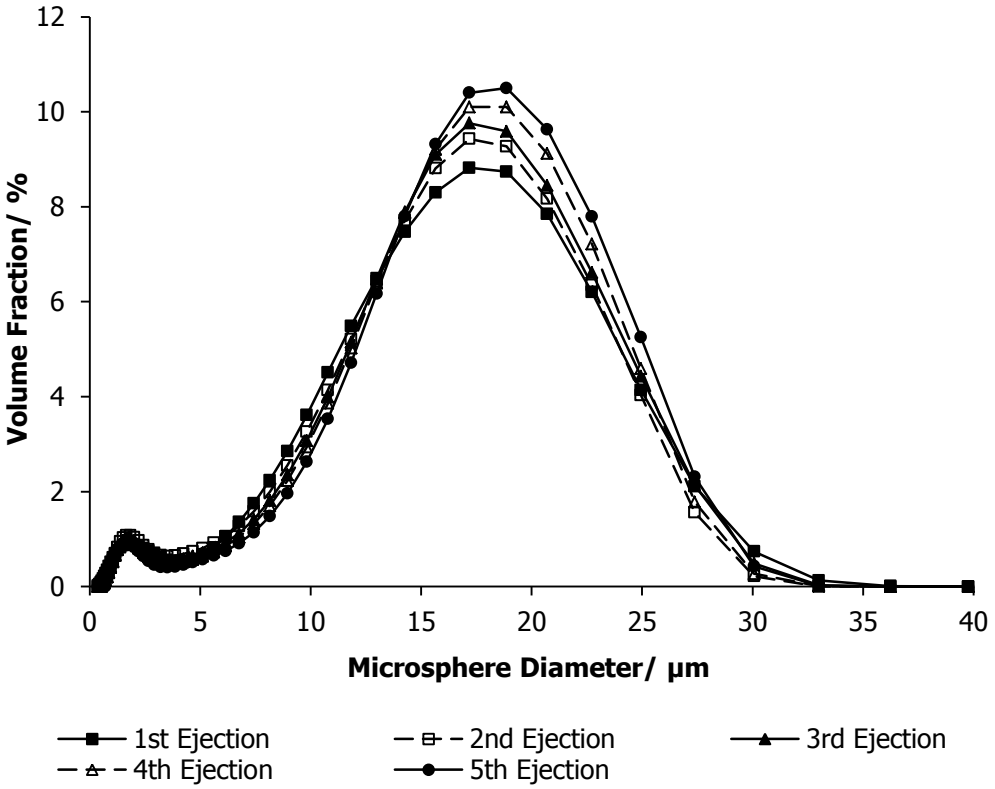

Figure 3.25 – Laser diffraction-derived size distributions resulting from series of five consecutive ejections of 1 µl of 50% (w/v) suspension of '15 µm' microspheres from a total volume of 5 µl (plunger-in-needle syringe, 260 µm inner diameter needle). Six series pooled for analysis to generate sufficient obscuration for accurate laser diffraction-based microsphere sizing.

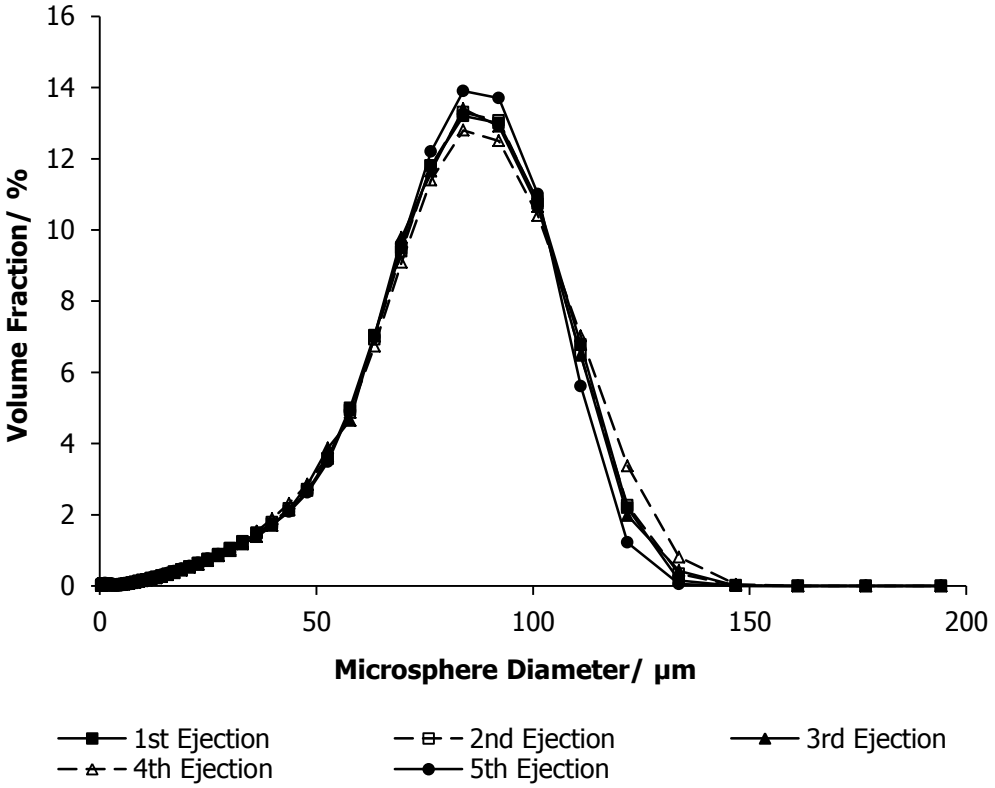

Figure 3.26 – Laser diffraction-derived size distributions resulting from series of five consecutive injections of 1 µl of 10% (w/v) suspension of '100 µm' microspheres from a total volume of 5 µl (microlitre syringe, 24 G needle). Six series pooled for analysis to generate sufficient obscuration for accurate laser diffraction-based microsphere sizing.

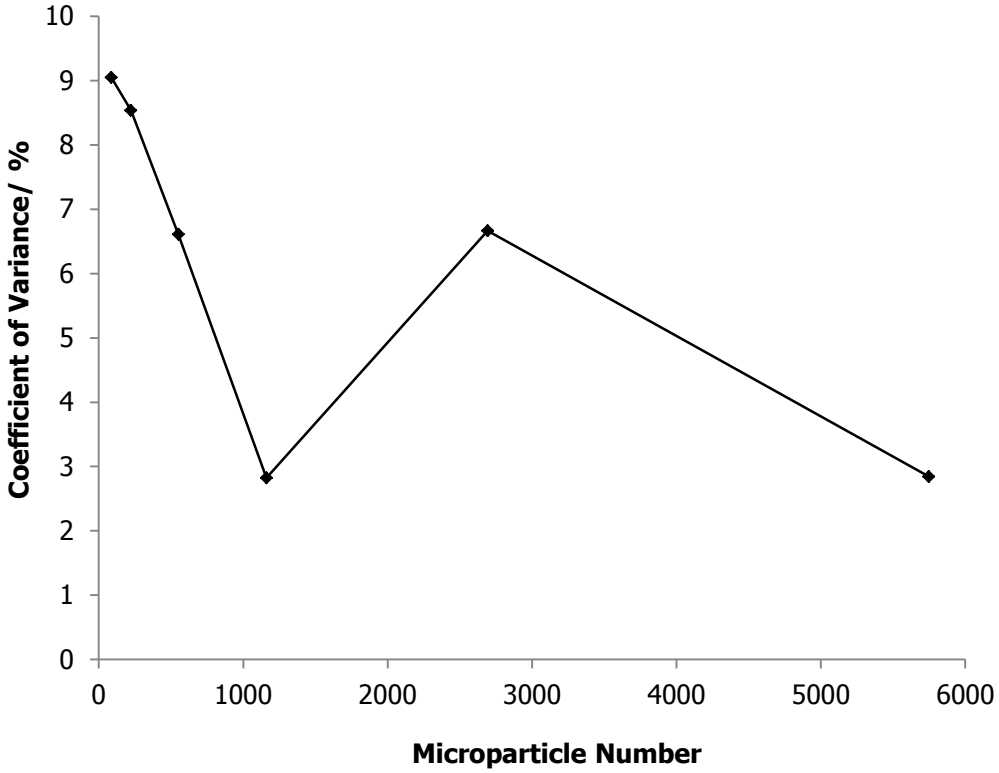

Figure 3.27 – Assessment of the reliability of light blocking as a method to count microspheres. A 70 µm microsphere size and count standard was counted at a variety of nominal microsphere numbers (n = 6) and the coefficient of variance (the standard deviation as a proportion of the mean) of the counting process derived at all levels.

Figure 3.28 shows a comparison of the microsphere counts resulting from two sets of six series of six 1 µL repeated ejections of 20% (w/v) '100 µm' microsphere suspension through a 20 G needle. One set of results utilised 0.5% and the other utilised 1% (w/v) CMC as the suspension fluid. The stark difference between the two demonstrated the significant effect that an alteration in fluid viscosity could have on the consistency of delivery. These results also demonstrated the ability of the light blocking-based counting technique to distinguish between consistent and inconsistent delivery conditions.

Later results utilising microlitre and plunger-in-needle syringes for patterning of microspheres (see Section 3.3.5) demonstrated that these simple delivery systems were not capable of exerting control at the single microsphere level. A more sophisticated system was pursued for the purpose of patterning (see Section 3.3.6) and therefore a full systematic screening study of syringe-based delivery conditions was not undertaken.

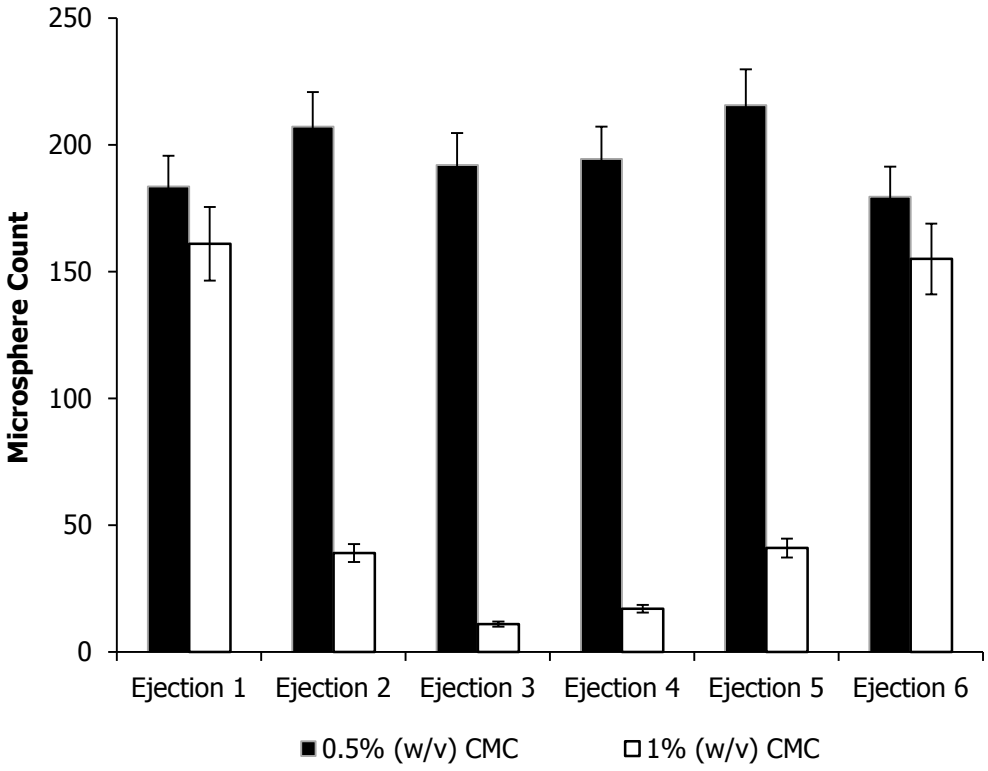

Figure 3.28 – '100 µm' PLGA microsphere numbers as measured by light blocking for exemplar microinjection-based delivery conditions to illustrate the ability of the technique to distinguish between consistent and inconsistent delivery. Six series of six repeated ejections of 20% (w/v) suspension (1 µL per ejection) were performed through a 20 G needle using either 0.5 or 1% (w/v) CMC as the suspension fluid. Means are plotted with error bars showing the 'process variability'.

3.3.5 Patterning of Microspheres via Manual Microinjection & Micromanipulation

Initial patterning attempts were made using microlitre and plunger-in-needle syringes in conjunction with a manual micromanipulator. Sub-microlitre volumes of microsphere suspension were delivered into 0.75% (w/v) agar as a simple-to-produce, readily-available model hydrogel. Microspheres were fluorescently-labelled with acridine orange to allow for successful visualisation. Volumes as low as 0.1 µL could be delivered and these volumes could be separated by as little as 750 µm whilst still remaining distinct.

Figures 3.29 and 3.30 show representative fluorescence microscopy images of grids formed from multiple consecutive sub-microlitre deliveries of suspensions of '15 µm' and '100 µm' microspheres respectively. As can be seen in these images it was found that the number of microspheres contained within each injection site and the shape and size of the injection sites varied widely. Additionally, and particularly for '15 µm' microspheres the numbers of microspheres in each site were still relatively large even at the smallest deliverable volumes. Although the grids appeared regular it was found that the separations between individual sites of delivery could vary by as much as 100 µm either side of the nominal spacing. As a result of these observations patterning with this MM system was not pursued further.

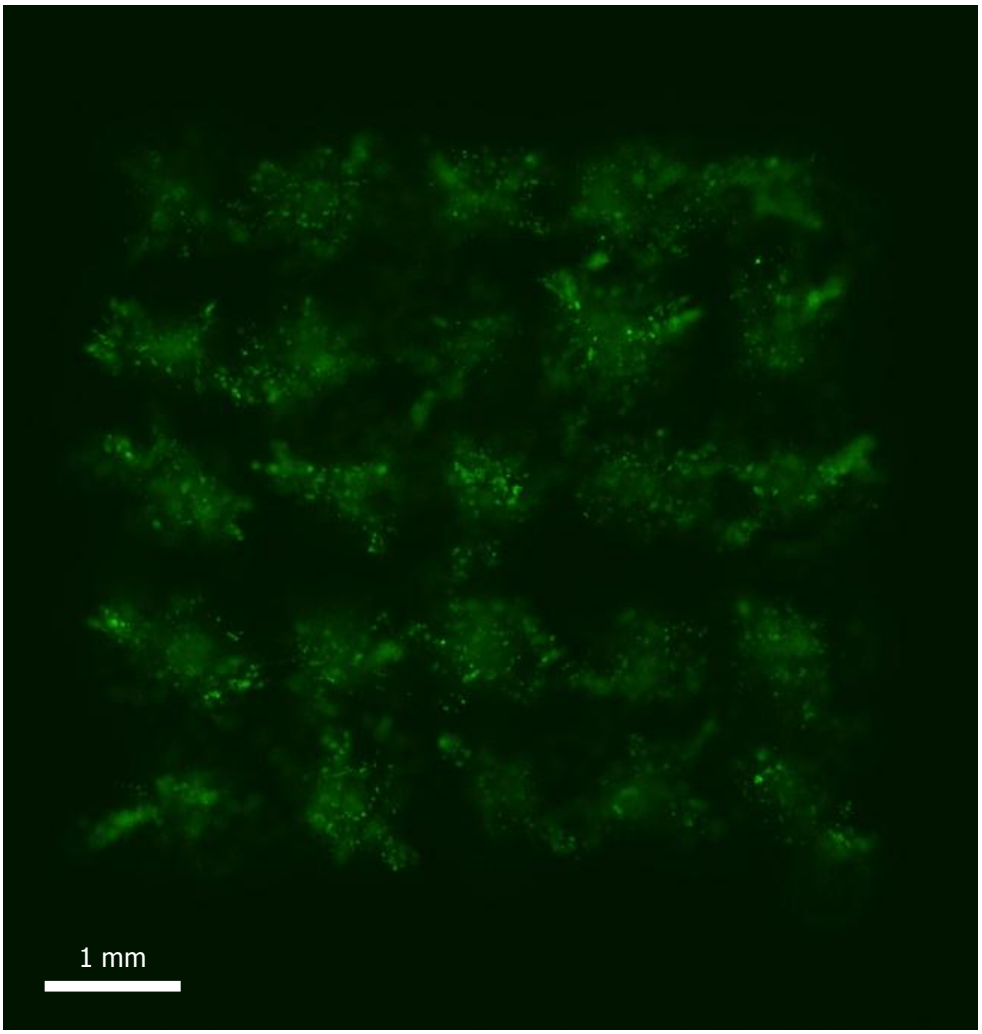

Figure 3.29 - Representative fluorescence microscope image showing 0.1 µl volumes of 10% (w/v) suspension of '15 µm' fluorescent PLGA microspheres in 1% (w/v) CMC delivered into 0.75% (w/v) agar gel at nominal spacings of 1 mm using a manual micromanipulator in conjunction with a plunger-in-needle microlitre syringe.

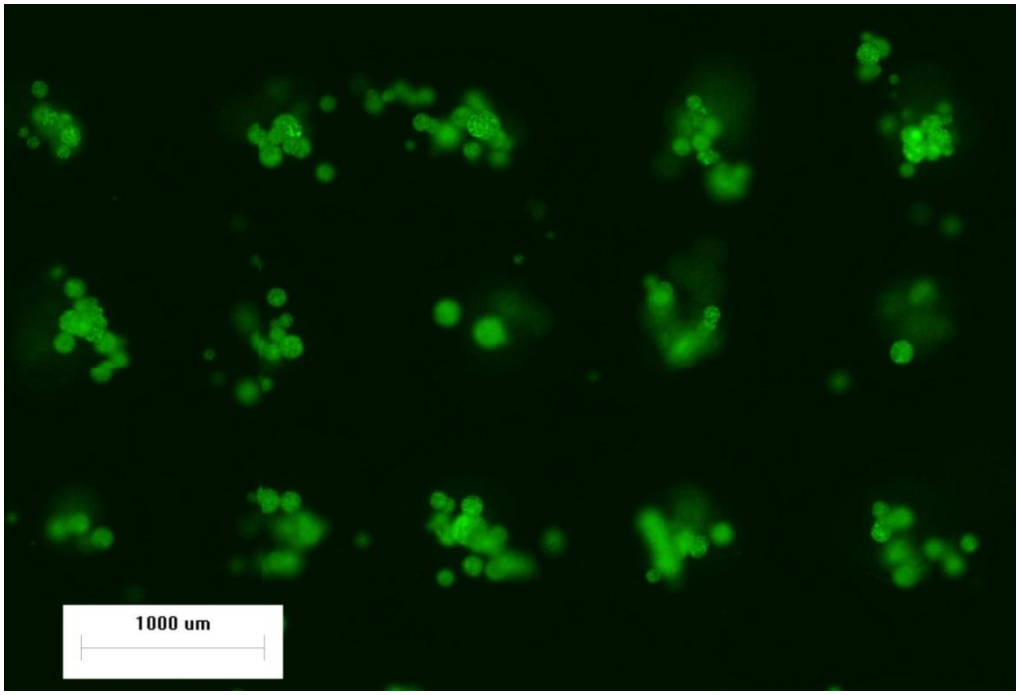

Figure 3.30 - Representative image showing 0.1 µl volumes of 10% (w/v) suspension of '100 µm' fluorescent PLGA microspheres in 0.5% (w/v) CMC delivered into 0.75% (w/v) agar gel at nominal spacings of 1 mm using a manual micromanipulator in conjunction with a plunger-in-needle microlitre syringe.

3.3.6 Patterning of Microspheres via Semi-Automated Microinjection & Micromanipulation

To overcome the limitations of the fully manual MM system utilised above a manual microinjector was used in conjunction with programmable micromanipulators to pattern microspheres individually into cooling/setting agarose. The exemplar images shown in Figure 3.31 demonstrate that patterning of individual '100 μm' microspheres was achieved on length scales as small as around 100 μm.

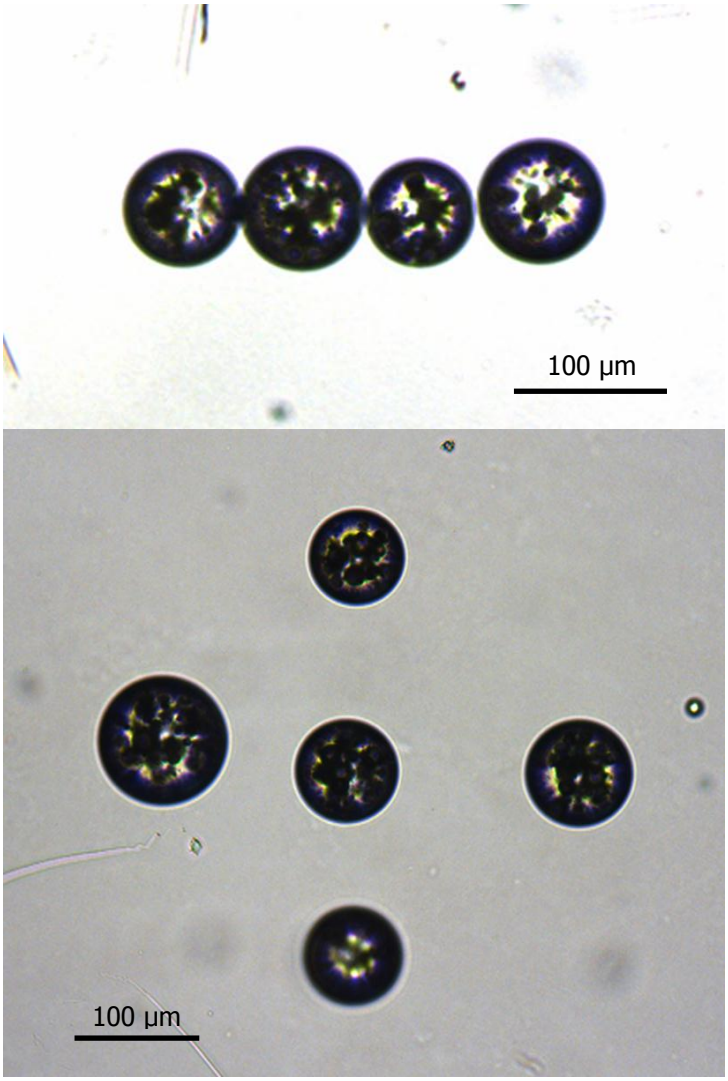

Figure 3.31 - Representative images showing '100 µm' PLGA microspheres positioned individually into 1% (w/v) agarose hydrogel using a manual microinjector in conjunction with a semi-automated, programmable micromanipulator.

3.4 Discussion

3.4.1 Generating Protocols for the Production of Three Sizes of Microspheres

Double emulsion microsphere fabrication protocols were generated which were capable of producing PLGA microspheres with three different mean sizes – around 2, around 15 and around 100 µm. This fulfilled the criterion outlined in Section 3.1.5 that the protocols should be able to produce microspheres with mean sizes covering around two orders of magnitude. Furthermore the three size distributions showed distinct separation with little or no overlap as determined by laser diffraction-based size analysis. The availability of these microspheres of distinct sizes should allow for the generation of distinct release profiles to tailor the presentation of any given protein to match its natural expression pattern in the biological process to be replicated.

A range of homogenisation speeds were tested in conjunction with a 20% (w/v) PLGA concentration in the oil phase for the production of microspheres with mean sizes of around 100 µm. Subsequently a range of polymer concentrations were evaluated for use with the maximum 9000 rpm speed of the high speed homogeniser to generate microspheres with means around one and two orders of magnitude lower. The resulting mean sizes and the final conditions for manufacture are shown in Table 3.5.

	`2 µm `Microspheres	`15 µm` Microspheres	`100 µm' Microspheres
Actual Mean Microsphere Size/ µm	2.02	13.6	84.4
Polymer Concentration/ % (w/v)	2	17	20
Primary Homogenisation Speed/ rpm	9000	9000	2000
Internal Aqueous Volume/ µl	1000	118	100
Beaker Size/ ml	100	25	25
Secondary Homogenisation Speed/ rpm	9000	9000	2000
External Aqueous Volume/ ml	500	200	200
Beaker Size/ ml	600	250	250

Table 3.5 – Optimised production conditions for three different sizes of microsphere using double emulsion manufacture with external aqueous phases consisting of 0.3% (w/v) PVA and overnight stirring at 300 rpm for microsphere hardening.

The mean size shown in Table 3.5 for '2 μm' microspheres is derived from the first three batches produced which showed single-peaked size distributions and only 4% variation in mean. However subsequent batches showed multiple peaks per size distribution indicating high degrees of oil droplet aggregation in the secondary emulsion prior to microsphere hardening. Additionally, very high batch-to-batch variation showed that this process was not sufficiently robust.

All nine batches of this smallest microsphere size showed a main peak around 2 μm and there are a number of examples in the literature of the use of double emulsion techniques to produce microspheres of this size and smaller[329,345-349]. Many of these protocols utilise sonication for at least one emulsification step in the place of homogenisation. It may be that the high speed homogenisers used here do not produce a powerful enough emulsification effect to act on the whole of the relatively large volumes of liquid involved in small microsphere manufacture. If this is the case then it is likely to also be true that the stirring used during microsphere hardening was insufficient to ensure maintenance of separation of the original oil droplets. A reduction in the total batch mass may therefore help to overcome the problems experienced producing microspheres of around 2 μm mean size.

For '15 μm' and '100 μm' microspheres all size distributions were single-peaked and the distributions from multiple batches showed good visual overlap. The coefficients of variance for the mean sizes of these two types of microspheres were found to be 9.3 and 18.5% respectively. It is difficult to give these figures a proper context since the issue of batch-to-batch variability is rarely explicitly addressed in published studies. However significant batch-to-batch behavioural differences were not seen in the work presented in this thesis. In other words different batches of microspheres prepared using the same conditions showed very similar flow behaviour and protein release.

SEM imaging of both sizes of microspheres confirmed the size distributions seen by laser diffraction and showed them to be predominantly spherical with surfaces which

were smooth and almost completely lacking in pores. This surface smoothness suggests that the microparticles should have a relatively low burst release for their size[350-352], which is highly desirable in most protein release applications.

3.4.2 Production of Fluorescent Microspheres

To attempt to produce fluorescent '2 μm' microspheres which could be successfully imaged once delivered into tissue engineering scaffolds, the encapsulation of acridine orange via the double emulsion process was evaluated. However significant aggregation was evidenced by the multi-peaked nature of the size distributions, which extended to sizes of up to around 50 μm. To ensure that fluorescent microspheres could be used as accurate models for non-fluorescent microspheres in patterning studies it was important that their size distributions closely matched. As a result none of the attempts undertaken could be considered successful. Since the concentration of fluorophore used did not seem to affect the degree of aggregation seen in the microsphere production process, this approach was not pursued further.

Encapsulation of fluorescein via a single emulsion technique was also evaluated but this tended to result in a greater degree of aggregation than was seen with double emulsion-based labelling. As with acridine orange labelling the amount of fluorophore used did not appear to affect the degree of aggregation. As a result this approach was also discontinued. Due to the problems encountered with consistent production of '2 μm' microspheres, fluorescent or otherwise, the effective labelling of this size of microsphere was no longer considered a priority.

Fluorescent versions of the larger two sizes of microparticles ('15 μm' and '100 μm') were successfully produced via double emulsion by utilisation of 0.1 mg mL^{-1} acridine orange as the inner aqueous phase. Mean sizes of these two populations of fluorescent microspheres closely reflected those of the blank versions (14.4 and 91.0 μm for fluorescent versions as compared to 13.6 and 84.4 μm for blank). Batch-to-

batch variabilities in both cases were low (4.9 and 9.1% coefficients of variance respectively) with good visual overlap of size distributions. In both cases the addition of fluorophore actually appeared to reduce batch-to-batch variation, but the statistical significance of this result could not be assessed. SEM imaging was performed on batches of both sizes and confirmed the size distributions seen via laser diffraction. It also showed the spherical nature and almost entirely smooth and non-porous surfaces of the microspheres to have been maintained upon addition of the fluorophore.

3.4.3 Effect of Triblock Incorporation on Protein Release Rate from Microspheres

It was found that increasing the proportion of Triblock in the polymer mix used for microsphere manufacture led to more rapid release of encapsulated protein. This trend was particularly clear once the first 24 hours of release (the burst release) was discounted. Since a very large burst release of protein is often highly undesirable or even detrimental biologically, it is envisaged that many clinical applications of these microspheres would involve a pre-washing and incubation step designed to avoid the burst release protein being administered. As a result the burst-subtracted release curves seen in Figure 3.20 (b) may actually be the more clinically-relevant.

Previous work involving the addition of hydrophilic release modifiers to PLGA (microparticulate) scaffolds has shown similar trends of increasing rate of protein release with increasing hydrophilic content[308,353-355]. As stated earlier it is believed that this acceleration is due to the encouragement of greater water ingress into the polymer matrix. This results in more rapid diffusion of protein through the matrix as well as more rapid polymer degradation. For instance, it has been explicitly demonstrated that a PLGA-PEG-PLGA copolymer exhibited greater water uptake than plain PLGA[356]. In the work presented here a 30% (w/w) Triblock level led to

particularly accelerated release and a fundamentally-altered release profile which lacked the lag phase of a normal tri-phasic PLGA release profile. This result has also been demonstrated using pure PLGA-PEG-PLGA copolymer microspheres[353], suggesting that there is some critical threshold above which protein release occurs in a single phase. This switch to a single phase profile is expected to be accompanied by a change to a release mechanism which is mediated only by diffusion and not by polymer degradation.

It is well-established in the literature that variation of microsphere size can have a dramatic effect on the release rate of proteins encapsulated therein[294,343,346]. Together with the Triblock-based manipulation discussed above this means that the suite of protocols developed here should allow the development of complex controlled release formulations for the independent delivery of multiple proteins.

3.4.4 Consistency of Delivery of Microspheres via Microlitre and Plunger-in-Needle Syringes

A major aim of the work undertaken in this chapter was to establish whether microlitre and plunger-in-needle syringes were viable delivery systems for PLGA microspheres. It was found that with appropriate choice of needle size suspensions as dense as 75% (w/v) in water could be repeatedly drawn up and ejected from these syringes. The minimum needle inner diameters which could be used with '15 μm' and '100 μm' microspheres were found to be 260 and 310 μm respectively. These sizes were important as they provided a lower limit to the separation between injection sites which could be used for later patterning studies and thus the maximum patterning resolution which could theoretically be achieved.

Another key consideration was the ability of these syringes to eject microsphere suspension in a way which would result in the delivery of a consistent mass of encapsulated protein. Under challenging conditions the microsphere size

distributions resulting from different ejections were found to be consistent with one another for both microsphere sizes. Under the assumption that microspheres had uniform density and that the mass of a microsphere determined its encapsulated protein load this meant that the number of microspheres in an ejection was a valid surrogate measure of the protein load.

Initial studies using haemocytometer-based microsphere counting demonstrated that consecutive ejections could contain highly variable microsphere numbers when using water as the suspension fluid. It was postulated that the low viscosity of the fluid may have led to rapid settling out of microspheres from suspension and/or preferential ejection of suspension fluid in early ejections. CMC was assessed as a viscosity modifier for improving consistency of delivery. It was found that the addition of 1% (w/v) CMC to suspension fluids could increase the time taken for microspheres to settle out of suspension by almost two orders of magnitude. The downside to CMC addition was that it lowered the maximum suspension density of microspheres which could be used in conjunction with a given needle size. It also increased the minimum needle size which could be used with each size of microsphere, thus decreasing any potential future patterning resolution.

Based on repeated measurements of a count standard light blocking-based particle counting was found to be an effective method to quantify microspheres in sub-microlitre ejection volumes. Across the entire range studied coefficients of variance were found to be below 10%, with some as low as 3%. This suggested that relatively small variabilities in ejected microsphere numbers could be reliably detected, though this ability was less effective at very low numbers.

The utilisation of this technique allowed differentiation between delivery conditions which resulted in consistent microsphere numbers and those which did not. Early results demonstrated that ensuring consistent delivery was more complex than simply increasing the viscosity of the suspension fluid. In some cases increasing the viscosity by increasing the concentration of CMC led to increased variability.

Systematic assessment and optimisation of consistency was not conducted at this stage since delivery via microlitre and plunger-in-needle syringes was not found to be an effective route to fine-scale patterning. These syringes may however provide a suitable route of delivery for microspheres into single precise tissue locations as part of tissue engineering therapies. For these applications optimisation would be required for the specific microsphere population to be used. The size distribution of the population would be expected to be the dominant factor in defining its flow properties.

3.4.5 Patterning of Microspheres via Microinjection and Micromanipulation

Initial studies examined the ability of a manual micromanipulator in conjunction with microlitre and plunger-in-needle syringes to pattern fluorescently-labelled microspheres within 0.75% (w/v) agar as a model hydrogel. Test grids produced by multiple consecutive injections of microsphere suspension were visually regular in terms of their spacings. However quantitative assessment of the spacings showed that they were subject to deviations of up to 100 μm from that which was intended. The morphology and size of individual delivery sites were found to vary widely, along with the number of microspheres contained within them.

To resolve these issues a more sophisticated, semi-automated MM system was utilised which consisted of a manual microinjector combined with two programmable micromanipulators. This setup allowed '100 μm' microspheres to be individually positioned into cooling and setting agarose solutions with separations as low as around 100 μm. This technique has excellent potential utility for the creation of fine-scale complex protein environments such as interacting gradients. However it was found to be strongly dependent on operator skill level due to the need for delicate corrections to microsphere motions caused by fluid flows created during injections. This dependence could be alleviated to an extent if the technique could be refined to allow microspheres to be delivered dry. This may involve them being held on the

end of very narrow bore glass needles in the fashion of holding pipettes for intracytoplasmic sperm injection[357].

The relatively short times taken for agarose solutions to cool and set limited the number of microspheres which could be included in patterns. In order to create larger patterns it may be necessary to consider alternative patterning protocols in future studies. For instance, microspheres could be suspended in warm agarose and then transferred individually onto a patterning substrate in small volumes of solution which would set to secure the microspheres in place. Once the pattern was produced the hydrogel 'islands' could be lyophilised and the patterned microspheres stored for future use. Additionally and subsequently bulk hydrogels could be formed around the patterns with or without encapsulated cells, or indeed cells could be cultured on the original patterning substrate. This protocol was developed during unpublished work conducted by Dr. Glen Kirkham at the University of Nottingham.

Another limitation of this patterning approach is that agarose is known to be a poor substrate for *in vitro* cell growth due to its low capacity for cell adhesion[358,359]. An adaptation of a previously-published protocol was used to modify the agarose used here via conjugation with gelatin in order to improve its cell compatibility (see Appendix). Although further work remains to fully optimise this protocol and characterise the cell response to the resulting materials, they show promise as potential *in vitro* cell culture substrates.

The studies outlined in this chapter demonstrate that MM techniques can be used to individually pattern PLGA microspheres with high resolution. They can be patterned into hydrogel environments which can be rendered conducive to cell proliferation. This patterning is intended to allow the creation of complex protein signal environments which may replicate those seen in normal and perturbed developmental and repair processes. These environments could then be used to study fundamental cell biology and to evaluate potential tissue engineering therapies *in vitro*.

The final steps in the development of MM techniques to this end are to demonstrate that the microsphere patterns created are converted into the expected protein signal patterns and that these are then translated into patterns of cellular behaviour. Proteins released from patterned microspheres in cell-free conditions would be expected to form gradients and other heterogeneous distributions only transiently. It is believed that the presence of cells to act as a sink for the diffusing protein could stabilise these heterogeneous distributions for long enough to allow them to exert a biological effect. Demonstrating and quantifying both stabilisation and biological efficacy will be a key step in the development of MM patterning techniques.

It should also be noted that the patterning presented thus far is conducted in two dimensions for ease and effectiveness of imaging and assessment. However the micromanipulators used in these studies function equally effectively in each of the three spatial dimensions. The extension of patterning into the third dimension is therefore predominantly a practical and logistical challenge and mainly concerns the development of a patterning protocol allowing real-time positioning and visualisation across multiple focal planes.

4. Generation of Hydrogels from the Extracellular Matrix of Bovine Bone

4.1 Introduction

4.1.1 The Extracellular Matrix

The extracellular matrix (ECM) surrounds the cells in every tissue in the body and is a complex mix of proteins, glycosaminoglycans (GAGs) and proteoglycans (PGs) which is vital to effective tissue function[360-362]. Collagen in its many forms is the most abundant protein in the ECM[363] but others which are common to many tissues include fibronectin[364], laminin[365] and elastin[366]. GAGs are nitrogen-containing polysaccharides which bind as side-chains to core proteins to form PGs[367]. PGs commonly found in the human body include aggrecan[368], fibromodulin[369], decorin[370], biglycan[370,371], perlecan[372] and versican[370,373].

Perhaps the most basic function of the ECM is to provide overall structure to tissues and therefore to control and define their mechanical properties. In connective tissues such as tendons and ligaments fibrillar proteins including collagen and elastin provide resistance to tensile loading[374-376]. In contrast in tissues such as articular cartilage the high PG content ensures the maintenance of adequate tissue hydration for the even distribution of compressive load[368,377].

Another major function of the ECM is to provide anchorage for the cell types constituting each tissue in the complex arrangements which are necessary for correct function. In this regard the ECM may be divided into the interstitial matrices which surrounds the cells in mesenchymal tissues and the basement membranes (BMs) on which various epithelial and endothelial cell layers sit. BMs have specialised structures in which collagen, fibrillin and laminin are important constituent

proteins[365,378]. Across both types of matrix much of the adhesion of cells to the ECM is mediated through the binding of integrins on the cell surface to arginine-glycine-aspartic acid (RGD) peptide sequences[379-382]. These are particularly common in fibronectin[383] but are also found in other major ECM proteins[384-386].

It had been thought that the function of the fibrillar proteins of the ECM was restricted to those purposes discussed thus far i.e. providing mechanical strength and supporting the growth of adherent cells. However it has subsequently been found that these 'structural' proteins can have biological functionality and can affect cell phenotype[361,387,388]. This creates a 'dynamic reciprocity' between a cell and its local ECM microenvironment in that cells can modulate their local matrix and vice versa. This process is further enhanced by the ability of GAGs in the matrix (especially heparin) to bind growth factors and other important signalling proteins[389]. In this way signals can either be sequestered locally to protect them from degradation and/or more efficiently presented to cell surface receptors.

4.1.2 Decellularised ECM as a Biomaterial

The ultimate aim of any treatment developed in tissue engineering is to recreate the native architecture and function of the tissue being repaired or replaced[390]. Much effort has gone into achieving this aim through the development and modification of synthetic biomaterials to reproduce some or all of the functions of the ECM[391-393]. However an alternative route has also been taken in which the native ECM is itself used as a biomaterial[394,395]. With appropriate preparation ECM-derived materials can recapitulate the functions of the native ECM more completely than can stepwise-modified synthetic materials.

The first requirement for any biomaterial prepared from ECM is that it should be decellularised to ensure the removal of any material which may provoke immune response on implantation[396]. Decellularisation may be achieved via a number of

approaches[397,398] including the use of ionic[399-402] or non-ionic detergents[401-404], enzymatic treatments[404-406], acid treatment[407-409], induction of osmotic shock and lysis[410,411], application of high hydrostatic pressures[412-414] or combinations thereof[405,415-422]. These different approaches have relative advantages and disadvantages but they all inevitably cause some alteration to both the structure and biological functionality of the matrices on which they are utilised. The aim of any optimised decellularisation protocol is to minimise these alterations whilst still removing cellular and genetic material to an acceptable extent. The approach taken to achieve this aim will depend on the biochemical composition, density and cellularity of the tissue to be processed.

ECM materials have been extracted from several species and from a wide range of different tissues[399-401,403,405,407,409-414,416-420,423-438]. Since ECMs derived from different tissues will often be composed of similar constituents it may be supposed that a single tissue could provide a 'one size fits all' ECM material for universal use. However recent results in the literature have shown tissue-specificity of the beneficial effects exerted by decellularised ECM materials[420,425,439,440]. As a result ensuring the ability to successfully decellularise a wide range of tissues remains a priority if ECM-derived scaffolds are to be broadly clinically-applicable.

The results of *in vivo* pre-clinical studies utilising a number of these materials demonstrate their potential as therapies for the repair of tissue defects[408,409,411,417,423,426,430,436,441,442]. The implantation of ECM scaffold materials is typically associated with an early inflammatory response which is indicative of constructive remodelling[396,443-445]. Following this the scaffolds are typically resorbed within 3 months of implantation and completely replaced by new host tissue[411,442,446-448]. The precise mechanisms involved in this remodelling process are yet to be fully understood. However the positive results obtained with these materials in pre-clinical studies have led to the launch of a number of products which have been successfully utilised in the clinic[432,449].

Despite the successes achieved with ECM-derived scaffold materials in (pre-)clinical tissue engineering there has been little attempt to generate criteria for defining a material as decellularised. A recent publication set three such criteria which were the absence of visible nuclei in appropriately-stained histological sections, a residual double-stranded DNA (dsDNA) level of less than 50 ng per mg of dry material and an absence of DNA fragments of more than 200 base pairs in length[450]. However it is not clear what the scientific basis is for these particular figures and few of the materials used successfully in the studies referred to above had been explicitly assessed against these criteria.

A recent development in the use of ECM scaffold materials has been the conversion of sheets and powders into hydrogels. This has typically been achieved by the use of pepsin to digest and solubilise the materials, resulting in solutions which can be induced to form hydrogels by altering the pH and/or temperature to normal physiological levels[421,439,451-457]. Homogenisation in high salt buffers has also been used and this too results in solutions which can be induced to gel by changes in pH or temperature[458-461]. These hydrogels have been shown to be favourable *in vitro* culture environments for cells isolated from the tissues from which the gels are derived[421,439,452,455,458,459].

Pre-gel ECM-derived solutions constitute truly injectable scaffolds and are potentially compatible with a range of construct production and processing technologies including bioplotting (see Section 1.2.6). It has been shown that when ECM scaffold materials are enzymatically degraded this results in the production of peptide fragments which can exhibit strong chemotactic and anti-microbial effects[429,454,462-465]. When these materials are implanted as sheets or powders then these bioactive peptides are not available immediately upon implantation, leading to delays in progenitor cell recruitment and bacterial infection suppression. However hydrogels composed of peptide fragments produced by enzymatic digestion of decellularised ECM may exert these effects with only a minimal delay.

4.1.3 Bone Grafting and Demineralised Bone Matrix

For the treatment of volumetric tissue loss in bone autograft is still considered the gold standard treatment since it provides patient-specific cells and matrix to achieve optimal repair[466-468]. Nevertheless issues of donor site morbidity and lack of sufficient tissue availability have led to the desire for alternative treatments. In this regard terminally-sterilised cadaveric allograft has found extensive use in orthopaedic surgery[468,469]. However the mineralised nature of bone ECM results in sub-optimal availability of osteoinductive constituents which may limit the rate and extent of new bone formation[470,471].

To this end protocols have been developed to produce demineralised forms of allograft bone, known as demineralised bone matrix (DBM)[472,473]. DBM is typically produced by acid demineralisation and organic solvent treatment for lipid extraction[470,474-476]. Some studies have shown DBM formulations to be osteoinductive *in vitro* and potentially able to match the performance of autograft and/or allograft[476-480]. These positive *in vitro* results can be attributed at least in part to the retention of both osteogenic and angiogenic growth factors within DBM materials[481-484].

Some *in vivo* studies utilising DBM materials have shown them to have comparable or superior performance to autograft and/or allograft in ectopic implantation[476], bone repair[485-487] and spinal fusion[481,488,489]. However not all studies show consistently beneficial effects[474,490-492] and the efficacy of DBM formulations appears to be more variable *in vivo* than *in vitro*[484,493]. Despite this a large number of DBM products are in current clinical use[473].

There are a number of suggested reasons why clinical results with DBM may be so variable including issues of batch-to-batch, process and donor variability[473,479,483,484,494,495] and also the sterilisation method used[472]. The preferred form of DBM for use in surgery is one in which the powder is suspended in a viscous liquid carrier to form a putty or paste which can be injected or moulded to fill cavities

and defects[477,492,495-497]. The carriers used in these formulations have been suggested as another source of variation in outcome[492,495,498,499]. Indeed significant nephrotoxicity has been demonstrated in rat models for one commonly-used carrier (glycerol)[499,500].

If DBM could be processed into a form which was capable of gelation then this would mean that it could be delivered minimally-invasively via injection. Additionally it could be used to localise cells and exogenous growth factors to the defect site. This material could also be used as a carrier for DBM powder in load-bearing areas where the gel alone may not be mechanically competent. This carrier may have reduced toxicity as well as additional bioactivity relative to those currently utilised. The generation of ECM-derived hydrogels has not yet been demonstrated in bone, perhaps due to concerns that the harsh processing used to demineralise the tissue may cause damage to the protein structure which would inhibit the ability of the material to undergo gelation.

4.1.4 Aims & Objectives

The overall aim of the work presented in this chapter is to generate hydrogels from the ECM of bovine bone. These materials would have the direct clinical utility discussed above but in addition they would have the potential to be formed into microparticles for microinjection-based patterning (see Chapter 3) and to be used for bioplotting-based construct patterning (see Chapter 5). An additional aim is to address the question of whether demineralisation alone is truly sufficient to adequately decellularise bone.

More specific objectives include the demonstration of complete demineralisation and the assessment of the extent of decellularisation in both DBM and decellularised DBM (referred to as DECM). Enzymatic digestion will be used to solubilise both DBM and DECM and the ability of these materials to gel will be assessed along with their

gelation kinetics. The gel structures, mechanical properties and cell compatibilities *in vitro* will also be evaluated.

The final objective of this work is to demonstrate that the ECM-derived materials can be formed into gel particles or beads. This would allow exogenous growth factors and other proteins to be incorporated into the beads and potentially released at a cell-mediated rate.

4.2 Materials and Methods

4.2.1 Demineralisation of Bovine Bone

See Section 2.11.

4.2.2 Decellularisation of Demineralised Bone Matrix

See Section 2.12.

4.2.3 Micro-Computed Tomography (µCT) Imaging

See Section 2.16.

4.2.4 Haemotoxylin and Eosin (H & E) Staining of Demineralised and Decellularised Bovine Bone

See Section 2.14.

4.2.5 Purification & Extraction Protocol for Pico Green Assay to Quantify DNA

See Section 2.15.

4.2.6 Hydroxyproline Assay for Collagen Quantification

See Section 2.17.

4.2.7 Hydrogel Formation from Demineralised and Decellularised Bovine Bone

See Section 2.13.

4.2.8 Spectrophotometric Analysis of Gelation Kinetics

See Section 2.18.

4.2.9 Rheological Analysis of Hydrogel Gelation and Mechanical Properties

See Section 2.19.

4.2.10 Scanning Electron Microscopy (SEM) Imaging

See Section 2.6 for general methodology. Imaging was performed using a Philips XL30 electron microscope and three samples were imaged for each condition examined.

4.2.11 Assessment of Cell Proliferation on ECM-Derived Hydrogels

Collagen, DBM and DECM pre-gel solutions at 3 and 6 mg mL^{-1} were plated into 96-well plates (100 µL per well, n = 12) and allowed to gel for one hour at 37°C. After this, human osteosarcoma (hOS) or murine primary calvarial (mPC) cells were added to each well in 100 µL of their respective media at a variety of seeding densities (5 – 20,000 cells per well). At each of 48 and 72 hours post-seeding, six wells were

assessed for cellular proliferation with respect to unseeded gel controls and in comparison with tissue culture plastic (TCP). Assessment of proliferation was via the MTS assay (see Section 2.25).

4.2.12 Bead Formation from Alginate and ECM-Derived Hydrogels

See Section 2.20.

4.3 Results

4.3.1 Demineralisation and Decellularisation of Bovine Bone

As stated earlier the first aim of the work presented in this chapter was to demonstrate effective demineralisation of bovine bone. A subsequent step was to assess whether a decellularisation step was necessary post-demineralisation to ensure adequate removal of cellular material. The approach used to address these aims was developed by Dr. Lisa White, William Bowen, Paramjeet Dhadda and Hareklea Markides at the University of Nottingham based on previously-published protocols[406,470,501]. Full details are in Sections 2.8 & 2.9 but in brief – milled bovine bone was soaked in 0.5 M HCl for 5, 18 or 24 hours and this was followed by lipid extraction in chloroform/methanol. After this came an optional 24 hour decellularisation step in trypsin/EDTA and finally lyophilisation for 48 hours. The appearance of the bone-derived material at each stage can be seen in Figure 4.1. It was found that only a 24 hour acid soak was sufficient to completely demineralise the bone tissue as assessed by μCT imaging (Figure 4.2). This time span was used for all future production of both DBM and DECM.

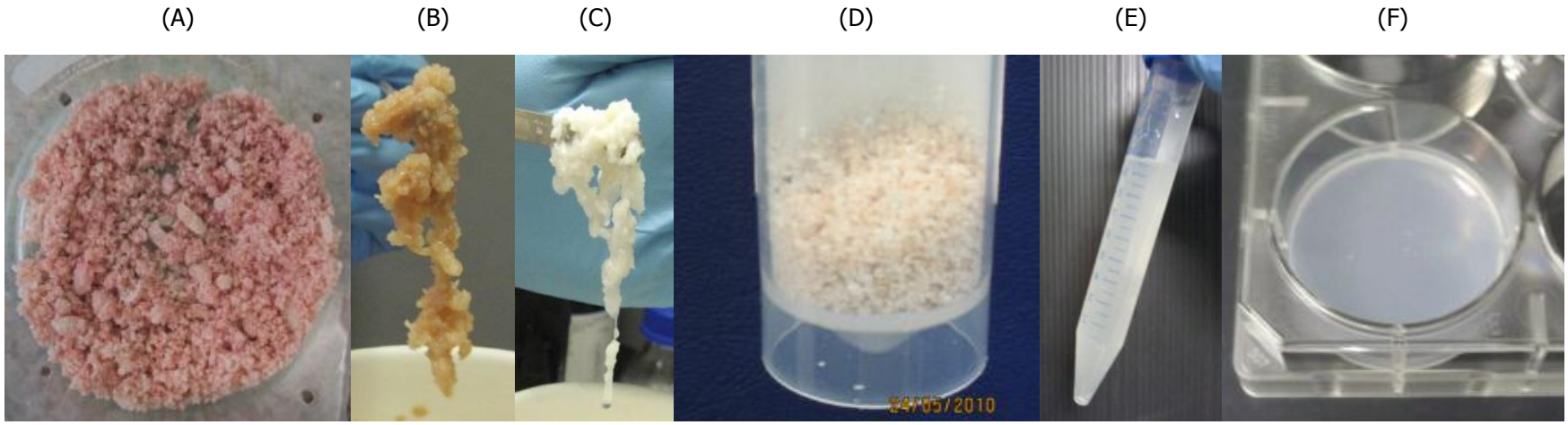

Figure 4.1 – Representative images showing the appearance of bovine bone-derived materials at various stages of processing. Left-to-right – bone chips resulting from milling of cancellous bone (A), bone chips after demineralisation (B), hydrated DBM matrix post-lipid extraction (C), powder resulting from freeze drying of lipid extracted material with (DECM) or without (DBM) decellularisation step (D), pepsin-digested DBM/DECM-derived solution (E) and hydrogel formed from pepsin-digested material (F).

The next step was to assess the extent of decellularisation in both DBM and DECM, in order to deduce whether the enzymatic decellularisation step was necessary to sufficiently reduce cellular content. Imaging of H & E stained histological sections showed that DBM contained intact cell nuclei whilst DECM contained no visible nuclear material (Figure 4.3). Quantification of the dsDNA content of the materials was undertaken using the PicoGreen® assay. Results showed that both materials had residual dsDNA levels which were significantly below the 50 ng per mg dry material which has been quoted in the literature as a criterion for effective decellularisation[450] (Figure 4.4). Furthermore there was no statistically-significant difference between the dsDNA contents of the two materials when normalised to mass (1.96 ng mg^{-1} for DBM, 2.35 ng mg^{-1} for DECM). However when the change in material mass pre- to post-decellularisation was taken into account it was found that approximately 40% of the total dsDNA content of DBM was removed by trypsin/EDTA treatment.

The final characterisation technique performed on the DBM and DECM materials was the hydroxyproline assay for quantification of collagen. The collagen contents of the two materials were found to be 93 and 92% by weight for DBM and DECM respectively (Figure 4.5). There was no statistically-significant difference between these results and so based on this parameter at least it seems that the trypsin/EDTA decellularisation step may not significantly alter the biochemical composition of the material.

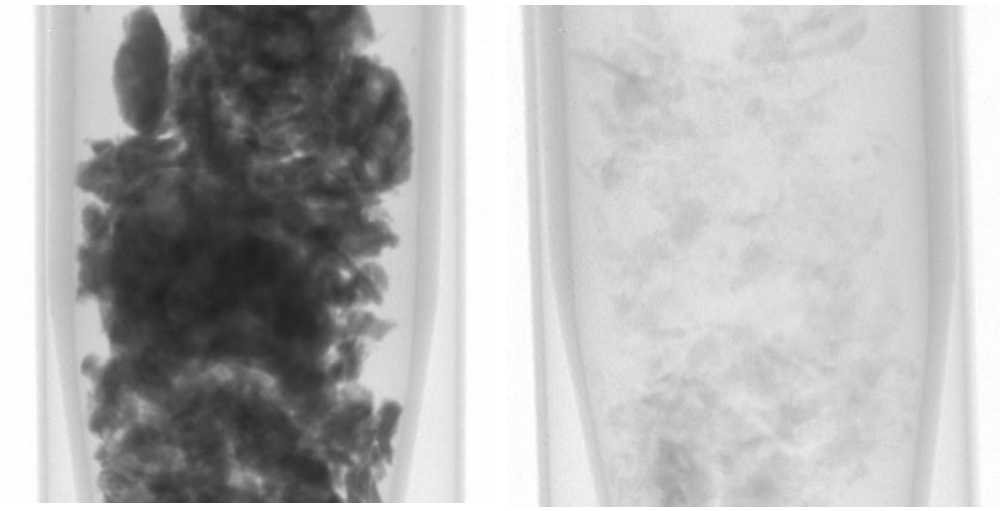

Figure 4.2 – Representative transmission images from μCT analysis of milled bone chips (left) and DBM (right) to show qualitative loss of mineral (dark grey/black) during processing. Images provided by Dr. Lisa White, Paramjeet Dhadda and Hareklea Markides.

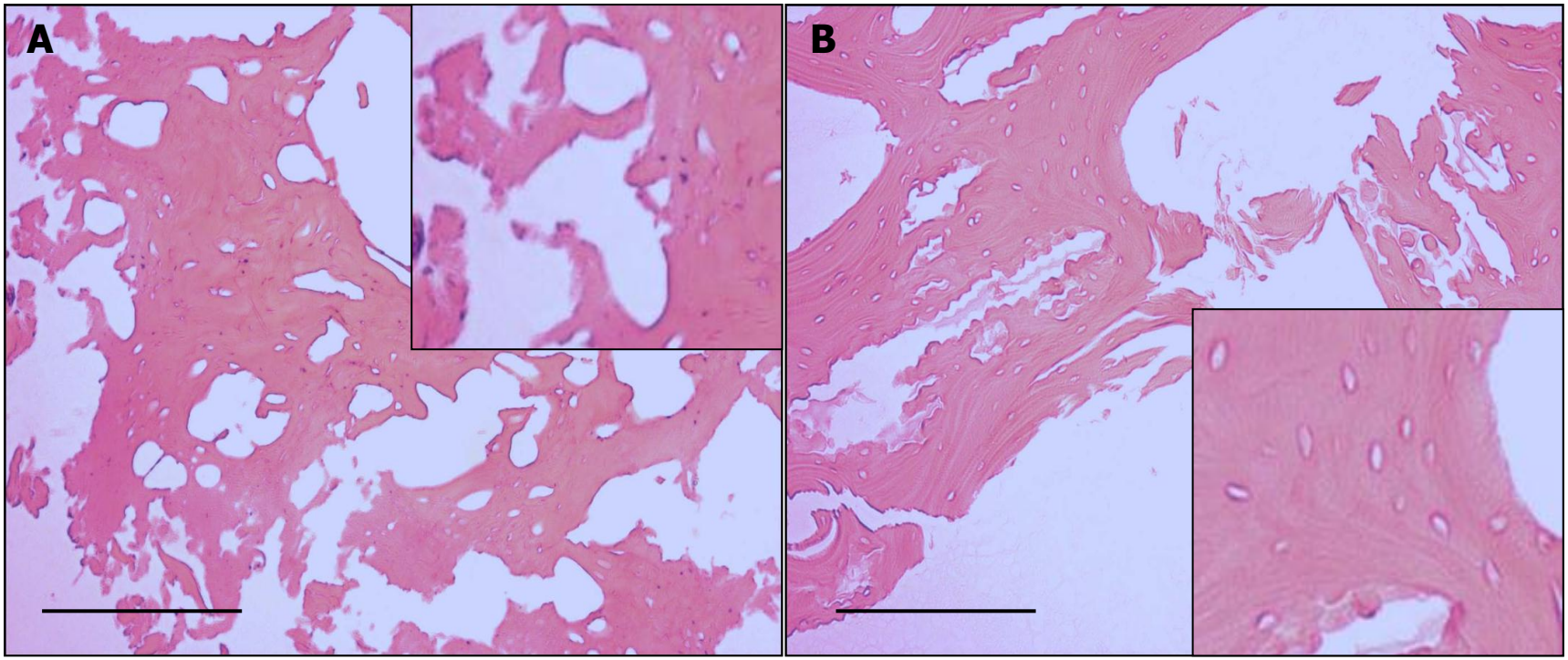

Figure 4.3 – Representative bright field microscopy images of sections of DBM (A) and DECM (B) stained with haemotoxylin to show cell nuclei in blue/black and counterstained with eosin to show matrix constituents. Insets show high magnification images and scale bars are 100 μm. Images provided by Dr. Lisa White, Paramjeet Dhadda and Hareklea Markides.

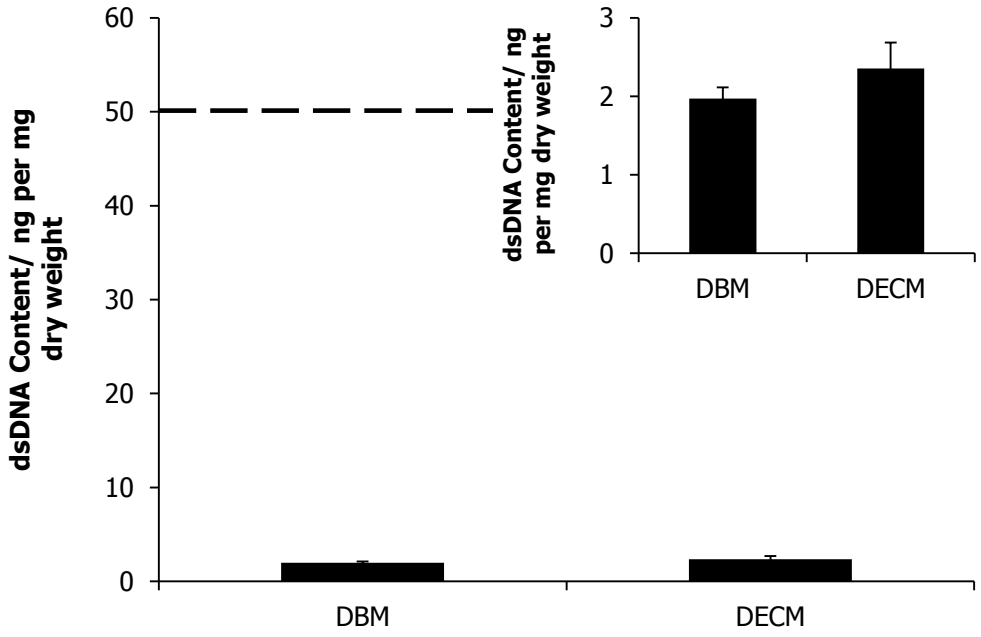

Figure 4.4 – Quantification of dsDNA for DBM and DECM via phenol/chloroform/isoamyl alcohol extraction and the PicoGreen® assay. Also shown is a widely-used criterion for consideration of a material as successfully decellularised (50 ng dsDNA per mg dry material). The inset graph shows more closely the values obtained for DBM and DECM. Error bars show one standard deviation for three samples, each of which was assayed in triplicate.

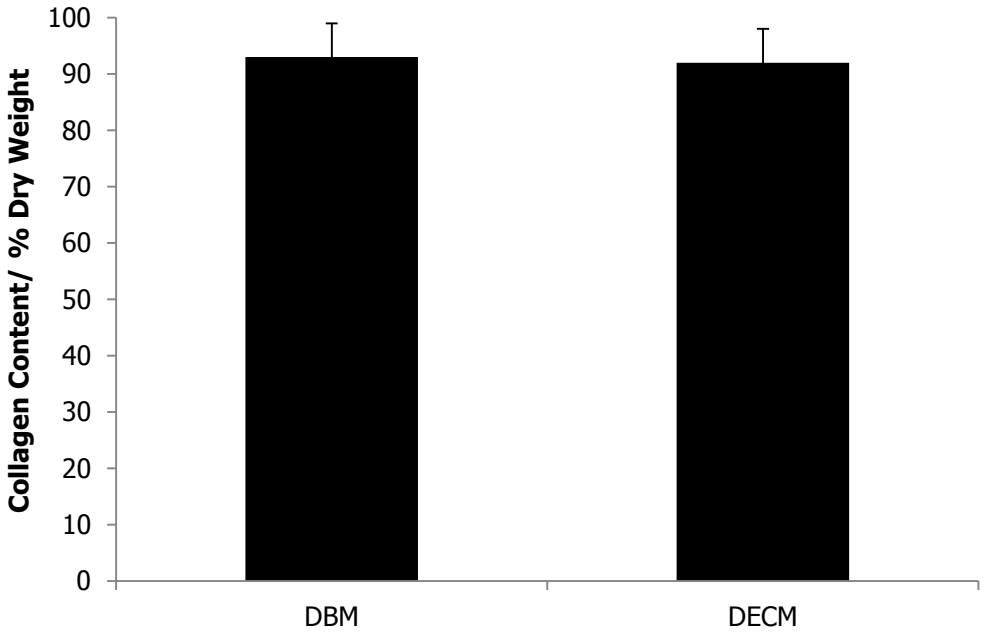

Figure 4.5 – Quantification of the collagen content (fraction of dry weight) of DBM and DECM powders via quantification of the non-proteinogenic amino acid hydroxyproline. Error bars are one standard error resulting from assaying four samples of each material in triplicate.

4.3.2 Generation of Hydrogels from Demineralised and Decellularised Bovine Bone

Both DBM and DECM could be successfully solubilised by room temperature incubation with pepsin at low pH, resulting in viscous cloudy liquids. These liquids could be induced to form hydrogels by neutralisation and incubation at 37°C (see Figure 4.1 for appearance of the materials before and after gelation).

Spectrophotometric analysis was used to assess the gelation kinetics of DBM and DECM-derived materials using collagen as a comparator since this was the major constituent of the pre-digestion ECM-derived powders. Figure 4.6 (a) shows that DBM-derived hydrogels display very similar optical properties to collagen, whilst DECM-derived hydrogels are significantly more opaque. Figure 4.6 (b) shows the normalised results of this analysis which more clearly illustrate the kinetics of gel formation. As expected, 6 mg mL^{-1} gels form more quickly than 3 mg mL^{-1} for all materials, though this difference is largest for DECM-derived gels. Collagen undergoes the most rapid gelation, followed by DECM-derived gels with DBM-derived gels being the slowest to completion (cessation of change of optical properties). The majority of the change in absorbance for ECM-derived materials has occurred by 15 – 30 minutes after the initiation of incubation, but gelation is not complete until around 30 minutes later.

Rheological analysis was used to assess the evolution of the mechanical properties of the three materials during gelation (Figure 4.7). As defined rheologically (storage modulus greater than loss modulus) all materials were considered to be gels almost immediately upon the temperature being raised to 37°C. At both concentrations collagen gelled very quickly, reaching its maximal storage modulus within 2 – 3 minutes. ECM-derived materials were found to have profiles which were much more distinct from collagen's than those observed spectrophotometrically.

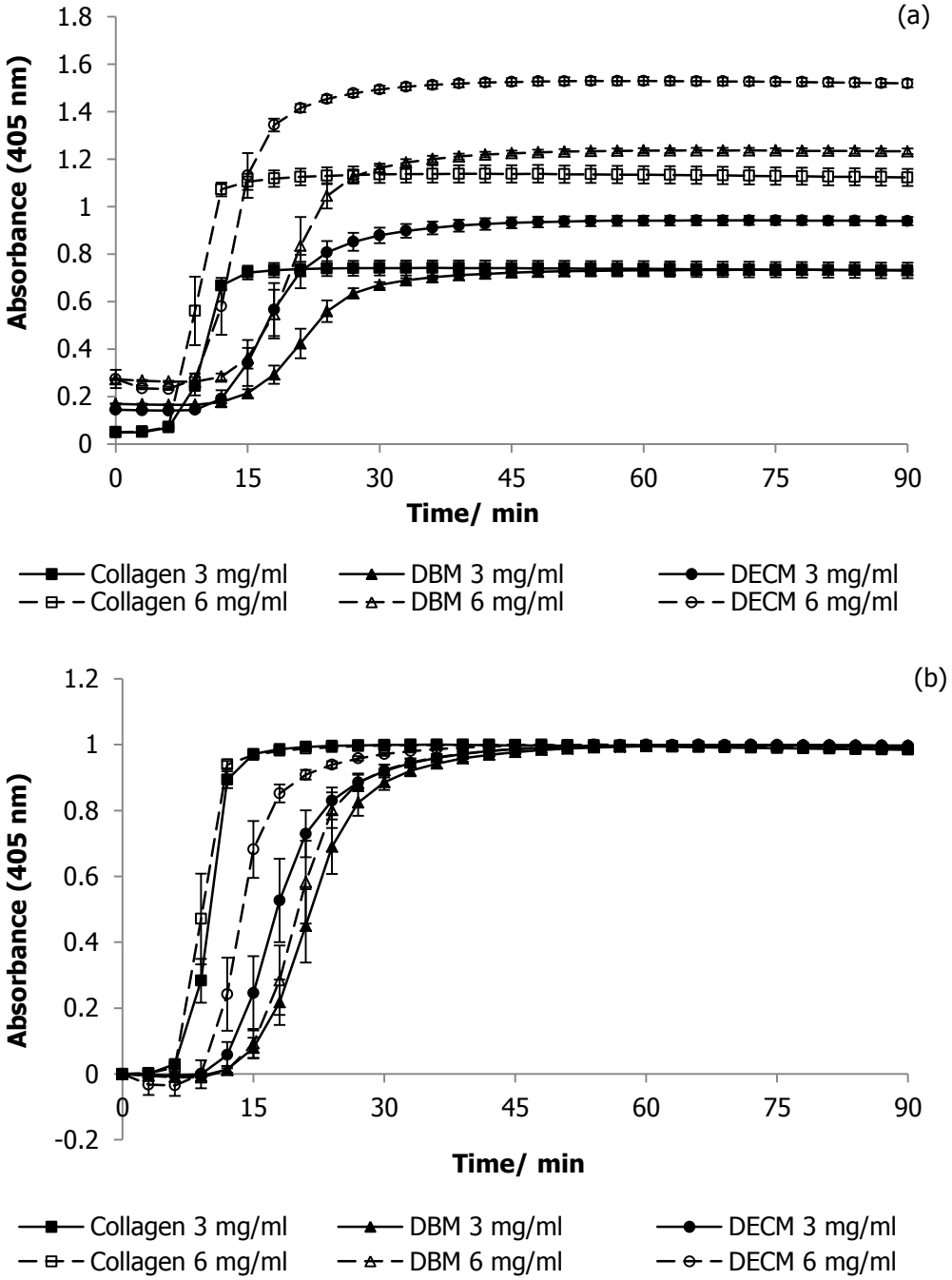

Figure 4.6 – Spectrophotometric assessment of gelation kinetics for collagen, DBM and DECM (n = 6) via absorbance measurements at 405 nm. Error bars are one standard deviation. Shown are both raw values (a) and values which are normalised (b) such that the initial reading is zero and the maximum value reached is one.

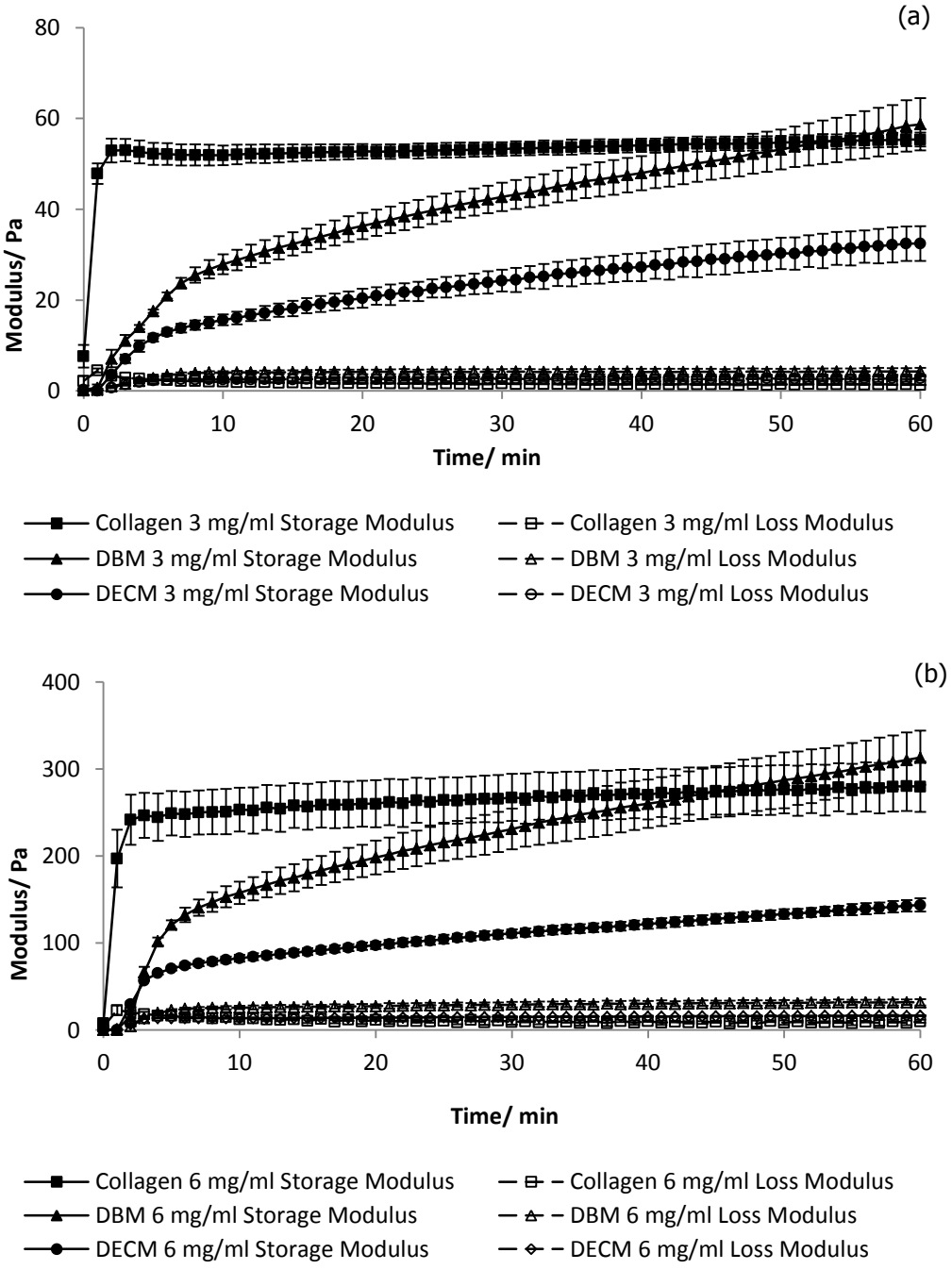

Figure 4.7 – Rheological assessment of gelling solutions of collagen, DBM and DECM via the application of an oscillating 1% shear strain at a constant strain rate of 1 rad s^{-1} in a humidified atmosphere at 37°C. Assessment was performed at 3 mg mL^{-1} (a) and 6 mg mL^{-1} (b) final gel concentrations. Error bars are one standard deviation (n = 6).

Both materials showed two-phase evolution of mechanical properties with the first phase lasting for around five minutes and contributing the most rapid evolution of mechanical properties. The second phase lasted from this point for at least another 55 minutes at which point the storage moduli of the gels still appeared to be changing. Measurements were not continued beyond this point as the samples began to dry out when studied beyond 60 minutes and this had a significant effect on the mechanical properties. Despite the continued gradual evolution of storage moduli at 60 minutes it was clear that DECM-derived hydrogels would never achieve moduli as high as those seen for collagen. DBM-derived hydrogels in contrast had already begun to display moduli in excess of those measured for collagen. Statistical analysis of the differences between the storage moduli of the various materials at 60 minutes seemed to support these conclusions (Table 4.1).

Rheological analysis of the viscoelastic behaviour of collagen and ECM-derived hydrogels was continued with an amplitude sweep of gels which had been allowed one hour to form (Figure 4.8). This was designed to assess the extent to which ECM-derived hydrogels would display the shear stiffening behaviour expected of collagen. It was also intended to derive the failure strain for the ECM-derived materials i.e. the strain beyond which the storage modulus was seen to display a rapid fall indicating disruption of the hydrogel structure. At both concentrations both ECM-derived materials were found to display shear stiffening as expected for collagen-based materials. DECM gels of both concentrations were found to have statistically-significantly lower failure strains than collagen and to have lower storage moduli at failure (though this difference was only statistically significant for 6 mg mL^{-1} gels). Contrastingly, the only instance in which DBM-derived gels showed significantly different performance to collagen was in the case of the failure strain for 6 mg mL^{-1} gels.

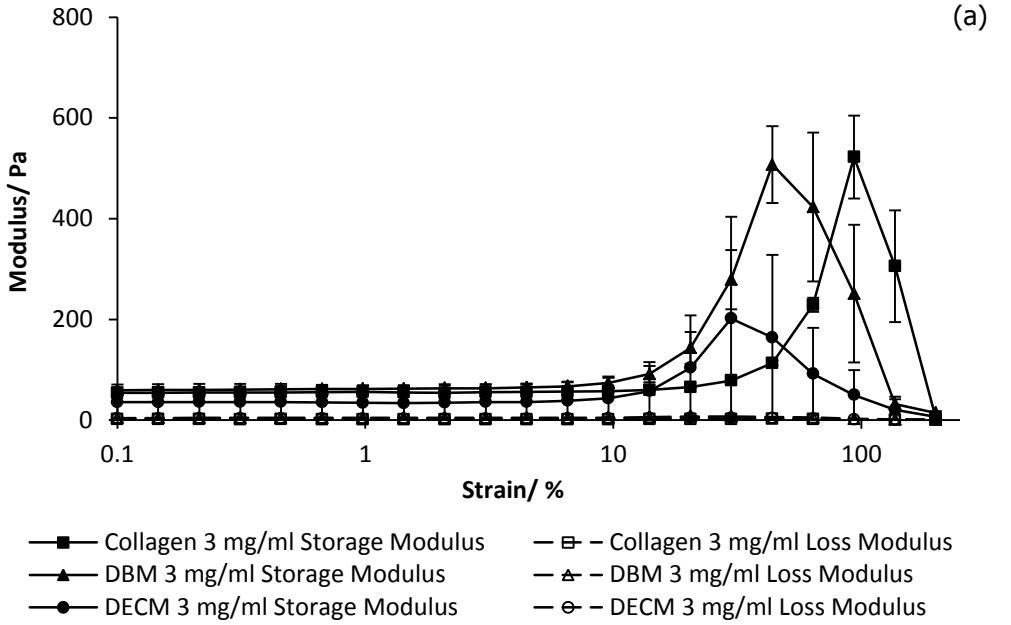

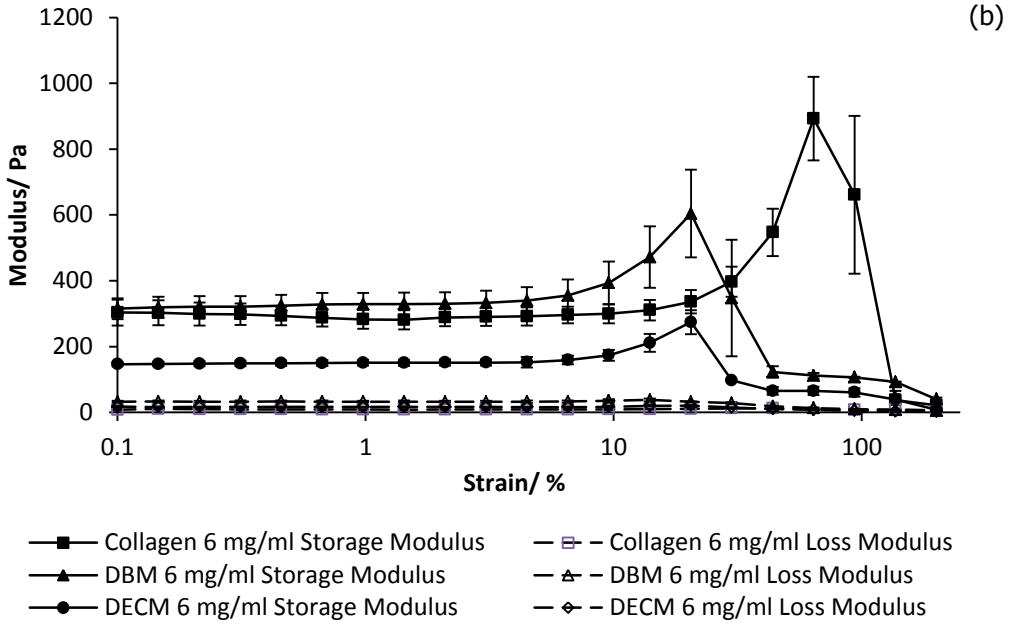

Figure 4.8 – Rheological assessment of hydrogels derived from collagen, DBM and DECM. An amplitude sweep was performed covering the strain range 0.1 – 200% at a constant shear rate of 1 rad s^{-1} applied in a humidified atmosphere at 37°C. All materials were assessed at 3 mg mL^{-1} (a) and 6 mg mL^{-1} (b) gel concentrations and were allowed to undergo gelation for one hour prior to testing. Error bars are one standard deviation (n = 6).

Gel Concentration/ mg mL^{-1}	Gel Type	Storage Modulus at 60 Minutes Incubation/ Pa	Failure Strain/ %	Storage Modulus at Failure/ Pa
3	Collagen	55 ± 2	93.6 ± 0	520 ± 80
	DBM	59 ± 6	50 ± 10	540 ± 20
	DECM	32 ± 4*†	35 ± 8*	260 ± 80
6	Collagen	280 ± 30	64 ± 0	890 ± 130
	DBM	310 ± 30	24 ± 5*	640 ± 80
	DECM	144 ± 8*†	30.6 ± 0*	270 ± 40*†

Table 4.1 – Summary of rheological parameters for ECM-derived hydrogels and collagen gels displayed as mean ± standard deviation (n = 6). Storage moduli at 60 minutes incubation measured after the application of an oscillating 1% shear strain at a constant strain rate of 1 rad s^{-1} in a humidified atmosphere at 37^{o}C for one hour. Other parameters derived from a subsequent amplitude sweep covering the strain range 0.1 – 200% at a constant shear rate of 1 rad s^{-1} applied in a humidified atmosphere at 37^{o}C. Statistically-significant difference ($p < 0.05$) to equivalent collagen parameter is indicated by (*) and to equivalent DBM parameter by (†).

SEM imaging was used to visualise and compare the structures of collagen and ECM-derived hydrogels (Figure 4.9). No apparent visual difference could be discerned between the fibrillar structures or fibre diameters of the different types of gel irrespective concentration. All gels presented highly porous structures in which the pores were strongly interconnected. Pore sizes appeared large with respect to the fibre diameters, though this size ratio would be expected to be different in the fully hydrated gels.

The final stage of ECM-derived gel characterisation was to examine the response of cells to the gels as *in vitro* culture surfaces. hOS and mPC cells were cultured on the surfaces of collagen, DBM and DECM hydrogels as well as on TCP for 72 hours. Figures 4.10 & 4.11 show results utilising 20,000 and 10,000 cells per well seeding densities respectively, but similar trends were observed at 5,000 cells per well for both cell types except where specifically noted. No experimental condition was examined under which either ECM-derived hydrogel was found to support statistically-significantly reduced cell numbers when compared to collagen. In the majority of cases, particularly for mPC cells, the ECM-derived gels supported significantly lower cell numbers than TCP. However under certain conditions cell numbers on these gels significantly exceeded those on collagen and achieved statistical similarity to those on TCP. This was most notably the case for mPC cells grown on 3 mg mL^{-1} DECM-derived gels for 72 hours, but was also found to be the case for three of the four conditions utilising DECM-derived gels as a growth substrate for hOS cells.

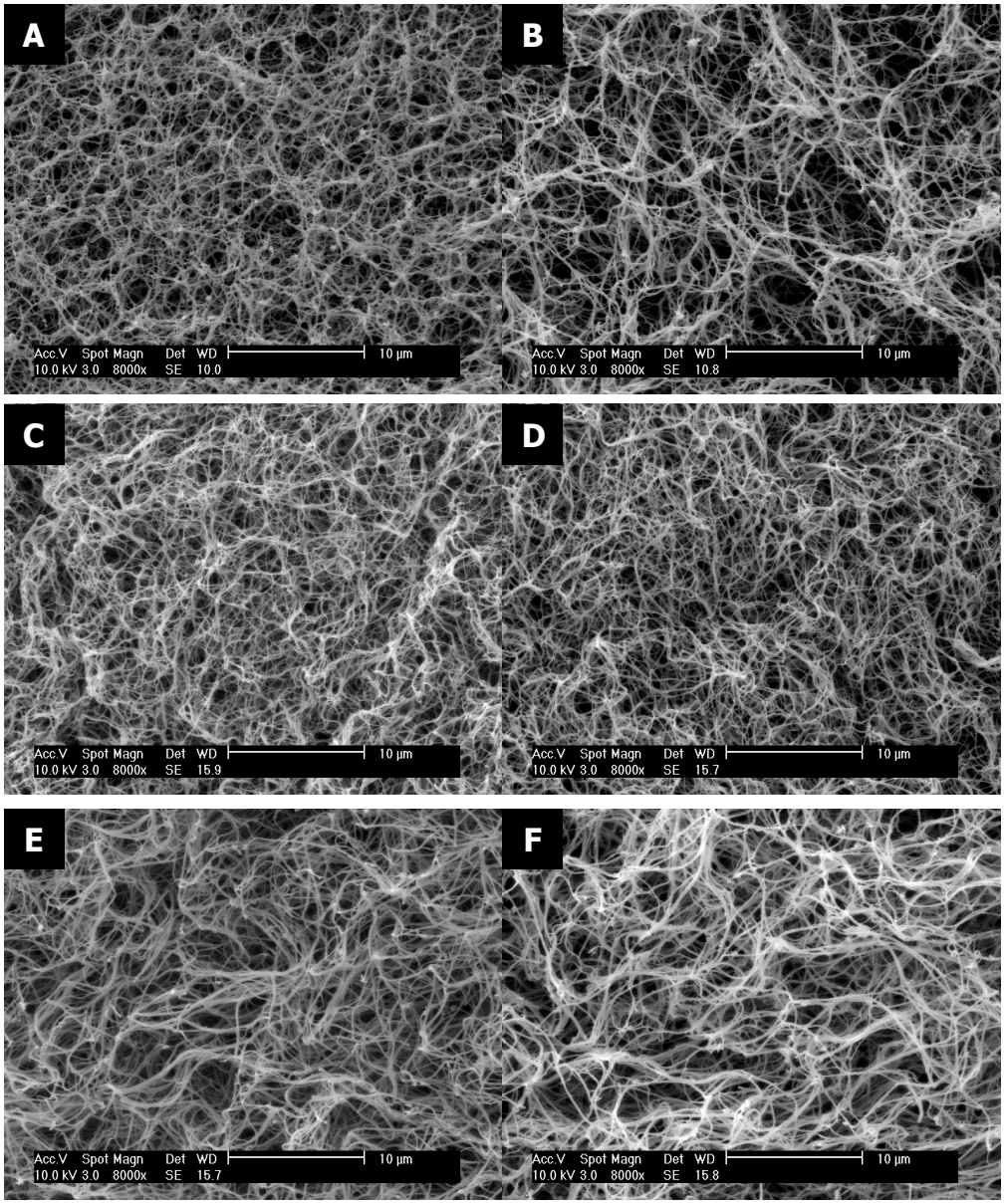

Figure 4.9 – Representative SEM images of 3 mg mL^{-1} DECM (A), 6 mg mL^{-1} DECM (B), 3 mg mL^{-1} DBM (C), 6 mg mL^{-1} DBM (D), 3 mg mL^{-1} collagen (E) and 6 mg mL^{-1} collagen (F) hydrogels. Gels were subjected to dehydration by washing in increasing concentrations of ethanol prior to critical point drying and sputter coating with platinum.

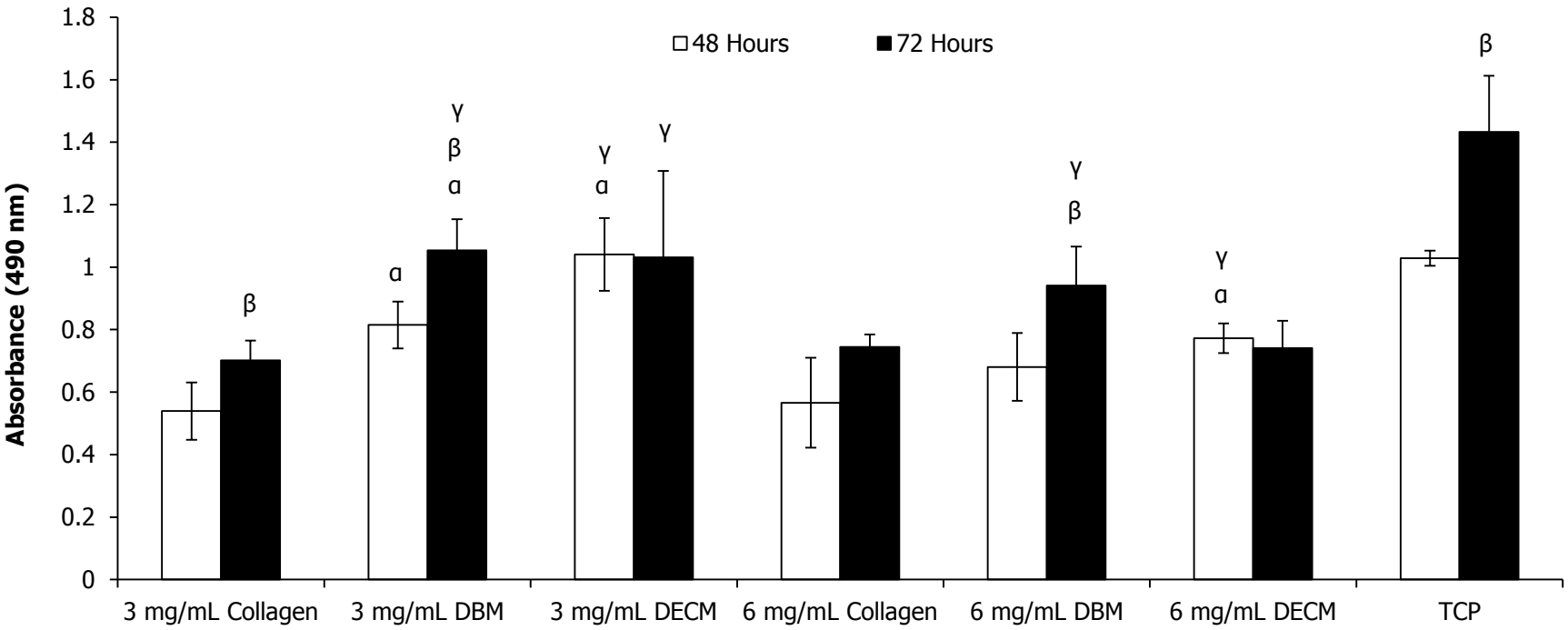

Figure 4.10 – Metabolic activity of hOS cells seeded on collagen, DBM and DECM hydrogels or on tissue culture plastic (TCP) assessed via the MTS assay. Cells were seeded at 20,000 cells per well onto 100 µL gels in 96-well plates (n = 6) after the gels had been allowed to form for one hour at 37°C. Error bars are one standard deviation. Statistically significant ($p < 0.05$) differences to equivalent collagen (α) and 48 hour (β) results and statistical similarity to equivalent TCP results (γ) are shown.

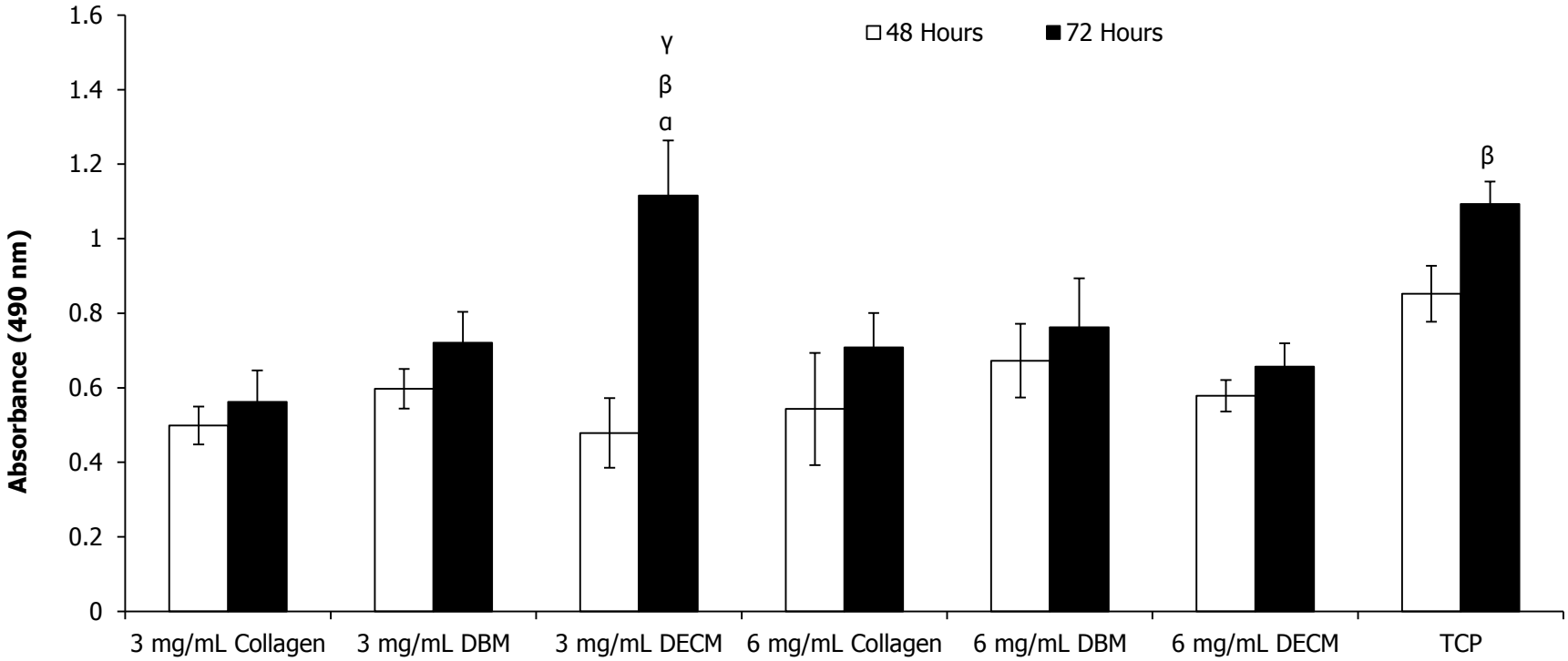

Figure 4.11 – Metabolic activity of mPC cells seeded on collagen, DBM and DECM hydrogels or on tissue culture plastic (TCP) assessed via the MTS assay. Cells were seeded at 10,000 cells per well onto 100 µL gels in 96-well plates (n = 6) after the gels had been allowed to form for one hour at 37°C. Error bars are one standard deviation. Statistically significant ($p < 0.05$) difference to equivalent collagen (α) and 48 hour (β) results and statistical similarity to equivalent TCP results (γ) are shown.

4.3.3 Fabrication of ECM-Derived Hydrogel Beads

One of the stated aims of the work presented in this chapter (see Section 4.1.4) was to demonstrate the production of beads composed of DBM or DECM hydrogels. Since the gelation kinetics for these highly-processed materials were found to be relatively slow, the key challenge in pursuing this aim was the stabilisation of pre-gel liquid droplets for sufficient time to allow gelation to be completed. To provide this stabilisation an indirect route to ECM-derived bead production was adopted which involved the use of calcium-crosslinked alginate as a temporary support structure (see Section 2.19).

Initially a variety of ratios of alginate solution to DECM digest were tested for bead formation and the beads were collected and dried to attempt to quantify the efficiency of DECM incorporation (n = 1). It was found that 1:1 and 2:1 (v:v) DECM:alginate ratios resulted in rounded beads which were visually similar to those produced using alginate alone. A 3:1 ratio resulted in highly irregularly-shaped beads which were prone to widespread aggregation prior to the completion of gelation and this ratio was discounted as a condition for bead production.

The dry weights of all batches of beads were found to be very much in excess of the total masses of alginate and/or DECM which had been included in the preparation. This was attributed to the encapsulation of large quantities of salt in the beads and made accurate quantification of DECM incorporation impossible. Instead the incorporation efficiency (the proportion of the DECM contained within the pre-gel mixture which was retained in the gel beads) was estimated for 2:1 and 3:1 ratios relative to the 1:1 ratio. This estimation was based on the assumption that both alginate and DECM gels retained salt at fixed mass ratios across all conditions. There appeared to be no loss of incorporation efficiency upon changing the DECM:alginate ratio (Table 4.2). The 2:1 ratio was chosen for future work based on containing the minimal amount of alginate necessary to achieve desirable morphology.

DECM:Alginate/ v:v	Incorporation Efficiency (I.E.)/ %	Mean I.E. ± Standard Deviation/ %
1:1	100	-
2:1	111, 105.2, 101.2	106 ± 5
3:1	106.3	-

Table 4.2 – Incorporation efficiency of DECM into DECM/alginate beads at a variety of ratios of the two constituents. Incorporation efficiency is defined as the proportion of the DECM contained within the pre-gel mixture which is retained within the hydrogel beads. Values are relative to the 1:1 (v:v) ratio condition and based on certain assumptions (see Section 4.3.3).

Further evaluation of the beads resulting from a 2:1 (v:v) DECM:alginate ratio was then undertaken. This began with a more reliable (n = 3) estimation of the relative incorporation efficiency which showed a low degree of batch-to-batch variation (Table 4.2). Subsequently the principle of citrate treatment to remove the alginate content was demonstrated and a clear change in the bead opacity and size could be discerned (Figure 4.12). The softness of the resulting beads and the alginate content of the suspension fluid meant it was not possible to reliably collect the beads for dry weight measurement.

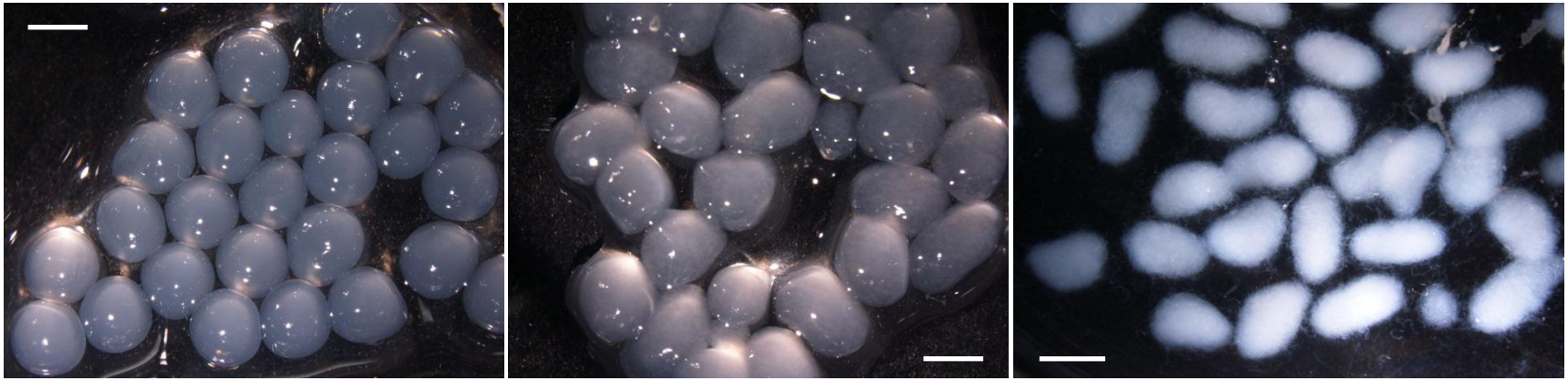

Figure 4.12 – Representative bright field microscopy images of (left to right) – hydrogel beads composed of alginate alone, beads produced from a 2:1 (v:v) ratio of DECM digest to alginate solution and beads produced from the same ratio of DECM to alginate imaged after treatment for 10 minutes with 0.25 M sodium citrate to remove the alginate component. Scale bars represent 2 mm.

4.4 Discussion

4.4.1 Successful Demineralisation and Decellularisation of Bovine Bone

Protocols were developed to demineralise milled bovine bone, to extract lipid content and subsequently to decellularise the processed bone. Powder-form materials were extracted after the lipid extraction step (DBM) and after the decellularisation step (DECM). DBM was found to be completely devoid of mineral content, which was expected since the protocol utilised was based on procedures which had been successfully used previously[470,501]. DBM is generally considered to be an acellular material[473] but in this work acid demineralisation plus chloroform/methanol lipid extraction was not found to be sufficient to remove all cells from the matrix. This was evidenced by the presence of visible nuclei in H & E stained histological sections. This discrepancy may be explained by the absence of a terminal sterilisation step in the protocol used here since this would be expected to cause death and lysis of any remaining cells. It should be noted that despite the presence of these intact cell nuclei the dsDNA level present in DBM was still found to be significantly below a widely-quoted criterion for successful decellularisation[450]. Additionally the levels found in DBM in this study compare favourably with those measured in other ECM-derived materials which have been used successfully both *in vitro* and *in vivo*[400,403,410,412,414,418,427,433,434,437,454,502-504]. Furthermore, as will be discussed below (see Section 4.4.2), there is no adverse cell response to this material to suggest levels of cell or DNA retention which are detrimental to material performance.

The trypsin/EDTA enzymatic decellularisation step utilised in this study did not produce a fall in the dsDNA level of the material when normalised to total mass. The total dsDNA content was reduced but the overall mass was reduced to a similar extent, leading to the proportional lack of change. This is perhaps to be expected due to the use of a non-specific protease treatment for decellularisation which has

previously been found to result in significant loss of ECM constituents[404-406,505,506]. The initial aim in this work was not to derive a fully-optimised decellularisation protocol but merely to achieve adequate reduction of cellular material. In future work other decellularisation regimes may need to be considered, such as ionic or non-ionic detergent treatments.

The trypsin/EDTA treatment utilised in this work leads to a total elimination of visible cell nuclei but only removes around 40% of dsDNA. This may suggest that it is more efficient at causing cell lysis than at removing cellular debris from the matrix. As a result additional DNase and RNase treatments may be important additions to future decellularisation protocols[422,428,507-509].

As would be expected for demineralised bone both DBM and DECM were found to be composed of around 90% collagen by weight with no significant change caused by the enzymatic decellularisation step[473,510]. The cell response data obtained (see Section 4.4.2) suggests that both DBM and DECM may contain other proteins, PGs or GAGs which have a beneficial signalling effect on the proliferation of bone-derived cells. An important step in the further study of these materials and their gel derivatives would be to establish what these other constituents are and to what extent their activity is maintained in both powder and gel forms. Other constituents which may be expected to be present in these materials include fibronectin[511-514], osteopontin[513,515], bone sialoprotein[513-515] and a number of BMPs[481,484,510,514,516].

4.4.2 Production of Hydrogels from Demineralised and Decellularised Bovine Bone

It was demonstrated in the work presented in this thesis that a pepsin solubilisation step which has been used to produce hydrogels from a number of soft tissue-derived ECMs[421,439,451-457] could also be applied to demineralised bone tissue. The concern in taking this approach was that the ECM may have been processed and altered to such

an extent that the resulting protein fragments would be incapable of polymerising or aggregating to form a hydrogel structure. This was particularly true for the DECM-derived material which had been subjected to an additional enzymatic processing step. In practice both DBM and DECM could be digested with pepsin and these solubilised materials induced to form hydrogels at concentrations of 1 mg mL^{-1} and above.

The similarity of the gelation kinetics of ECM-derived materials to those of collagen suggested that it was digested collagen fragments that were responsible for gelation. Both ECM-derived materials gelled more slowly than collagen with DBM being the slower of the two. Previously reported ECM-derived hydrogels show a very wide range of times for complete gelation which extends around an order of magnitude either side of the figures obtained in this work (around 45 – 60 minutes)[451,453,458,459,461,517].

Spectrophotometric measurements showed the gels that were formed from DBM digest to be optically similar to collagen with DECM-derived gels being substantially more opaque. However SEM imaging showed very similar structures of both DBM and DECM-derived hydrogels to their corresponding collagen gels. All gels showed randomly-oriented fibrillar structures which were highly porous and had highly interconnected pore structures. This further suggested that collagen and its derivative peptides were controlling the gelation and physical structure of these materials.

Rheological analysis suggested that although collagen may be the causative element for gelation the complex composition of the pepsin digests was giving rise to a distinct gel formation mechanism. Collagen's storage modulus reached its maximum value in one continuous phase of change lasting two to three minutes. On the other hand, the storage moduli of ECM-derived hydrogels showed two distinct phases of change. An initial rapid increase was seen for around five minutes after the temperature was raised to 37°C. Following this the rate of change slowed into a

second phase during which the storage moduli continued to increase up to the maximum 60 minute incubation time studied. It is likely that these altered gelation kinetics were the result of two distinct differences between the pre-gel collagen solutions studied and the ECM-derived pepsin digests. Firstly the collagen peptide chains in the pepsin-digested DBM and DECM would have been very much shorter than those in the collagen solution. Secondly the ECM digests contained around 10% by weight non-collagenous material and it has previously been shown that the presence of other ECM constituents such as GAGs can alter the kinetics of collagen gelation[518-520].

The slower gelation kinetics of the ECM-derived materials may in practice make them more usable injectable scaffold materials since the window of time during which they are able to maintain flow at room temperature is larger. However it will likely also render them more difficult to form into beads and more challenging to use in bioplotting applications as suggested in Section 4.1.4.

The additional enzymatic processing applied to DECM prior to pepsin digestion was found to lead to significantly reduced final gel stiffness, but DBM-derived gels were ultimately stiffer than collagen equivalents. The stiffnesses of both types of ECM-derived gel, as measured by their storage moduli under shear strain, are considerably higher than those seen previously for some ECM-derived gels[451,453-455,457,517]. This suggests they may be more suitable for applications in bone repair, perhaps indicating a degree of 'mechanical tissue specificity'. It should be remembered however, that the experimental conditions used to gather these measurements were different and that this will have affected the precise values obtained. The lower stiffness of DECM gels for a given gel concentration means that a higher concentration would have to be used to achieve similar mechanical properties. This would by definition be a denser gel which may be less conducive to supporting the growth of encapsulated cells. However SEM imaging did show that gels remained highly porous even at the higher concentration studied here.

In most cases the gels formed from bone-derived materials were found to fail at lower strains than collagen gels when subjected to amplitude sweeps. This suggested they would be more likely to fail if used as load-bearing biomaterials *in vivo*. DECM-derived gels at 6 mg mL^{-1} faired particularly poorly in this regard as they had statistically-significantly lower storage moduli at failure than collagen. This in turn suggested that they would fail under the influence of particularly low stresses. It should be noted however, that the properties derived here under shear conditions do not relate directly to behaviour under the predominantly compressive loads which would be experienced in many bone implantation sites *in vivo*.

The mechanical properties of the ECM-derived hydrogels studied here appear to be inferior to those of the collagen of which they are predominantly composed. However they compare favourably with those of other ECM-derived gels which have previously been reported. Additionally, in the case of bone it is perhaps not envisaged that a hydrogel alone would be a suitable biomaterial for all applications but rather that it would act as a bioactive supplement for a stronger material of either synthetic or natural origin[496,521,522].

The potentially beneficial bioactivity of DECM and DBM-derived gels was demonstrated by their successful utilisation as *in vitro* cell culture substrates. For all combinations of two gel concentrations, two cell types, two time points and two cell seeding densities both materials performed at least as well as collagen based on cell metabolic activity. Under some conditions ECM-derived gels significantly outperformed collagen and even showed equivalence with tissue culture plastic, the gold standard *in vitro* substrate. A particularly significant demonstration of this occurred when murine primary calvarial cells were cultured at 10,000 cells per 96-well plate well on 3 mg mL^{-1} DECM-derived gels. These primary cells are more sensitive to their environment than the cancer-derived hOS cell line and under the conditions described they proliferated very significantly between 48 and 72 hour time points.

Further work is clearly required to understand the sensitivity of bone-relevant cell types to the conditions used for culture both on and within bone-derived hydrogels. It will also be important to understand which non-collagenous constituents of the materials are exerting the beneficial effects seen on cell growth. As suggested earlier these may include fibronectin and bone morphogenetic proteins. Finally it may be instructive to compare the ECM-derived hydrogels produced here with their undigested counterparts and with native bone tissue as cell culture substrates. This would allow an understanding of the effects of each processing step on the bioactivity and biocompatibility of these materials. Despite these unknowns the initial positive results seen here demonstrate that such hydrogels may have great potential as adjuncts to or replacements for DBM in bone grafting procedures.

4.4.3 Fabrication of ECM-Derived Hydrogel Beads

As outlined in Section 4.1.4 one of the objectives of the work presented in this chapter was to demonstrate the ability of ECM-derived hydrogels to be formed into particles or beads. These bead formulations would constitute injectable suspensions with increased room temperature stability compared to pre-gel solutions. This may render them a useful alternative formulation, although they would not then undergo gelation after delivery and may not be as well retained at the defect site. Formulation into beads would also present the possibility for exogenous growth factors to be encapsulated within them for controlled delivery *in vitro* or *in vivo*. In the simplest instance these proteins would then be released by diffusion through the gel. However it has been shown recently that decellularised matrices may retain binding sites for growth factors such as basic fibroblast growth factor and hepatocyte growth factor even when processed to form hydrogels[431,517,523]. The presence of these functional growth factor binding sites may offer a route to cell-mediated release of a wide range of growth factors.

The initial protocol evaluated for bead formation was relatively simple, with beads produced by ejecting a mixture of alginate and DECM digest into a calcium chloride bath at 37°C. This induced gelation of the alginate into rounded beads which retained the DECM digest for sufficient time to allow it to undergo complete gelation. Beads could be formed containing 6 mg mL^{-1} DECM and as little as 0.33% (w/v) alginate with no drop in estimated incorporation efficiency relative to beads containing 0.5% (w/v) alginate. Although the DECM-containing beads did not maintain the close-to-spherical morphology of alginate-only beads they were fairly uniform with sizes around 2 mm.

The amount of DECM in the beads could not be accurately quantified due to the retention of a large amount of salt within them. However citrate treatment did indicate qualitatively the presence of fully-formed DECM-derived hydrogel within the beads, since there was a clear change in size and opacity post-treatment but discrete beads could still be observed.

The work described here has demonstrated that the formation of beads consisting of DECM-derived hydrogel is possible. However the protocol used may need refining to be suitable for some applications. The beads are relatively large to be considered as easily injectable and fundamentally different protocols may be needed should a very large reduction in size be required. The need to include alginate in the production process is perhaps not ideal because if it is retained in the final beads then it acts to dilute the bioactivity of the DECM. Alternatively if it is removed via citrate treatment then a portion of any cell population or protein incorporated in the formulation will inevitably be lost in production. To combat these issues water-in-oil emulsion techniques could be considered a promising alternative route to bead production[524-526]. However, organic-aqueous interfaces can be detrimental to protein activity[527,528] and protocols of this type would necessitate extensive washing to remove organic solvent residues.

Arguably a better approach would be to develop alternative methods of delivery of the alginate/DECM mixture into the calcium chloride bath in order to produce droplets of smaller size. Further to this a larger calcium chloride bath combined with more efficient modes of stirring may prevent the irregular morphology seen with higher DECM-to-alginate ratios and allow the alginate content of the beads to be further lowered. Taken together these modifications of a technique which is fundamentally effective could alleviate the potential issues foreseen in future applications.

5. Fabrication of Patterned Constructs via Bioplotting

5.1 Introduction

5.1.1 Thermoresponsive Sintering of a Microparticulate Scaffold Material

Many scaffolds used for bone tissue engineering are composed of calcium phosphate-based ceramics which can be engineered with excellent mechanical properties[182,191,194,198]. These scaffolds have been shown to be capable of supporting significant proliferation of bone-derived cells *in vitro*[188,191,529]. However the high temperature processing required prevents the incorporation of cells or proteins into the production process[182,191,193,194,198]. This limits the biological functionality which the scaffolds can display and it also severely limits the complexity of patterning which can be achieved within them.

The use of synthetic polymers as scaffold materials removes the requirement for very high temperature processing. This strategy also allows an acceptable level of mechanical strength to be maintained[88,157,178,204,211,530]. However the majority of scaffold fabrication techniques still require these polymers to be processed at (mildly) elevated temperatures[157,204,209-211,530] and/or in the process of organic solvents[112,178,277,353,531-533]. This can be circumvented by the use of supercritical carbon dioxide ($scCO_2$) as a solvent for polymer processing[308,534-539]. The use of $scCO_2$ allows proteins to be encapsulated within polymer scaffolds whilst remaining active[308,534,536,538]. However $scCO_2$ processing requires the application of high pressures and this renders these techniques non-cell compatible.

A novel microparticulate polymer formulation has recently been developed which undergoes thermoresponsive liquid sintering under physiological conditions to form porous solid scaffolds[270-273,540,541]. The microparticles in this formulation are composed of a melt blend of poly(lactic-co-glycolic acid) (PLGA) and poly(ethylene

glycol) (PEG). The PEG component acts to lower the glass transition of the mixture such that it is just below body temperature[270,273]. These microparticles can be suspended in an aqueous carrier to form a paste for use as an injectable defect filler. When the temperature of the paste is raised to 37°C the microparticles soften and form adhesion bridges to one another. The presence of the aqueous carrier then allows the hydrophilic PEG component to leach from the microspheres. This causes the polymer and thus the microparticle-to-microparticle adhesion bridges to resolidify. A porous solid scaffold is formed with mechanical properties which are comparable to those of cancellous bone[270-273,542-545].

The mild processing conditions used for the fabrication of these PLGA-PEG scaffolds allow active proteins to be loaded into them by dissolution in the carrier[540]. Alternatively proteins can be encapsulated in polymer microspheres which are then mixed into the formulation and which can deliver them in a time-controlled manner (see Chapter 3)[272,541]. Cells can also be suspended in the carrier and then be retained and proliferate within the fully-formed scaffolds[270,272]. The ability to formulate these microparticles as injectable pastes also renders them compatible with extrusion-based construct fabrication and patterning by bioplotting (see Section 1.2.6).

5.1.2 Bioplotting as a Tissue Engineering Construct Fabrication Technology

Due to the very mild conditions used for bioplotting the technique has predominantly been used to produce constructs from natural and synthetic polymer hydrogels (see Section 1.2.6)[226,227,229,230,232,240,242,243,245-247,249-251,546]. These constructs do not have sufficient mechanical strength to be used for the repair of defects in load-bearing bones. A number of publications describe the extrusion at ambient conditions of pastes containing ceramic particulates[190,547,548]. However as with ceramic scaffolds produced via other means, these required very high temperature post-production sintering[190,547,548] and could not incorporate proteins or cells for biological

functionality. This means that to date the production of bone-appropriate tissue engineering constructs via a pure bioplotting approach has not been demonstrated.

5.1.3 Aims & Objectives

The overall aim of the work presented in this chapter is to evaluate the potential of bioplotting techniques for the production of patterned constructs for osteochondral defect repair. However much of the data obtained is also more widely informative and applicable.

The first step in achieving this aim is to assess the feasibility of bioplotting the PLGA-PEG microparticulate scaffold material described above. Should this prove feasible then the process will be optimised with the aim of achieving suitable mechanical properties for bone repair. Consideration will also be given to bioplotting of cell-laden alginate hydrogels similar to those which have been used elsewhere in tissue engineering[226,227,229,230,232,245,546]. Alginate gels encapsulating chondrocytes or mesenchymal stem cells in particular have proved effective for the generation of cartilage tissue *in vitro* and *in vivo*[230,244,245].

Further to this the production of constructs containing both PLGA-PEG and alginate phases will be attempted. These constructs may be suitable for the repair of bone and cartilage simultaneously. Another important step in the development of bioplotting for osteochondral construct fabrication will be to determine whether viable cells can be incorporated in the PLGA-PEG phase.

Finally the ability of a bioplotting platform to simultaneously pattern materials, protein signals and cell populations will be considered. It may be necessary to perform patterning of this complexity to achieve truly effective defect repair and this ability would also render the technique very widely-applicable.

5.2 Materials and Methods

5.2.1 Use of Fab@Home Bioplotting Platform

See Section 2.22 for general protocols for bioplotting of PLGA-PEG microparticulate pastes and alginate hydrogels with or without cells. In the following text '1.5% alginate hydrogel' is used to refer to a mixture composed of a 3:1 (v:v) ratio of 2% (w/v) alginate solution (Acros Organics) and 1% (w/v) calcium sulphate (Alfa Aesar). In a similar fashion '2% alginate hydrogel' refers to a 2:1 (v:v) mixture of 3% (w/v) alginate solution (FMC Biopolymer) and 1% calcium sulphate (Sigma-Aldrich).

5.2.2 Production of PLGA-PEG Microparticles

See Section 2.21.

5.2.3 PLGA Microsphere Fabrication via Refined Double Emulsion Technique

See Section 2.4.3.

5.2.4 Microsphere Size Distribution Analysis via Laser Diffraction

See Section 2.5.

5.2.5 Scanning Electron Microscopy (SEM)

See Section 2.6.

5.2.6 Unconstrained Compression Testing

See Section 2.23.

5.2.7 Micro Computed Tomography (μCT) Imaging and Three-Dimensional Analysis

See Section 2.16.

5.2.8 Live/Dead Staining of Cells in Alginate Hydrogels

See Section 2.24.

5.3 Results

5.3.1 Feasibility of Production of Patterned Constructs Containing PLGA-PEG Microparticulate Material via Bioplotting

The Fab@Home Model 1 platform[274] was used for an initial study assessing the feasibility of bioplotting as a fabrication technique for osteochondral tissue engineering. Figure 5.1 shows representative images of 2% alginate hydrogel constructs produced using this system. The resolution of a bioplotting process is essentially defined by the width of the material filament which is deposited. This provides a lower limit to the size of structure that can be reproduced and is in turn limited by the inner diameter of the tip which is used to deposit the material. In the case of the constructs shown in Figure 5.1 this was 630 μm but 2% alginate hydrogels could also be deposited using tips with inner diameters as small as 250 μm.

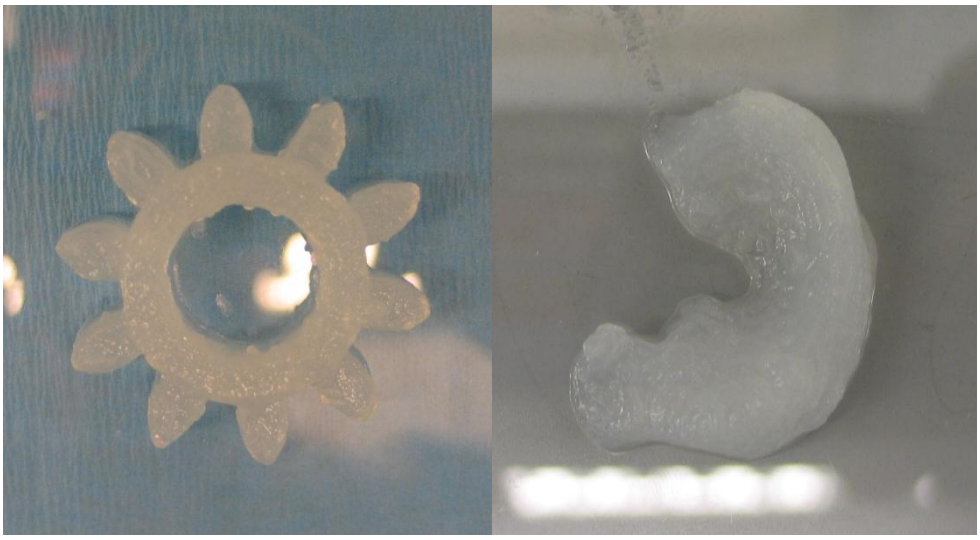

Figure 5.1 – Representative images of constructs produced via bioplotting of 2% alginate hydrogels. Shown are a 'gear' test design (left) and a construct shaped to match a bovine meniscus (right).

The next stage in this study was to assess whether the deposition of PLGA-PEG microparticulate pastes using the Fab@Home Model 1 was feasible. Previous studies utilising PLGA-PEG microparticles had focused on the 100 – 200 μm size fraction[270-273,540,541]. In this study it was found that microparticles of this size could not be deposited by bioplotting even when the inner diameter of the syringe tip was as large as 1.36 mm.

Deposition was achieved using a smaller microparticle size fraction (50 – 100 μm). A number of conditions were varied to achieve and then optimise deposition within certain practical constraints. Parameters considered included the inner diameter of the tip, the concentration of medium viscosity carboxymethyl cellulose (CMC) used as the carrier liquid, the carrier:solid (v:w) ratio and the material flow rate. The result was optimised with respect to the achievement of total deposition of all material, the maintenance of consistent flow during deposition and the ability to discern individual deposition paths in constructs which nevertheless maintained their integrity. Figure 5.2 shows constructs produced using a tip with an inner diameter of 1.19 mm, 3% (w/v) medium viscosity CMC as the carrier, a 1.5:1 carrier:solid ratio and a material flow rate of 38.8 μL s^{-1}. These constructs could be sintered for 24 hours at 37^{o}C to achieve appreciable mechanical strength and rigidity with minimal change of size and shape.

Another important step in this study was the demonstration that PLGA microspheres could be incorporated into PLGA-PEG constructs to provide the potential for controlled protein delivery. Figure 5.3 shows constructs bioplotted using the conditions described above excepting that 25% (w/w) of the solid was replaced by '100 μm' PLGA microspheres. These microspheres had been manually sieved to remove the sub-50 μm size fraction as this significantly improved the flow of microparticulate pastes. With the inclusion of microspheres the ability to discern by eye the location of individual deposition paths was lost. However the constructs could still be sintered with minimal changes in size and shape.

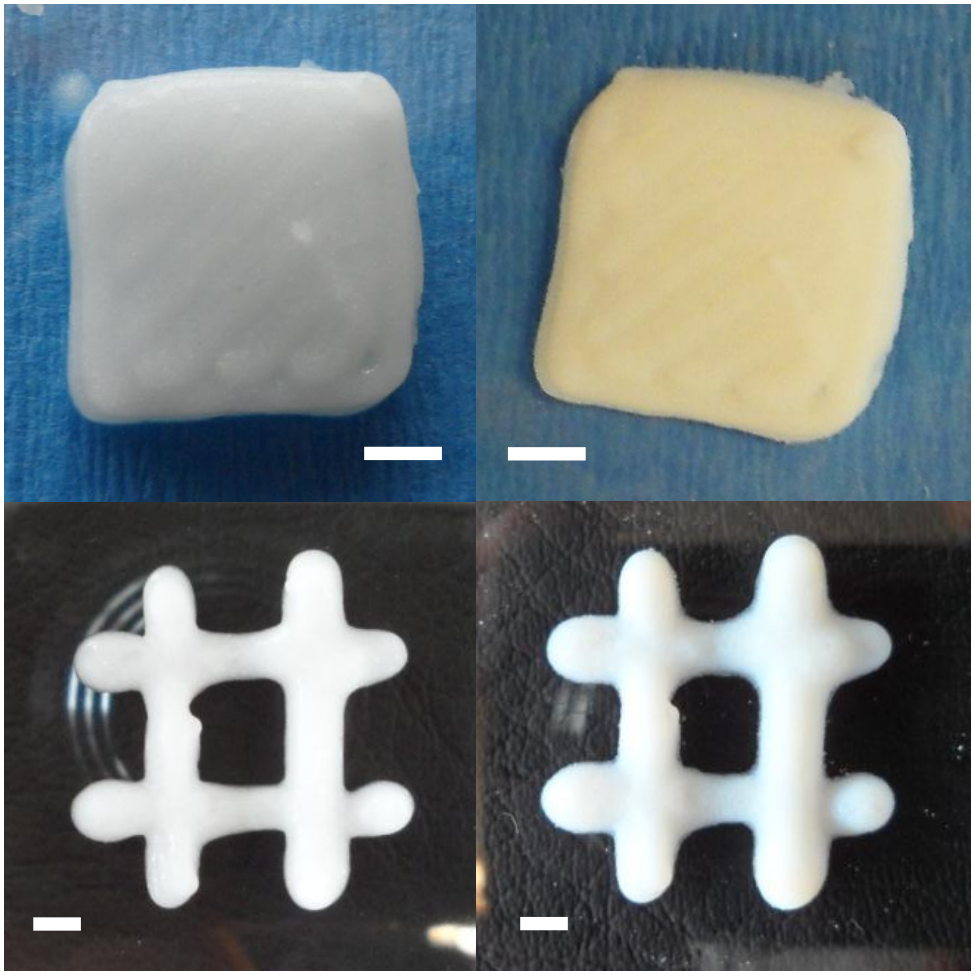

Figure 5.2 – Representative images of constructs produced via bioplotting PLGA-PEG microparticles suspended in 3% (w/v) medium viscosity CMC at a 1.5:1 (v:w) ratio of solid to aqueous carrier. Images are shown of constructs both before (left) and after (right) 24 hours sintering. Scale bars represent 2 mm.

Figure 5.3 – Representative images of constructs produced via bioplotting of PLGA-PEG microparticles and '100 μm' PLGA microspheres suspended in 3% (w/v) medium viscosity CMC at a 1.5:1 (v:w) ratio of solid to aqueous carrier. The ratio of microparticles to microspheres was 3:1 (w:w). Images are shown of constructs both before (left) and after (right) 24 hours sintering. Scale bars represent 2 mm.

When imaged via SEM (Figure 5.4) and μCT (Figure 5.5) scaffolds were seen to contain interconnected pore structures. Microparticle-to-microparticle bridging appeared to be very extensive at the surface of the constructs but less so in the interior. This apparently incomplete sintering process was reflected in the mechanical properties of the constructs as assessed by unconstrained compression testing. The mean yield stress for the constructs was significantly lower than those observed in previous studies of this material at 0.026 MPa (n = 3)[270-273].

The next step in this feasibility study was to evaluate the ability of the Fab@Home platform to produce dual material scaffolds containing both alginate and PLGA-PEG microparticle phases. Figure 5.6 shows dual material scaffolds produced using the settings described above for individual materials. It was noted that when constructs were sintered under standard conditions the alginate component reverted to an aqueous solution and was removed from them. In this case the alginate was acting as a temporary support to stabilise PLGA-PEG microparticle structures which were not capable of self-supporting. The alginate phase could instead be retained if sintering was conducted using a 0.66% (w/v) calcium chloride solution in place of the standard 0.9% (w/v) sodium chloride. This allowed the alginate to function as a true construct component, in which cells and/or proteins could be delivered. The presence of the alginate component did not appear to affect the ability of the PLGA-PEG microparticles to sinter in either case.

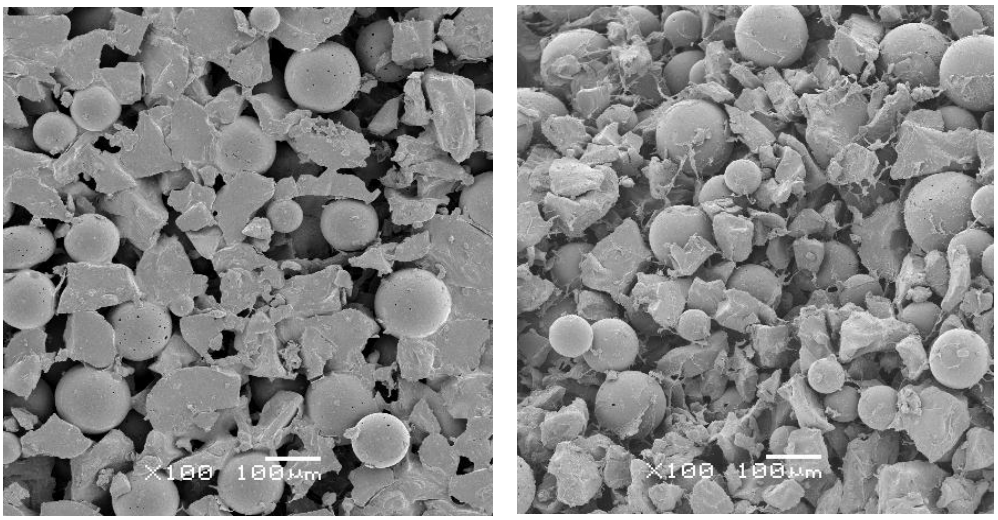

Figure 5.4 – Representative SEM images of constructs produced via bioplotting of PLGA-PEG microparticles and '100 µm' PLGA microspheres suspended in 3% (w/v) medium viscosity CMC at a 1.5:1 (v:w) ratio of solid to aqueous carrier. The ratio of microparticles to microspheres was 3:1 (w:w). Images show construct surface (left) and cross-section (right) after 24 hours sintering.

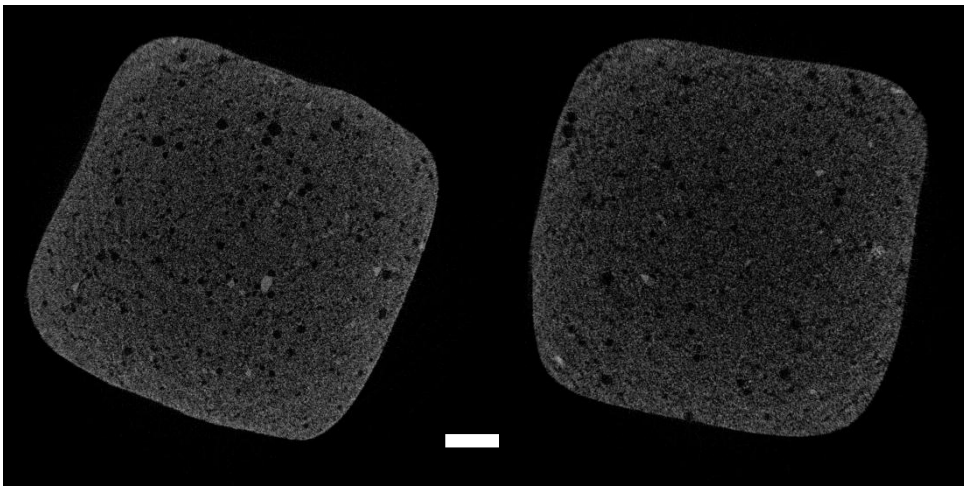

Figure 5.5 – Representative μCT-derived cross-sectional images of constructs produced via bioplotting of PLGA-PEG microparticles and '100 μm' PLGA microspheres suspended in 3% (w/v) medium viscosity CMC at a 1.5:1 (v:w) ratio of solid to aqueous carrier. The ratio of microparticles to microspheres was 3:1 (w:w) and constructs were imaged after 24 hours sintering. Scale bar represents 2 mm.

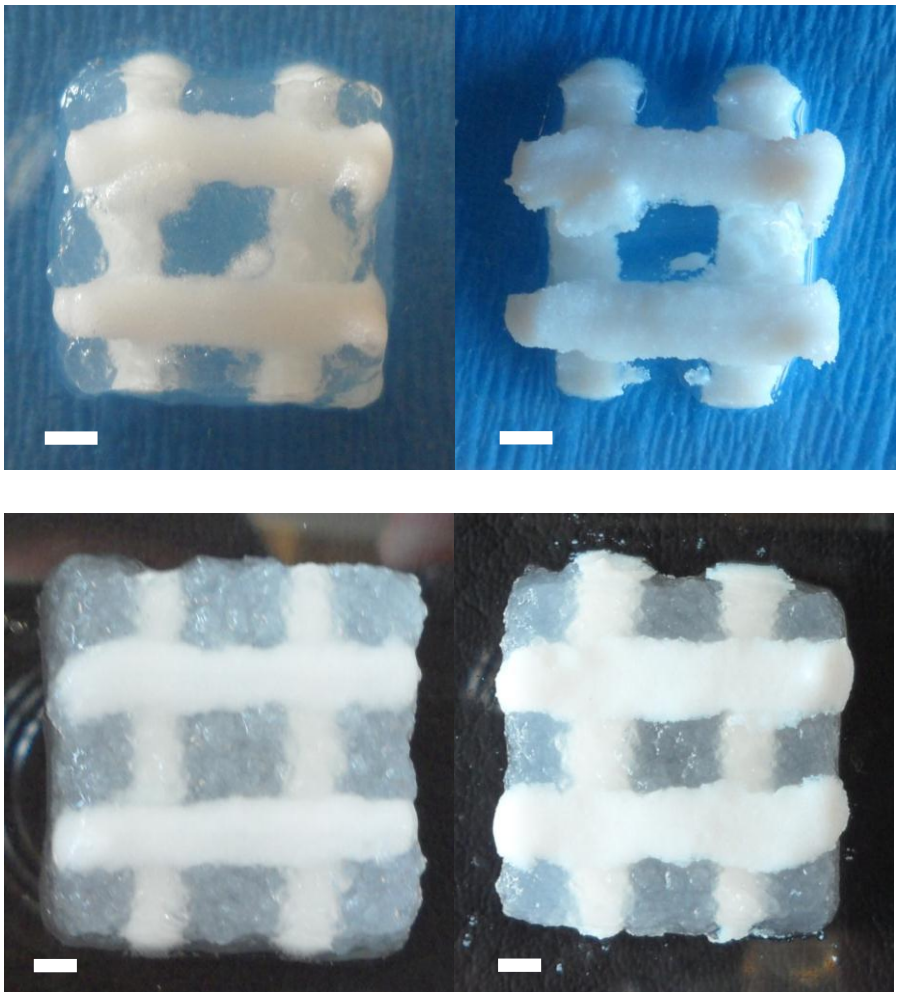

Figure 5.6 – Representative images of constructs produced via bioplotting of PGLA-PEG microparticulate and 2% alginate hydrogel phases. PLGA-PEG phase consisted of microparticles suspended in 3% (w/v) medium viscosity CMC at a 1.5:1 (v:w) ratio of solid to aqueous carrier. Images are shown before (left) and after (right) 24 hours sintering. Top images show constructs sintered in 0.9% (w/v) sodium chloride and bottom images show constructs sintered in 0.66% (w/v) calcium chloride. Scale bars represent 2 mm.

Next the ability of cells contained within alginate hydrogels to remain viable across the bioplotting process was assessed. Relevant cell types for osteochondral repair strategies were suspended in 2% alginate hydrogels to a final concentration of 500,000 cells mL^{-1}. These cell-laden gels were then bioplotted as per the conditions described above. Post-plot viabilities were assessed via live/dead staining and compared to pre-plot viabilities as measured via trypan blue staining. Representative images of live/dead stained MC3T3-E1 murine pre-osteoblasts and bovine articular chondrocytes are shown in Figure 5.7. These cell types had mean (± standard deviation) post-plot viabilities (n = 3) of 78 ± 9% and 80 ± 2% respectively.

The final stage of the feasibility study undertaken here was designed to assess the ability of the Fab@Home Model 1 to simultaneously pattern materials, cells and proteins. Constructs were produced which contained four different phases – alginate hydrogels encapsulating two different cell populations and PLGA-PEG microparticle pastes containing two different types of PLGA microsphere. Figure 5.8 shows the schematic design on which the constructs were based and a representative confocal microscopy image of a bioplotted construct. The latter is also shown in Figure 5.9 with magnified images of the individual phases. The fidelity of design replication was lowered for these multiple phase constructs relative to single phase constructs. However the overall patterns of construct phases were in good general agreement with those in the designs.

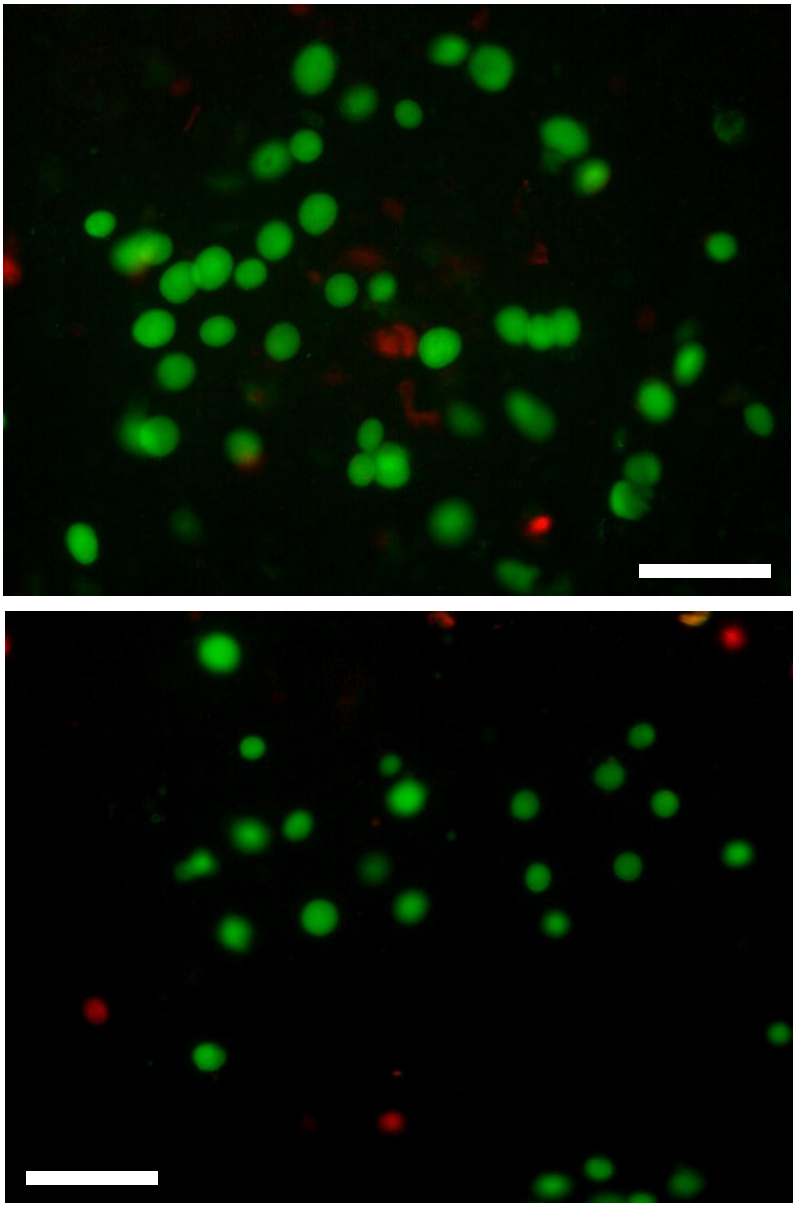

Figure 5.7 – Representative fluorescence microscopy images of MC3T3-E1 cells (top) and bovine chondrocytes (bottom) bioplotted in 2% alginate hydrogel at 500,000 cells mL^{-1}. Cells have been live/dead (green/red) stained for 30 minutes with 2 μM calcein AM and ethidium homodimer-1 respectively. Scale bars represent 10 μm.

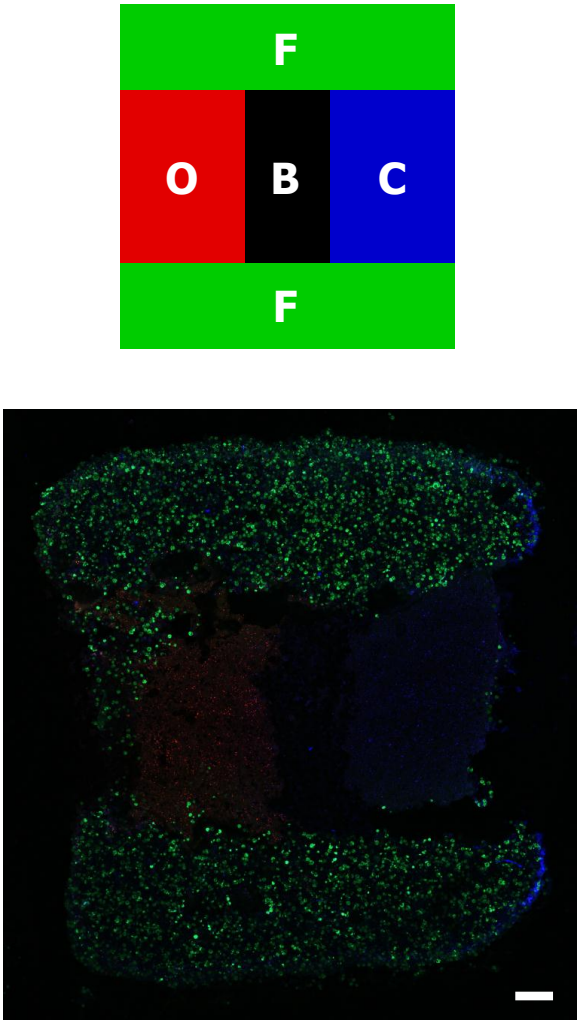

Figure 5.8 – Schematic (top) showing design of four phase construct and confocal microscopy image (bottom) of bioplotted construct produced from design. Phases consisted of 2% alginate hydrogel containing MC3T3-E1 cells labelled with a far red dye (O), 2% alginate hydrogel containing bovine chondrocytes labelled with DAPI (C), PLGA-PEG microparticle paste containing blank PLGA microspheres (B) and PLGA-PEG microparticle paste containing PLGA microspheres encapsulating FITC-lysozyme (F). Alginate phases contained 500,000 cells mL^{-1} and PLGA-PEG pastes consisted of PLGA-PEG microparticles and '100 μm' PLGA microspheres suspended in 3% (w/v) medium viscosity CMC at a 1.5:1 (v:w) ratio of solid to aqueous carrier. The ratio of microparticles to microspheres was 3:1 (w:w). Scale bar represents 1 mm.

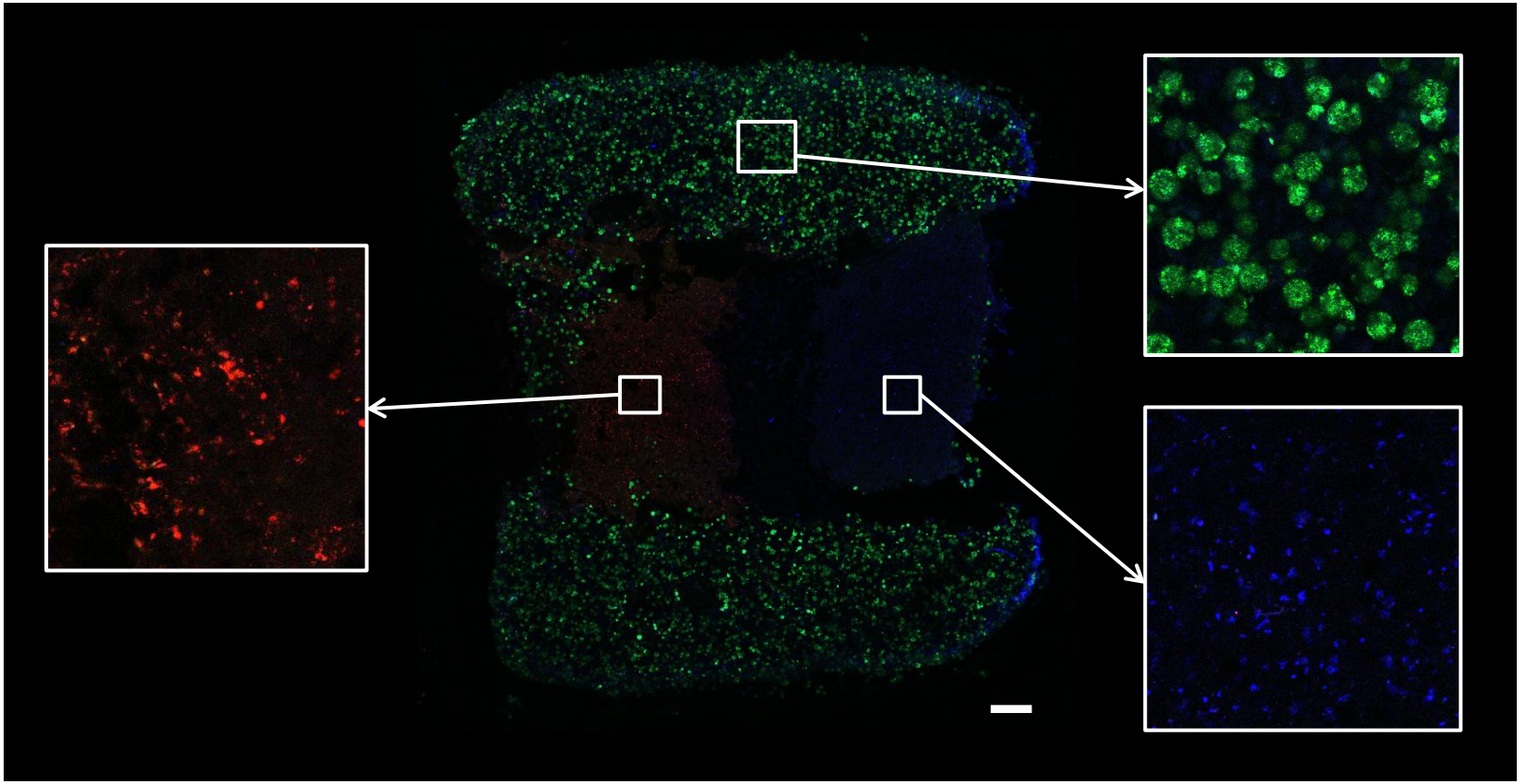

Figure 5.9 – Confocal microscopy image of four phase bioplotted construct shown in Figure 5.8 with magnified images of individual phases. Scale bar represents 1 mm.

5.3.2 Optimisation of Bioplotting of PLGA-Based Microparticulate Scaffold Material

PLGA-PEG microparticulate constructs produced during the feasibility study described above had mechanical which were significantly below those required for repair of load-bearing bones. Three possible effects were identified which may have been detrimental to the observed mechanical properties. Firstly the pastes incorporated non-sintering microspheres, leading to the formation of less of the adhesion bridges from which the strength of the constructs was drawn. Secondly the constructs produced were too large to undergo compression testing intact and instead sections had to be punched out of them for this analysis. This caused considerable damage, particularly at the edges of the punched sections. Finally it had not been possible to fully optimise the conditions used for deposition since only one suitable carrier had been available and the supply of microparticles had been limited.

A systematic study was designed which would optimise the deposition of PLGA-PEG microparticles using the Fab@Home Model 2 platform with respect to mechanical properties and pore structure. The effects of the first two factors described above were eliminated by depositing microparticles without microspheres and into cylindrical poly(tetrafluoroethylene) (PTFE) moulds (6 mm diameter, 12 mm height). The latter led to the production of constructs of exactly reproducible shape which could be compression tested without the need for size reduction. Since no significant change in size was seen during sintering of previous constructs the restriction of deposited pastes by the moulds was not considered to exert a significant effect on construct architecture.

An important consideration in this work was to ensure that PLGA-PEG microparticulate paste compositions and thus mechanical properties were consistent throughout the constructs produced. Consistency in this sense was very challenging

to assess quantitatively and so a simpler qualitative measure was needed. If a microparticulate paste could not be bioplotted in its entirety but instead resulted in a wasted remnant of material in the syringe barrel then this indicated that consistency was certainly not achieved. Complete deposition of all material was therefore considered as a first criterion for defining conditions under which consistent deposition was possible.

Minimising the amount of carrier needed to achieve complete deposition was considered important since smaller amounts of carrier would result in greater mechanical strengths and lower levels of post-bioplotting microparticle flow. As a result the first analysis undertaken in this optimisation study was to determine the minimum carrier:solid (v:w) ratios needed for a range of aqueous carriers to ensure that the entirety of microparticulate pastes prepared with them could be bioplotted. Medium viscosity CMC, high viscosity CMC and Pluronic® F127 were considered as potential aqueous carriers and were assessed at a range of concentrations (Table 5.1). The three carrier/concentration combinations that resulted in the lowest minimum ratios were taken forward for further investigation and optimisation. These were 3% (w/v) medium viscosity CMC , 2% (w/v) high viscosity CMC and 3% (w/v) high viscosity CMC at corresponding carrier:solid (v:w) ratios of 1.4:1, 1.4:1 and 1.3:1.

Carrier	Minimum Carrier:Solid Ratio (v:w)
0.5% (w/v) Medium Viscosity CMC	1.7:1
1% (w/v) Medium Viscosity CMC	1.7:1
2% (w/v) Medium Viscosity CMC	1.6:1
3% (w/v) Medium Viscosity CMC	1.4:1
0.5% (w/v) High Viscosity CMC	1.7:1
1% (w/v) High Viscosity CMC	1.5:1
2% (w/v) High Viscosity CMC	1.4:1
3% (w/v) High Viscosity CMC	1.3:1
0.5% (w/v) Pluronic® F127	1.6:1
1% (w/v) Pluronic® F127	1.5:1
2% (w/v) Pluronic® F127	1.5:1
3% (w/v) Pluronic® F127	1.5:1

Table 5.1 – Minimum v:w ratios of a variety of aqueous carriers to PLGA-PEG microparticles (solid) required to produce pastes which could be completely deposited (i.e. extruded in their entirety) by Fab@Home Model 2 bioplotting platform.

These three most effective carriers were used to produce constructs for unconstrained compression testing at the ratios described above and at one ratio each side of these values (n = 3). Yield stresses (Figure 5.10) and Young's moduli (Figure 5.11) were analysed. There were no statistically-significant differences between different ratios for the same carrier based on either parameter. The majority of results obtained using different carriers were also statistically similar. However 2% (w/v) high viscosity CMC at 1.3:1 and 1.4:1 ratios and 3% (w/v) high viscosity CMC at 1.3:1 and 1.4:1 ratios showed statistically-significantly ($p < 0.05$) greater values than some of those obtained with 3% (w/v) medium viscosity CMC for at least one parameter.

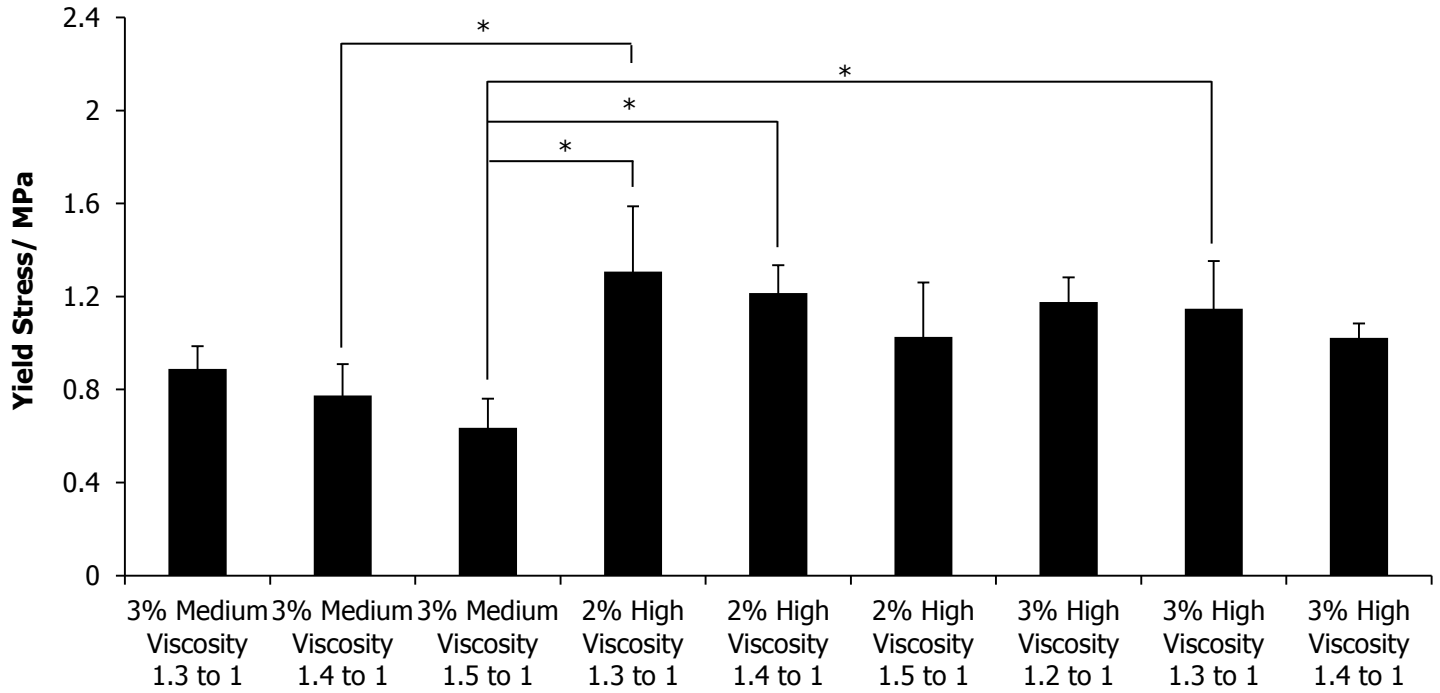

Figure 5.10 – Yield stresses for bioplotted PLGA-PEG microparticulate scaffolds as assessed by unconstrained compression testing (n = 3). PLGA-PEG microparticles were suspended in a variety of aqueous carriers at a variety of carrier:solid (v:w) ratios for bioplotting into cylindrical PTFE moulds. Samples were tested after 24 hours sintering. Error bars show one standard deviation and statistically-significant differences are denoted by (*).

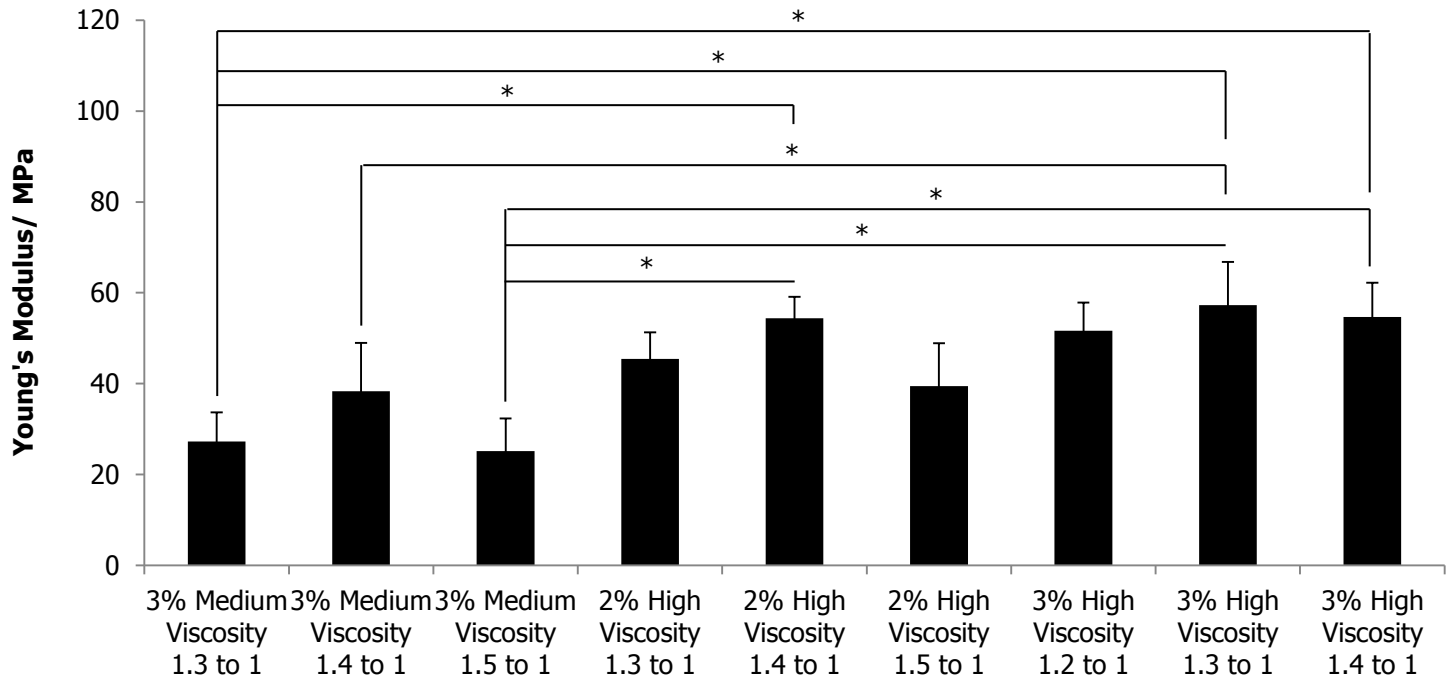

Figure 5.11 – Young's moduli for bioplotted PLGA-PEG microparticulate scaffolds as assessed by unconstrained compression testing (n = 3). PLGA-PEG microparticles were suspended in a variety of aqueous carriers at a variety of carrier:solid (v:w) ratios for bioplotting into cylindrical PTFE moulds. Samples were tested after 24 hours sintering. Error bars show one standard deviation and statistically-significant differences are denoted by (*).

Next μCT analysis was undertaken to determine the porosity and mean pore size of constructs produced using the three carriers utilised above. This analysis was conducted only on the central of the three ratios investigated earlier (n = 3). No significant differences had been observed between the mechanical properties of constructs produced with the same carrier but at different concentrations. As a result of this observation it was considered unlikely that there would be significant pore structure differences and so other ratios were not investigated. No statistically-significant ($p < 0.05$) differences were found between the three groups based on porosity (Figure 5.12). However the 2% (w/v) high viscosity CMC group was found to have a significantly lower mean pore size than the other groups (Figure 5.13).

μCT analysis of bioplotted constructs also highlighted that the standard PLGA-PEG microparticulate scaffold sintering conditions utilised may not have been allowing the completion of the sintering process. This was evidenced by macroscopic reductions in diameter of the construct portions which were illuminated by the x-ray source during imaging (Figure 5.14). This shrinkage was thought to be caused by softening and/or sintering of microparticles which still contained PEG upon loading into the μCT instrument.

Finally constructs produced using the three carriers were subjected to SEM imaging to visually confirm the results of the microCT analysis (Figure 5.15). The structures seen in SEM images did appear to reflect the trends seen in Figures 5.12 and 5.13 in that the 3% medium viscosity CMC constructs had the largest pores and highest overall porosities.

As a result of all the analyses considered in this optimisation study the most promising carriers and ratios for PLGA-PEG bioplotting were considered to be 2% (w/v) high viscosity CMC at a 1.4:1 (v:w) carrier:solid ratio and 3% (w/v) high viscosity CMC at a 1.3:1 ratio.

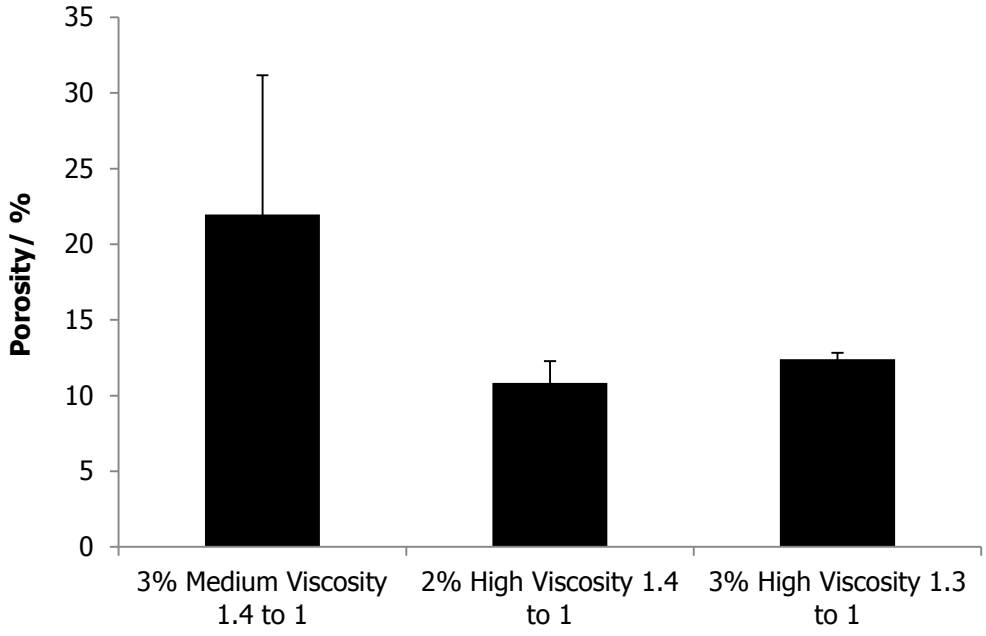

Figure 5.12 – Porosities of bioplotted PLGA-PEG microparticulate scaffolds as assessed by μCT imaging and analysis (n = 3). PLGA-PEG microparticles were suspended in a variety of aqueous carriers at different carrier:solid (v:w) ratios for bioplotting into cylindrical PTFE moulds. Samples were tested after 24 hours sintering. Error bars show one standard deviation.

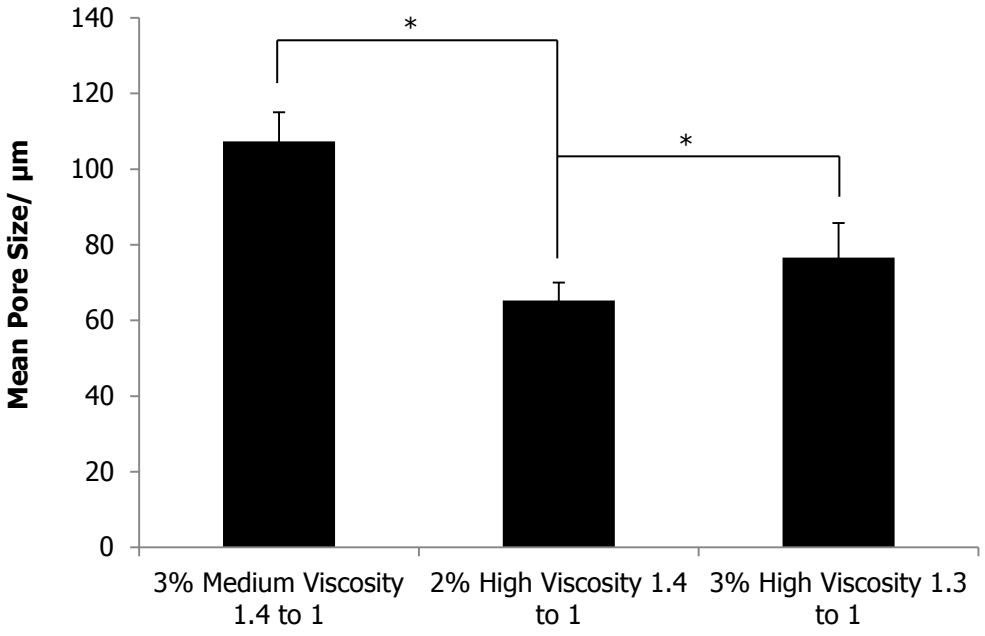

Figure 5.13 – Mean pore sizes of bioplotted PLGA-PEG microparticulate scaffolds as assessed by µCT imaging and analysis (n = 3). PLGA-PEG microparticles were suspended in a variety of aqueous carriers at different carrier:solid (v:w) ratios for bioplotting into cylindrical PTFE moulds. Samples were tested after 24 hours sintering. Error bars show one standard deviation and Statistically-significant ($p < 0.05$) differences are denoted by (*).

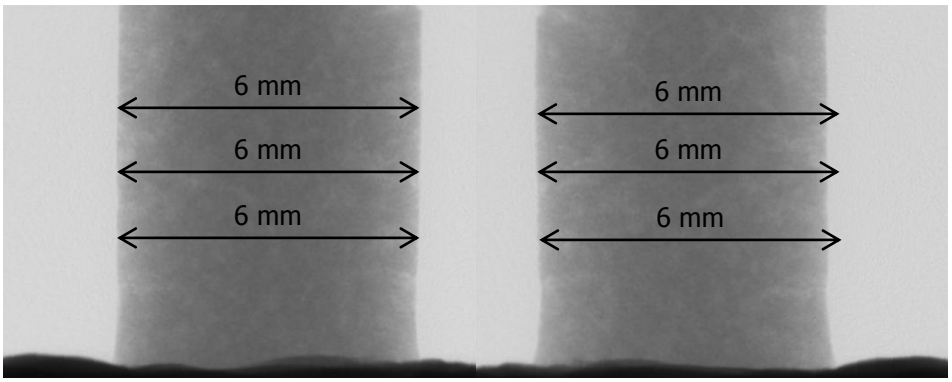

Figure 5.14 – µCT transmission images from early (left) and late (right) stages of the acquisition process. Shrinking can be seen due to thermally-mediated sintering of constructs which were incompletely sintered upon initiation of the acquisition process. PLGA-PEG microparticles were suspended in 3% (w/v) medium viscosity CMC at a 1.4:1 (v:w) ratio of liquid:solid for bioplotting into cylindrical PTFE moulds. Samples were tested after 24 hours sintering.

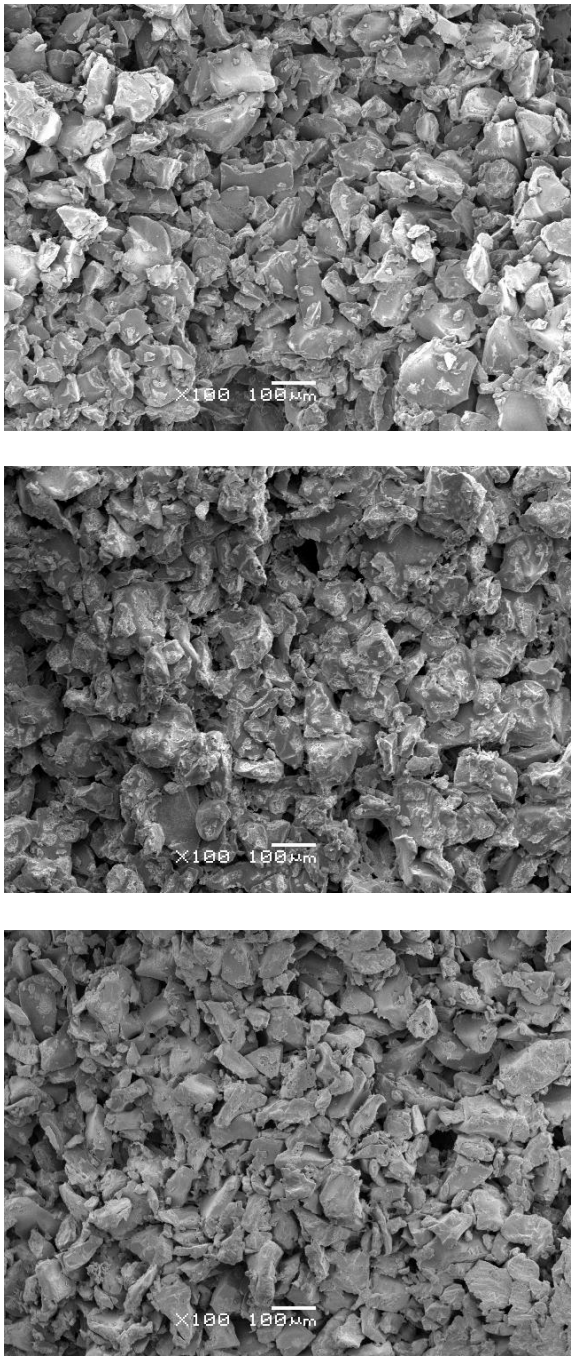

Figure 5.15 – Representative SEM images of fracture surfaces of bioplotted PLGA-PEG microparticulate scaffolds. PLGA-PEG microparticles were suspended in a range of aqueous carriers for bioplotting into cylindrical PTFE moulds. Samples were sintered for 24 hours prior to fracture and imaging. Top-to-bottom: 3% (w/v) medium viscosity CMC used at 1.4:1 (v:w) liquid:solid ratio, 2% (w/v) high viscosity CMC at 1.4:1 ratio and 3% (w/v) high viscosity CMC at 1.3:1 ratio.

5.3.3 Investigation of the Effect on Cell Viability of the Bioplotting Process

Following on from the cell-laden hydrogel bioplotting presented earlier (see Section 5.3.1) a more extensive study was undertaken to assess the compatibility of a number of cell types with the bioplotting process. Cells were suspended at 500,000 mL^{-1} in 1.5% alginate hydrogels and pre- and post-plot viabilities were assessed as before. The results of this study are summarised in Table 5.2. Figure 5.16 shows representative fluorescence microscopy images of live/dead stained bioplotted cells in 1.5% alginate hydrogels. Mean post-bioplotting cell viabilities were in the range 79 – 94% as proportions of pre-plot viabilities. Mean post-plot viability for C2C12 myoblasts was found to be statistically-significantly ($p < 0.05$) higher than that for other cell types. Additionally immortalised human mesenchymal stem cells (ihMSCs) had significantly higher post-plot viability than 3T3 fibroblasts and human osteosarcoma (hOS) cells.

Cell Type	Post-Bioplotting Viability/ %
3T3 Murine Fibroblast	83 ± 1
C2C12 Murine Myoblast	94 ± 1
Human Osteosarcoma	79 ± 3
Human Mesenchymal Stem Cell	89 ± 2

Table 5.2 – Post-bioplotting viabilities of a number of cell types suspended in 1.5% alginate hydrogels at 500,000 mL^{-1}. Viabilities were assessed by live/dead staining (n = 3) for 30 minutes with 2 μM calcein AM/ethidium homodimer-1 and are displayed as proportions of pre-plot viabilities (mean ± standard deviation).

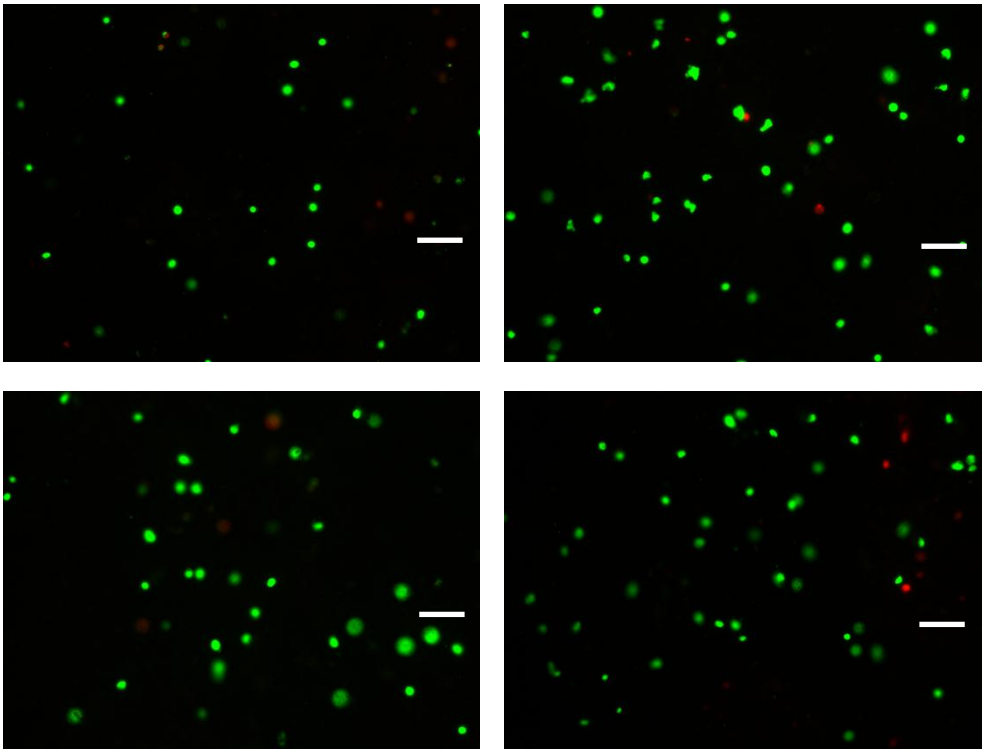

Figure 5.16 – Representative fluorescence microscopy images of cells bioplotted in 1.5% alginate hydrogels at 500,000 cells mL^{-1}. Cells have been live/dead (green/red) stained for 30 minutes with 2 μM calcein AM and ethidium homodimer-1 respectively. Clockwise from top left – 3T3 murine fibroblasts, C2C12 murine myoblasts, hOS cells and ihMSCs. Scale bars represent 100 μm.

The next step in the evaluation of live cell incorporation in alginate bioplotting was to understand which steps of the process were causing the largest losses of viability. 1.5% alginate hydrogel constructs containing ihMSCs were produced via bioplotting and the viability of the cells was assessed at three stages of the process. Viability was measured after mixing the alginate solution with the calcium sulphate crosslinker, after allowing 30 minutes for crosslinking to occur and after bioplotting ($n = 3$). Figure 5.17 summarises these results, which showed that the mean cell viabilities at all stages of the process were statistically-significantly ($p < 0.05$) different to pre-plot viability but statistically-similar to one another. An alternative presentation of this data is shown in Figure 5.18, depicting the loss of viability across each process step as a proportion of the loss across the whole process. This shows that more than 75% of the viability loss was caused by the mixing step, with the bioplotting step itself causing only around 20% of the loss (or around 2 – 4% absolute drop in cell viability).

The final analysis undertaken was designed to assess whether the final concentration of alginate within the hydrogels could influence the viability of cells encapsulated within them. In all cases, the w:w ratio of alginate to calcium sulphate was kept constant at 6:1. Across the range considered (1 – 2% (w/v) alginate concentration) no statistically-significant ($p < 0.05$) variation in cell viability was measured (Figure 5.19).

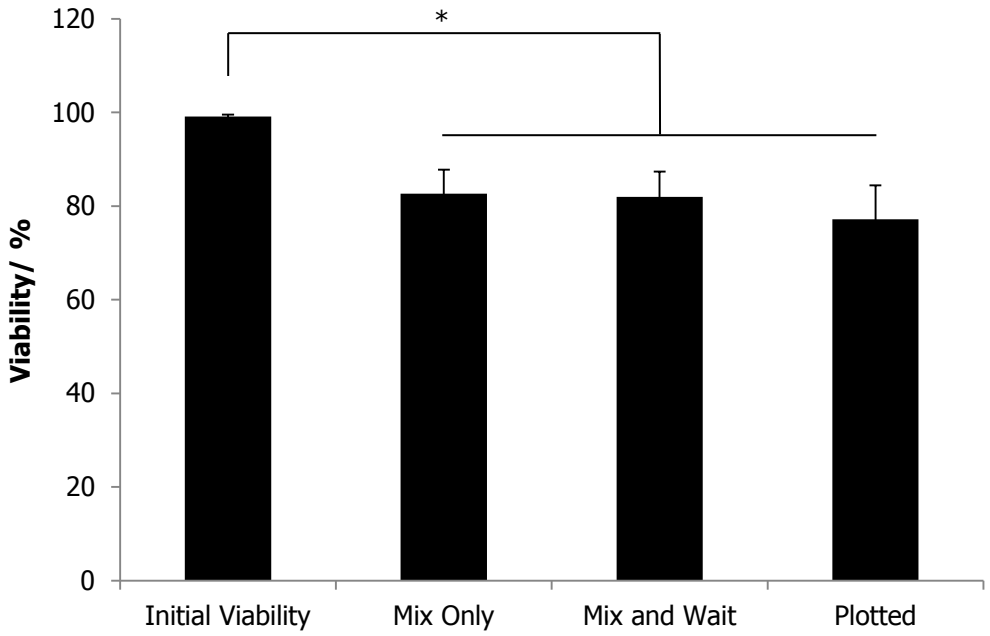

Figure 5.17 – Mean viabilities of ihMSCs at various stages of the bioplotting process (n = 3). Cells were suspended in 1.5% alginate hydrogels at 500,000 mL^{-1}. Cell viabilities were assessed by live/dead staining for 30 minutes with 2 µM calcein AM and ethidium homodimer-1 respectively. Viabilities were measured after alginate/calcium sulphate mixing, after 30 minutes wait for crosslinking and after bioplotting. Error bars are one standard deviation and statistically-significant differences to initial viability are denoted by (*).

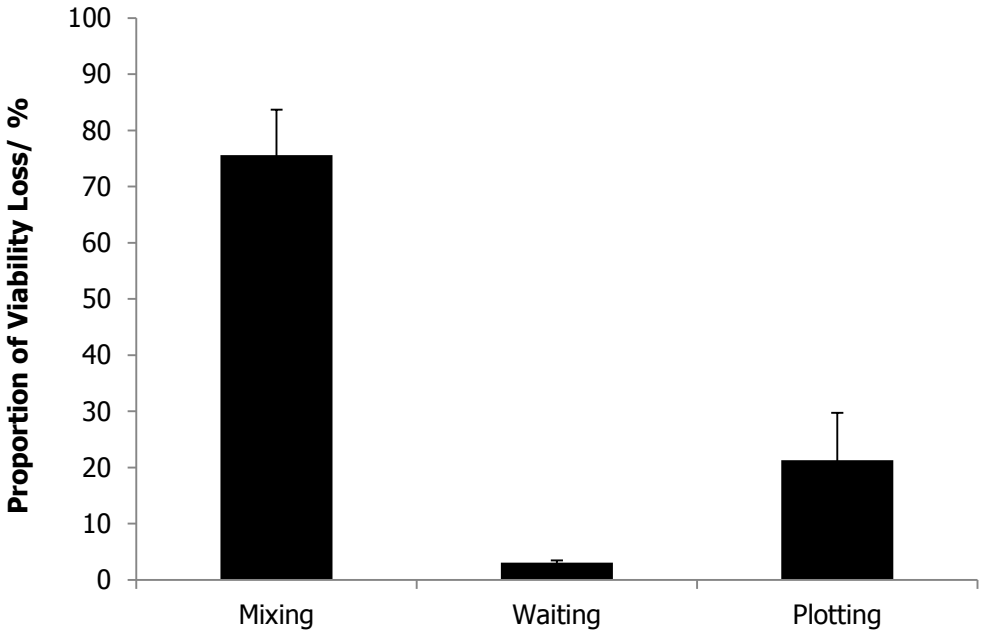
Proportion of Viability Loss/ %
100
90
80
70
60
50
40
30
20
10
0
Mixing
Waiting
Plotting

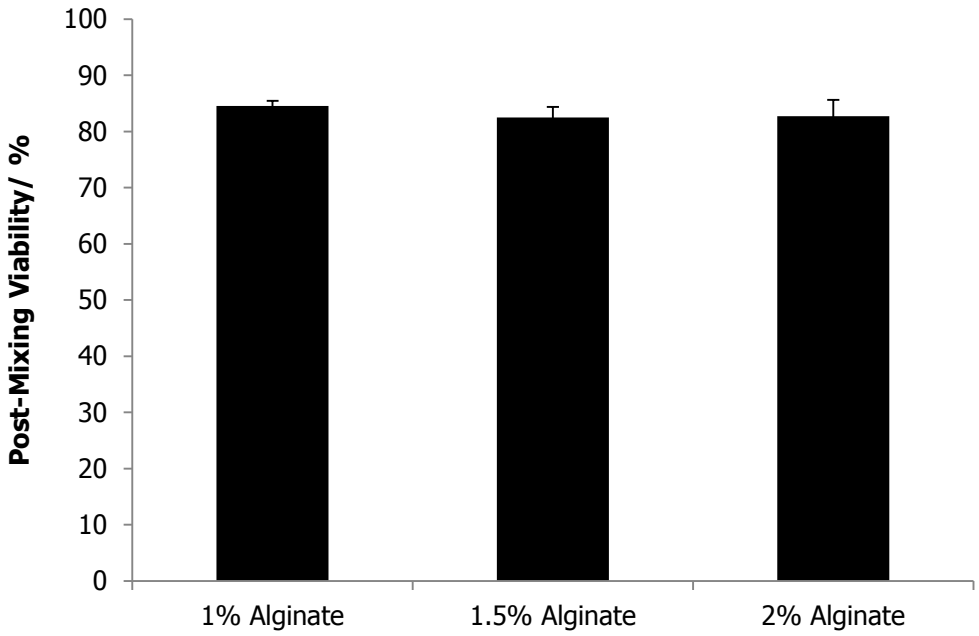
Post-Mixing Viability/ %
100
90
80
70
60
50
40
30
20
10
0
1% Alginate
1.5% Alginate
2% Alginate

5.4 Discussion

5.4.1 Feasibility of Bioplotting as a Patterned Construct Fabrication Technique for Osteochondral Defect Repair

The initial study undertaken with the Fab@Home Model 1 bioplotting platform demonstrated that this technique could be used to produce patterned constructs containing materials suitable for osteochondral repair. Crosslinked alginate hydrogels could be deposited to recreate shapes with high resolution and bone and cartilage-derived cells could be bioplotted within these gels whilst maintaining around 80% viability. The ability of such chondrocyte-loaded alginate gels to generate cartilage tissue *in vitro* is well-established[230,244,245].

It was also shown that the Fab@Home platform could be used to bioplot constructs composed of a PLGA-based synthetic polymer microparticle paste which could subsequently undergo thermoresponsive liquid sintering to form solid structures[270-273,540,541]. Similar formulations have been shown previously to be capable of forming constructs with mechanical properties similar to normal cancellous bone[270-273]. PLGA microspheres could be incorporated into the microparticle pastes without disrupting the sintering process. SEM and μCT imaging confirmed that microparticle-to-microparticle bridging had occurred and a porous sintered solid had been formed. The incorporation of microspheres allows for the temporally-controlled delivery of proteins from bioplotted constructs[272,541].

Dual material constructs could also be produced using the Fab@Home Model 1. These constructs contained both alginate hydrogel and PLGA-PEG microparticulate phases. The inclusion of alginate hydrogel phases did not disrupt the successful sintering of the PLGA-PEG phases contained within the same constructs. By appropriate choice of liquid sintering medium the alginate phases of dual material scaffolds could either be retained or removed during the sintering process. The

former allowed the gel to act as a reservoir for cells and/or proteins whilst the latter allowed it to act as a temporary reinforcement to prevent collapse of non-self-supporting PLGA-PEG structures.

Finally the work undertaken showed that it was possible to use a bioplotting construct fabrication technique to simultaneously and independently pattern materials, cell populations and protein signals. This suggested that techniques of this type could be used to produce constructs for simultaneous repair of multiple tissues in complex osteochondral defects.

The initial study described above demonstrated that bioplotting techniques have great potential for tissue engineering and modelling. However weaknesses were identified in the process and constructs as applied and produced at this stage. The mechanical properties of the constructs were inferior to those of constructs produced from PLGA-PEG microparticles in previous studies[270-273]. Though the particular paste formulations used in this and previous studies differ the key consideration is that the mechanical properties measured here were not sufficient for the support of defects in load-bearing bones. Additionally the cell viabilities measured in bioplotted alginate hydrogels were at the lower end of those published in other bioplotting studies[226,229,230,232,234,238,240,242,243,249,549]. As a result of these identified weaknesses more systematic evaluation and optimisation was undertaken using a Fab@Home Model 2 bioplotting system.

5.4.2 Optimisation of Bioplotting of PLGA-PEG Microparticle Pastes

A study was undertaken which was designed to maximise the mechanical properties of bioplotted PLGA-PEG microparticulate constructs in order to render them more suitable for bone defect repair. The study also assessed the pore structures of these constructs as maintenance of adequate porosity and pore size are important considerations for ensuring tissue ingrowth *in vivo*. Two different inherent viscosities

of CMC were assessed as viscosity modifiers for use in carrier solutions along with Pluronic® F127 as a lubricant for microparticle-microparticle interactions. The most promising combinations of carrier and concentration were chosen on the basis of requiring the smallest carrier:solid (v:w) ratio to achieve complete deposition of all material. Complete deposition was considered to be a minimum requirement for achieving consistency of paste composition throughout the bioplotting process.

On the basis of the yield stresses and Young's moduli of bioplotted PLGA-PEG constructs 2 and 3% (w/v) high viscosity CMC appeared to be the most promising carriers for construct fabrication. In particular these carriers performed well when mixed with microparticles at the minimum carrier:solid ratios derived earlier. At these ratios the constructs had yield stresses of 1.22 and 1.15 MPa respectively and Young's moduli of 54.4 and 57.3 Mpa. These properties are lower than those for many ceramic[182,191,194,198] and synthetic polymer[88,157,178,204,211,530] constructs used in bone tissue engineering. However they are within the normal ranges for cancellous bone[542-545].

The mean porosities of constructs produced using these carriers at these ratios were relatively low at only 10.8 and 12.4% for 2 and 3% high viscosity CMC respectively. These values are reflected in the relatively dense structures seen via SEM imaging and they are lower than those of some other bone tissue engineering constructs with similar or better mechanical properties[88,157,191,194,198,204,211,530]. The mean pore sizes for constructs produced using these carriers were 65.3 and 76.6 μm. It has been suggested that an optimal construct for bone regeneration needs to contain a significant amount of pores of around 200 – 400 μm in size in order to maximise tissue ingrowth[550-553]. The pores produced here were clearly smaller than this suggested range but equally they were large enough to allow cell motion through and proliferation in the constructs. Additionally the pore size distributions of bioplotted constructs showed small but appreciable population fractions which were within this optimal size range (data not shown).

Further progress on improving both the overall porosity and pore sizes of bioplotted PLGA-PEG microparticle constructs may be required for successful application *in vivo*. The simplest way to achieve this would be via the use of larger microparticles with a more uniform size distribution. Greater uniformity would result in less efficient packing and thus greater porosity whilst larger microparticle sizes would result in larger pores. Work so far on PLGA-PEG microparticle bioplotting suggests that using larger rough milled microparticles may not be a feasible option. Additionally it is difficult to ensure uniformity of size in a population of objects with irregular shapes and potentially very high aspect ratios.

One option which may be feasible is the use of PLGA-PEG microspheres as the solid component of the pastes. Microparticles with regular spherical morphology would pack less efficiently than those with irregular morphology. Microspheres would also flow over one another more efficiently which may allow carrier:solid ratios and tip inner diameters to be lowered relative to the values used in this work. These changes could result in improved mechanical properties and improved patterning resolution respectively.

5.4.3 Evaluation of the Effect of the Bioplotting Process on the Viability of Cells in Hydrogels

Following on from the results of the feasibility study described earlier (see Sections 5.3.1 and 5.4.1) cells derived from a number of tissues were bioplotted in 1.5% alginate hydrogels and their post-plot viabilities assessed. These were typically in the range 75 – 95% as proportions of pre-plot viability. This range is in good agreement with the viabilities reported in other studies involving bioplotting of cell-laden alginate[226,229,230,232] and other hydrogels[226,234,238,240,242,243,249,549]. Statistically-significant ($p < 0.05$) differences were seen between different cell types and understanding the reasons for these differences will be a key step in the further

optimisation of bioplotting protocols. It may be supposed that cells derived from tissues which experience very large mechanical loads, such as bone, would be more resilient to the stresses imposed on them during bioplotting. However in this case hOS cells were found to withstand the process less successfully than C2C12 myoblasts, suggesting that the reasons for such variation are more complex than this one single factor.

It was identified that the key step of the sample preparation and bioplotting process which was most detrimental to cell viability was the significant amount of mixing needed to combine the alginate and calcium sulphate solutions. This step caused over 75% of the observed loss of viability whilst the deposition itself caused only 20% of it (equating to around a 2 – 4% absolute loss of viability). This suggests that the loss of cell viability across the bioplotting process as a whole could potentially be very low for cells encapsulated in materials which require less mixing or other processing to formulate them for extrusion. It also suggests that the results obtained here are comparable with those obtained in previous studies which involved the deposition of cells in alginate solutions without calcium crosslinking[226,232].

The final concentration of alginate in crosslinked, cell-laden hydrogels was varied whilst keeping the alginate:calcium sulphate (w:w) ratio constant and the effect on cell viability post-mixing was assessed. Within the range studied varying this parameter did not significantly affect the cell viability. The range studied was relatively narrow but it was difficult to vary the alginate concentration further. Utilising lower concentrations resulted in materials which were not sufficiently solid to allow retention of structure after deposition. Hydrogels with higher alginate concentrations could not be produced utilising the alginate considered in this study as it was not soluble at sufficiently high concentrations. Only one previous study has directly compared post-plot cell viabilities for alginate hydrogels of different concentrations[232]. This study was performed using a very different range of concentrations (5 – 10% (w/v)) and a different alginate product but nevertheless

also found no significant effect of concentration. Other studies have utilised alginate concentrations individually across the range 1.33 – 2% (w/v) and no very large differences in post-plot cell viability have been observed[226,229,230].

Another parameter which could be considered when optimising the bioplotting of cell-laden hydrogels would be the cell density within them. It may be expected that increasing the cell density would lead to a greater level of cell damage and death since they would then constitute a larger volume fraction of the material and thus be less likely to be stress shielded by the gel.

As well as optimising the cell density it may be possible to find alternative mixing protocols which would result in lower mechanical loading of the cell-laden hydrogels. Previous work indicates that the extensive mixing utilised in the work presented in this chapter is necessary to ensure consistency of material properties through the bioplotting process[554]. This suggests that significant reduction of the amount of mixing may not be possible. As a result it may be important to consider automation or at least improved control of the mixing process which is currently used. In the current protocol mixing is by hand and the mixing rate is controlled only by operator judgement. This results in a process which is relatively poorly-controlled and potentially has a very high degree of variability. Superior control of the process would allow the mixing rate to be varied and optimised for both mixing efficiency and eventual cell viability. Such control could be exercised via the use of programmable syringe pumps or similar to drive the motion of the syringe plungers at more tightly-defined rates.

5.4.4 The Potential of Bioplotting for Patterned Construct Fabrication

The feasibility study presented in Section 5.3.1 demonstrated that the Fab@Home bioplotting platform could produce constructs containing patterned materials, patterned protein signals and patterned cell populations. However it also highlighted

that the 'quality' of result that could be obtained with multiple scaffold phases was inferior to that obtained when only a single phase was needed. The processes used to produce complex constructs require further optimisation from a practical and logistical standpoint to ensure that this 'quality' is improved.

An additional requirement is the demonstration that patterns generated during construct production are converted into patterns of cell behaviour *in vitro* or tissue formation *in vivo*. This issue was discussed earlier in relation to microinjection/micromanipulation-based patterning (see Section 3.4.5). Requirements include the demonstration that patterns of cell populations can be maintained when cells are afforded the opportunity to adhere and move through the constructs. Also needed is evidence that signal patterns generated by protein release from patterned microspheres can be stabilised by the ability of cells to act as signal sinks. Furthermore it is necessary to demonstrate that these stabilised patterns can then be converted into patterned cellular behaviour.

In order to achieve truly functional patterning and cell-populated construct phases which are suitable for bone repair the incorporation of viable cells in bioplotted PLGA-PEG pastes is an important step. This has not been demonstrated in the work presented here but other results in this chapter along with those obtained previously[270,272] suggest it is achievable. The work presented in this chapter has demonstrated that the deposition step of the bioplotting process does not cause significant cell death, at least for cells deposited in alginate hydrogels. Previous work utilising PLGA-PEG microparticle pastes has shown that constructs can be formed from this material containing populations of live cells which go on to proliferate post-production[270,272]. The existence of these prior studies does not render the successful bioplotting of viable cells in PLGA-PEG microparticle pastes a trivial achievement. However it does suggest that with appropriate optimisation of the process it should be possible.

6. Conclusions & Future Work

6.1 Three-Dimensional Patterning in Tissue Engineering

As highlighted in the introduction to this thesis (see Chapter 1) three-dimensional patterning technologies are likely be important in the development of future tissue engineering therapies and engineered tissue models. *In vitro* tissue models which could reproduce some of the structural complexity and cell-cell interactions of native tissue would be a useful alternative or addition to pre-clinical animal models for drug screening and development. Future tissue engineering therapies may also benefit from, or even require the heterogeneous distribution of construct constituents to achieve fully-functional tissue repair. This may be particularly true for applications involving large, complex defects incorporating multiple tissue types.

The work presented in this thesis has addressed aspects of such three-dimensional patterning strategies in tissue engineering. Some of the work focused on the production of biomaterial formulations for use in patterning. Poly(lactic-co-glycolic acid)-based (PLGA-based) microsphere formulations were considered (see Chapter 3) along with hydrogels derived from the extracellular matrix (ECM) of bovine bone (see Chapter 4). The remainder of the work related to the patterning techniques themselves. The techniques utilised were microinjection/micromanipulation (MM) (see Chapter 3) and bioplotting (see Chapter 5). These techniques were intended to address different aims, with the former used to attempt patterning of individual PLGA-based microspheres within *in vitro* culture environments. This was envisaged to be useful for the deduction of fundamental cell and molecular biology by replication of developmental and repair environments and processes. In contrast bioplotting was intended as an approach to patterning materials, cells and protein signals at a higher level. The constructs created by this coarser patterning were

intended to be useful both as *in vitro* tissue models and potential future tissue engineering therapies.

6.2 Production and Patterning of PLGA-Based Microspheres

Double emulsion-based protocols were developed for the production of PLGA microspheres with size distributions centred on means of around 15 and 100 μm and with low batch-to-batch variabilities. These distinctly-different size distributions could give rise to distinctly-different release kinetics[294,343,346]. These release kinetics could be further modified by supplementing the PLGA of which the microspheres were composed with a PLGA-poly(ethylene glycol)-PLGA (PLGA-PEG-PLGA) triblock copolymer ('Triblock')[267]. The hydrophilic PEG component of the copolymer acted to increased water ingress into the microspheres and thus accelerate protein release in a dose-dependent manner. Further tailoring of the Triblock concentration and/or the combination of multiple microsphere types into a single formulation would allow more sophisticated control of the protein release profiles. In particular the combination of a fast-releasing type with a slow-releasing type may have the potential to generate a zero-order release profile for sustained and consistent biological action.

Both sizes of microsphere could be suspended in water and delivered via ejection from microlitre syringes at densities as high as 75% (w/v). The number of microspheres contained within individual ejection volumes was used as a measure of the consistency of the delivery process. Based upon this output the delivery of microspheres suspended in water alone was subject to very significant variation. In some, though not all cases supplementing the suspension fluid with carboxymethyl cellulose (CMC) led to improved ejection-to-ejection consistency. This was attributed to the fact that CMC addition could significantly extend the time taken for microspheres to settle out of suspension. Further work is needed to deduce optimal conditions for the delivery of microsphere suspensions but this was not undertaken

here since microlitre syringes proved to be insufficiently precise delivery systems for the intended patterning work.

A semi-automated MM system was successfully used to pattern microspheres individually into agarose hydrogels with inter-microsphere spacings as small as 100 μm. This suggested that the technology may have the potential to produce environments for the deduction of fundamental cell and developmental biology. However further work is required on a number of aspects of the process in order to fully realise this potential. The protocol used for patterning in this work was highly-dependent on operator skill and did not allow the production of patterns containing more than a few microspheres. Furthermore agarose is not a suitable cell culture environment due to its poor cell adhesion properties[358,359] and the gelatin conjugation process[555] which was used here to overcome this problem proved promising but unreliable (see Appendix). Alternative modification with RGD-containing peptide sequences[131,140] and logistically-different patterning protocols may allow truly effective three-dimensional patterning into hydrogels which could support cell growth. Finally the ability to pattern cells in addition to microspheres via MM techniques would allow still greater control over the assessment of cellular responses to protein gradient environments.

6.3 Production of Hydrogels from the Extracellular Matrix of Bovine Bone

The work presented in Chapter 4 includes the generation of demineralised bone matrix (DBM) powder from bovine bone and the subsequent decellularisation of this material to produce decellularised extracellular matrix (DECM). Both of these materials could be solubilised by enzymatic digestion and the resulting solutions could undergo temperature- and pH-responsive gelation at physiological conditions. These materials may therefore be suitable for use as injectable scaffolds for tissue engineering therapies. This idea is further supported by the positive results obtained when utilising these ECM-derived hydrogels as *in vitro* cell culture surfaces. Across

two cell types and a number of different conditions the ECM-derived gels consistently outperformed collagen and could in some cases match tissue culture plastic, the gold standard culture surface. Further work is nevertheless required to understand the observed significant response differences between different cell types and to deduce the identity of any beneficial DBM and DECM constituents.

These solubilised ECM-derived materials may be incorporated into both patterning techniques considered in this thesis. Work presented in Chapter 4 showed that, by the use of an alginate intermediate, these materials could be formed into beads. These beads have inherent bioactivity but could also potentially be used to encapsulate proteins for subsequent release by cell-mediated degradation of the beads. As a result ECM-derived hydrogel beads may be useful for MM-based strategies in tissue modelling. A similar approach to that used for bead formation could also be used to bioplot ECM-derived gel constructs. This approach would help to circumvent any issues which may be caused by the relatively slow gelation kinetics of these materials. One limitation to this approach would be that cell encapsulation in the hybrid alginate/ECM material would inevitably be associated with significant losses during the alginate elimination step.

6.4 Bioplotting for the Production of Patterned Tissue Engineering Constructs

As has been found in a number of previous studies[226,229,230,232,234,238,240,242,243,249,549] the work presented in Chapter 5 demonstrated that alginate hydrogels could be bioplotted containing cells which retained a high degree of viability (around 75% or more). It also established that the majority of the loss of viability which was observed was due to sample preparation and not the bioplotting process itself. This suggested that hydrogels of similar rheological properties but requiring less physical mixing during preparation could be used to bioplot cells with only around 2 – 4% loss of viability. Future work may seek to further explore the cell type-to-cell type

differences in post-plot viability observed here in order to tailor bioplotting protocols to individual populations.

A novel application of bioplotting was also considered in which it was used to extrude pastes composed of thermoresponsive PLGA-PEG microparticles suspended in aqueous carriers. These extruded pastes could be sintered under physiological conditions resulting in constructs with bone-appropriate mechanical properties[270-273] (yield stresses up to 1.22 MPa and Young's moduli as high as 57.3 MPa). The porosities of these constructs were lower than would be desirable and may need to be increased in order to achieve effective tissue repair in future *in vivo* applications. Additional work may also be needed to increase the number of pores falling within the 200 – 400 μm size range which has been considered ideal for achieving *in vivo* bone ingrowth[550-553]. Achieving these aims may be significantly aided by the use of PLGA-PEG microspheres in place of the rough milled microparticles used in this work. This would reduce the packing efficiency of individual objects within the pastes resulting in increased porosity. The improved flow properties of microspheres relative to microparticles may also allow the use of larger objects, giving rise to increased pore sizes.

Work presented in this thesis also demonstrated the capability of the Fab@Home bioplotting platform to produce dual material constructs containing both alginate and PLGA-PEG phases. Furthermore it showed that the platform could produce constructs containing four separate phases and patterns of materials, cell populations and protein signals. This complex patterning capability gives the technique excellent and widely-applicable potential for use in tissue engineering and *in vitro* modelling and particularly in construct fabrication for osteochondral repair. Lessons learnt during the bioplotting of cell-laden alginate hydrogels are especially widely-applicable since it can be assumed that the rheological properties of the hydrogel are the dominant factor in determining the cell response to applied mechanical stresses. This means that the fate of cells bioplotted in alginate gels should be similar to that of

cells in other hydrogels with similar rheological properties, regardless of their biochemical nature.

6.5 Current & Future Directions

Overall it can be said that the results presented here have helped to demonstrate and extend the potential of three-dimensional patterning techniques in tissue engineering. The application of MM techniques in this field has been very limited but in this thesis it has been shown that they can be powerful tools for the recreation of complex heterogeneous signal environments *in vitro*. Previously-published studies utilising bioplotting in this field have almost exclusively used hydrogels as construct materials[226,227,229,230,232,240,242,243,245-247,249-251,546] and this has limited the application of the technique to bone tissue engineering. Here the potential of bioplotting in this specific area has been enhanced by the utilisation of synthetic polymer microparticulate pastes as scaffold materials. These can be extruded and sintered at mild conditions but nevertheless achieve bone-appropriate mechanical properties[270-273].

The use of synthetic polymer microspheres and/or ECM-derived hydrogel beads as protein delivery vehicles allows these signals to be presented in a temporally-controlled manner. This is in addition to the spatial control exerted by the patterning technologies themselves. Indeed MM techniques in particular could even be used to introduce new protein-loaded elements and/or cell populations during post-production *in vitro* culture.

Taken together these techniques potentially allow the recreation of tissue architecture and cellular microenvironments across a very large range of length scales. This may be useful for a range of applications, from the replication of key developmental processes to the restoration of large volumes of lost tissue.

References

[1] Lundkvist, A., Lee, S. *et al.* Growth factor gradients in vascular patterning. *Novartis Foundation Symposium* **283**, 194-241, (2007).

[2] Ashe, H.L. & Briscoe, J. The interpretation of morphogen gradients. *Development* **133(3)**, 385-394, (2006).

[3] Tseng, Q., Duchemin-Pelletier, E. *et al.* Spatial organization of the extracellular matrix regulates cell-cell junction positioning. *Proceedings of the National Academy of Sciences of the United States of America* **109(5)**, 1506-1511, (2012).

[4] Kollmannsberger, P., Bidan, C.M. *et al.* The physics of tissue patterning and extracellular matrix organisation: how cells join forces. *Soft Matter* **7(20)**, 9549-9560, (2011).

[5] Lelievre, S.A. Contributions of extracellular matrix signaling and tissue architecture to nuclear mechanisms and spatial organization of gene expression control. *Biochimica Et Biophysica Acta - General Subjects* **1790(9)**, 925-935, (2009).

[6] Cavalcanti-Adam, E.A., Tomakidi, P. *et al.* Geometric organization of the extracellular matrix in the control of integrin-mediated adhesion and cell function in osteoblasts. *Progress in Orthodontics* **6(2)**, 232-237, (2005).

[7] Martins, A., da Silva, M.L.A. *et al.* The influence of patterned nanofiber meshes on human mesenchymal stem cell osteogenesis. *Macromolecular Bioscience* **11(7)**, 978-987, (2011).

[8] Patel, S., Kurpinski, K. *et al.* Multilayer fibrous polymer scaffolds, methods of production and methods of use. US20100233115 (2010).

[9] Mehrotra, S., Lynam, D. *et al.* Time controlled protein release from layer-by-layer assembled multilayer functionalized agarose hydrogels. *Advanced Functional Materials* **20(2)**, 247-258, (2010).

[10] Detamore, M.S., Singh, M. *et al.* Microsphere-based materials with predefined 3D spatial and temporal control of biomaterials, porosity and/or bioactive signals. WO2009049230 (2009).

[11] Dormer, N.H., Singh, M. *et al.* Osteochondral interface tissue engineering using macroscopic gradients of bioactive signals. *Annals of Biomedical Engineering* **38**, 2167-2182, (2010).

[12] Wang, X., Wenk, E. *et al.* Growth factor gradients via microsphere delivery in biopolymer scaffolds for osteochondral tissue engineering. *Journal of Controlled Release* **134**, 81-90, (2009).

[13] Singh, M., Morris, C.P. *et al.* Microsphere-based seamless scaffolds containing macroscopic gradients of encapsulated factors for tissue engineering. *Tissue Engineering Part C - Methods* **14(4)**, 299-309, (2008).

[14] Anselme, K., Davidson, P. *et al.* The interaction of cells and bacteria with surfaces structured at the nanometre scale. *Acta Biomaterialia* **6(10)**, 3824-3846, (2010).

[15] Ganesan, R., Kratz, K. *et al.* Multicomponent protein patterning of material surfaces. *Journal of Materials Chemistry* **20(35)**, 7322-7331, (2010).

[16] Ringeisen, B.R., Othon, C.M. *et al.* Jet-based methods to print living cells. *Biotechnology Journal* **1(9)**, 930-948, (2006).

[17] Campbell, P.G. & Weiss, L.E. Tissue engineering with the aid of inkjet printers. *Expert Opinion on Biological Therapy* **7(8)**, 1123-1127, (2007).

[18] Schiele, N.R., Corr, D.T. *et al.* Laser-based direct-write techniques for cell printing. *Biofabrication* **2(3)**, doi: 10.1088/1758-5082/1082/1083/032001, (2010).

[19] Gagnon, Z.R. Cellular dielectrophoresis: applications to the characterization, manipulation, separation and patterning of cells. *Electrophoresis* **32(18)**, 2466-2487, (2011).

[20] Inamdar, N.K. & Borenstein, J.T. Microfluidic cell culture models for tissue engineering. *Current Opinion in Biotechnology* **22(5)**, 681-689, (2011).

[21] Yeo, L.Y., Chang, H.C. *et al.* Microfluidic devices for bioapplications. *Small* **7(1)**, 12-48, (2011).

[22] Quist, A.P. & Oscarsson, S. Micropatterned surfaces: techniques and applications in cell biology. *Expert Opinion on Drug Discovery* **5(6)**, 569-581, (2010).

[23] Alves, N.M., Pashkuleva, I. *et al.* Controlling cell behavior through the design of polymer surfaces. *Small* **6(20)**, 2208-2220, (2010).

[24] Lu, R.Y., Yang, L.H. *et al.* Stereotaxic microinjection of adenovirus-mediated human tissue Kallikrein gene reduces apoptosis in a rat model of middle cerebral artery occlusion. *Neural Regeneration Research* **3(8)**, 847-852, (2008).

[25] Poliacek, I., Wang, C. *et al.* Microinjection of codeine into the region of the caudal ventral respiratory column suppresses cough in anesthetized cats. *Journal of Applied Physiology* **108**, 858-865, (2010).

[26] Erfanparast, A., Tamaddonfard, E. *et al.* Effect of microinjection of histamine into the dorsal hippocampus on the orofacial formalin-induced pain in rats. *European Journal of Pharmacology* **627**, 119-123, (2010).

[27] Emamian, S., Naghdi, N. *et al.* Learning impairment caused by intra-CA1 microinjection of testosterone increases the number of astrocytes. *Behavioural Brain Research* **208**, 30-37, (2010).

[28] Garcia Pelosi, G., Fiacadori Tavares, R. *et al.* Cardiovascular effects of noradrenaline microinjection into the medial part of the superior colliculus of unanesthetized rats. *Brain Research* **1290**, 21-27, (2009).

[29] Davidson, S., Truong, H. *et al.* A microinjection technique for targeting regions of embryonic and neonatal mouse brain in vivo. *Brain Research* **1307**, 43-52, (2010).

[30] Siniscalco, D., Giordano, C. *et al.* Intra-brain microinjection of human mesenchymal stem cells decreases allodynia in neuropathic mice. *Cellular and Molecular Life Sciences* **67**, 655-669, (2010).

[31] Bible, E., Chau, D.Y.S. *et al.* The support of neural stem cells transplanted into stroke-induced brain cavities by PLGA particles. *Biomaterials* **30(16)**, 2985-2994, (2009).

[32] Bible, E., Chau, D.Y.S. *et al.* Attachment of stem cells to scaffold particles for intra-cerebral transplantation. *Nature Protocols* **4(10)**, 1440-1453, (2009).

[33] Masuzaki, T., Ayukawa, Y. *et al.* The effect of a single remote injection of statin-impregnated poly(lactic-co-glycolic acid) microspheres on osteogenesis around titanium implants in rat tibia. *Biomaterials* **31**, 3327-3334, (2010).

[34] Shishatskaya, E.I., Voinova, O.N. *et al.* Tissue reaction to intramuscular injection of resorbable polymer microparticles. *Bulletin of Experimental Biology and Medicine* **144**, 786-790, (2007).

[35] Sun, Y. & Nelson, B.J. Biological cell injection using an autonomous microrobotic system. *International Journal of Robotics Research* **21(10-11)**, 861-868, (2002).

[36] Matsuoka, H., Komazaki, T. *et al.* High throughput easy microinjection with a single-cell manipulation supporting robot. *Journal of Biotechnology* **116(2)**, 185-194, (2005).

[37] Wang, W., Liu, X. *et al.* A fully automated robotic system for microinjection of zebrafish embryos. *PLoS One* **2(9)**, doi: 10.1371/journal.pone.0000862, (2007).

[38] Huang, H.B., Sun, D. *et al.* Robotic cell injection system with position and force control: toward automatic batch biomanipulation. *IEEE Transactions on Robotics* **25(3)**, 727-737, (2009).

[39] Truong, H.H., de Sonneville, J. *et al.* Automated microinjection of cell-polymer suspensions in 3D ECM scaffolds for high-throughput quantitative cancer invasion screens. *Biomaterials* **33(1)**, 181-188, (2012).

[40] Leach, J., Sinclair, G. *et al.* 3D manipulation of particles into crystal structures using holographic optical tweezers. *Optics Express* **12(1)**, 220-226, (2004).

[41] Watson, D., Hagen, N. *et al.* Elastic light scattering from single cells: orientational dynamics in optical trap. *Biophysical Journal* **87(2)**, 1298-1306, (2004).

[42] Akselrod, G.M., Timp, W. *et al.* Laser-guided assembly of heterotypic three-dimensional living cell microarrays. *Biophysical Journal* **91(9)**, 3465-3473, (2006).

[43] Townes-Anderson, E., St Jules, R.S. *et al.* Micromanipulation of retinal neurons by optical tweezers. *Molecular Vision* **4**, 12, (1998).

[44] Ashkin, A. Acceleration and trapping of particles by radiation pressure. *Physical Review Letters* **24(4)**, 156-159, (1970).

[45] Ashkin, A., Dziedzic, J.M. *et al.* Observation of a single-beam gradient force optical trap for dielectric particles. *Optics Letters* **11(5)**, 288-290, (1986).

[46] Ashkin, A. & Dziedzic, J.M. Optical trapping and manipulation of viruses and bacteria. *Science* **235(4795)**, 1517-1520, (1987).

[47] Ashkin, A., Dziedzic, J.M. *et al.* Optical trapping and manipulation of single cells using infrared-laser beams. *Nature* **330(6150)**, 769-771, (1987).

[48] Seeger, S., Monajembashi, S. *et al.* Application of laser optical tweezers in immunology and molecular-genetics. *Cytometry* **12(6)**, 497-504, (1991).

[49] Steubing, R.W., Cheng, S. *et al.* Laser-induced cell-fusion in combination with optical tweezers - the laser cell-fusion trap. *Cytometry* **12(6)**, 505-510, (1991).

[50] Visscher, K., Brakenhoff, G.J. *et al.* Micromanipulation by multiple optical traps created by a single fast scanning trap integrated with the bilateral confocal scanning laser microscope. *Cytometry* **14(2)**, 105-114, (1993).

[51] Ogura, Y., Kagawa, K. *et al.* Optical manipulation of microscopic objects by means of vertical-cavity surface-emitting laser array sources. *Applied Optics* **40(30)**, 5430-5435, (2001).

[52] Gruber, L., Grier, D. *et al.* Configurable dynamic three dimensional array. US20040180363 (2004).

[53] Ozkan, M., Esener, S. *et al.* Manipulation of live cells and inorganic objects with optical micro beam arrays. US7049579 (2006).

[54] Liesener, J., Reicherter, M. *et al.* Multi-functional optical tweezers using computer-generated holograms. *Optics Communications* **185(1-3)**, 77-82, (2000).

[55] Curtis, J.E., Koss, B.A. *et al.* Dynamic holographic optical tweezers. *Optics Communications* **207(1-6)**, 169-175, (2002).

[56] Sinclair, G., Jordan, P. *et al.* Assembly of 3-dimensional structures using programmable holographic optical tweezers. *Optics Express* **12(22)**, 5475-5480, (2004).

[57] Polin, M., Ladavac, K. *et al.* Optimized holographic optical traps. *Optics Express* **13(15)**, 5831-5845, (2005).

[58] Gibson, G., Barron, L. *et al.* An optical trapped gripper for manipulating micron-sized particles. in *Optical Trapping and Optical Micromanipulation III* (Eds Dholakia, K. & Spalding, G.C.), U230-234 (Society of Photo-Optical Instrumentation Engineers, 2006).

[59] Whyte, G., Gibson, G. *et al.* An optical trapped microhand for manipulating micron-sized objects. *Optics Express* **14(25)**, 12497-12502, (2006).

[60] Fukuchi, N. & Igasaki, Y. Optical tweezers. US20070114371 (2007).

[61] Hu, S.Y. & Sun, D. Automatic transportation of biological cells with a robot-tweezer manipulation system. *International Journal of Robotics Research* **30(14)**, 1681-1694, (2011).

[62] Lucio, A.D., Santos, R.A.S. *et al.* Measurements and modeling of water transport and osmoregulation in a single kidney cell using optical tweezers and videomicroscopy. *Physical Review E* **68(4)**, doi: 10.1103/PhysRevE.1168.041906, (2003).

[63] Buican, T.N., Smyth, M.J. *et al.* Automated single-cell manipulation and sorting by light trapping. *Applied Optics* **26(24)**, 5311-5316, (1987).

[64] Ericsson, M., Hanstorp, D. *et al.* Sorting out bacterial viability with optical tweezers. *Journal of Bacteriology* **182(19)**, 5551-5555, (2000).

[65] Grover, S.C., Gauthier, R.C. *et al.* Analysis of the behaviour of erythrocytes in an optical trapping system. *Optics Express* **7(13)**, 533-539, (2000).

[66] Herzenberg, L.A., Parks, D. *et al.* The history and future of the fluorescence activated cell sorter and flow cytometry: a view from Stanford. *Clinical Chemistry* **48(10)**, 1819-1827, (2002).

[67] MacDonald, M.P., Neale, S. *et al.* Cell cytometry with a light touch: sorting microscopic matter with an optical lattice. *Journal of Biological Regulators and Homeostatic Agents* **18(2)**, 200-205, (2004).

[68] Ozkan, M., Wang, M. *et al.* Optical manipulation of objects and biological cells in microfluidic devices. *Biomedical Microdevices* **5(1)**, 61-67, (2003).

[69] Rodrigo, P.J., Eriksen, R.L. *et al.* Shack-Hartmann multiple-beam optical tweezers. *Optics Express* **11(3)**, 208-214, (2003).

[70] Enger, J., Goksor, M. *et al.* Optical tweezers applied to a microfluidic system. *Lab on a Chip* **4(3)**, 196-200, (2004).

[71] MacDonald, M.P., Spalding, G.C. *et al.* Microfluidic sorting in an optical lattice. *Nature* **426(6965)**, 421-424, (2003).

[72] Rodrigo, P.J., Daria, V.R. *et al.* Four-dimensional optical manipulation of colloidal particles. *Applied Physics Letters* **86(7)**, doi: 10.1063/1061.1866646, (2005).

[73] Wang, M.M., Tu, E. *et al.* Microfluidic sorting of mammalian cells by optical force switching. *Nature Biotechnology* **23(1)**, 83-87, (2005).

[74] Cran-McGreehin, S., Krauss, T.F. *et al.* Integrated monolithic optical manipulation. *Lab on a Chip* **6(9)**, 1122-1124, (2006).

[75] Dholakia, K., MacDonald, M.P. *et al.* Cellular and colloidal separation using optical forces. in *Laser Manipulation of Cells and Tissues* (Eds Berns, M.W. & Greulich, K.O.), 467-495 (Elsevier Academic Press Inc., 2007).

[76] Rohrbach, A. & Landenberger, B. Microfluidic sorting apparatus with optical tweezers. WO2010063478 (2010).

[77] Grier, D.G. & Korda, P.T. Apparatus and process for the lateral deflection and separation of flowing particles by a static array of optical tweezers. EP1425944 (2004).

[78] Eriksson, E., Enger, J. *et al.* A microfluidic system in combination with optical tweezers for analyzing rapid and reversible cytological alterations in single cells upon environmental changes. *Lab on a Chip* **7(1)**, 71-76, (2007).

[79] Jordan, P., Leach, J. *et al.* Creating permanent 3D arrangements of isolated cells using holographic optical tweezers. *Lab on a Chip* **5(11)**, 1224-1228, (2005).

[80] Hull, C.W. Apparatus for production of three-dimensional objects by stereolithography. US4575330 (1986).

[81] Melchels, F.P.W., Feijen, J. *et al.* A review on stereolithography and its applications in biomedical engineering. *Biomaterials* **31(24)**, 6121-6130, (2010).

[82] Matsuda, T., Mizutani, M. *et al.* Molecular design of photocurable liquid biodegradable copolymers. 1. Synthesis and photocuring characteristics. *Macromolecules* **33(3)**, 795-800, (2000).

[83] Lee, J.W., Lan, P.X. *et al.* 3D scaffold fabrication with PPF/DEF using micro-stereolithography. *Microelectronic Engineering* **84(5-8)**, 1702-1705, (2007).

[84] Lee, J.W., Lan, P.X. *et al.* Fabrication and characteristic analysis of a poly(propylene fumarate) scaffold using micro-stereolithography technology. *Journal of Biomedical Materials Research Part B - Applied Biomaterials* **87B(1)**, 1-9, (2008).

[85] Lan, P.X., Lee, J.W. *et al.* Development of 3D PPF/DEF scaffolds using micro-stereolithography and surface modification. *Journal of Materials Science - Materials in Medicine* **20(1)**, 271-279, (2009).

[86] Brandi, F., Anjum, F. *et al.* Rigid biodegradable photopolymer structures of high resolution using deep-UV laser photocuring. *Journal of Micromechanics and Microengineering* **21(5)**, doi: 10.1088/0960-1317/1021/1085/054007, (2011).

[87] Melchels, F.P.W., Feijen, J. *et al.* A poly(D,L-lactide) resin for the preparation of tissue engineering scaffolds by stereolithography. *Biomaterials* **30(23-24)**, 3801-3809, (2009).

[88] Melchels, F.P.W., Bertoldi, K. *et al.* Mathematically defined tissue engineering scaffold architectures prepared by stereolithography. *Biomaterials* **31(27)**, 6909-6916, (2010).

[89] Elomaa, L., Teixeira, S. *et al.* Preparation of poly(epsilon-caprolactone)-based tissue engineering scaffolds by stereolithography. *Acta Biomaterialia* **7(11)**, 3850-3856, (2011).

[90] Qiu, Y.Z., Zhang, N. *et al.* Chemically modified light-curable chitosans with enhanced potential for bone tissue repair. *Journal of Biomedical Materials Research Part A* **89A(3)**, 772-779, (2009).

[91] Wang, S., Foo, C.W.P. *et al.* Gradient lithography of engineered proteins to fabricate 2D and 3D cell culture micro environments. *Biomedical Microdevices* **11(5)**, 1127-1134, (2009).

[92] Hinczewski, C., Corbel, S. *et al.* Ceramic suspensions suitable for stereolithography. *Journal of the European Ceramic Society* **18(6)**, 583-590, (1998).

[93] Hinczewski, C., Corbel, S. *et al.* Stereolithography for the fabrication of ceramic three-dimensional parts. *Rapid Prototyping Journal* **4(3)**, 104-111, (1998).

[94] Zhang, X., Jiang, X.N. *et al.* Micro-stereolithography of polymeric and ceramic microstructures. *Sensors and Actuators A - Physical* **77(2)**, 149-156, (1999).

[95] Licciulli, A., Corcione, C.E. *et al.* Laser stereolithography of ZrO_2 toughened Al_2O_3. *Journal of the European Ceramic Society* **25(9)**, 1581-1589, (2005).

[96] Bian, W.G., Li, D.C. *et al.* Design and fabrication of a novel porous implant with pre-set channels based on ceramic stereolithography for vascular implantation. *Biofabrication* **3(3)**, doi: 10.1088/1758-5082/1083/1083/034103, (2011).

[97] Dhariwala, B., Hunt, E. *et al.* Rapid prototyping of tissue-engineering constructs, using photopolymerizable hydrogels and stereolithography. *Tissue Engineering* **10(9-10)**, 1316-1322, (2004).

[98] Arcaute, K., Mann, B.K. *et al.* Stereolithography of three-dimensional bioactive poly(ethylene glycol) constructs with encapsulated cells. *Annals of Biomedical Engineering* **34(9)**, 1429-1441, (2006).

[99] Tsang, V.L., Chen, A.A. *et al.* Fabrication of 3D hepatic tissues by additive photopatterning of cellular hydrogels. *FASEB Journal* **21(3)**, 790-801, (2007).

[100] Mapili, G., Lu, Y. *et al.* Laser-layered microfabrication of spatially patterned functionalized tissue-engineering scaffolds. *Journal of Biomedical Materials Research Part B - Applied Biomaterials* **75B(2)**, 414-424, (2005).

[101] Lee, J.W., Kang, K.S. *et al.* Bone regeneration using a microstereolithography-produced customized poly(propylene fumarate)/diethyl fumarate photopolymer 3D scaffold incorporating BMP-2 loaded PLGA microspheres. *Biomaterials* **32**, 744-752, (2011).

[102] Lee, J.W., Ahn, G. *et al.* Evaluating cell proliferation based on internal pore size and 3D scaffold architecture fabricated using solid freeform fabrication technology. *Journal of Materials Science - Materials in Medicine* **21**, 3195-3205, (2010).

[103] Sohn, Y.S., Jung, J.W. *et al.* Investigation of bi-pore scaffold based on the cell behaviors on 3D scaffold patterns. *Tissue Engineering and Regenerative Medicine* **8(4)**, 66-72, (2011).

[104] Kim, K., Yeatts, A. *et al.* Stereolithographic bone scaffold design parameters: osteogenic differentiation and signal expression. *Tissue Engineering Part B - Reviews* **16(5)**, 523-539, (2010).

[105] Chan, V., Zorlutuna, P. *et al.* Three-dimensional photopatterning of hydrogels using stereolithography for long-term cell encapsulation. *Lab on a Chip* **10(16)**, 2062-2070, (2010).

[106] Arcaute, K., Mann, B. *et al.* Stereolithography of spatially controlled multi-material bioactive poly(ethylene glycol) scaffolds. *Acta Biomaterialia* **6(3)**, 1047-1054, (2010).

[107] Zorlutuna, P., Jeong, J.H. *et al.* Stereolithography-Based Hydrogel Microenvironments to Examine Cellular Interactions. *Advanced Functional Materials* **21(19)**, 3642-3651, (2011).

[108] Bertsch, A., Bernhard, P. *et al.* Microstereolithography: concepts and applications. in *8th IEEE International Conference on Emerging Technologies and Factory Automation.* 289-298 (2001).

[109] John, H., Schillen, V. *et al.* Device and method for producing a three-dimensional object by means of mask exposure. US7894921 (2011).

[110] Fang, N.X., Xia, C. *et al.* Three-dimensional microfabricated bioreactors with embedded capillary network. WO2009042671 (2009).

[111] Choi, J.W., Wicker, R. *et al.* Fabrication of 3D biocompatible/biodegradable micro-scaffolds using dynamic mask projection microstereolithography. *Journal of Materials Processing Technology* **209(15-16)**, 5494-5503, (2009).

[112] Cheng, Y.L. & Lee, M.L. Development of dynamic masking rapid prototyping system for application in tissue engineering. *Rapid Prototyping Journal* **15(1)**, 29-41, (2009).

[113] Han, L.-H., Mapili, G. *et al.* Projection microfabrication of three-dimensional scaffolds for tissue engineering. *Journal of Manufacturing Science and Engineering - Transactions of the ASME* **130(2)**, doi: 10.1115/1111.2823079, (2008).

[114] Han, L.-H., Suri, S. *et al.* Fabrication of three-dimensional scaffolds for heterogeneous tissue engineering. *Biomedical Microdevices* **12**, 721-725, (2010).

[115] Choi, J.W., MacDonald, E. *et al.* Multi-material microstereolithography. *International Journal of Advanced Manufacturing Technology* **49(5-8)**, 543-551, (2010).

[116] Maruo, S., Nakamura, O. *et al.* Three-dimensional microfabrication with two-photon-absorbed photopolymerization. *Optics Letters* **22(2)**, 132-134, (1997).

[117] Maruo, S. & Kawata, S. Two-photon-absorbed near-infrared photopolymerization for three-dimensional microfabrication. *Journal of Microelectromechanical Systems* **7(4)**, 411-415, (1998).

[118] Goodman, S.L. & Campagnola, P. Apparatus for nanofabrication using multi-photon excitation. EP2144725 (2009).

[119] Kasko, A.M. & Wong, D.Y. Two-photon lithography in the future of cell-based therapeutics and regenerative medicine: a review of techniques for hydrogel patterning and controlled release. *Future Medicinal Chemistry* **2(11)**, 1669-1680, (2010).

120 Narayan, R.J., Doraiswamy, A. *et al.* Medical prototyping using two photon polymerization. *Materials Today* **13(12)**, 42-48, (2010).

121 Seidlits, S.K., Schmidt, C.E. *et al.* High-resolution patterning of hydrogels in three dimensions using direct-write photofabrication for cell guidance. *Advanced Functional Materials* **19(22)**, 3543-3551, (2009).

122 Nielson, R., Koehr, B. *et al.* Microreplication and design of biological architectures using dynamic-mask multiphoton lithography. *Small* **5(1)**, 120-125, (2009).

123 Pitts, J.D., Campagnola, P.J. *et al.* Submicron multiphoton free-form fabrication of proteins and polymers: studies of reaction efficiencies and applications in sustained release. *Macromolecules* **33(5)**, 1514-1523, (2000).

124 Kaehr, B. & Shear, J.B. Mask-directed multiphoton lithography. *Journal of the American Chemical Society* **129(7)**, 1904-1905, (2007).

125 Kaehr, B. & Shear, J.B. Multiphoton fabrication of chemically responsive protein hydrogels for microactuation. *Proceedings of the National Academy of Sciences of the United States of America* **105(26)**, 8850-8854, (2008).

126 Ovsianikov, A., Schlie, S. *et al.* Two-photon polymerization technique for microfabrication of CAD-designed 3D scaffolds from commercially available photosensitive materials. *Journal of Tissue Engineering and Regenerative Medicine* **1(6)**, 443-449, (2007).

127 Jeon, H., Hidai, H. *et al.* Fabrication of arbitrary polymer patterns for cell study by two-photon polymerization process. *Journal of Biomedical Materials Research Part A* **93A(1)**, 56-66, (2010).

128 Weiss, T., Hildebrand, G. *et al.* Two-photon polymerization for microfabrication of three-dimensional scaffolds for tissue engineering application. *Engineering in Life Sciences* **9(5)**, 384-390, (2009).

129 Engelhardt, S., Hoch, E. *et al.* Fabrication of 2D protein microstructures and 3D polymer-protein hybrid microstructures by two-photon polymerization. *Biofabrication* **3(2)**, doi: 10.1088/1758-5082/1083/1082/025003, (2011).

130 Nimmo, C.M. & Shoichet, M.S. Regenerative biomaterials that "click": simple, aqueous-based protocols for hydrogel synthesis, surface immobilization, and 3D patterning. *Bioconjugate Chemistry* **22(11)**, 2199-2209, (2011).

131 Luo, Y. & Shoichet, M.S. A photolabile hydrogel for guided three-dimensional cell growth and migration. *Nature Materials* **3(4)**, 249-253, (2004).

[132] Wylie, R.G. & Shoichet, M.S. Three-dimensional spatial patterning of proteins in hydrogels. *Biomacromolecules* **12(10)**, 3789-3796, (2011).

[133] Wylie, R.G., Ahsan, S. *et al.* Spatially controlled simultaneous patterning of multiple growth factors in three-dimensional hydrogels. *Nature Materials* **10(10)**, 799-806, (2011).

[134] Wosnick, J.H. & Shoichet, M.S. Three-dimensional chemical Patterning of transparent hydrogels. *Chemistry of Materials* **20(1)**, 55-60, (2008).

[135] Aizawa, Y., Wylie, R. *et al.* Endothelial cell guidance in 3D patterned scaffolds. *Advanced Materials* **22(43)**, 4831-4835, (2010).

[136] Aizawa, Y., Leipzig, N. *et al.* The effect of immobilized platelet derived growth factor AA on neural stem/progenitor cell differentiation on cell-adhesive hydrogels. *Biomaterials* **29(35)**, 4676-4683, (2008).

[137] Leipzig, N.D., Wylie, R.G. *et al.* Differentiation of neural stem cells in three-dimensional growth factor-immobilized chitosan hydrogel scaffolds. *Biomaterials* **32(1)**, 57-64, (2011).

[138] Leipzig, N.D., Xu, C.C. *et al.* Functional immobilization of interferon-gamma induces neuronal differentiation of neural stem cells. *Journal of Biomedical Materials Research Part A* **93A(2)**, 625-633, (2010).

[139] Rahman, N., Purpura, K.A. *et al.* The use of vascular endothelial growth factor functionalized agarose to guide pluripotent stem cell aggregates toward blood progenitor cells. *Biomaterials* **31(32)**, 8262-8270, (2010).

[140] Luo, Y. & Shoichet, M.S. Light-activated immobilization of biomolecules to agarose hydrogels for controlled cellular response. *Biomacromolecules* **5(6)**, 2315-2323, (2004).

[141] Wylie, R.G. & Shoichet, M.S. Two-photon micropatterning of amines within an agarose hydrogel. *Journal of Materials Chemistry* **18(23)**, 2716-2721, (2008).

[142] Shoichet, M., Wosnick, J. *et al.* Chemically patterned hydrogels, manufacture and use thereof. US20080286360 (2008).

[143] DeForest, C.A. & Anseth, K.S. Cytocompatible click-based hydrogels with dynamically tunable properties through orthogonal photoconjugation and photocleavage reactions. *Nature Chemistry* **3(12)**, 925-931, (2011).

144 DeForest, C.A., Polizzotti, B.D. *et al.* Sequential click reactions for synthesizing and patterning three-dimensional cell microenvironments. *Nature Materials* **8(8)**, 659-664, (2009).

145 Kloxin, A.M., Kasko, A.M. *et al.* Photodegradable hydrogels for dynamic tuning of physical and chemical properties. *Science* **324(5923)**, 59-63, (2009).

146 Kloxin, A.M., Tibbitt, M.W. *et al.* Synthesis of photodegradable hydrogels as dynamically tunable cell culture platforms. *Nature Protocols* **5(12)**, 1867-1887, (2010).

147 Kloxin, A.M., Tibbitt, M.W. *et al.* Tunable hydrogels for external manipulation of cellular microenvironments through controlled photodegradation. *Advanced Materials* **22(1)**, 61-66, (2010).

148 Polizzotti, B., Anseth, K. *et al.* Hydrogels and methods for producing and using the same. US20100291357 (2010).

149 Polizzotti, B.D., Fairbanks, B.D. *et al.* Three-dimensional biochemical patterning of click-based composite hydrogels via thiolene photopolymerization. *Biomacromolecules* **9(4)**, 1084-1087, (2008).

150 Fairbanks, B.D., Schwartz, M.P. *et al.* A versatile synthetic extracellular matrix mimic via thiol-norbornene photopolymerization. *Advanced Materials* **21(48)**, 5005-5010, (2009).

151 Bowman, C., Anseth, K. *et al.* Degradable thiol-ene polymers. US20080070786 (2008).

152 Lee, S.H., Moon, J.J. *et al.* Three-dimensional micropatterning of bioactive hydrogels via two-photon laser scanning photolithography for guided 3D cell migration. *Biomaterials* **29(20)**, 2962-2968, (2008).

153 Hoffmann, J.C. & West, J.L. Three-dimensional photolithographic patterning of multiple bioactive ligands in poly(ethylene glycol) hydrogels. *Soft Matter* **6(20)**, 5056-5063, (2010).

154 Hahn, M.S., Miller, J.S. *et al.* Three-dimensional biochemical and biomechanical patterning of hydrogels for guiding cell behavior. *Advanced Materials* **18(20)**, 2679-2684, (2006).

155 Deckard, C.R. Method and apparatus for producing parts by selective sintering. US4863538 (1989).

[156] Duan, B. & Wang, M. Selective laser sintering and its application in biomedical engineering. *MRS Bulletin* **36(12)**, 998-1005, (2011).

[157] Williams, J.M., Adewunmi, A. *et al.* Bone tissue engineering using polycaprolactone scaffolds fabricated via selective laser sintering. *Biomaterials* **26(23)**, 4817-4827, (2005).

[158] Partee, B., Hollister, S.J. *et al.* Selective laser sintering process optimization for layered manufacturing of CAPA$^{(R)}$ 6501 polycaprolactone bone tissue engineering scaffolds. *Journal of Manufacturing Science and Engineering-Transactions of the ASME* **128(2)**, 531-540, (2006).

[159] Leong, K.F., Wiria, F.E. *et al.* Characterization of a poly-epsilon-caprolactone polymeric drug delivery device built by selective laser sintering. *Bio-Medical Materials and Engineering* **17(3)**, 147-157, (2007).

[160] Niino, T., Hamajima, D. *et al.* Laser sintering fabrication of three-dimensional tissue engineering scaffolds with a flow channel network. *Biofabrication* **3(3)**, doi: 10.1088/1758-5082/1083/1083/034104, (2011).

[161] Lee, M.Y., Liu, S.W. *et al. In vitro* experiments on laser sintered porous PCL scaffolds with polymer hydrogle for bone repair. *Journal of Mechanics in Medicine and Biology* **11(5)**, 983-992, (2011).

[162] Chua, C.K., Leong, K.F. *et al.* Development of tissue scaffolds using selective laser sintering of polyvinyl alcohol/hydroxyapatite biocomposite for craniofacial and joint defects. *Journal of Materials Science - Materials in Medicine* **15(10)**, 1113-1121, (2004).

[163] Hao, L., Savalani, M.M. *et al.* Selective laser sintering of hydroxyapatite reinforced polyethylene composites for bioactive implants and tissue scaffold development. *Proceedings of the Institution of Mechanical Engineers Part H - Journal of Engineering in Medicine* **220(H4)**, 521-531, (2006).

[164] Zhou, W.Y., Lee, S.H. *et al.* Selective laser sintering of porous tissue engineering scaffolds from poly(L)/carbonated hydroxyapatite nanocomposite microspheres. *Journal of Materials Science - Materials in Medicine* **19(7)**, 2535-2540, (2008).

[165] Simpson, R.L., Wiria, F.E. *et al.* Development of a 95/5 poly(L-lactide-co-glycolide)/hydroxylapatite and beta-tricalcium phosphate scaffold as bone replacement material via selective laser sintering. *Journal of Biomedical Materials Research Part B - Applied Biomaterials* **84B(1)**, 17-25, (2008).

166 Duan, B., Cheung, W.L. *et al.* Optimized fabrication of Ca-P/PHBV nanocomposite scaffolds via selective laser sintering for bone tissue engineering. *Biofabrication* **3(1)**, doi: 10.1088/1758-5082/1083/1081/015001, (2011).

167 Duan, B. & Wang, M. Encapsulation and release of biomolecules from Ca-P/PHBV nanocomposite microspheres and three-dimensional scaffolds fabricated by selective laser sintering. *Polymer Degradation and Stability* **95(9)**, 1655-1664, (2010).

168 Wiria, F.E., Leong, K.F. *et al.* Poly-epsilon-caprolactone/hydroxyapatite for tissue engineering scaffold fabrication via selective laser sintering. *Acta Biomaterialia* **3(1)**, 1-12, (2007).

169 Eosoly, S., Brabazon, D. *et al.* Selective laser sintering of hydroxyapatite/poly-epsilon-caprolactone scaffolds. *Acta Biomaterialia* **6(7)**, 2511-2517, (2010).

170 Dyson, J.A., Genever, P.G. *et al.* Development of custom-built bone scaffolds using mesenchymal stem cells and apatite-wollastonite glass-ceramics. *Tissue Engineering* **13(12)**, 2891-2901, (2007).

171 Shuai, C.J., Gao, C.D. *et al.* Structure and properties of nano-hydroxypatite scaffolds for bone tissue engineering with a selective laser sintering system. *Nanotechnology* **22(28)**, doi: 10.1088/0957-4484/1022/1028/285703, (2011).

172 Lorrison, J.C., Dalgarno, K.W. *et al.* Processing of an apatite-mullite glass-ceramic and an hydroxyapatite/phosphate glass composite by selective laser sintering. *Journal of Materials Science - Materials in Medicine* **16(8)**, 775-781, (2005).

173 Russel, D., Hernandez, A. *et al.* Methods and apparatus for 3D printing. WO2005097476 (2005).

174 Sachs, E., Cima, M. *et al.* 3-dimensional printing - rapid tooling and prototypes directly from a CAD model. *Journal of Engineering for Industry - Transactions of the ASME* **114(4)**, 481-488, (1992).

175 Sachs, E.M., Haggerty, J.S. *et al.* Three-dimensional printing techniques. US5204055 (1993).

176 Serdy, J.G. & Sachs, E.M. Manufacturing process, such as three-dimensional printing, including solvent vapor filming and the like. US7815826 (2010).

[177] Sherwood, J.K., Riley, S.L. *et al.* A three-dimensional osteochondral composite scaffold for articular cartilage repair. *Biomaterials* **23(24)**, 4739-4751, (2002).

[178] Ge, Z., Wang, L. *et al.* Proliferation and differentiation of human osteoblasts within 3D printed poly-lactic-co-glycolic acid scaffolds. *Journal of Biomaterials Applications* **23(6)**, 533-547, (2009).

[179] Wu, W., Zheng, Q. *et al.* A programmed release multi-drug implant fabricated by three-dimensional printing technology for bone tuberculosis therapy. *Biomedical Materials* **4**, doi: 10.1088/1748-6041/1084/1086/065005, (2009).

[180] Butscher, A., Bohner, M. *et al.* Structural and material approaches to bone tissue engineering in powder-based three-dimensional printing. *Acta Biomaterialia* **7**, 907-920, (2011).

[181] Seitz, H., Deisinger, U. *et al.* Different Calcium Phosphate Granules for 3-D Printing of Bone Tissue Engineering Scaffolds. *Advanced Engineering Materials* **11(5)**, B41-B46, (2009).

[182] Seitz, H., Rieder, W. *et al.* Three-dimensional printing of porous ceramic scaffolds for bone tissue engineering. *Journal of Biomedical Materials Research Part B - Applied Biomaterials* **74B(2)**, 782-788, (2005).

[183] Leukers, B., Gulkan, H. *et al.* Hydroxyapatite scaffolds for bone tissue engineering made by 3D printing. *Journal of Materials Science-Materials in Medicine* **16(12)**, 1121-1124, (2005).

[184] Will, J., Melcher, R. *et al.* Porous ceramic bone scaffolds for vascularized bone tissue regeneration. *Journal of Materials Science - Materials in Medicine* **19(8)**, 2781-2790, (2008).

[185] Simon, J.L., Rekow, E.D. *et al.* MicroCT analysis of hydroxyapatite bone repair scaffolds created via three-dimensional printing for evaluating the effects of scaffold architecture on bone ingrowth. *Journal of Biomedical Materials Research Part A* **85A(2)**, 371-377, (2008).

[186] Fierz, F.C., Beckmann, F. *et al.* The morphology of anisotropic 3D-printed hydroxyapatite scaffolds. *Biomaterials* **29(28)**, 3799-3806, (2008).

[187] Warnke, P.H., Seitz, H. *et al.* Ceramic scaffolds produced by computer-assisted 3D printing and sintering: characterization and biocompatibility investigations. *Journal of Biomedical Materials Research Part B - Applied Biomaterials* **93B(1)**, 212-217, (2010).

[188] Detsch, R., Schaefer, S. *et al. In vitro* osteoclastic activity studies on surfaces of 3D printed calcium phosphate scaffolds. *Journal of Biomaterials Applications* **26(3)**, 359-380, (2011).

[189] Roy, T.D., Simon, J.L. *et al.* Performance of hydroxyapatite bone repair scaffolds created via three-dimensional fabrication techniques. *Journal of Biomedical Materials Research Part A* **67A(4)**, 1228-1237, (2003).

[190] Simon, J.L., Michna, S. *et al. In vivo* bone response to 3D periodic hydroxyapatite scaffolds assembled by direct ink writing. *Journal of Biomedical Materials Research Part A* **83A(3)**, 747-758, (2007).

[191] Khalyfa, A., Vogt, S. *et al.* Development of a new calcium phosphate powder-binder system for the 3D printing of patient specific implants. *Journal of Materials Science - Materials in Medicine* **18(5)**, 909-916, (2007).

[192] Bergmann, C., Lindner, M. *et al.* 3D printing of bone substitute implants using calcium phosphate and bioactive glasses. *Journal of the European Ceramic Society* **30(12)**, 2563-2567, (2010).

[193] Butscher, A., Bohner, M. *et al.* Printability of calcium phosphate powders for three-dimensional printing of tissue engineering scaffolds. *Acta Biomaterialia* **8(1)**, 373-385, (2012).

[194] Fielding, G.A., Bandyopadhyay, A. *et al.* Effects of silica and zinc oxide doping on mechanical and biological properties of 3D printed tricalcium phosphate tissue engineering scaffolds. *Dental Materials* **28(2)**, 113-122, (2012).

[195] Gbureck, U., Hozel, T. *et al.* Resorbable dicalcium phosphate bone substitutes prepared by 3D powder printing. *Advanced Functional Materials* **17(18)**, 3940-3945, (2007).

[196] Vorndran, E., Klammert, U. *et al.* Simultaneous immobilization of bioactives during 3D powder printing of bioceramic drug-release matrices. *Advanced Functional Materials* **20(10)**, 1585-1591, (2010).

[197] Maier, A.-K., Dezmirean, L. *et al.* Three-dimensional printing of flash-setting calcium aluminate cement. *Journal of Materials Science* **46**, 2947-2954, (2011).

[198] Shanjani, Y., De Croos, J.N.A. *et al.* Solid freeform fabrication and characterization of porous calcium polyphosphate structures for tissue engineering purposes. *Journal of Biomedical Materials Research Part B - Applied Biomaterials* **93B(2)**, 510-519, (2010).

199 Crump, S.S. Apparatus and method for creating three-dimensional objects. US5121329 (1992).

200 Endres, M., Hutmacher, D.W. *et al.* Osteogenic induction of human bone marrow-derived mesenchymal progenitor cells in novel synthetic polymer-hydrogel matrices. *Tissue Engineering* **9(4)**, 689-702, (2003).

201 Hutmacher, D.W., Schantz, T. *et al.* Mechanical properties and cell cultural response of polycaprolactone scaffolds designed and fabricated via fused deposition modeling. *Journal of Biomedical Materials Research* **55(2)**, 203-216, (2001).

202 Schantz, J.T., Hutmacher, D.W. *et al.* Repair of calvarial defects with customised tissue-engineered bone grafts - II. evaluation of cellular efficiency and efficacy *in vivo*. *Tissue Engineering* **9**, S127-S139, (2003).

203 Schantz, J.T., Teoh, S.H. *et al.* Repair of calvarial defects with customized tissue-engineered bone grafts - I. evaluation of osteogenesis in a three-dimensional culture system. *Tissue Engineering* **9**, S113-S126, (2003).

204 Zein, I., Hutmacher, D.W. *et al.* Fused deposition modeling of novel scaffold architectures for tissue engineering applications. *Biomaterials* **23(4)**, 1169-1185, (2002).

205 Teoh, S.H., Hutmacher, D.W. *et al.* Three-dimensional bioresorbable scaffolds for tissue engineering applications. US7968026 (2011).

206 Schantz, J.T., Brandwood, A. *et al.* Osteogenic differentiation of mesenchymal progenitor cells in computer designed fibrin-polymer-ceramic scaffolds manufactured by fused deposition modeling. *Journal of Materials Science - Materials in Medicine* **16(9)**, 807-819, (2005).

207 Russias, J., Saiz, E. *et al.* Fabrication and *in vitro* characterization of three-dimensional organic/inorganic scaffolds by robocasting. *Journal of Biomedical Materials Research Part A* **83A(2)**, 434-445, (2007).

208 Park, S., Kim, G. *et al.* 3D polycaprolactone scaffolds with controlled pore structure using a rapid prototyping system. *Journal of Materials Science - Materials in Medicine* **20(1)**, 229-234, (2009).

209 Seyednejad, H., Gawlitta, D. *et al.* Preparation and characterization of a three-dimensional printed scaffold based on a functionalized polyester for bone tissue engineering applications. *Acta Biomaterialia* **7(5)**, 1999-2006, (2011).

[210] Muller, D., Chim, H. *et al.* Vascular guidance: microstructural scaffold patterning for inductive neovascularization. *Stem Cells International* **2011**, doi: 10.4061/2011/547247, (2011).

[211] Park, S.A., Lee, S.H. *et al.* Fabrication of porous polycaprolactone/hydroxyapatite (PCL/HA) blend scaffolds using a 3D plotting system for bone tissue engineering. *Bioprocess and Biosystems Engineering* **34(4)**, 505-513, (2011).

[212] Woodfield, T.B.F., Malda, J. *et al.* Design of porous scaffolds for cartilage tissue engineering using a three-dimensional fiber-deposition technique. *Biomaterials* **25(18)**, 4149-4161, (2004).

[213] Tellis, B.C., Szivek, J.A. *et al.* Trabecular scaffolds created using micro CT guided fused deposition modeling. *Materials Science & Engineering C - Biomimetic and Supramolecular Systems* **28(1)**, 171-178, (2008).

[214] Whatley, B.R., Kuo, J. *et al.* Fabrication of a biomimetic elastic intervertebral disk scaffold using additive manufacturing. *Biofabrication* **3(1)**, doi: 10.1088/1758-5082/1083/1081/015004, (2011).

[215] Hoque, M.E., Hutmacher, D.W. *et al.* Fabrication using a rapid prototyping system and in vitro characterization of PEG-PCL-PLA scaffolds for tissue engineering. *Journal of Biomaterials Science - Polymer Edition* **16(12)**, 1595-1610, (2005).

[216] Centola, M., Rainer, A. *et al.* Combining electrospinning and fused deposition modeling for the fabrication of a hybrid vascular graft. *Biofabrication* **2(1)**, doi: 10.1088/1758-5082/1082/1081/014102, (2010).

[217] Schumann, D., Ekaputra, A.K. *et al.* Design of bioactive, multiphasic PCL/collagen type I and type II-PCL-TCP/collagen composite scaffolds for functional tissue engineering of osteochondral repair tissue by using electrospinning and FDM techniques. in *Methods in Molecular Medicine* (Ed Hauser, H.), 101-124 (Humana Press Inc, 2007).

[218] Owida, A., Chen, R. *et al.* Artery vessel fabrication using the combined fused deposition modeling and electrospinning techniques. *Rapid Prototyping Journal* **17(1)**, 37-44, (2011).

[219] Malda, J., Woodfield, T.B.F. *et al.* The effect of PEGT/PBT scaffold architecture on the composition of tissue engineered cartilage. *Biomaterials* **26(1)**, 63-72, (2005).

[220] Landers, R., Hubner, U. *et al.* Rapid prototyping of scaffolds derived from thermoreversible hydrogels and tailored for applications in tissue engineering. *Biomaterials* **23(23)**, 4437-4447, (2002).

[221] Landers, R., Pfister, A. *et al.* Fabrication of soft tissue engineering scaffolds by means of rapid prototyping techniques. *Journal of Materials Science* **37(15)**, 3107-3116, (2002).

[222] Chang, C.C., Boland, E.D. *et al.* Direct-write bioprinting three-dimensional biohybrid systems for future regenerative therapies. *Journal of Biomedical Materials Research Part B - Applied Biomaterials* **98B(1)**, 160-170, (2011).

[223] Fedorovich, N.E., Alblas, J. *et al.* Hydrogels as extracellular matrices for skeletal tissue engineering: state-of-the-art and novel application in organ printing. *Tissue Engineering* **13(8)**, 1905-1925, (2007).

[224] Nakamura, M., Iwanaga, S. *et al.* Biomatrices and biomaterials for future developments of bioprinting and biofabrication. *Biofabrication* **2(1)**, doi: 10.1088/1758-5082/1082/1081/014110, (2010).

[225] Chang, R. & Sun, W. Effects of dispensing pressure and nozzle diameter on cell survival from solid freeform fabrication-based direct cell writing. *Tissue Engineering Part A* **14(1)**, 41-48, (2008).

[226] Fedorovich, N.E., Dewijn, J.R. *et al.* Three-dimensional fiber deposition of cell-laden, viable, patterned constructs for bone tissue printing. *Tissue Engineering Part A* **14(1)**, 127-133, (2008).

[227] Fedorovich, N.E., Kuipers, E. *et al.* Scaffold porosity and oxygenation of printed hydrogel constructs affect functionality of embedded osteogenic progenitors. *Tissue Engineering Part A* **17(19-20)**, 2473-2486, (2011).

[228] Khalil, S., Nam, J. *et al.* Multi-nozzle deposition for construction of 3D biopolymer tissue scaffolds. *Rapid Prototyping Journal* **11(1)**, 9-17, (2005).

[229] Khalil, S. & Sun, W. Bioprinting endothelial cells with alginate for 3D tissue constructs. *Journal of Biomechanical Engineering* **131**, doi: 10.1115/1111.3128729, (2009).

[230] Cohen, D.L., Malone, E. *et al.* Direct freeform fabrication of seeded hydrogels in arbitrary geometries. *Tissue Engineering* **12(5)**, 1325-1335, (2006).

[231] Song, S.J., Choi, J. *et al.* Sodium alginate hydrogel-based bioprinting using a novel multinozzle bioprinting system. *Artificial Organs* **35(11)**, 1132-1136, (2011).

[232] Gaetani, R., Doevendans, P.A. *et al.* Cardiac tissue engineering using tissue printing technology and human cardiac progenitor cells. *Biomaterials* **33(6)**, 1782-1790, (2012).

[233] Ahn, S., Koh, Y.H. *et al.* A three-dimensional hierarchical collagen scaffold fabricated by a combined solid freeform fabrication (SFF) and electrospinning process to enhance mesenchymal stem cell (MSC) proliferation. *Journal of Micromechanics and Microengineering* **20**, 065015, (2010).

[234] Smith, C.M., Christian, J.J. *et al.* Characterizing environmental factors that impact the viability of tissue-engineered constructs fabricated by a direct-write bioassembly tool. *Tissue Engineering* **13(2)**, 373-383, (2007).

[235] Shim, J.H., Kim, J.Y. *et al.* Development of a hybrid scaffold with synthetic biomaterials and hydrogel using solid freeform fabrication technology. *Biofabrication* **3(3)**, doi: 10.1088/1758-5082/1083/1083/034102, (2011).

[236] Smith, C.M., Stone, A.L. *et al.* Three-dimensional bioassembly tool for generating viable tissue-engineered constructs. *Tissue Engineering* **10(9-10)**, 1566-1576, (2004).

[237] Wang, X.H., Yan, Y.N. *et al.* Generation of three-dimensional hepatocyte/gelatin structures with rapid prototyping system. *Tissue Engineering* **12(1)**, 83-90, (2006).

[238] Xu, W., Wang, X.H. *et al.* Rapid prototyping three-dimensional cell/gelatin/fibrinogen constructs for medical regeneration. *Journal of Bioactive and Compatible Polymers* **22(4)**, 363-377, (2007).

[239] Yan, Y.N., Wang, X.H. *et al.* Fabrication of viable tissue-engineered constructs with 3D cell-assembly technique. *Biomaterials* **26(29)**, 5864-5871, (2005).

[240] Cheng, J., Lin, F. *et al.* Rheological properties of cell-hydrogel composites extruding through small-diameter tips. *Journal of Manufacturing Science and Engineering - Transactions of the ASME* **130(2)**, doi: 10.1115/1111.2896215, (2008).

[241] Pham, C.B., Leong, K.F. *et al.* Rapid freeze prototyping technique in bio-plotters for tissue scaffold fabrication. *Rapid Prototyping Journal* **14(4)**, 246-253, (2008).

[242] Lee, W., Debasitis, J.C. *et al.* Multi-layered culture of human skin fibroblasts and keratinocytes through three-dimensional freeform fabrication. *Biomaterials* **30(8)**, 1587-1595, (2009).

[243] Lee, Y.-B., Polio, S. *et al.* Bio-printing of collagen and VEGF-releasing fibrin gel scaffolds for neural stem cell culture. *Experimental Neurology* **223**, 645-652, (2010).

[244] Fedorovich, N.E., Schuurman, W. *et al.* Biofabrication of osteochondral tissue equivalents by printing topologically defined, cell-laden hydrogel scaffolds. *Tissue Engineering Part C - Methods* **18(1)**, 33-44, (2012).

[245] Fedorovich, N.E., Wijnberg, H.M. *et al.* Distinct tissue formation by heterogeneous printing of osteo- and endothelial progenitor cells. *Tissue Engineering Part A* **17(15-16)**, 2113-2121, (2011).

[246] Maher, P.S., Keatch, R.P. *et al.* Construction of 3D biological matrices using rapid prototyping technology. *Rapid Prototyping Journal* **15(3)**, 204-210, (2009).

[247] Barry, R.A., Shepherd, R.F. *et al.* Direct-write assembly of 3D hydrogel scaffolds for guided cell growth. *Advanced Materials* **21(23)**, 2407-2410, (2009).

[248] Lewis, J.A., Shepherd, R.F. *et al.* Viscoeleastic ink for direct writing of hydrogel structures. WO2011119607 (2011).

[249] Censi, R., Schuurman, W. *et al.* A printable photopolymerizable thermosensitive p(HPMAm-lactate)-PEG hydrogel for tissue engineering. *Advanced Functional Materials* **21(10)**, 1833-1842, (2011).

[250] Skardal, A., Zhang, J. *et al.* Photocrosslinkable hyaluronan-gelatin hydrogels. *Tissue Engineering Part A* **16(8)**, 2675-2685, (2010).

[251] Skardal, A., Zhang, J. *et al.* Bioprinting vessel-like constructs using hyaluronan hydrogels crosslinked with tetrahedral polyethylene glycol tetracrylates. *Biomaterials* **31**, 6173-6181, (2010).

[252] Prestwich, G.D., Skardal, A. *et al.* Modified macromolecules and methods of making and using thereof. US20100330143 (2010).

[253] Lee, W., Lee, V. *et al.* On-demand three-dimensional freeform fabrication of multi-layered hydrogel scaffold with fluidic channels. *Biotechnology and Bioengineering* **105(6)**, 1178-1186, (2010).

[254] Mironov, V., Prestwich, G. *et al.* Bioprinting living structures. *Journal of Materials Chemistry* **17**, 2054-2060, (2007).

[255] Mironov, V., Visconti, R.P. *et al.* Organ printing: tissue spheroids as building blocks. *Biomaterials* **30(12)**, 2164-2174, (2009).

[256] Rivron, N.C., Rouwkema, J. *et al.* Tissue assembly and organization: developmental mechanisms in microfabricated tissues. *Biomaterials* **30(28)**, 4851-4858, (2009).

[257] Jakab, K., Norotte, C. *et al.* Tissue engineering by self-assembly and bio-printing of living cells. *Biofabrication* **2**, doi: 10.1088/1758-5082/1082/1082/022001, (2010).

[258] Norotte, C., Marga, F.S. *et al.* Scaffold-free vascular tissue engineering using bioprinting. *Biomaterials* **30**, 5910-5917, (2009).

[259] Jakab, K., Damon, B. *et al.* Three-dimensional tissue constructs built by bioprinting. *Biorheology* **43(3-4)**, 509-513, (2006).

[260] Jakab, K., Neagu, A. *et al.* Engineering biological structures of prescribed shape using self-assembling multicellular systems. *Proceedings of the National Academy of Sciences of the United States of America* **101(9)**, 2864-2869, (2004).

[261] Jakab, K., Norotte, C. *et al.* Tissue engineering by self-assembly of cells printed into topologically defined structures. *Tissue Engineering Part A* **14(3)**, 413-421, (2008).

[262] Forgacs, G., Marga, F.S. *et al.* Self-assembling multicellular bodies and methods of producing a three-dimensional biological structure using the same. US20100041134 (2010).

[263] Khatiwala, C., Murphy, K. *et al.* Multilayered vascular tubes. WO2011116125 (2011).

[264] Forgacs, G., Jakab, K. *et al.* Self-assembling cell aggregates and methods of making engineered tissue using the same. US20080070304 (2008).

[265] Williams, D.F. On the mechanisms of biocompatibility. *Biomaterials* **29(20)**, 2941-2953, (2008).

[266] Okamoto, T., Aoyama, T. *et al.* Clonal heterogeneity in differentiation potential of immortalized human mesenchymal stem cells. *Biochemical and Biophysical Research Communications* **295(2)**, 354-361, (2002).

[267] Kirby, G.T.S., White, L.J. *et al.* PLGA-based microparticles for the sustained release of BMP-2. *Polymers* **3(1)**, 571-586, (2011).

[268] Wiechelman, K.J., Braun, R.D. *et al.* Investigation of the bicinchoninic acid protein assay - identification of the groups responsible for color formation. *Analytical Biochemistry* **175(1)**, 231-237, (1988).

[269] Woessner, J.F. Determination of hydroxyproline in tissue and protein samples containing small proportions of this imino acid. *Archives of Biochemistry and Biophysics* **93(2)**, 440-447, (1961).

[270] Dhillon, A., Rahman, C. *et al.* Physical and biological characterisation of a novel injectable scaffold formulation. *Journal of Pharmacy and Pharmacology* **62(10)**, 1510-1511, (2010).

[271] Dhillon, A., Schneider, P. *et al.* Analysis of sintered polymer scaffolds using concomitant synchrotron computed tomography and in situ mechanical testing. *Journal of Materials Science - Materials in Medicine* **22(12)**, 2599-2605, (2011).

[272] Hamilton, L.G., Quirk, R.A. *et al.* An injectable scaffold for cell and growth factor delivery. *Journal of Pharmacy and Pharmacology* **62(10)**, 1498-1499, (2010).

[273] Rahman, C.V., Cox, H.C. *et al.* Injectable scaffold for bone tissue engineering applications. *Journal of Pharmacy and Pharmacology* **62(10)**, 1508-1509, (2010).

[274] Malone, E. & Lipson, H. Fab@Home: the personal desktop fabricator kit. *Rapid Prototyping Journal* **13**, 245-255, (2007).

[275] Li, M., Rouaud, O. *et al.* Microencapsulation by solvent evaporation: state of the art for process engineering approaches. *International Journal of Pharmaceutics* **363(1-2)**, 26-39, (2008).

[276] Sokolsky-Papkov, M., Agashi, K. *et al.* Polymer carriers for drug delivery in tissue engineering. *Advanced Drug Delivery Reviews* **59(4-5)**, 187-206, (2007).

[277] Mundargi, R.C., Babu, V.R. *et al.* Nano/micro technologies for delivering macromolecular therapeutics using poly(D,L-lactide-co-glycolide) and its derivatives. *Journal of Controlled Release* **125(3)**, 193-209, (2008).

[278] Langer, R. Biomaterials in drug delivery and tissue engineering: one laboratory's experience. *Accounts of Chemical Research* **33(2)**, 94-101, (2000).

[279] Lim, T.Y., Poh, C.K. *et al.* Poly (lactic-co-glycolic acid) as a controlled release delivery device. *Journal of Materials Science - Materials in Medicine* **20(8)**, 1669-1675, (2009).

[280] Mohamed, F. & van der Walle, C.F. Engineering biodegradable polyester particles with specific drug targeting and drug release properties. *Journal of Pharmaceutical Sciences* **97(1)**, 71-87, (2008).

[281] Anderson, J.M. & Shive, M.S. Biodegradation and biocompatibility of PLA and PLGA microspheres. *Advanced Drug Delivery Reviews* **28(1)**, 5-24, (1997).

[282] Lassalle, V. & Ferreira, M.L. PLA nano- and microparticles for drug delivery: an overview of the methods of preparation. *Macromolecular Bioscience* **7(6)**, 767-783, (2007).

[283] Amrite, A.C., Ayalasomayajula, S.P. *et al.* Single periocular injection of celecoxib-PLGA microparticles inhibits diabetes-induced elevations in retinal PGE2,VEGF, and vascular leakage. *Investigative Ophthalmology & Visual Science* **47(3)**, 1149-1160, (2006).

[284] Ye, M., Kim, S. *et al.* Issues in long-term protein delivery using biodegradable microparticles. *Journal of Controlled Release* **In Press, Uncorrected Proof**.

[285] Dorati, R., Colonna, C. *et al.* Effect of porogen on the physico-chemical properties and degradation performance of PLGA scaffolds. *Polymer Degradation and Stability* **95(4)**, 694-701.

[286] Sun, L., Zhou, S.B. *et al.* Preparation and characterization of porous biodegradable microspheres used for controlled protein delivery. *Colloids and Surfaces A - Physicochemical and Engineering Aspects* **345(1-3)**, 173-181, (2009).

[287] Kuo, Y.C. & Leou, S.N. Effects of composition, solvent, and salt particles on the physicochemical properties of polyglycolide/poly(lactide-co-glycolide) scaffolds. *Biotechnology Progress* **22(6)**, 1664-1670, (2006).

[288] Tai, H.Y., Mather, M.L. *et al.* Control of pore size and structure of tissue engineering scaffolds produced by supercritical fluid processing. *European Cells & Materials* **14**, 64-76, (2007).

[289] Kretlow, J.D., Klouda, L. *et al.* Injectable matrices and scaffolds for drug delivery in tissue engineering. *Advanced Drug Delivery Reviews* **59(4-5)**, 263-273, (2007).

290 Suciati, T., Howard, D. *et al.* Zonal release of proteins within tissue engineering scaffolds. *Journal of Materials Science-Materials in Medicine* **17(11)**, 1049-1056, (2006).

291 Narayan, D. & Venkatraman, S.S. Effect of pore size and interpore distance on endothelial cell growth on polymers. *Journal of Biomedical Materials Research Part A* **87A(3)**, 710-718, (2008).

292 Graziano, A., d'Aquino, R. *et al.* Concave pit-containing scaffold surfaces improve stem cell-derived osteoblast performance and lead to significant bone tissue formation. *PLoS One* **2(6)**, (2007).

293 Petrie Aronin, C.E., Sadik, K.W. *et al.* Comparative effects of scaffold pore size, pore volume, and total void volume on cranial bone healing patterns using microsphere-based scaffolds. *Journal of Biomedical Materials Research Part A* **89(3)**, 632-641, (2009).

294 Freiberg, S. & Zhu, X. Polymer microspheres for controlled drug release. *International Journal of Pharmaceutics* **282(1-2)**, 1-18, (2004).

295 Freitas, S., Merkle, H.P. *et al.* Microencapsulation by solvent extraction/evaporation: reviewing the state of the art of microsphere preparation process technology. *Journal of Controlled Release* **102(2)**, 313-332, (2005).

296 Chu, D.F., Tian, J.W. *et al.* Poly(lactic-co-glycolic acid) microspheres for the controlled release of huperzine A: In vitro and in vivo studies and the application in the treatment of the impaired memory of mice. *Chemical & Pharmaceutical Bulletin* **55(4)**, 625-628, (2007).

297 Zhang, P.C., Chen, L.L. *et al.* In vitro and in vivo evaluation of donepezil-sustained release microparticles for the treatment of Alzheimer's disease. *Biomaterials* **28(10)**, 1882-1888, (2007).

298 Dawes, G.J.S., Fratila-Apachitei, L.E. *et al.* Size effect of PLGA spheres on drug loading efficiency and release profiles. *Journal of Materials Science-Materials in Medicine* **20(5)**, 1089-1094, (2009).

299 Chen, X.Q., Yang, Y.Y. *et al.* Effects of inner water volume on the peculiar surface morphology of microspheres fabricated by double emulsion technique. *Journal of Microencapsulation* **18(5)**, 637-649, (2001).

300 Jiang, G., Woo, B.H. *et al.* Assessment of protein release kinetics, stability and protein polymer interaction of lysozyme encapsulated poly (D,L-lactide-co-glycolide) microspheres. *Journal of Controlled Release* **79(1-3)**, 137-145, (2002).

[301] Intra, J. & Salem, A.K. Fabrication, Characterization and In Vitro Evaluation of Poly(D,L-Lactide-co-Glycolide) Microparticles Loaded With Polyamidoamine-Plasmid DNA Dendriplexes for Applications in Nonviral Gene Delivery. *Journal of Pharmaceutical Sciences* **99(1)**, 368-384.

[302] Morita, T., Horikiri, Y. *et al.* Formation and isolation of spherical fine protein microparticles through lyophilization of protein-poly(ethylene glycol) aqueous mixture. *Pharmaceutical Research* **17(11)**, 1367-1373, (2000).

[303] Morita, T., Sakamura, Y. *et al.* Protein encapsulation into biodegradable microspheres by a novel s/o/w emulsion method using poly(ethylene glycol) as a protein micronization adjuvant. *Journal of Controlled Release* **69(3)**, 435-444, (2000).

[304] Takada, S., Yamagata, Y. *et al.* Sustained release of human growth hormone from microcapsules prepared by a solvent evaporation technique. *Journal of Controlled Release* **88(2)**, 229-242, (2003).

[305] Paillard-Giteau, A., Tran, V.T. *et al.* Effect of various additives and polymers on lysozyme release from PLGA microspheres prepared by an s/o/w emulsion technique. *European Journal of Pharmaceutics and Biopharmaceutics* **75(2)**, 128-136.

[306] de Jalon, E.G., Blanco-Prieto, M.J. *et al.* PLGA microparticles: possible vehicles for topical drug delivery. *International Journal of Pharmaceutics* **226(1-2)**, 181-184, (2001).

[307] Chau, D.Y.S., Agashi, K. *et al.* Microparticles as tissue engineering scaffolds: manufacture, modification and manipulation. *Materials Science and Technology* **24(9)**, 1031-1044, (2008).

[308] Ginty, P.J., Barry, J.J.A. *et al.* Controlling protein release from scaffolds using polymer blends and composites. *European Journal of Pharmaceutics and Biopharmaceutics* **68(1)**, 82-89, (2008).

[309] Wischke, C., Lorenzen, D. *et al.* Preparation of protein loaded poly(D,L-lactide-co-glycolide) microparticles for the antigen delivery to dendritic cells using a static micromixer. *European Journal of Pharmaceutics and Biopharmaceutics* **62(3)**, 247-253, (2006).

[310] Zhu, L.P., Li, Y.G. *et al.* Fabrication of monodisperse, large-sized, functional biopolymeric microspheres using a low-cost and facile microfluidic device. *Biomedical Microdevices* **12(1)**, 169-177.

[311] Kim, B.S., Oh, J.M. *et al.* BSA-FITC-loaded microcapsules for *in vivo* delivery. *Biomaterials* **30(5)**, 902-909, (2009).

[312] Rondeau, E. & Cooper-White, J.J. Biopolymer microparticle and nanoparticle formation within a microfluidic device. *Langmuir* **24(13)**, 6937-6945, (2008).

[313] Ribeiro-Costa, R.M., da Cunha, M.R. *et al.* Preparation of protein-loaded-PLGA microspheres by an emulsion/solvent evaporation process employing LTCC micromixers. *Powder Technology* **190(1-2)**, 107-111, (2009).

[314] Gong, X.Q., Wen, W.J. *et al.* Microfluidic fabrication of porous polymer microspheres: dual reactions in single droplets. *Langmuir* **25(12)**, 7072-7077, (2009).

[315] Jordan, F., Naylor, A. *et al.* Sustained release hGH microsphere formulation produced by a novel supercritical fluid technology: In vivo studies. *Journal of Controlled Release* **141(2)**, 153-160.

[316] Liu, S., Danquah, M.K. *et al.* Preparation and characterization of poly(lactic-co-glycolic acid) microparticles containing DNA molecules encoding a malaria vaccine candidate. *Journal of Chemical Technology and Biotechnology* **84(5)**, 782-788, (2009).

[317] Stolnik, S. & Shakesheff, K. Formulations for delivery of therapeutic proteins. *Biotechnology Letters* **31(1)**, 1-11, (2009).

[318] Wu, F. & Jin, T. Polymer-Based Sustained-Release Dosage Forms for Protein Drugs, Challenges, and Recent Advances. *AAPS PharmSciTech* **9(4)**, 1218-1229, (2008).

[319] Jeon, O., Song, S.J. *et al.* Enhancement of ectopic bone formation by bone morphogenetic protein-2 released from a heparin-conjugated poly(L-lactic-co-glycolic acid) scaffold. *Biomaterials* **28(17)**, 2763-2771, (2007).

[320] Kirker-Head, C.A. Potential applications and delivery strategies for bone morphogenetic proteins. *Advanced Drug Delivery Reviews* **43(1)**, 65-92, (2000).

[321] Kempen, D.H.R., Lu, L. *et al.* Retention of *in vitro* and *in vivo* BMP-2 bioactivities in sustained delivery vehicles for bone tissue engineering. *Biomaterials* **29(22)**, 3245-3252, (2008).

[322] Barry, J.J.A., Silva, M. *et al.* Using plasma deposits to promote cell population of the porous interior of three-dimensional poly(D,L-lactic acid) tissue-engineering scaffolds. *Advanced Functional Materials* **15(7)**, 1134-1140, (2005).

[323] Berchane, N.S., Jebrail, F.F. *et al.* Optimization of PLG microspheres for tailored drug release. *International Journal of Pharmaceutics* **383(1-2)**, 81-88.

[324] Thote, A.J., Chappell, J.T. *et al.* Reduction in the initial-burst release by surface crosslinking of PLGA microparticles containing hydrophilic or hydrophobic drugs. *Drug Development and Industrial Pharmacy* **31(1)**, 43-57, (2005).

[325] Jaraswekin, S., Prakongpan, S. *et al.* Effect of poly(lactide-co-glycolide) molecular weight on the release of dexamethasone sodium phosphate from microparticles. *Journal of Microencapsulation* **24(2)**, 117-128, (2007).

[326] Shelke, N.B., Rokhade, A.P. *et al.* Preparation and Evaluation of Novel Blend Microspheres of Poly(lactic-co-glycolic) acid and Pluronic F68/127 for Controlled Release of Repaglinide. *Journal of Applied Polymer Science* **116(1)**, 366-372.

[327] Jung, G.Y., Na, Y.E. *et al.* Preparation of sustained release microparticles with improved initial release property. *Archives of Pharmacal Research* **32(3)**, 359-365, (2009).

[328] Wang, Y., Gao, J.Q. *et al.* Triblock copolymer Pluronic (R) F127 sustains insulin release and reduces initial burst of microspheres - in vitro and in vivo study. *Colloid and Polymer Science* **285(2)**, 233-238, (2006).

[329] Sheikh Hassan, A., Sapin, A. *et al.* Composite microparticles with *in vivo* reduction of the burst release effect. *European Journal of Pharmaceutics and Biopharmaceutics* **73(3)**, 337-344, (2009).

[330] Dunne, M., Corrigan, O.I. *et al.* Influence of particle size and dissolution conditions on the degradation properties of polylactide-co-glycolide particles. *Biomaterials* **21(16)**, 1659-1668, (2000).

[331] Berkland, C., Kim, K. *et al.* PLG microsphere size controls drug release rate through several competing factors. *Pharmaceutical Research* **20(7)**, 1055-1062, (2003).

[332] Berkland, C., Pollauf, E. *et al.* Macromolecule release from monodisperse PLG microspheres: control of release rates and investigation of release mechanism. *Journal of Pharmaceutical Sciences* **96(5)**, 1176-1191, (2007).

[333] Berkland, C., King, M. *et al.* Precise control of PLG microsphere size provides enhanced control of drug release rate. *Journal of Controlled Release* **82(1)**, 137-147, (2002).

[334] Bertram, J.P., Jay, S.M. *et al.* Functionalized poly(lactic-co-glycolic acid) enhances drug delivery and provides chemical moieties for surface engineering while preserving biocompatibility. *Acta Biomaterialia* **5(8)**, 2860-2871, (2009).

[335] Koppolu, B., Rahimi, M. *et al.* Development of multiple-layer polymeric particles for targeted and controlled drug delivery. *Nanomedicine-Nanotechnology Biology and Medicine* **6(2)**, 355-361.

[336] Basmanav, F.B., Kose, G.T. *et al.* Sequential growth factor delivery from complexed microspheres for bone tissue engineering. *Biomaterials* **29(31)**, 4195-4204, (2008).

[337] Lee, J. & Lee, K.Y. Local and sustained vascular endothelial growth factor delivery for angiogenesis using an injectable system. *Pharmaceutical Research* **26(7)**, 1739-1744, (2009).

[338] Lee, J. & Lee, K.Y. Injectable Microsphere/Hydrogel Combination Systems for Localized Protein Delivery. *Macromolecular Bioscience* **9(7)**, 671-676, (2009).

[339] Schoubben, A., Blasi, P. *et al.* Novel composite microparticles for protein stabilization and delivery. *European Journal of Pharmaceutical Sciences* **36(2-3)**, 226-234, (2009).

[340] Ye, M., Kim, S. *et al.* Issues in long-term protein delivery using biodegradable microparticles. *Journal of Controlled Release* **146**, 241-260, (2010).

[341] Dorati, R., Colonna, C. *et al.* Effect of porogen on the physico-chemical properties and degradation performance of PLGA scaffolds. *Polymer Degradation and Stability* **95**, 694-701, (2010).

[342] Barry, J.J.a., Silva, M.M.C.G. *et al.* Using Plasma Deposits to Promote Cell Population of the Porous Interior of Three-Dimensional Poly(D,L-Lactic Acid) Tissue-Engineering Scaffolds. *Advanced Functional Materials* **15**, 1134-1140, (2005).

[343] Berchane, N.S., Jebrail, F.F. *et al.* Optimization of PLG microspheres for tailored drug release. *International Journal of Pharmaceutics* **383**, 81-88, (2010).

[344] Thote, A., Chappell, J. *et al.* Reduction in the Initial-Burst Release by Surface Crosslinking of PLGA Microparticles Containing Hydrophilic or Hydrophobic Drugs. *Drug Development and Industrial Pharmacy* **31**, 43-57, (2005).

345 Wischke, C. & Borchert, H.-H. Influence of the primary emulsification procedure on the characteristics of small protein-loaded PLGA microparticles for antigen delivery. *Journal of Microencapsulation* **23**, 435-448, (2006).

346 Dawes, G.J.S., Fratila-Apachitei, L.E. *et al.* Size effect of PLGA spheres on drug loading efficiency and release profiles. *Journal of Materials Science - Materials in Medicine* **20**, 1089-1094, (2009).

347 Feczko, T., Toth, J. *et al.* Optimization of protein encapsulation in PLGA nanoparticles. *Chemical Engineering and Processing* **50(8)**, 757-765, (2011).

348 Wang, F., Song, Y.-l. *et al.* Sustained release of insulin-like growth factor-1 from poly(lactide-co-glycolide) microspheres improves osseointegration of dental implants in type 2 diabetic rats. *European Journal of Pharmacology* **640**, 226-232, (2010).

349 Van de Ven, H., Verrneersch, M. *et al.* PLGA nanoparticles loaded with the antileishmanial saponin beta-aescin: factor influence study and *in vitro* efficacy evaluation. *International Journal of Pharmaceutics* **420(1)**, 122-132, (2011).

350 Luan, X.S., Skupin, M. *et al.* Key parameters affecting the initial release (burst) and encapsulation efficiency of peptide-containing poly(lactide-co-glycolide) microparticles. *International Journal of Pharmaceutics* **324(2)**, 168-175, (2006).

351 Lee, J., Oh, Y.J. *et al.* Facile control of porous structures of polymer microspheres using an osmotic agent for pulmonary delivery. *Journal of Controlled Release* **In Press, Corrected Proof**.

352 Yushu, H. & Venkatraman, S. The effect of process variables on the morphology and release characteristics of protein-loaded PLGA particles. *Journal of Applied Polymer Science* **101(5)**, 3053-3061, (2006).

353 Tran, V.T., Karam, J.P. *et al.* Protein-loaded PLGA-PEG-PLGA microspheres: a tool for cell therapy. *European Journal of Pharmaceutical Sciences* **45(1-2)**, 128-137, (2012).

354 Buske, J., Konig, C. *et al.* Influence of PEG in PEG-PLGA microspheres on particle properties and protein release. *European Journal of Pharmaceutics and Biopharmaceutics* **81(1)**, 57-63, (2012).

355 Shelke, N.B., Rokhade, A.P. *et al.* Preparation and evaluation of novel blend microspheres of poly(lactic-co-glycolic acid) and Pluronic F68 / 127 for controlled release of repaglinide. *Journal of Applied Polymer Science* **116(1)**, 366-372, (2009).

[356] Kissel, T., Li, Y.X. *et al.* ABA-triblock copolymers from biodegradable polyester A-blocks and hydrophilic poly(ethylene oxide) B-blocks as a candidate for *in situ* forming hydrogel delivery systems for proteins. *Advanced Drug Delivery Reviews* **54(1)**, 99-134, (2002).

[357] Palermo, G., Joris, H. *et al.* Pregnancies after intracytoplasmic injection of single spermatazoon into an oocyte. *Lancet* **340(8810)**, 17-18, (1992).

[358] Yuspa, S.H., Hawleynelson, P. *et al.* A survery of transformation markers in differentiating epidermal-cell lines in culture. *Cancer Research* **40(12)**, 4694-4703, (1980).

[359] Lafyatis, R., Remmers, E.F. *et al.* Anchorage-independent growth of synoviocytes from arthritic and normal joints - stimulation by exogenous platelet-derived growth-factor and inhibition by transforming growth factor-beta and retinoids. *Journal of Clinical Investigation* **83(4)**, 1267-1276, (1989).

[360] Badylak, S.F. Regenerative medicine and developmental biology: the role of the extracellular matrix. *The Anatomical Record Part B: The New Anatomist* **287**, 36-41, (2005).

[361] Daley, W.P., Peters, S.B. *et al.* Extracellular matrix dynamics in development and regenerative medicine. *Journal of Cell Science* **121(3)**, 255-264, (2008).

[362] Rosso, F., Giordano, A. *et al.* From cell-ECM interactions to tissue engineering. *Journal of Cellular Physiology* **199(2)**, 174-180, (2004).

[363] van der Rest, M. & Garrone, R. Collagen family of proteins. *FASEB Journal* **5(13)**, 2814-2823, (1991).

[364] Schwarzbauer, J.E. Fibronectin: from gene to protein. *Current Opinion in Cell Biology* **3(5)**, 786-791, (1991).

[365] Schwarzbauer, J. Basement membranes: putting up the barriers. *Current Biology* **9(7)**, R242-244, (1999).

[366] Debelle, L. & Tamburro, A.M. Elastin: molecular description and function. *International Journal of Biochemistry & Cell Biology* **31(2)**, 261-272, (1999).

[367] Iozzo, R.V. Matrix proteoglycans: from molecular design to cellular function. *Annual Review of Biochemistry* **67**, 609-652, (1998).

[368] Kiani, C., Chen, L. *et al.* Structure and function of aggrecan. *Cell Research* **12(1)**, 19-32, (2002).

[369] Hedlund, H., Mengarelliwidholm, S. *et al.* Fibromodulin distribution and association with collagen. *Matrix Biology* **14(3)**, 227-232, (1994).

[370] Kinsella, M.G., Bressler, S.L. *et al.* The regulated synthesis of versican, decorin, and biglycan: extracellular matrix proteoglycans that influence cellular phenotype. *Critical Reviews in Eukaryotic Gene Expression* **14(3)**, 203-234, (2004).

[371] Wadhwa, S., Embree, M.C. *et al.* Regulation, regulatory activities, and function of biglycan. *Critical Reviews in Eukaryotic Gene Expression* **14(4)**, 301-315, (2004).

[372] Iozzo, R.V. Perlecan - a gem of a proteoglycan. *Matrix Biology* **14(3)**, 203-208, (1994).

[373] Wight, T.N. Versican: a versatile extracellular matrix proteoglycan in cell biology. *Current Opinion in Cell Biology* **14(5)**, 617-623, (2002).

[374] Kastelic, J., Galeski, A. *et al.* Multicomposite structure of tendon. *Connective Tissue Research* **6(1)**, 11-23, (1978).

[375] Gentleman, E., Lay, A.N. *et al.* Mechanical characterization of collagen fibers and scaffolds for tissue engineering. *Biomaterials* **24(21)**, 3805-3813, (2003).

[376] Kato, Y.P., Christiansen, D.L. *et al.* Mechanical-properties of collagen-fibers - a comparison of reconstituted and rat tail tendon fibers. *Biomaterials* **10(1)**, 38-41, (1989).

[377] Huang, C.Y., Mow, V.C. *et al.* The role of flow-independent viscoelasticity in the biphasic tensile and compressive responses of articular cartilage. *Journal of Biomechanical Engineering - Transactions of the ASME* **123(5)**, 410-417, (2001).

[378] Kalluri, R. Basement membranes: structure, assembly and role in tumour angiogenesis. *Nature Reviews Cancer* **3(6)**, 422-433, (2003).

[379] Howe, A., Aplin, A.E. *et al.* Integrin signaling and cell growth control. *Current Opinion in Cell Biology* **10(2)**, 220-231, (1998).

[380] Ruoslahti, E. & Pierschbacher, M.D. New perspectives in cell adgesion - RGD and integrins. *Science* **238(4826)**, 491-497, (1987).

[381] Hynes, R.O. Integrins - a family of cell-surface receptors. *Cell* **48(4)**, 549-554, (1987).

[382] Hynes, R.O. Integrins - versatility, modulation, and signaling in cell adhesion. *Cell* **69(1)**, 11-25, (1992).

[383] Pierschbacher, M.D. & Ruoslahti, E. Cell attachment activity of fibronectin can be duplicated by small synthetic fragments of the molecule. *Nature* **309(5963)**, 30-33, (1984).

[384] Dedhar, S., Ruoslahti, E. *et al.* A cell-surface receptor complex for collagen type-I recognises the Arg-Gly-Asp sequence. *Journal of Cell Biology* **104(3)**, 585-593, (1987).

[385] Ginsberg, M., Pierschbacher, M.D. *et al.* Inhibition of fibronectin binding to platelets by proteolytic fragments and synthetic peptides which support fibroblast adhesion. *Journal of Biological Chemistry* **260(7)**, 3931-3936, (1985).

[386] Plow, E.F., Pierschbacher, M.D. *et al.* The effect of Arg-Gly-Asp-containing peptides on fibrinogen and von Willebrand factor binding to platelets. *Proceedings of the National Academy of Sciences of the United States of America* **82(23)**, 8057-8061, (1985).

[387] Guilak, F., Cohen, D.M. *et al.* Control of stem cell fate by physical interactions with the extracellular matrix. *Cell Stem Cell* **5(1)**, 17-26, (2009).

[388] Geiger, B., Bershadsky, A. *et al.* Transmembrane extracellular matrix-cytoskeleton crosstalk. *Nature Reviews Molecular Cell Biology* **2(11)**, 793-805, (2001).

[389] Macri, L., Silverstein, D. *et al.* Growth factor binding to the pericellular matrix and its importance in tissue engineering. *Advanced Drug Delivery Reviews* **59(13)**, 1366-1381, (2007).

[390] Langer, R. & Vacanti, J.P. Tissue engineering. *Science* **260(5110)**, 920-926, (1993).

[391] Williams, D.F. On the nature of biomaterials. *Biomaterials* **30(30)**, 5897-5909, (2009).

[392] Tibbitt, M.W. & Anseth, K.S. Hydrogels as extracellular matrix mimics for 3D cell culture. *Biotechnology and Bioengineering* **103(4)**, 655-663, (2009).

[393] Ma, P.X. Biomimetic materials for tissue engineering. *Advanced Drug Delivery Reviews* **60(2)**, 184-198, (2008).

[394] Badylak, S.F. The extracellular matrix as a biologic scaffold material. *Biomaterials* **28**, 3587-3593, (2007).

[395] Badylak, S.F., Freytes, D.O. *et al.* Extracellular matrix as a biological scaffold material: structure and function. *Acta Biomaterialia* **5**, 1-13, (2009).

[396] Badylak, S.F. & Gilbert, T.W. Immune response to biologic scaffold materials. *Seminars in Immunology* **20**, 109-116, (2008).

[397] Badylak, S.F., Taylor, D. *et al.* Whole-organ tissue engineering: decellularization and recellularization of three-dimensional matrix scaffolds. in *Annual Review of Biomedical Engineering* (Eds Yarmush, M.L., S., D.J. *et al.*), 27-53 (2011).

[398] Gilbert, T.W., Sellaro, T.L. *et al.* Decellularization of tissues and organs. *Biomaterials* **27**, 3675-3683, (2006).

[399] Deeken, C.R., White, A.K. *et al.* Method of preparing a decellularized porcine tendon using tributyl phosphate. *Journal of Biomedical Materials Research Part B - Applied Biomaterials* **96(2)**, 199-206, (2011).

[400] DeQuach, J.A., Yuan, S.H. *et al.* Decellularized porcine brain matrix for cell culture and tissue engineering scaffolds. *Tissue Engineering Part A* **17(21-22)**, 2583-2592, (2011).

[401] Du, L., Wu, X. *et al.* Histological evaluation and biomechanical characterisation of an acellular porcine cornea scaffold. *The British Journal of Ophthalmology* **95(3)**, 410-414, (2011).

[402] Lumpkins, S.B., Pierre, N. *et al.* A mechanical evaluation of three decellularization methods in the design of a xenogeneic scaffold for tissue engineering the temporomandibular joint disc. *Acta Biomaterialia* **4(4)**, 808-816, (2008).

[403] Mendoza-Novelo, B., Avila, E.E. *et al.* Decellularization of pericardial tissue and its impact on tensile viscoelasticity and glycosaminoglycan content. *Acta Biomaterialia* **7(3)**, 1241-1248, (2011).

[404] Grauss, R.W., Hazekamp, M.G. *et al.* Histological evaluation of decellularised porcine aortic valves: matrix changes due to different decellularisation methods. *European Journal of Cardio-Thoracic Surgery* **27(4)**, 566-571, (2005).

[405] Zhou, J., Fritze, O. *et al.* Impact of heart valve decellularization on 3-D ultrastructure, immunogenicity and thrombogenicity. *Biomaterials* **31(9)**, 2549-2554, (2010).

406 Schenke-Layland, K., Vasilevski, O. *et al.* Impact of decellularization of xenogeneic tissue on extracellular matrix integrity for tissue engineering of heart valves. *Journal of Structural Biology* **143(3)**, 201-208, (2003).

407 Gilbert, T.W., Wognum, S. *et al.* Collagen fiber alignment and biaxial mechanical behavior of porcine urinary bladder derived extracellular matrix. *Biomaterials* **29**, 4775-4782, (2008).

408 Wood, J.D., Simmons-Byrd, A. *et al.* Use of a particulate extracellular matrix bioscaffold for treatment of acquired urinary incontinence in dogs. *Journal of the American Veterinary Medical Association* **226**, 1095-1097, (2005).

409 Gilbert, T.W., Nieponice, A. *et al.* Repair of the thoracic wall with an extracellular matrix scaffold in a canine model. *The Journal of Surgical Research* **147**, 61-67, (2008).

410 Gillies, A.R., Smith, L.R. *et al.* Method for decellularizing skeletal muscle without detergents or proteolytic enzymes. *Tissue Engineering Part C - Methods* **17(4)**, 383-389, (2011).

411 Xu, C.C., Chan, R.W. *et al.* A bovine acellular scaffold for vocal fold reconstruction in a rat model. *Journal of Biomedical Materials Research Part A* **92(1)**, 18-32, (2010).

412 Hashimoto, Y., Funamoto, S. *et al.* Preparation and characterization of decellularized cornea using high-hydrostatic pressurization for corneal tissue engineering. *Biomaterials* **31(14)**, 3941-3948, (2010).

413 Funamoto, S., Nam, K. *et al.* The use of high-hydrostatic pressure treatment to decellularize blood vessels. *Biomaterials* **31(13)**, 3590-3595, (2010).

414 Sasaki, S., Funamoto, S. *et al. In vivo* evaluation of a novel scaffold for artificial corneas prepared by using ultrahigh hydrostatic pressure to decellularize porcine corneas. *Molecular Vision* **15**, 2022-2028, (2009).

415 Hong, Y., Takanari, K. *et al.* An elastomeric patch electrospun from a blended solution of dermal extracellular matrix and biodegradable polyurethane for rat abdominal wall repair. *Tissue Engineering Part C - Methods* **18(2)**, 122-132, (2012).

416 Reing, J.E., Brown, B.N. *et al.* The effects of processing methods upon mechanical and biologic properties of porcine dermal extracellular matrix scaffolds. *Biomaterials* **31(33)**, 8626-8633, (2010).

[417] Merritt, E.K., Hammers, D.W. *et al.* Functional assessment of skeletal muscle regeneration utilizing homologous extracellular matrix as scaffolding. *Tissue Engineering Part A* **16(4)**, 1395-1405, (2010).

[418] Yang, B., Zhang, Y. *et al.* Development of a porcine bladder acellular matrix with well-preserved extracellular bioactive factors for tissue engineering. *Tissue Engineering Part C - Methods* **16(5)**, 1201-1211, (2010).

[419] Flynn, L.E. The use of decellularized adipose tissue to provide an inductive microenvironment for the adipogenic differentiation of human adipose-derived stem cells. *Biomaterials* **31(17)**, 4715-4724, (2010).

[420] Cortiella, J., Niles, J. *et al.* Influence of acellular natural lung matrix on murine embryonic stem cell differentiation and tissue formation. *Tissue Engineering Part A* **16(8)**, 2565-2580, (2010).

[421] Singelyn, J.M., DeQuach, J.A. *et al.* Naturally derived myocardial matrix as an injectable scaffold for cardiac tissue engineering. *Biomaterials* **30(29)**, 5409-5416, (2009).

[422] Zhao, Y., Zhang, S. *et al.* The development of a tissue-engineered artery using decellularized scaffold and autologous ovine mesenchymal stem cells. *Biomaterials* **31(2)**, 296-307, (2010).

[423] Remlinger, N.T., Czajka, C.a. *et al.* Hydrated xenogeneic decellularized tracheal matrix as a scaffold for tracheal reconstruction. *Biomaterials* **31**, 3520-3526, (2010).

[424] Gilbert, T.W., Agrawal, V. *et al.* Liver-derived extracellular matrix as a biologic scaffold for acute vocal fold repair in a canine model. *The Laryngoscope* **119**, 1856-1863, (2009).

[425] Uygun, B.E., Soto-Gutierrez, A. *et al.* Organ reengineering through development of a transplantable recellularized liver graft using decellularized liver matrix. *Nature Medicine* **16(7)**, 814-U120, (2010).

[426] Valentin, J.E., Turner, N.J. *et al.* Functional skeletal muscle formation with a biologic scaffold. *Biomaterials* **31**, 7475-7484, (2010).

[427] Daly, K.A., Stewart-Akers, A.M. *et al.* Effect of the alpha gal epitope on the response to small intestinal submucosa extracellular matrix in a nonhuman primate model. *Tissue Engineering Part A* **15(12)**, 3877-3888, (2009).

[428] Ingram, J.H., Korossis, S. *et al.* The use of ultrasonication to aid recellularization of acellular natural tissue scaffolds for use in anterior cruciate ligament reconstruction. *Tissue Engineering* **13(7)**, 1561-1572, (2007).

[429] Brennan, E.P., Tang, X.-H. *et al.* Chemoattractant activity of degradation products of fetal and adult skin extracellular matrix for keratinocyte progenitor cells. *Journal of Tissue Engineering and Regenerative Medicine* **2(8)**, 491-498, (2008).

[430] Gui, L., Muto, A. *et al.* Development of decellularized human umbilical arteries as small-diameter vascular grafts. *Tissue Engineering Part A* **15(9)**, 2665-2676, (2009).

[431] Xu, C.C., Chan, R.W. *et al.* Controlled release of hepatocyte growth factor from a bovine acellular scaffold for vocal fold reconstruction. *Journal of Biomedical Materials Research Part A* **93(4)**, 1335-1347, (2010).

[432] Karabekmez, F.E., Duymaz, A. *et al.* Early clinical outcomes with the use of decellularized nerve allograft for repair of sensory defects within the hand. *Hand* **4(3)**, 245-249, (2009).

[433] Wilshaw, S.-P., Kearney, J.N. *et al.* Production of an acellular amniotic membrane matrix for use in tissue engineering. *Tissue Engineering* **12(8)**, 2117-2129, (2006).

[434] Ozeki, M., Narita, Y. *et al.* Evaluation of decellularized esophagus as a scaffold for cultured esophageal epithelial cells. *Journal of Biomedical Materials Research Part A* **79(4)**, 771-778, (2006).

[435] Flynn, L., Semple, J.L. *et al.* Decellularized placental matrices for adipose tissue engineering. *Journal of Biomedical Materials Research Part A* **79(2)**, 359-369, (2006).

[436] Narita, Y., Kagami, H. *et al.* Decellularized ureter for tissue-engineered small-caliber vascular graft. *Journal of Artificial Organs* **11(2)**, 91-99, (2008).

[437] Stapleton, T.W., Ingram, J. *et al.* Development and characterization of an acellular porcine medial meniscus for use in tissue engineering. *Tissue Engineering Part A* **14(4)**, 505-518, (2008).

[438] Nakayama, K.H., Batchelder, C.A. *et al.* Decellularized rhesus monkey kidney as a three-dimensional scaffold for renal tissue engineering. *Tissue Engineering Part A* **16(7)**, 2207-2216, (2010).

[439] Sellaro, T.L., Ranade, A. *et al.* Maintenance of human hepatocyte function *in vitro* by liver-derived extracellular matrix gels. *Tissue Engineering Part A* **16**, 1075-1082, (2010).

[440] Petersen, T.H., Calle, E.A. *et al.* Tissue-engineered lungs for *in vivo* implantation. *Science* **329(5991)**, 538-541, (2010).

[441] Nieponice, A., McGrath, K. *et al.* An extracellular matrix scaffold for esophageal stricture prevention after circumferential EMR. *Gastrointestinal Endoscopy* **69**, 289-296, (2009).

[442] Robinson, K.A., Li, J. *et al.* Extracellular matrix scaffold for cardiac repair. *Circulation* **112**, I135-143, (2005).

[443] Brown, B.N., Valentin, J.E. *et al.* Macrophage phenotype and remodeling outcomes in response to biologic scaffolds with and without a cellular component. *Biomaterials* **30(8)**, 1482-1491, (2009).

[444] Badylak, S.F., Valentin, J.E. *et al.* Macrophage phenotype as a determinant of biologic scaffold remodeling. *Tissue Engineering Part A* **14**, 1835-1842, (2008).

[445] Brown, B.N., Londono, R. *et al.* Macrophage phenotype as a predictor of constructive remodeling following the implantation of biologically derived surgical mesh materials. *Acta Biomaterialia* **8(3)**, 978-987, (2012).

[446] Gilbert, T.W., Stewart-Akers, A.M. *et al.* Degradation and remodeling of small intestinal submucosa in canine Achilles tendon repair. *The Journal Of Bone And Joint Surgery (American)* **89**, 621-630, (2007).

[447] Gilbert, T.W., Stewart-Akers, A.M. *et al.* A quantitative method for evaluating the degradation of biologic scaffold materials. *Biomaterials* **28**, 147-150, (2007).

[448] Record, R.D., Hillegonds, D. *et al. In vivo* degradation of C-14-labeled small intestinal submucosa (SIS) when used for urinary bladder repair. *Biomaterials* **22(19)**, 2653-2659, (2001).

[449] Mostow, E.N., Haraway, G.D. *et al.* Effectiveness of an extracellular matrix graft (OASIS Wound Matrix) in the treatment of chronic leg ulcers: a randomized clinical trial. *Journal of Vascular Surgery* **41(5)**, 837-843, (2005).

[450] Crapo, P.M., Gilbert, T.W. *et al.* An overview of tissue and whole organ decellularization processes. *Biomaterials* **32(12)**, 3233-3243, (2011).

[451] Freytes, D.O., Martin, J. *et al.* Preparation and rheological characterization of a gel form of the porcine urinary bladder matrix. *Biomaterials* **29**, 1630-1637, (2008).

[452] Seif-Naraghi, S.B., Salvatore, M.A. *et al.* Design and characterization of an injectable pericardial matrix gel: a potentially autologous scaffold for cardiac tissue engineering. *Tissue Engineering Part A* **16(6)**, 2017-2027, (2010).

[453] Wolf, M.T., Daly, K.A. *et al.* A hydrogel derived from decellularized dermal extracellular matrix. *Biomaterials* **33(29)**, 7028-7038, (2012).

[454] DeQuach, J.A., Lin, J.E. *et al.* Injectable skeletal muscle matrix hydrogel promotes neovascularization and muscle cell infiltration in a hindlimb ischemia model. *European Cells & Materials* **23**, 400-412, (2012).

[455] Young, D.A., Ibrahim, D.O. *et al.* Injectable hydrogel scaffold from decellularized human lipoaspirate. *Acta Biomaterialia* **7(3)**, 1040-1049, (2011).

[456] Singelyn, J.M., Sundaramurthy, P. *et al.* Catheter-deliverable hydrogel derived from decellularized ventricular extracellular matrix increases endogenous cardiomyocytes and preserves cardiac function post-myocardial infarction. *Journal of the American College of Cardiology* **59(8)**, 751-763, (2012).

[457] Johnson, T.D., Lin, S.Y. *et al.* Tailoring material properties of a nanofibrous extracellular matrix derived hydrogel. *Nanotechnology* **22(49)**, 494015, (2011).

[458] Uriel, S., Huang, J.-J. *et al.* The role of adipose protein derived hydrogels in adipogenesis. *Biomaterials* **29(27)**, 3712-3719, (2008).

[459] Uriel, S., Labay, E. *et al.* Extraction and assembly of tissue-derived gels for cell culture and tissue engineering. *Tissue Engineering Part C - Methods* **15(3)**, 309-321, (2009).

[460] Francis, D., Abberton, K. *et al.* Myogel supports the *ex vivo* amplification of corneal epithelial cells. *Experimental Eye Research* **88(3)**, 339-346, (2009).

[461] Cheng, M.-H., Uriel, S. *et al.* Dermis-derived hydrogels support adipogenesis *in vivo*. *Journal of Biomedical Materials Research Part A* **92A(3)**, 852-858, (2010).

[462] Reing, J.E., Zhang, L. *et al.* Degradation products of extracellular matrix affect cell migration and proliferation. *Tissue Engineering Part A* **15**, 605-614, (2009).

[463] Sarikaya, A., Record, R. *et al.* Antimicrobial activity associated with extracellular matrices. *Tissue Engineering* **8(1)**, 63-71, (2002).

[464] Brennan, E.P., Reing, J. *et al.* Antibacterial activity within degradation products of biological scaffolds composed of extracellular matrix. *Tissue Engineering* **12**, 2949-2955, (2006).

[465] Beattie, A.J., Gilbert, T.W. *et al.* Chemoattraction of progenitor cells by remodeling extracellular matrix scaffolds. *Tissue Engineering Part A* **15**, 1119-1125, (2009).

[466] Vaccaro, A.R., Chiba, K. *et al.* Bone grafting alternatives in spinal surgery. *The Spine Journal* **2(3)**, 206-215, (2002).

[467] Kolk, A., Handschel, J. *et al.* Current trends and future perspectives of bone substitute materials - from space holders to innovative biomaterials. *Journal of Cranio-Maxillofacial Surgery*, (2012).

[468] Dinopoulos, H., Dimitriou, R. *et al.* Bone graft substitutes: what are the options? *The Surgeon* **10(4)**, 230-239, (2012).

[469] Bostrom, M.P.G. & Seigerman, D.A. The clinical use of allografts, demineralized bone matrices, synthetic bone graft substitutes and osteoinductive growth factors: a survey study. *HSS Journal* **1(1)**, 9-18, (2005).

[470] Pietrzak, W.S., Ali, S.N. *et al.* BMP depletion occurs during prolonged acid demineralization of bone: characterization and implications for graft preparation. *Cell and Tissue Banking* **12(2)**, 81-88, (2011).

[471] Sampath, T.K. & Reddi, A.H. Distribution of bone inductive proteins in mineralized and demineralized extracellular-matrix. *Biochemical and Biophysical Research Communications* **119(3)**, 949-954, (1984).

[472] Chakkalakal, D.A., Strates, B.S. *et al.* Demineralized bone matrix as a biological scaffold for bone repair. *Tissue Engineering* **7(2)**, 161-177, (2001).

[473] Gruskin, E., Doll, B.A. *et al.* Demineralized bone matrix in bone repair: history and use. *Advanced Drug Delivery Reviews*, (2012).

[474] Ozdemir, M.T. & Kir, M.C. Repair of long bone defects with demineralized bone matrix and autogenous bone composite. *Indian Journal of Orthopaedics* **45(3)**, 226-230, (2011).

[475] Thomas, C.B., Maxson, S. *et al.* Preparation and characterization of a composite of demineralized bone matrix fragments and polylactide beads for bone tissue engineering. *Journal of Biomaterials Science - Polymer Edition* **22(4-6)**, 589-610, (2011).

[476] Mauney, J.R., Jaquiery, C. *et al. In vitro* and *in vivo* evaluation of differentially demineralized cancellous bone scaffolds combined with human bone marrow stromal cells for tissue engineering. *Biomaterials* **26(16)**, 3173-3185, (2005).

[477] Moore, S.T., Katz, J.M. *et al.* Osteoconductivity and osteoinductivity of Puros(R) DBM putty. *Journal of Biomaterials Applications* **26(2)**, 151-171, (2011).

[478] Supronowicz, P., Gill, E. *et al.* Human adipose-derived side population stem cells cultured on demineralized bone matrix for bone tissue engineering. *Tissue Engineering Part A* **17(5-6)**, 789-798, (2011).

[479] Han, B., Tang, B.W. *et al.* Quantitative and sensitive *in vitro* assay for osteoinductive activity of dernineralized bone matrix. *Journal of Orthopaedic Research* **21(4)**, 648-654, (2003).

[480] Kasten, P., Luginbuhl, R. *et al.* Comparison of human bone marrow stromal cells seeded on calcium-deficient hydroxyapatite, beta-tricalcium phosphate and demineralized bone matrix. *Biomaterials* **24(15)**, 2593-2603, (2003).

[481] Wildemann, B., Kadow-Romacker, A. *et al.* Quantification of various growth factors in different demineralized bone matrix preparations. *Journal of Biomedical Materials Research Part A* **81A(2)**, 437-442, (2007).

[482] Shi, Y., Niedzinski, J.R. *et al.* Adipose-derived stem cells combined with a demineralized cancellous bone substrate for bone regeneration. *Tissue Engineering Part A* **18(13-14)**, 1313-1321, (2012).

[483] Katz, J.M., Nataraj, C. *et al.* Demineralized bone matrix as on osteoinductive biomaterial and *in vitro* predictors of its biological potential. *Journal of Biomedical Materials Research Part B - Applied Biomaterials* **89B(1)**, 127-134, (2009).

[484] Bae, H., Zhao, L. *et al.* Variability across ten production lots of a single demineralized bone matrix product. *Journal Of Bone And Joint Surgery (American)* **92A(2)**, 427-435, (2010).

[485] Servin-Trujillo, M.A., Reyes-Esparza, J.A. *et al.* Use of a graft of demineralized bone matrix along with TGF-beta 1 leads to an early bone repair in dogs. *Journal of Veterinary Medical Science* **73(9)**, 1151-1161, (2011).

[486] Pieske, O., Wittmann, A. *et al.* Autologous bone graft versus demineralized bone matrix in internal fixation of ununited long bones. *Journal of Trauma Management & Outcomes* **3**, 11, (2009).

[487] Hoffer, M.J., Griffon, D.J. *et al.* Clinical applications of demineralized bone matrix: a retrospective and case-matched study of seventy-five dogs. *Veterinary Surgery* **37(7)**, 639-647, (2008).

[488] Vaccaro, A.R., Stubbs, H.A. *et al.* Demineralized bone matrix composite grafting for posterolateral spinal fusion. *Orthopedics* **30(7)**, 567-570, (2007).

[489] Martin, G.J., Boden, S.D. *et al.* New formulations of demineralized bone matrix as a more effective graft alternative in experimental posterolateral lumbar spine arthrodesis. *Spine* **24(7)**, 637-645, (1999).

[490] Kawcak, C.E., Trotter, G.W. *et al.* Comparison of bone healing by demineralized bone matrix and autogenous cancellous bone in horses. *Veterinary Surgery* **29(3)**, 218-226, (2000).

[491] Piattelli, A., Scarano, A. *et al.* Comparison of bone regeneration with the use of mineralized and demineralized freeze-dried bone allografts: a histological and histochemical study in man. *Biomaterials* **17(11)**, 1127-1131, (1996).

[492] Acarturk, T.O. & Hollinger, J.O. Commercially available demineralized bone matrix compositions to regenerate calvarial critical-sized bone defects. *Plastic and Reconstructive Surgery* **118(4)**, 862-873, (2006).

[493] Peterson, B., Whang, P.G. *et al.* Osteoinductivity of commercially available demineralized bone matrix - preparations in a spine fusion model. *Journal Of Bone And Joint Surgery (American)* **86A(10)**, 2243-2250, (2004).

[494] Takikawa, S., Bauer, T.W. *et al.* Comparative evaluation of the osteoinductivity of two formulations of human demineralized bone matrix. *Journal of Biomedical Materials Research Part A* **65A(1)**, 37-42, (2003).

[495] Markel, D.C., Guthrie, S.T. *et al.* Characterization of the inflammatory response to four commercial bone graft substitutes using a murine biocompatibility model. *Journal of Inflammation Research* **5**, 13-18, (2012).

[496] Tian, M., Yang, Z. *et al.* Delivery of demineralized bone matrix powder using a thermogelling chitosan carrier. *Acta Biomaterialia* **8(2)**, 753-762, (2012).

[497] Kaya, Y., Yalim, M. *et al.* Comparison of applying particulate demineralized bone matrix (DBM), putty DBM and open flap debridement in periodontal horizontal bone defects. A 12-month longitudinal, multi-center, triple-blind, split-mouth, randomized, controlled clinical study. Part 1 - clinical and radiographic evaluation. *Journal of Oral Rehabilitation* **36(7)**, 524-534, (2009).

[498] Sandhu, H.S., Khan, S.N. *et al.* Demineralized bone matrix, bone morphogenetic proteins, and animal models of spine fusion: an overview. *European Spine Journal* **10**, S122-S131, (2001).

[499] Bostrom, M.P.G., Yang, X. *et al.* An unexpected outcome during testing of commercially available demineralized bone graft materials - how safe are the nonallograft components? *Spine* **26(13)**, 1425-1428, (2001).

[500] Wang, J.C., Kanim, L.E.A. *et al.* Dose-dependent toxicity of a commercially available demineralized bone matrix material. *Spine* **26(13)**, 1429-1435, (2001).

[501] Lomas, R.J., Gillan, H.L. *et al.* An evaluation of the capacity of differently prepared demineralised bone matrices (DBM) and toxic residuals of ethylene oxide (EtOx) to provoke an inflammatory response *in vitro*. *Biomaterials* **22(9)**, 913-921, (2001).

[502] Schenke-Layland, K., Opitz, F. *et al.* Complete dynamic repopulation of decellularized heart valves by application of defined physical signals - an *in vitro* study. *Cardiovascular Research* **60(3)**, 497-509, (2003).

[503] Rosario, D.J., Reilly, G.C. *et al.* Decellularization and sterilization of porcine urinary bladder matrix for tissue engineering in the lower urinary tract. *Regenerative Medicine* **3(2)**, 145-156, (2008).

[504] Gilbert, T.W., Freund, J.M. *et al.* Quantification of DNA in biologic scaffold materials. *The Journal of Surgical Research* **152**, 135-139, (2009).

[505] Liao, J., Joyce, E.M. *et al.* Effects of decellularization on the mechanical and structural properties of the porcine aortic valve leaflet. *Biomaterials* **29(8)**, 1065-1074, (2008).

[506] Meyer, S.R., Chiu, B. *et al.* Comparison of aortic valve allograft decellularization techniques in the rat. *Journal of Biomedical Materials Research Part A* **79(2)**, 254-262, (2006).

[507] Iop, L., Renier, V. *et al.* The influence of heart valve leaflet matrix characteristics on the interaction between human mesenchymal stem cells and decellularized scaffolds. *Biomaterials* **30(25)**, 4104-4116, (2009).

[508] Xu, C.C., Chan, R.W. *et al.* A biodegradable, acellular xenogeneic scaffold for regeneration of the vocal fold lamina propria. *Tissue Engineering* **13(3)**, 551-566, (2007).

[509] Dong, X., Wei, X. *et al.* RGD-modified acellular bovine pericardium as a bioprosthetic scaffold for tissue engineering. *Journal of Materials Science - Materials in Medicine*, (2009).

[510] Lee, K.J.H., Roper, J.G. *et al.* Demineralized bone matrix and spinal arthrodesis. *The Spine Journal* **5(6 Suppl)**, 217S-223S, (2005).

[511] Dalton, B.A., McFarland, C.D. *et al.* Role of the heparin-binding domain of fibronectin in attachment and spreading of human bone-derived cells. *Journal of Cell Science* **108**, 2083-2092, (1995).

[512] Weiss, R.E. & Reddi, A.H. Appearance of fibronectin during the differentiation of cartilage, bone, and bone-marrow. *Journal of Cell Biology* **88(3)**, 630-636, (1981).

[513] Flores, M.E., Norgard, M. *et al.* RGD-directed attachment of isolated rat osteoclasts to osteopontin, bone sialoprotein, and fibronectin. *Experimental Cell Research* **201(2)**, 526-530, (1992).

[514] Shigeyama, Y., Derrico, J.A. *et al.* Commercially-prepared allograft material has biological-activity *in-vitro*. *Journal of Periodontology* **66(6)**, 478-487, (1995).

[515] Roach, H.I. Why does bone-matrix contain noncollagenous proteins - the possible roles of osteocalcin, osteonectin, osteopontin and bone sialoprotein in bone mineralization and resorption. *Cell Biology International* **18(6)**, 617-628, (1994).

[516] Pietrzak, W.S., Woodell-May, J. *et al.* Assay of bone morphogenetic protein-2,-4, and-7 in human demineralized bone matrix. *Journal of Craniofacial Surgery* **17(1)**, 84-90, (2006).

[517] Seif-Naraghi, S.B., Horn, D. *et al.* Injectable extracellular matrix derived hydrogel provides a platform for enhanced retention and delivery of a heparin-binding growth factor. *Acta Biomaterialia*, (2012).

[518] Keech, M.K. Formation of fibrils from collagen solutions. 4. Effect of mucopolysaccharides and nucleic acids - an electron microscope study. *Journal of Biophysical and Biochemical Cytology* **9(1)**, 193-&, (1961).

519 McPherson, J.M., Sawamura, S.J. *et al.* The effects of heparin on the physicochemical properties of reconstituted collagen. *Collagen and Related Research* **8(1)**, 65-82, (1988).

520 Nemethcsoka, M. & Kovacsay, A. The effect of glycosaminoglycans (GAG) on the intramolecular bindings of collagen. *Acta Biologica Academiae Scientiarum Hungaricae* **30(4)**, 303-308, (1979).

521 Jayasuriya, A.C. & Ebraheim, N.A. Evaluation of bone matrix and demineralized bone matrix incorporated PLGA matrices for bone repair. *Journal of Materials Science - Materials in Medicine* **20(8)**, 1637-1644, (2009).

522 Bibbo, C. & Patel, D.V. The effect of demineralized bone matrix-calcium sulfate with vancomycin on calcaneal fracture healing and infection rates: a prospective study. *Foot & Ankle International* **27(7)**, 487-493, (2006).

523 Lai, P.-H., Chang, Y. *et al.* Acellular biological tissues containing inherent glycosaminoglycans for loading basic fibroblast growth factor promote angiogenesis and tissue regeneration. *Tissue Engineering* **12(9)**, 2499-2508, (2006).

524 Li, Y., Kong, M. *et al.* Preparation and property of layer-by-layer alginate hydrogel beads based on multi-phase emulsion technique. *Journal of Sol-Gel Science and Technology* **62(2)**, 217-226, (2012).

525 Matalanis, A. & McClements, D.J. Impact of encapsulation within hydrogel microspheres on lipid digestion: an *in vitro* study. *Food Biophysics* **7(2)**, 145-154, (2012).

526 Schachschal, S., Adler, H.-J. *et al.* Encapsulation of enzymes in microgels by polymerization/cross-linking in aqueous droplets. *Colloid and Polymer Science* **289(5-6)**, 693-698, (2011).

527 Couvreur, P., BlancoPrieto, M.J. *et al.* Multiple emulsion technology for the design of microspheres containing peptides and oligopeptides. *Advanced Drug Delivery Reviews* **28(1)**, 85-96, (1997).

528 Sah, H. Protein behavior at the water/methylene chloride interface. *Journal of Pharmaceutical Sciences* **88**, 1320-1325, (1999).

529 Leukers, B., Gulkan, H. *et al.* Hydroxyapatite scaffolds for bone tissue engineering made by 3D printing. *Journal of Materials Science - Materials in Medicine* **16(12)**, 1121-1124, (2005).

[530] Ang, K.C., Leong, K.F. *et al.* Investigation of the mechanical properties and porosity relationships in fused deposition modelling-fabricated porous structures. *Rapid Prototyping Journal* **12(2)**, 100-105, (2006).

[531] Chen, V.J., Smith, L.a. *et al.* Bone regeneration on computer-designed nano-fibrous scaffolds. *Biomaterials* **27**, 3973-3979, (2006).

[532] Berry, S.M., Warren, S.P. *et al.* Endothelial cell scaffolds generated by 3D direct writing of biodegradable polymer microfibers. *Biomaterials* **32(7)**, 1872-1879, (2011).

[533] Weigel, T., Schinkel, G. *et al.* Design and preparation of polymeric scaffolds for tissue engineering. *Expert Review of Medical Devices* **3**, 835-851, (2006).

[534] Jordan, F., Naylor, A. *et al.* Sustained release hGH microsphere formulation produced by a novel supercritical fluid technology: *in vivo* studies. *Journal of Controlled Release* **141(2)**, 153-160, (2010).

[535] White, L.J., Hutter, V. *et al.* Controlling the morphology and mechanical properties of supercritical fluid foamed scaffolds. *Journal of Pharmacy and Pharmacology* **62(10)**, 1503-1504, (2010).

[536] Kelly, C.A., Howdle, S.M. *et al.* Stability of human growth hormone in supercritical carbon dioxide. *Journal of Pharmaceutical Sciences* **101(1)**, 56-67, (2012).

[537] Davies, O.R., Lewis, A.L. *et al.* Applications of supercritical CO_2 in the fabrication of polymer systems for drug delivery and tissue engineering. *Advanced Drug Delivery Reviews* **60(3)**, 373-387, (2008).

[538] Yang, X.B.B., Whitaker, M.J. *et al.* Human osteoprogenitor bone formation using encapsulated bone morphogenetic protein 2 in porous polymer scaffolds. *Tissue Engineering* **10(7-8)**, 1037-1045, (2004).

[539] Yeo, S.D. & Kiran, E. Formation of polymer particles with supercritical fluids: a review. *Journal of Supercritical Fluids* **34(3)**, 287-308, (2005).

[540] Rahman, C.V., Ben-David, D. *et al.* Controlled release of BMP-2 from a sintered polymer scaffold enhances bone repair in a mouse calvarial defect model. *Journal of Tissue Engineering and Regenerative Medicine*, (2012).

[541] Boussahel, A., Rahman, C. *et al.* An injectable scaffold with sustained release of rhBMP2 for bone regeneration. *Journal of Pharmacy and Pharmacology* **62(10)**, 1499-1500, (2010).

[542] Morgan, E.F. & Keaveny, T.M. Dependence of yield strain of human trabecular bone on anatomic site. *Journal of Biomechanics* **34(5)**, 569-577, (2001).

[543] Kopperdahl, D.L. & Keaveny, T.M. Yield strain behavior of trabecular bone. *Journal of Biomechanics* **31(7)**, 601-608, (1998).

[544] Lotz, J.C., Gerhart, T.N. *et al.* Mechanical properties of trabecular bone from the proximal femur - a quantitative CT study. *Journal of Computer Assisted Tomography* **14(1)**, 107-114, (1990).

[545] Carter, D.R. & Hayes, W.C. Bone compressive strength - influence of density and strain rate. *Science* **194(4270)**, 1174-1176, (1976).

[546] Buyukhatipoglu, K., Jo, W. *et al.* The role of printing parameters and scaffold biopolymer properties in the efficacy of a new hybrid nano-bioprinting system. *Biofabrication* **1(3)**, (2009).

[547] Michna, S., Wu, W. *et al.* Concentrated hydroxyapatite inks for direct-write assembly of 3-D periodic scaffolds. *Biomaterials* **26(28)**, 5632-5639, (2005).

[548] Fu, Q., Saiz, E. *et al.* Direct ink writing of highly porous and strong glass scaffolds for load-bearing bone defects repair and regeneration. *Acta Biomaterialia* **7(10)**, 3547-3554, (2011).

[549] Moon, S., Hasan, S.K. *et al.* Layer by layer three-dimensional tissue epitaxy by cell-laden hydrogel droplets. *Tissue Engineering Part C - Methods* **16**, 157-166, (2010).

[550] Tsuruga, E., Takita, H. *et al.* Pore size of porous hydroxyapatite as the cell-substratum controls BMP-induced osteogenesis. *Journal of Biochemistry* **121(2)**, 317-324, (1997).

[551] Klawitter, J.J. & Hulbert, S.F. Application of porous ceramics for the attachment of load bearing internal orthopedic applications. *Journal of Biomedical Materials Research Biomedical Materials Symposium* **2**, 161-229, (1972).

[552] Robinson, B.P., Hollinger, J.O. *et al.* Calvarial bone repair with porous D,L-polylactide. *Otolaryngology - Head and Neck Surgery* **112(6)**, 707-713, (1995).

[553] Whang, K., Healy, K.E. *et al.* Engineering bone regeneration with bioabsorbable scaffolds with novel microarchitecture. *Tissue Engineering* **5(1)**, 35-51, (1999).

554 Cohen, D.L., Lo, W. *et al.* Increased mixing improves hydrogel homogeneity and quality of three-dimensional printed constructs. *Tissue Engineering Part C - Methods* **17(2)**, 239-248, (2011).

555 Sakai, S., Hashimoto, I. *et al.* Synthesis of an agarose-gelatin conjugate for use as a tissue engineering scaffold. *Journal of Bioscience and Bioengineering* **103(1)**, 22-26, (2007).

Appendix – Modification of Agarose to Improve its Cell Compatibility

A1 - Introduction

Agarose was chosen as a substrate for microinjection/micromanipulation-based patterning partly due to its excellent optical properties. Additionally the cooling/setting-based gelation mechanism allowed effective positioning of microspheres without residual damage to the hydrogel. However agarose is known to allow only poor adhesion of cells in *in vitro* culture[358,359]. To allow cells to be grown on or in hydrogels in which protein signals had been patterned it was necessary to modify the agarose to improve its cell adhesiveness. This was achieved by conjugating gelatin to it using a protocol based on one which was previously published[555].

A2 – Materials & Methods

A2.1 – Agarose-Gelatin Conjugate Synthesis

First 0.4 g of agarose was dissolved in 10 mL dimethyl sulphoxide (DMSO) at 80^{o}C and the resulting solution cooled to room temperature. Following this 17.545 mg of 1,1-carbonyldiimidazole (CDI) in 4 mL DMSO was added to the agarose solution and the mixture stirred for one hour at room temperature. This allowed reaction of the CDI with hydroxyl groups on the agarose molecules. Subsequently 0.4 g of gelatin in 6 mL DMSO was added and stirred for 16 hours at room temperature to allow the CDI bound to the agarose chains to react with amine groups on the gelatin molecules. The resulting material was dialysed against 4 L dH_2O for 2 days to remove DMSO and unreacted CDI (dialysis tubing – catalogue number D0405, Sigma-

Aldrich, Poole, UK). During this period the water was changed three times per day to ensure sink conditions. After removal from the dialysis tubing the hydrogel product was broken into fragments by rapid ejection from a 10 mL Luer lock syringe. These hydrogel fragments were soaked in 0.1 M sodium bicarbonate buffer (4 L, pH 8.5) for 4 days at room temperature to remove uncrosslinked gelatin. During this soak the buffer was changed a total of 6 times. Finally the hydrogel product was washed in 4 L dH_2O for one day to remove the bicarbonate buffer and during this time the water was changed twice. At the end of this period the final product was snap frozen in liquid nitrogen and lyophilised for five days before dry mass measurement to assess the degree of gelatin incorporation. The lyophilised material could be stored at room temperature and reconstituted by addition of dH_2O or PBS and incubation at 80^{o}C with regular agitation.

A2.2 – PrestoBlue™ Assay to Measure Cell Proliferation on Agarose-Based Hydrogels

The agarose-gelatin conjugate material used in this study was kindly provided by Giles Kirby (University of Nottingham). Solutions were prepared at 1% (w/v) of agarose, agarose-gelatin conjugate and a mixture of agarose and gelatin at the same mass ratio as contained within the conjugate. These solutions were transferred to the wells of 12-well tissue culture plates (200 µL per well) and the plates incubated at 4^{o}C for 2 hours to form hydrogels. Immortalised human mesenchymal stem cells (ihMSCs) were seeded on the gels and also on tissue culture plastic (TCP) at 20,000 cells per well in 1 mL of complete medium (n = 6). Medium was changed once per day for 7 days and total cell metabolism on the gels assessed at 1, 3, 5 and 7 days. Results for each surface were assessed relative to cell-free controls incubated under the same conditions.

Resazurin (7-Hydroxy-3H-phenoxazin-3-one 10-oxide) is a non-fluorescent blue compound which becomes the red-fluorescent dye resorufin when reduced in the intracellular environment of living cells. This has been exploited in the development of several resazurin-based cell viability assays, among which is the PrestoBlue™ Cell Viability Reagent assay.

This assay was used to perform the cell metabolism assessment described above. To the 1 mL of culture medium in each well 111 µL of PrestoBlue™ reagent was added and the combination incubated at 37°C in the dark for 30 minutes. From each well 100 µL of reaction mixture was transferred to a black 96-well plate well and the fluorescence intensity read at 560 nm excitation and 590 nm emission.

A3 – Results & Discussion

A3.1 – Agarose-Gelatin Conjugate Preparation

In the course of the work presented here three different batches of conjugate were fabricated by two different operators (one batch prepared by Giles Kirby). The mass fractions of gelatin in these batches were found to be 25.2, 26.0 and 25.8%. These figures were in good agreement with those presented in the original publication[555] and also indicated a low level of bath-to-batch variability for the process.

However two of the batches prepared were found to be incompletely dissolved in either PBS or water at concentrations as low as 0.5% (w/v). This observation was made even after two hours incubation in a water bath at 80°C. The cause of this lack of solubility is not yet fully understood but it can most likely be attributed either to agarose-agarose or gelatin-gelatin conjugation occurring instead of the intended agarose-gelatin interaction. A fuller understanding of the alterations to the reaction mechanism that caused this issue may allow it to be prevented in future conjugate production.

A3.2 – Cell Compatibility of Agarose-Gelatin Conjugate Hydrogels

One day after seeding very few ihMSCs were seen on agarose or agarose-gelatin mixture hydrogels and those that were present showed rounded morphology. By three days after seeding these hydrogels were largely absent in the wells where they had been created suggesting they had dissolved or degraded. These materials were therefore deemed to be unsuitable as *in vitro* cell culture substrates.

Figure A1 shows representative phase contrast images of ihMSCs on the other two surfaces (TCP and agarose-gelatin conjugate). These images show that cells cultured on the conjugate hydrogel exhibited similar morphology to those cultured on TCP. Total cell metabolism on the hydrogels as assessed via the PrestoBlue™ assay was statistically-significantly ($p < 0.05$) lower than that on TCP at all time points (Figure A2).

When the results on both surfaces were normalised to their own day 1 results these significant differences were no longer seen at day 3 or day 7. This suggested that the difference between the two surfaces was one of differing levels of initial cell adhesion rather than differing rates of proliferation. This in turn suggested that agarose-gelatin conjugate hydrogels could function as excellent cell growth environments.

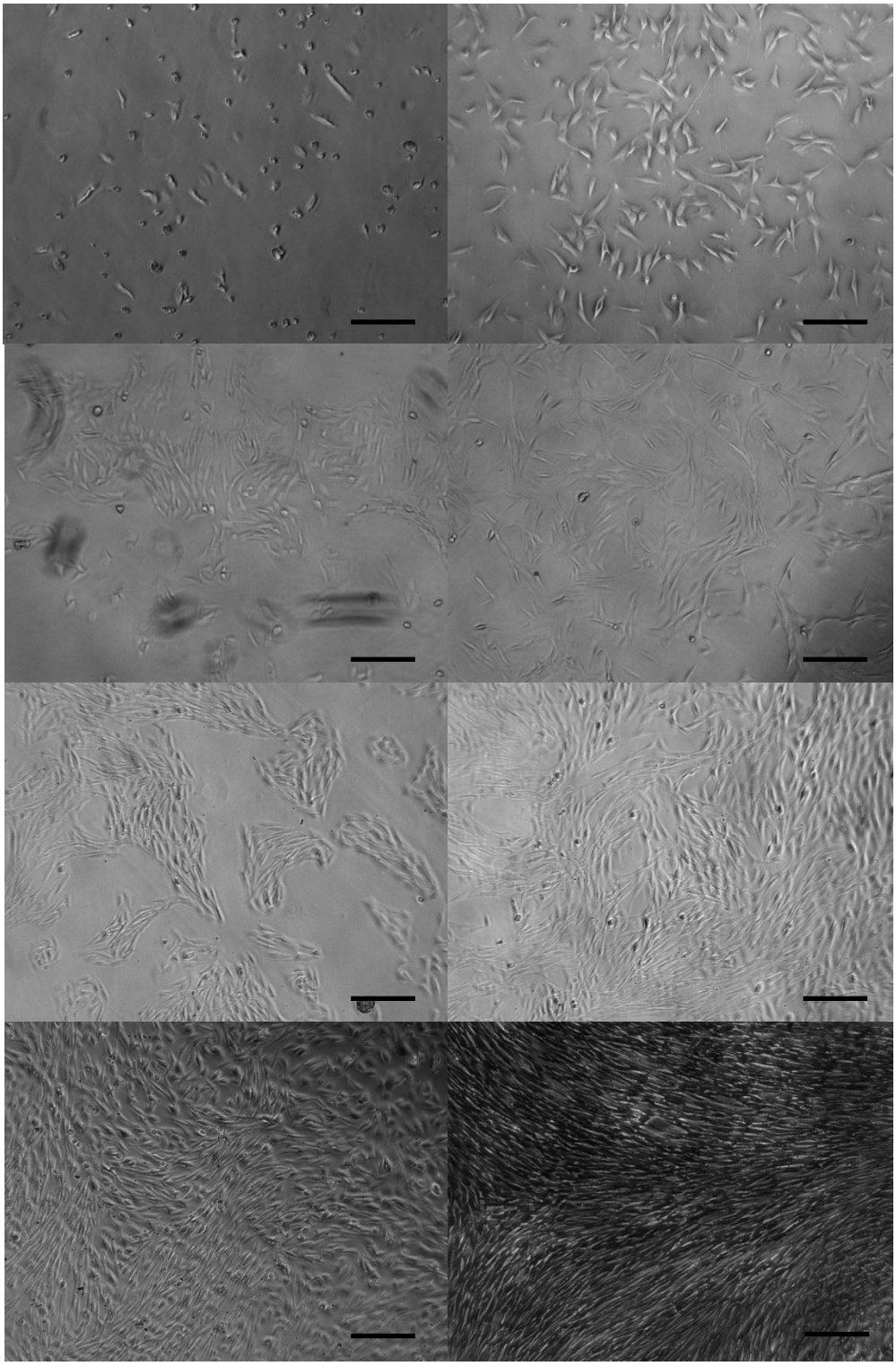

Figure A1 - Representative phase contrast images showing ihMSCs cultured on agarose-gelatin conjugate hydrogel (left) or TCP (right) and imaged at various time points. Top-to-bottom – one day, three days, five days and seven days after seeding at 20,000 cells per well in 12-well plates. Scale bars represent 250 µm.

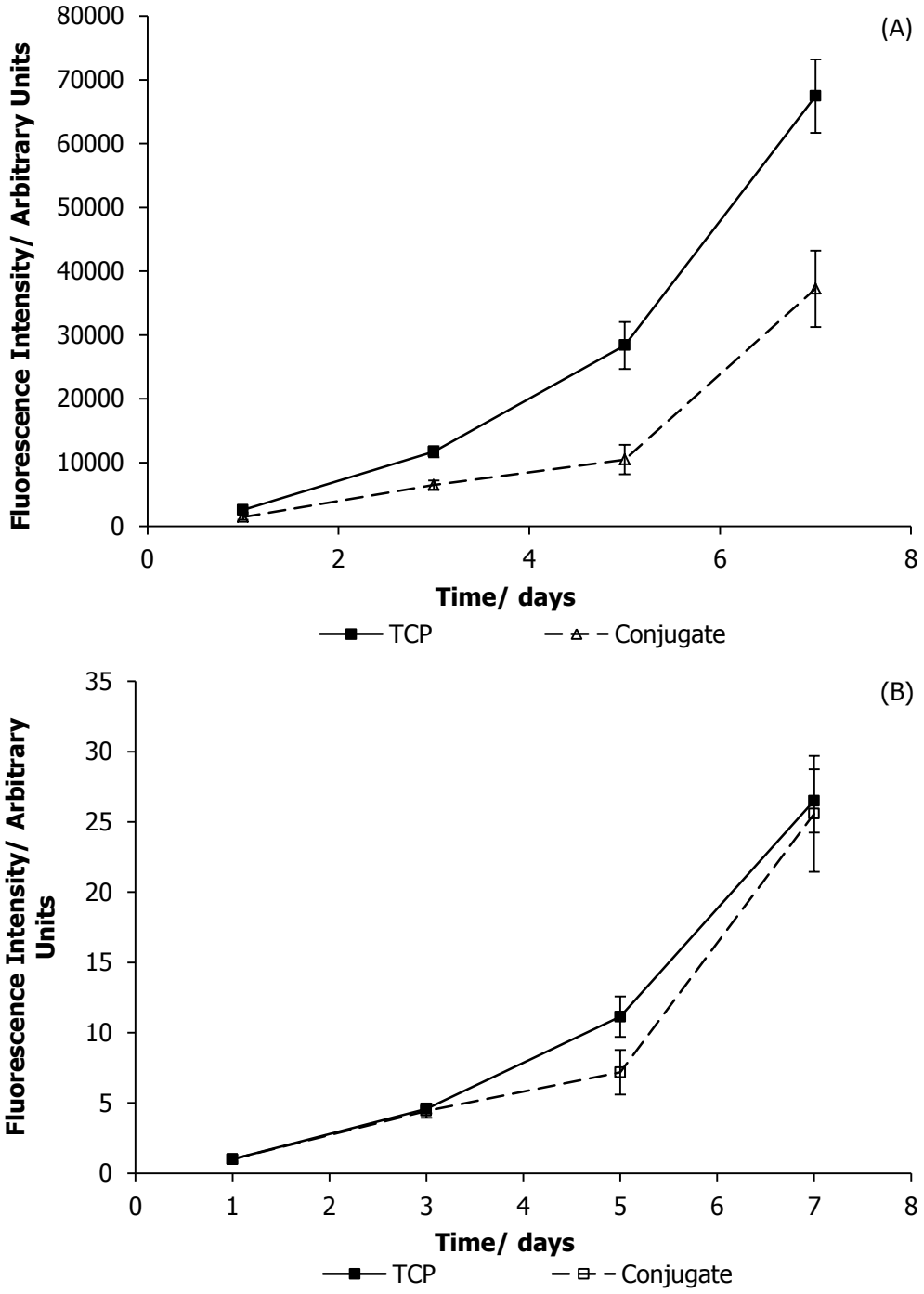

Figure A2 – Total ihMSC metabolism on TCP and on an agarose-gelatin conjugate hydrogel at a variety of time points as measured by PrestoBlue™ assay (n = 6). Cells were seeded at 20,000 cells per well in 12-well plates at time zero. Fluorescence intensities are shown both as measured (A) and normalised to day 1 results (B). Error bars are on standard deviation and statistically-significant differences ($p < 0.05$) between the two groups are denoted by (*).